THE UNIVERSITY
of EDINBURGH

The Early Macrophage Response to *Mycobacterium avium* subspecies *paratuberculosis*

Heather Mathie

A thesis submitted in fulfilment of the requirements for the degree of Doctor of Philosophy

University of Edinburgh

2017

Author's Declaration

I declare that this thesis has been composed solely by myself and that the work presented is entirely my own, except where stated otherwise by reference or acknowledgement, and that it has not been submitted, in whole or in part, in any previous application for a degree or other professional qualification

Signed……

Date...……

Contents

Table of Figures

Table of tables

Acknowledgements

First and foremost, I would like to thank my wonderful supervisors Prof. Jayne Hope, Prof. Liz Glass, and Dr Jo Stevens, for offering me the opportunity to undertake this project, and for providing valuable insight, advice, and support, throughout. A particular thank you to Jayne, not only for your vast immunological knowledge and helpful advice, but for the continuous support and encouragement you have given me over the past four years – I couldn't have gotten here without you.

I would also like to give a special mention to Tom McCahill, without whom I never would have developed an interest in biology. Thank you for all the enthusiasm you instilled in me.

Thanks must be given to Eastbio DTP for funding this project and for providing multiple training opportunities that have broadened my horizons.

I would like to thank Prof. Neil Mabbot and Dr Mike McGrew for sitting on my thesis committee and offering practical advice on experimental design and the direction of the project.

Particular thanks must be given to Dr Kirsty Jensen, who has been the most wonderful teacher – thank you so much for all your wisdom, and for all the time you dedicated to helping me succeed.

Thank you, as well, to Rodrigo Bacigalupe, who performed the bioinformatics analysis for this project. I couldn't have done it without you, and really appreciate you selflessly giving up your time in the middle of a move!

In addition, I would like to add a big thank you to all the members of the Hope, Glass and Stevens groups (past and present) – you have all offered help and advice at some point throughout my project, and have made the lab a fun and friendly place during my time here.

I don't know if I would still be sane at this point if it wasn't for the amazing friends I've made throughout my time at Roslin. Particular thanks to Emma, Ailbhe, Anna,

Craig, Abi, and Maeve – our lunch-time chats and after-work drinks got me through the toughest of weeks. You have been my shoulders to cry on when things have gone wrong, and have always been on hand to pop the prosecco during moments of triumph. Even though we are all moving on to bigger and better things, I know that we'll be Phriends Phor life!

To my many other wonderful friends from school and university - Thank you for being so incredibly supportive. You don't know how much comfort your small gestures of kindness and patience have brought me, and I promise you'll be seeing a lot more of me from now on.

I know I wouldn't be here today without the loving support of my family. Mum and Dad – thank you so much for all you have done for me, not just during these last four years, but throughout my life. You are the people who fostered a love of learning in me from a young age, and always encouraged me to aim high and be the best that I can be. This achievement is just as much yours as it is mine.

Karen – who could ask for a better sister? Thank you so much for all the support and encouragement (and cheering up!) you have given me throughout my PhD. Now let's have some celebrations!

Last but not least, I would like to thank my amazing fiancé David. I know it hasn't been easy living with me over the last six months so I can't thank you enough for putting up with me! You have been so encouraging and supportive, constantly driving me back and forth to the library, providing me with chocolate, take-out food, and even ball games, to keep my spirits up, and (mostly) knowing when to just keep out of my way! I honestly do not know how I would have managed to get through this without you. You inspire me every day with your drive and positivity, and always manage to bring a smile to my face, even in the darkest of times. I love you, and can't wait to become Dr Baird!

Abstract

Mycobacterium avium subsp. *paratuberculosis* (MAP) is the causative agent of Johne's disease, a chronic enteritis that has a damaging economic and welfare impact on the livestock industry. Johne's disease in cattle is known to reduce milk yield and carcass value, making it of economic concern to both dairy and beef farmers. In addition, there is cause for concern regarding zoonotic transmission, as there is an unconfirmed but potential relationship between MAP infection and human Crohn's disease, which presents similar clinical symptoms.

MAP is most often contracted by neonates through the faecal-oral route, but can also be spread through contact with contaminated milk and colostrum, as well as in utero. Once the host receives an oral dose, the bacteria traverse the gut epithelium and are phagocytosed by gut macrophages residing in the lamina propria and Peyer's patches. MAP are able to evade the macrophage response by resisting intracellular degradation within phagosomes. Infected macrophages respond to the infection by secreting several pro-inflammatory cytokines that drive the downstream immune response and granuloma formation.

This work aimed to elucidate key early responses of bovine monocyte derived macrophages (MDM) to MAP infection, and determine the reliability of using the reference strain, K10 (which is likely to have undergone lab adaptation) to model the infection *in vitro*, by comparing the MDM response to K10 with the response to a recent clinical isolate, C49.

At a multiplicity of infection of 5 (MOI 5), there was a significant decrease in K10 intracellular survival (~90%), compared to C49 intracellular survival, over a 24 hour infection time-course. This suggests that K10 may have lost some virulence mechanism through lab adaptation. Understanding the mechanisms of how MDM respond to these two strains could be informative for the design of targeted vaccines

When further investigating the MDM response to both strains, it was found that, at MOI 5, MDM infected with K10 secreted higher levels of IL-1β and IL-10, compared to MDM infected with C49. Both cytokines are associated with

mycobacterial infection and could perhaps indicate that MDM are more responsive to the K10 strain at early time-points.

In addition, MDM infected with K10 produced significantly higher levels of reactive nitrogen species (RNS). RNS are antimicrobial products that can destroy invading pathogens, and have been shown to have bactericidal effects on MAP. The production of RNS could, therefore be a potential mechanism by which MDM are able to kill K10 more efficiently than C49.

An additional aim of this project was to understand the importance of the route of phagocytosis in determining the outcome of MAP infection. MDM express several phagocytic receptors, including Fc receptors (FcRs), complement receptors (CR), C-type lectin receptors and scavenger receptors. This project mainly focused on the role of the mannose receptor (MR) on bacterial uptake and downstream immune responses, as past studies have suggested that other species of mycobacteria such as *M. tuberculosis*, target the mannose receptor in order to regulate macrophage immune responses. Blocking the MR reduced intracellular survival for both strains of MAP; however, the mechanism by which the MR influences intracellular survival remains poorly understood

The effect of opsonisation on MAP prior to uptake by phagocytic cells was also investigated, as presence of opsonins, such a complement proteins and antibody, can change the mechanism by which pathogens are phagocytosed. MAP were incubated in serum from either MAP- negative or MAP- positive cattle, prior to infection and the percentage uptake and survival assessed by performing colony counts. Opsonisation in serum from Johne's negative cattle resulted in marked increase in MAP uptake but not intracellular survival, whereas opsonisation in serum from Johne's positive cattle did not increase uptake but decreased the intracellular survival rate by 24 HPI. This finding highlights a potential protective role of antibody early in the infection process, and could significantly impact how the infection is modelled in future, as anti-MAP antibody may be present in contaminated milk at the point of infection.

Taken together, the data presented in this thesis show that bacterial strain has a significant impact on MDM response to MAP infection, which may have important implications for the interpretation of previous studies and the design of future studies investigating host-pathogen interactions in the context of paratuberculosis. Additionally, this work has shown that RNS production and the mechanism of uptake can affect intracellular survival rates, and although this needs further investigation, the findings could have implications for the design of future vaccines.

Lay Abstract

Johne's disease in cattle is an inflammatory disease of the intestine, caused by infection with the *Mycobacterium avium* subspecies *paratuberculosis* (MAP). The disease can have a detrimental animal-welfare and economic impact on infected farms, as it causes reduced milk yield and carcass value of infected cattle. There is also a tentative link between MAP infection and human Crohn's disease (which presents similar clinical symptoms to Johne's disease) that further underlines the need to understand how this bacterium interacts with its host.

In most cases, a cow will be infected with MAP within the first 6 months of its life, by contact with contaminated milk or colostrum from the mother, or by contact with contaminated faeces. Once MAP enters the gut of the infected animal, it will cross the epithelium (a thin layer of tissue forming the internal surface of the gut) and be ingested by host immune cells called macrophages. Macrophages are cells of the innate immune system that take up and destroy foreign material through a process known as phagocytosis. However, MAP are able to evade the destruction process and go on to live within the macrophages, in a dormant state. Infected macrophages respond to the infection by secreting immune regulators known as cytokines which drives an influx of other immune cells to the site of infection. These newly recruited immune cells essentially 'wall off' the infected macrophages at the centre of a structure known as a granuloma. This process allows an infected cow to live for several years, whilst displaying no clinical symptoms. However, eventually a breakdown in protective immunity will ensue, dormant MAP will reactivate, and the infected cow will display clinical symptoms, including diarrhoea, chronic wasting and the shedding of large numbers of bacteria in the faeces.

The mechanisms that determine the process of this infection are still not fully understood, and this projected hypothesised that early MAP-macrophage interactions may play a pivotal role in determining the downstream immune response and infection outcome.

This work aimed to identify key features in the early responses of bovine macrophages to MAP, and determine the reliability of using the lab-adapted K10

strain to study the macrophage response to MAP. In order to investigate this, bovine macrophages were infected with either the K10 strain or the C49 strain, a recent MAP clinical isolate (taken from a cow presenting clinical symptoms of Johne's disease), at the same dose, and the macrophage response to the 2 strains was compared over a 24-hour time-course.

At the lowest dose tested, K10 had significantly reduced survival within macrophages (~90%), compared to C49, suggesting that the K10 strain may not be as capable of causing disease as the recent clinical isolate, C49. This could possibly be due to the fact that K10 has adapted to survive in the lab for several years, which could have caused it to lose some genes required for successful infection. Macrophages infected with the K10 strain also produced higher levels of cytokines associated with Mycobacterial infection (IL-1β and IL-10), perhaps indicating that macrophages are more responsive to the K10 strain at early time-points.

In addition, bovine macrophages infected with K10 produced significantly higher levels of antimicrobial products called reactive nitrogen species (RNS). RNS are toxic substances that can destroy invading bacteria, and have been previously shown to have a detrimental effect on MAP survival at high concentrations. Therefore, the production of RNS could be a potential mechanism by which macrophages are able to kill K10 more efficiently than C49.

An additional aim of this project was to understand the importance of the route of phagocytosis in determining the outcome of MAP infection. This is due to the fact that macrophages express several types of phagocytic receptors (all of which are capable of inducing macrophages to take up bacteria) but uptake via each can lead to different responses within the cell. This project mainly focused on the role of the MR on bacterial uptake and downstream immune responses, as past studies have suggested that other species of Mycobacteria such as *M. tuberculosis*, target the MR in order to regulate macrophage immune responses. Blocking the mannose receptor reduced survival of both strains of MAP over a 24-hour time-course.

Proteins known as 'antibodies' and 'complement' circulate in the blood and coat foreign substances, in order to aid phagocytosis by immune cells such as

macrophages. This process is known as opsonisation, and a further aim of this project was to investigate the effect of MAP opsonisation on the macrophage response to infection. MAP was incubated in serum from either Johne's negative (no MAP-specific antibody) or Johne's positive (MAP-specific antibody) cattle, prior to infection, and the percentage uptake and survival assessed. Opsonisation in serum from Johne's negative cattle resulted in marked increase in MAP uptake by macrophages but did not affect MAP survival, whereas opsonisation in serum from Johne's positive cattle did not increase uptake but decreased MAP survival over a 24-hour time-course. This finding warrants further study as antibody may be present in contaminated milk, which can cause infection in new-borns.

Taken together, the data presented in this thesis demonstrates that bacterial strain has a significant impact on the macrophage response to MAP infection, which may have important implications for the interpretation of previous studies and the design of future studies investigating how MAP causes disease. Additionally, this work has shown that RNS production and the mechanism of uptake can affect MAP survival rates within macrophages, and although this requires further investigation, it could have implications for the design of future vaccines.

Abbreviations:

AF647: Alexa Fluor 647

AIM2: Absent in melanoma 2

BCG: Bacillus Calmette-Guerin

BLAST: Basic Local Alignment Search Tool

Bp: Base pair

BWA: Burrows Wheeler Aligner

CARD: Caspase activation recruitment domain

cDNA: Complementary deoxyribonucleic acid

CFU: Colony forming unit

CGD: Chronic granulomatous disease

CHeCS: Cattle Health Certification Standards

CR: Complement receptor

CSM: Cell Surface Molecule

CRISPR: Clustered regularly interspaced short palindromic repeat

DAF: Decay accelerating factor

DAMP: Danger associated molecular pattern

DC: Dendritic cell

DIVA: Differentiating infected from vaccinated animals

DNA: Deoxyribonucleic Acid

ELISA: Enzyme Linked Immunosorbent Assay

eNOS: Endothelial nitric oxide synthase

ERK: Extracellular-signal-regulated kinase

EtOH: Ethanol

FBS: Foetal bovine serum

FcRs: Fc Receptors

FSC: Forward Scatter

GALT: Gut associated lymphoid tissue

GATK: Genome analysis toolkit

GCN: Genome copy number

gDNA: Genomic deoxyribonucleic acid

GM: Geometric mean

H/in: Heat inactivated

HNS: Heat-inactivated naïve sera

HPI: Hours post infection

HT-J: High throughput-Johne's

IBD: Inflammatory bowel disease

IFN: Interferon

IFNγR: Interferon gamma receptor

IGRA: Interferon gamma release assay

IL: Interleukin

IL-1R: Interleukin 1 receptor

iNOS: Inducible nitric oxide synthase

IS: Immune sera

JAK: Janus kinase

JDIP: Johne's disease integrated program

Kb: Kilobase

KD: Knockdown

LPS: Lipopolysaccharide

LUT: Lookup table

M. abscessus: Mycobacterium abscessus

M. bovis: *Mycobacterium bovis*

M. kansasii: Mycobacterium kansasii

M. marinum: *Mycobacterium marinum*

M. smegmatis: *Mycobacterium smegmatis*

M. tb: *Mycobacterium tuberculosis*

M: Molar

MAC: Membrane attack complex

Man-LAM: Mannose-capped lipoarabinomannan

MAP: *Mycobacterium avium* subsp. *paratuberculosis*

MAPK: Mitogen activated protein kinase

MARCO: Macrophage receptor with collagenous structure

MBL: Mannose binding lectin

MDM: Monocyte derived macrophage

mg: milligrams

mm: Millimetre

μm: Micrometre

mM: Millimolar

MOI: Multiplicity of infection

MR: Mannose receptor

MVA: Modified Vaccinia Ankara

NADPH: Nicotinamide adenine dinucleotide phosphate reduced

NC: Negative control

NCBI: National Centre for Biotechnology Information

NK cells: Natural killer cells

NLR: Nod-like receptor

NLRP: NLR Family Pyrin Domain Containing

nm: Nanometre

nNOS: Neuronal nitric oxide synthase

NO: Nitric oxide

NS: Naïve sera

NTC: Non-template control

OD: Optical density

PAMP: Pathogen associated molecular pattern

PBMC: Peripheral blood mononuclear cell

PCR: Polymerase chain reaction

PFA: Paraformaldehyde

PFU: Plaque forming unit

PI3P: Phosphatidylinositol 3-phosphate

PPA: Paratuberculosis protoplasmic antigen

PPD: Purified protein derivative

PRR: Pattern recognition receptor

PYD: Pyrin domain

qPCR: Quantitative polymerase chain reaction

qRT-PCR: Quantitative reverse transcription polymerase chain reaction

RANKL: Receptor activator of nuclear factor kappa-B ligand

RNA: Ribonucleic acid

RNS: Reactive nitrogen species

ROI: Region of Interest

ROS: Reactive oxygen species

RPMI: Roswell Park Memorial Institute (media)

SD: Standard deviation

SEM: Standard Error of the Mean

siRNA: small interfering

SNP: Single nucleotide polymorphism

SSC: Side scatter

STAT: Signal Transducer and Activator of Transcription

TC: Transfection control

TCR: T-cell receptor

TGF: Transforming growth factor

TLR: Toll-like receptor

TNF: Tumour necrosis factor

V-ATPase: Vesicular-H+-ATPase

VDAC: Voltage-dependent anion channels

1 Introduction

1.1 Johne's disease in cattle

Johne's disease is a chronic inflammatory disease of the intestine, caused by *Mycobacterium avium* subsp. *paratuberculosis* (MAP) infection. There is a long subclinical period to MAP infection, referred to as 'paratuberculosis', caused by the formation of granulomatous lesions in the intestines of infected animals (section 1.9.4) Johne's disease is the clinical manifestation of paratuberculosis, which occurs upon the breakdown of protective immunity. Symptoms include wasting, diarrhoea, reduced milk production, and premature death of infected cattle (Arsenault et al. 2014), causing MAP infection to have a detrimental economic impact on the beef and dairy industry.

1.2 Prevalence and economic cost of paratuberculosis

Understanding the prevalence of paratuberculosis is essential for the design of effective control programmes, however data on prevalence is severely hindered by the lack of sensitive and specific diagnostic tests (discussed in section 1.3.1). In addition, Johne's disease is not considered a notifiable infection in the UK, meaning there is no legal duty to report an outbreak to the government, causing a lack of reliable data. A 1998 postal survey of 3772 farmers in England and Wales demonstrated that 4.9% of respondents had had clinical cases of Johne's disease within the last ten years and that 17.4% of respondents reported that they had been affected by clinical Johne's disease at some point in the past (Cetinkaya et al. 1998). In addition, assessment of raw bulk-tank milk by PCR estimated UK prevalence to be 7.8%, however the sample size was relatively small (241 approved dairy processing establishments) (Grant et al. 2002). The lack of statutory testing in the UK makes it likely that the prevalence (and therefore economic cost) of Johne's disease is underestimated. The economic cost of the disease is associated with increased involuntary culling of infected cattle, reduced carcass value and reduced milk yield (McAloon et al. 2016; Richardson & More 2009; Ott et al. 1999). In addition to disease-related costs, the long-term nature of the infection makes control programmes costly (Groenendaal et al. 2003; Kudahl et al. 2007). Although the

economic cost associated with Johne's disease is relatively low compared to other diseases of livestock, such as mastitis and bovine tuberculosis (Brooks-Pollock & Keeling 2009; Rollin et al. 2015), it is detrimental to the livestock industry and was estimated to cost the US dairy industry $200-250 million annually (Ott et al. 1999).

1.3 Control of Johne's disease

As discussed above, Johne's disease is not considered a notifiable infection in the UK meaning farmers are not required to report cases, and the disease is not subject to statutory testing. Thus, control is entirely dependent on voluntary livestock health schemes that can provide Cattle Health Certification Standards (CHeCS) accreditation. CHeCS provide a standard set of criteria that must be met, ensuring that the health status of one herd is equivalent to that of the other herds within the scheme (CHeCS 2016). 16% of UK dairy farms were reported to be enrolled in CHeCS licenced Johne's disease health schemes (Orpin et al. 2012; Geraghty et al. 2014). The schemes use a test-and-cull strategy to control the disease; one such health scheme - The Johne's Disease Risk-Level Certification Programme (for beef and dairy cattle) - requires that annual herd blood tests (or quarterly milk tests) be carried out. The most commonly used test to diagnose paratuberculosis infection is an Enzyme-Linked Immunosorbent Assay (ELISA) measuring the presence of MAP-specific antibodies in the serum. As control of Johne's disease must focus on within-herd transmission, due to the high risk of animals within the same herd being exposed to MAP when infected animals shedding MAP in their faeces are present. Seropositive animals must therefore be immediately isolated from the rest of the herd. A secondary test is carried out at one month, and the animal is ultimately culled if seropositive on a second round of testing. Additionally, seropositive animals cannot be used or sold for breeding purposes. Other health schemes also adhere to similar criteria, although culling is not always a strict requirement (CHeCS 2016). Control of the disease is hindered by the lack of reliable diagnostic tests and efficacious vaccines (discussed in sections 1.3.1 and 1.3.2, respectively). In addition, the existence of wildlife reservoirs (particularly rabbits) (Shaughnessy et al. 2013) and the ability of MAP to survive low temperatures in the environment for prolonged

periods of time (up to 55 weeks) (Whittington et al. 2004; Whittington et al. 2005) further complicate disease control.

1.3.1 Diagnosis

As discussed above, Johne's disease control programmes in the UK utilise a test-and-cull strategy in order to identify and remove infected animals. Test-and-cull methods rely on sensitive (unlikely to report a false negative) and specific (unlikely to report a false positive) ante-mortem tests, to identify infected animals for removal from the herd. However, there is currently a lack of reliable diagnostic tests for Johne's disease, which risks infected animals being missed upon testing, as well as increasing the possibility of removing uninfected animals, in error. Lack of sensitivity and specificity in diagnostic tests also creates the need for repeated testing, increasing the cost of control measures for farmers.

Serum ELISA is the most commonly used ante-mortem test and is often used alongside faecal culture of bacteria (Gonza et al. 2009). However, the sensitivity of the serum ELISA can range from 7% to 87%, while specificity ranges between 85-100% (Nielsen & Toft 2008). The lack of sensitivity of serum ELISA is likely due to the nature of the infection (described in section 1.6), as there is great variation in time taken for seroconversion to occur between individual animals; this variation is not yet fully understood, and lack of MAP-specific antibody is not necessarily indicative that the animal is free from infection. The specificity of the ELISA test is lowered by the possibility of antibodies against other mycobacterial species cross-reacting with MAP antigens (Osterstock et al. 2007).

Other diagnostic tests include culture and polymerase chain reaction (PCR) of faecal samples. Culture of MAP from faeces is 100% specific, but only 30-50% sensitive (Clark et al. 2008). The lack of sensitivity is due to the intermittent faecal shedding that occurs during subclinical infection (described in section 1.6.3). A secondary drawback to the use of faecal culture to diagnose paratuberculosis is that it can take up to 16 weeks to gain results, due to the slow-growing nature of the organism (described in section 1.5).

PCR and quantitative PCR (qPCR) have been employed to identify the presence of MAP in faecal samples, using primers targeting MAP-specific sequences, such as IS900 and F57 insertion sequences. A study by Kawaji et al. demonstrated that qPCR had similar sensitivity and specificity to bacterial culture (Kawaji et al. 2007). This method reduced the long wait-time to generate results associated with bacterial culture; however, the DNA extraction protocol was laborious and time-consuming, making it impractical for large-scale testing. Improvements in molecular diagnosis of paratuberculosis by qPCR are continually being developed: a novel test known as the High Throughput Johne's (HT-J) test, improved upon the labour-intensive aspects of qPCR for diagnosis, and demonstrated similar sensitivities and specificities compared to previous qPCR protocols (Plain et al. 2014; Kawaji et al. 2007; Khare et al. 2004).

Other methods for diagnosing MAP infection that are under development, and not currently widely used in the UK, include bacteriophage-based assays (often used in conjunction with PCR or other diagnostic methods). Bacteriophage have been utilised to detect the presence of MAP in blood, milk and faeces, to date (Swift et al. 2016; Stanley et al. 2007; Foddai & Grant 2017; Stewart et al. 2013). In addition, interferon (IFN)γ-release assays (IGRA) could potentially detect MAP-specific immune responses in the early stages of subclinical infection (a major defect of currently available diagnostics) (see section 1.9.3). Studies have recently been undertaken to assess the reliability and usefulness of IGRA (Dernivoix et al. 2017; Hughes et al. 2017), although further work will need to be done to identify specific and immunogenic antigens, as IFNγ production is not specific to MAP and could be induced due to cross-reactivity of antigens with other mycobacteria species. In addition, further investigations would be needed in order to effectively interpret IGRA results before this assay could be routinely used, as fluctuations in IFNγ production can be influenced by additional factors, such as age of infected animals (Dernivoix et al. 2017) and co-infections.

Post mortem tests to confirm a case of Johne's disease include histological assessment of the ileocecal junction and draining lymph node for granulomatous lesions (see section 1.9.4) and MAP culture. MAP PCR from multiple tissue

samples may also be performed (CHeCS 2016). These are useful in confirming the reliability of ante-mortem diagnostics. A detailed understanding of the early immune response to MAP infection could aid in the development of more sensitive and specific ante-mortem diagnostic tests that would likely greatly benefit paratuberculosis control. Improved ante-mortem diagnostics would increase identification of infected animals at early stages, which is of particular importance for reducing spread of infection.

1.3.2 Vaccines

There are currently three commercial vaccines against Johne's disease: Mycopar (manufactured by Boehringer), Gudair (manufactured by CZ Veterinaria and licenced only for use in sheep and goats), and Silirum (manufactured by Zoetis) (Park & Yoo 2016). All three commercial vaccines are inactivated whole-cell vaccines that lack efficacy as they cannot protect against infection or prevent faecal shedding of MAP, but merely delay the onset of clinical symptoms (Park & Yoo 2016). Live-attenuated vaccines provide superior protection than whole-cell inactive vaccines against MAP infection and have been shown to prevent faecal shedding of MAP in goats (Shippy et al. 2017), however no live attenuated MAP vaccines are currently licenced for use in the field. Live-attenuated and whole-cell inactivated MAP vaccines express an array of antigens which could cause reactivity to ante-mortem diagnostic tests for both paratuberculosis and bovine tuberculosis (Rosseels & Huygen 2008). Therefore, these are not licenced for use in cattle in several countries, including the UK. Vaccines should only be used alongside diagnostics with Differentiation of Infected from Vaccinated Animals (DIVA) test capability. Despite the limitations of commercially available Johne's disease vaccines, a meta-analysis by Bastida and Juste determined that vaccination is a useful strategy for preventing production losses from MAP infection and Johne's disease (Bastida & Juste 2011), suggesting that development of a more efficacious vaccine would be of benefit for disease control. An ideal Johne's disease vaccine should induce cell-mediated immunity to confer long-term protection from clinical disease, prevent faecal shedding of MAP, and have DIVA test capability (i.e. not interfere with

paratuberculosis diagnostics). Also of importance is a vaccine that would not interfere with diagnosis of other mycobacterial infections such as bovine tuberculosis. It is therefore likely that the development of a novel, efficacious sub-unit vaccine (used together with an appropriate adjuvant to induce protective Th-1 type immunity) would significantly benefit control of paratuberculosis and Johne's disease. Several advances have been made regarding the development of novel paratuberculosis vaccines in recent years. Bull et al. developed a fusion construct of 4 MAP antigens delivered in viral vectors (Bull et al. 2007). This construct conferred protective immune responses against MAP infection in calves, evidenced by priming and boosting of antigen-specific IFNγ producing T-cell populations, and a lack of faecal shedding in vaccinated calves over a 7 month period (although the study was not continued long enough to determine if calves were protected from clinical disease) (Bull et al. 2014). In addition, a cocktail of MAP antigens delivered in a cationic liposome adjuvant was reported to induce increased antigen-specific IFNγ secretion and IgG1 levels in the serum of vaccinated calves, and did not result in cross-reactivity with the standard tuberculin skin test (a diagnostic test for bovine tuberculosis) (Thakur et al. 2013). Souza et al. recently demonstrated that macrophages incubated with nanoparticles incorporated with MAP peptides and lipids produced high levels of TNFα and IL12p40, suggesting that nanoparticles could be an effective delivery system for subunit vaccines (Souza et al. 2017). Macrophages play a fundamental role in the early immune response to MAP infection, likely determining the outcome of infection or vaccination, and if an animal will become diseased. A detailed understating of the early immune response to MAP infection, focussing on macrophages, would therefore likely identify pathways that could be manipulated by the design of targeted vaccines against paratuberculosis, in order to confer protection.

1.3.3 Host genetics

Breeding for resistance may be an effective long-term preventative measure against Johne's disease, particularly due to the difficulties associated with current control measures discussed in sections 1.3.1 and 1.3.2. The heritability of an antibody response to paratuberculosis (measured by milk ELISA) has been reported to be between 0.06 and 0.095 (Pritchard et al. 2017; Attalla et al. 2010). However, the heritability of susceptibility to paratuberculosis has been reported to be between 0.78 and 0.283, when measured by faecal culture (Küpper et al. 2012), suggesting that faecal culture diagnosis may be a more useful tool as a selection criterion against Johne's disease. Collectively, genetic studies indicate that heritability scores are impacted by country, prevalence, and means of diagnosis (Pritchard et al. 2017; Attalla et al. 2010; Küpper et al. 2012; Zare et al. 2014). Improved diagnostics for paratuberculosis would likely improve genomic selection in the future. Although the heritability of susceptibility to MAP has been reported to be low-medium, it is likely that breeding for resistance would be of long-term benefit when used alongside other control measures, as genetic resistance confers permanent, cumulative protection against disease.

1.3.4 Treatment of Johne's disease

As stated in section 1.3, Johne's disease is controlled through test-and cull strategies, meaning there is little need to treat MAP-infected animals. However, there are specific situations where treatment may be desirable – for example, when the infected animal is of high genetic value, a pet, or used for sport such as rodeo. In these instances, some treatment options are available. While treatment is able to reduce faecal shedding and reverse clinical symptoms, there is no 'cure' for Johne's disease that results in MAP-negative tissues (Fecteau & Whitlock 2011). Cattle infected with MAP and receiving treatment should be isolated from uninfected animals and these animals should not be used in food production. Antimicrobials used to treat MAP-infected animals have the ability to enter mammalian cells (which is of importance since MAP is an intracellular pathogen), and include: isoniazid (Baldwin 1976), rifampin (Mondal et al. 1994; Zanetti et al. 2006), and clofazimine

(Merkal & Larsen 1973). These antimicrobials are often used in combination with each other or with additional antibiotics known to be effective against mycobacteria such as aminoglycosides (Zanetti et al. 2006). There is a risk of toxicity associated antimicrobial treatments and no large-scale studies have been carried out to assess the risk of these drugs. Adverse effects associated with treatment (particularly isoniazid) include: milk reduction, limb stiffness, renal problems, ataxia, and congenital anomalies (leading to abortion) (Fecteau & Whitlock 2011).

1.4 Potential Zoonosis

MAP poses a potential risk to human health, as there is an unconfirmed association between MAP infection and human Crohn's disease. The association is derived from the similarity in clinical symptoms and pathological outcomes of Johne's disease and Crohn's disease, as well as the successful isolation of MAP from tissues of Crohn's disease patients (Autschbach et al. 2005; Shafran 2000). A 2010 meta-analysis by Feller et al. demonstrated that the drug Clofazimine (traditionally used to treat leprosy) was beneficial in the treatment of human Crohn's disease (Feller et al. 2010), and the same drug has been demonstrated to reduce MAP faecal shedding and clinical symptoms in cattle testing positive for MAP infection (Feller et al. 2010; Fecteau & Whitlock 2011). Since MAP is able to survive Pasteurisation of milk, and has been isolated from commercial milk sold to the public (Ellingson et al. 2005), this may be a route by which genetically susceptible individuals within the human population could be exposed to MAP, contributing to the incidence of Crohn's disease. Although this association between Crohn's disease and MAP is still controversial, it emphasises the importance of further research into the pathogenesis of this organism and the requirement for cattle vaccines that would reduce the overall burden of MAP.

1.5 Mycobacterium avium subsp. paratuberculosis

MAP was first isolated from the intestine of a cow displaying clinical symptoms of Johne's disease, by Twort and Ingram in 1912 (Twort & Ingram 1912). Like other mycobacterial species, it is an acid-fast bacterium, meaning it cannot be decolourised by acid due to high lipid content in the cell wall, and requires techniques such as Ziehl-Neelsen staining to be visualised in tissues.

A notable phenotypic difference between MAP and other species of mycobacteria, is its inability to produce the siderophore, mycobactin, in culture, due to truncation of the *mbtA* gene (Li et al. 2005) . Mycobactin is responsible for the transport of iron into cells, which is an essential requirement for bacterial growth. Growth of most MAP strains in culture, therefore, depends on the exogenous addition of Mycobactin-J, an iron chelator purified from a strain of MAP adapted to growth on synthetic medium without exogenous mycobactin (Francis et al. 1953; Merkal & Mccullough 1982). MAP has an exceptionally long generation time of >24 hours in culture (Elguezabal et al. 2011) and takes between 3 and 5 weeks for colonies to appear in culture.

.

1.5.1 Host Range

MAP has a diverse host-range and has been isolated from several ruminant and non-ruminant species, including humans (Ghadiali et al. 2004; Motiwala et al. 2004; Beard et al. 2001). However, it is only known to cause Johne's disease in ruminants, deer, camelids, rabbits, and hares (Salgado et al. 2014; Mackintosh et al. 2016; Ghosh et al. 2012; Beard et al. 2001), although there is a tentative link between MAP and human Crohn's disease, (discussed in Section 1.4).

1.5.2 Genome

The genome of MAP (K10 strain) was first sequenced in 2005, demonstrating MAP to have a single, circular, chromosome, which is 4,829,781 base pairs (bp) in length (Li et al. 2005). The genome has a high GC content (69.3%) and encodes 4350 open

reading frames (ORFs). MAP is a close genetic relative of other pathogenic mycobacteria species; it shares 99% sequence identity with *Mycobacterium avium* subsp. *avium*, and genomic regions of MAP that map to *Mycobacterium marinum* (*M. marinum*), *Mycobacterium bovis* (*M. bovis*) and *Mycobacterium tuberculosis* (*M. tb*) show sequence identity of 90%, 86%, and 86%, respectively (Li et al. 2005; National Center for Biotechnology Information 2017). Some of the noticeable genomic differences between MAP and *M. tb* include genes that are involved in lipid metabolism, possibly resulting in differences in the types of lipids expressed on the cell surface of the two species. In addition, only 1% of the MAP genome encodes PE/PPE proteins, compared to 10% in the *M. tb* genome; these proteins are involved in antigenic variation, suggesting that some of the key genomic differences between MAP and *M. tb* are associated with immune recognition (Li et al. 2005).

1.5.3 MAP structure

The structure and composition of the MAP cell envelope (which encompasses the inner cell membrane and outer cell wall) is important when considering pathogen associated molecular patterns (PAMPs). PAMPs are recognised early in infection by pattern recognition receptors (PRRs) expressed on innate immune cells, such as macrophages. The recognition of PAMPs by innate immune cells can trigger phagocytosis and activate intracellular signalling pathways that will inform the immune response to follow. MAP shares several features of its cell envelope with other, genetically similar, mycobacterial species; the cell envelope is a highly adapted structure important for growth and virulence of mycobacteria, and is composed of three macromolecules: peptidoglycan, arabinogalactan and mycolic acids, surrounded by an outer capsule of proteins and polysaccharides (that can be recognised as PAMPs). Common features of the mycobacterial cell envelope mean that MAP shares several PAMPs with other mycobacterial species, such as mannose-capped lipoarabinomannan (Man-LAM), which is expressed by other species, including *M. tb*, *M. bovis*, *M. bovis* BCG, and *M. leprae* (Prinzis et al. 1993; Murray et al. 2007). Recently, work has been undertaken to identify MAP-specific PAMPs, which will be beneficial to understanding how MAP interacts with immune cells, and

likely improve specificity of MAP diagnostics, as current diagnostics utilise crude preparations of antigens that are not necessarily unique to MAP (discussed further in section 1.3.1 and 1.6.4). Mitachi et al have reported a MAP-specific cell surface lipopeptide (lipopeptide IIβ, 3) that exhibited high antibody binding activity in serum from MAP infected cattle (Mitachi et al. 2016). In addition, specific IFNγ has been measured in response to MAP antigens Ag6, MAP1637c, MAP3547c, and MAP0586c by IGRA (Dernivoix et al. 2017). A recent study by Karuppusamy et al. identified novel MAP-specific cell surface proteins using proteomic approaches. Of the cell surface molecules (CSM) identified, three (*sdhA, FadE25_2, and DesA2*) were recombinantly expressed in *E. coli*, purified, and successfully used to generate polyclonal antibodies, demonstrating that the proteins are antigenic (Karuppusamy et al. 2018). MAP-specific polyclonal antibodies could potentially be utilised to efficiently detect MAP in bovine faecal or milk samples, and the identification of MAP-specific antigens could improve the specificity of serum ELISAs. It should be noted that differences in both fatty acid and protein composition of the MAP cell envelope have been reported between different strains of MAP; this could provide an explanation for differences in virulence observed between strains (Alonso-Hearn et al. 2010; Karuppusamy et al. 2018)

1.5.4 Strains

There are several phylogenetically distinct strains of MAP that are grouped into two major types: C-type (Cow-type) and S-type (Sheep-type). The types are named for the animal that most isolates were originally cultured from. Strains isolated from other species, such as humans, also belong to one of these two types (human isolates are generally C-type) (Stevenson 2015). The reference strain, K10, is a C-type strain that is likely to have undergone lab adaptation (Bryant et al. 2016). Tools to identify genetic differences between strains of the same type have only become available in recent years (Hsu et al. 2011; Bryant et al. 2016). Whole genome sequencing has revealed that MAP strains can differ genetically from the reference strain through mutations such as single nucleotide polymorphisms (SNPs) and large sequence polymorphisms, including insertions, deletions, inversions, translocations, and

duplications. However, MAP strains within the same type, tend to be relatively homogeneous (Hsu et al. 2011; Bryant et al. 2016). There is currently very little information on how strain differences influence virulence and infection outcome. However, a study by Fernandez et al. demonstrated that intestinal lesions in lambs differed between animals experimentally infected with S-type strains, compared to C-type strains; S-type strains resulted in focal lesions, whereas C-type strains resulted in more severe diffuse lesions, at 150 days post infection. Additionally, the study found that the K10 strain produced less severe, multifocal lesions, compared to the diffuse lesions observed for the C-type strain (Fernández et al. 2014), indicating that K10 differs in virulence from other C-type strains. A recent study compared the association of different C-type genotypes with the presence of macroscopic lesions in cattle. Only a weak relationship was found between genotype and lesion severity (Möbius et al. 2017). To date, there have been no studies examining the differences in virulence between K10 and other C-type strains in cattle.

1.6 Pathogenesis of Johne's disease

1.6.1 Transmission

MAP has three main routes of transmission: faecal-oral, congenital and via contaminated milk and colostrum; making neonates the most at-risk of coming into contact with the bacteria and also the most vulnerable to infection, due to underdeveloped naïve immune systems and increased permeability of the intestines of very young animals. The presence of antibody in contaminated milk/colostrum could also increase the risk for neonates as antibody can enhance translocation of MAP across the gut epithelium (Lombard 2011; Everman & Bermudez 2015). Although neonates are at particular risk of infection with MAP, it is important to note that older animals are also susceptible. A study by Mortier et al. demonstrated that calves up to 12 months of age presented macroscopic lesions in the intestine and the draining lymph nodes of the intestine, when experimentally infected with either a high, or low dose of MAP ($5x10^9$ or $5x10^7$ CFU, respectively) (Mortier et al. 2013).

1.6.2 Invasion of the epithelium

There is still some debate regarding the primary point of entry of MAP; granulomatous lesions (see section 1.9.4) most commonly occur in the intestine, however an early *in vivo* study by Payne and Rankin suggested the primary point of MAP entry was the tonsils (Payne & Rankin 1961). Direct instillation of MAP into the tonsillar crypts resulted in bacterial colonisation of the tonsil, duodenum, ileum, and jejunum, as well as ileal, jejunal, and spiral colon lymph nodes (Waters et al. 2003). However, a study which used a surgical procedure to directly infect the intestine of calves showed colonisation of the mesenteric lymph-nodes within 1-2 hours post infection (HPI) (Wu et al. 2007), demonstrating that MAP is efficient at directly invading the intestinal epithelium. Additionally, *in vivo* experiments examining tissue colonisation with a more clinically relevant dose ($1.5x10^6$ CFU)suggest that the intestine is the primary point of entry for MAP as only

intestinal tissue and mesenteric lymph nodes were culture positive in calves infected with $1x10^6$ CFU at 3 weeks post infection (Sweeney et al. 2006).

MAP has been shown to be capable of invading the gut epithelium via multiple mechanisms, including direct invasion of Microfold cells (M-cells) and enterocytes. M-cells are specialised antigen sampling cells overlying follicles of gut associated lymphoid tissue (GALT), including Peyer's patches and isolated lymphoid follicles (Mabbott et al. 2013). Momotani et al first demonstrated that MAP could invade the gut epithelium via M-cells, using election microscopy (Momotani et al. 1988). In addition, a study by Secott et al demonstrated that MAP preferentially invaded M-cells in a murine gut loop model. These studies suggested that MAP target their uptake via M-cells by expression of a fibronectin attachment protein homologue which allows formation of a fibronectin bridge between MAP and integrins on M-cells (Secott et al. 2004). However, other studies have demonstrated that M-cells are not the only means by which MAP invades the gut epithelium. MAP has been shown to directly invade enterocytes, causing them to elicit an internalisation-dependent inflammatory response resulting in the secretion of the inflammatory chemokine CXCL2 (Pott et al. 2009; Bermudez et al. 2010). In addition, Khare et al. demonstrated that MAP actively suppresses host genes involved in maintaining tight junctions between cells, suggesting that MAP is capable of weakening the mucosal epithelium in order to assist direct passage into the GALT during infection (Khare et al. 2012; Bannantine & Bermudez 2013). Subsequent to invasion of the epithelium, MAP rapidly disseminate to mesenteric lymph nodes (within 1-2 hours) where granulomatous lesions form (in addition to lesions observed in the intestine) and the infection persists.

1.6.3 Subclinical infection and progression to clinical disease.

Subsequent to infection, there is a long subclinical period of the infection, during which infected cattle display no clinical symptoms. This long subclinical period is due to the ability of MAP to evade intracellular destruction and survive within the macrophage for a prolonged time. The macrophage response to MAP infection

within the lamina propria and mesenteric lymph-node drives the production of pro-inflammatory cytokines and chemokines that lead to a protective Th-1 response (characterised by IFNγ production) and granuloma formation (described in detail under section 1.9.4). Integrity of the granuloma structure prevents faecal shedding and keeps bacteria and infected macrophages isolated from surrounding tissue, preventing the development of clinical symptoms. MAP are predicted to enter a dormant state within granulomas, surviving for several years (Parrish et al. 2017; Whittington et al. 2004; Whittington et al. 2005). However, after a period of time a change in immune status occurs that results in faecal shedding of bacteria and progression towards clinical disease. This change in immune status has traditionally been thought of as a breakdown in cell-mediated immunity which causes a Th-2 type response to become dominant (Begg et al. 2010). However, it is likely that this is an over-simplification of the cause of the switch to faecal shedding. For example, 50% of lambs experimentally infected with MAP displayed a 'combined' response (i.e. they produced both IFNγ and MAP specific antibody) over the first 19 months post infection, whereas only 39% of lambs displayed a classical switch from Th-1 to Th-2 type immunity (i.e. the IFNγ response waned as the antibody response increased) (Begg et al. 2010). It is clear that immune status is directly correlated with faecal shedding and disease progression, and that Th-1 type immunity is correlated with protection (particularly at early time points) (Begg et al. 2010; Ganusov et al. 2015); however, what triggers the change in immune status that leads to increased faecal shedding, and the exact nature of the immune response associated with disease progression remains poorly understood. Faecal shedding most often first occurs prior to seroconversion while the infected animal remains subclinical (allowing infectious cattle to go undetected by serum ELISA), although this is not always the case (Sweeney *et al.*, 2006) (Figure 1-1). Certain infected animals within a herd may be 'super-shedders', shedding more than 10,000 colony forming units (CFU)/gram of faeces (Aly et al. 2012). It is thought that these cattle play a significant role in maintaining the infection status of a herd, due to the ability of MAP to survive in the environment for prolonged periods (Whittington et al. 2004), but there is still much to be learned about the immunological and bacteriological events which cause this phenomenon (Pradhan et al. 2011). During the shift to a Th-2 biased response, in

which animals are producing antibody against MAP, and shedding bacteria in the faeces, they can remain free of visible symptoms for up to several years (Sweeney 2011) although a reduction in milk production is observed concomitantly with seroconversion and faecal shedding (Gonda et al. 2007). Ultimately, loss of protective cell-mediated immunity and the dominance of a Th-2 response is associated with disease progression and development of clinical symptoms. This is due to granulomatous lesions becoming diffuse, and causing granulomatous enteritis throughout the intestine; this results in a thickening of the intestinal epithelium, causing malabsorption of nutrients and resulting in watery diarrhoea, which leads to weight loss (Sweeney 2011). It is likely that early events during subclinical infection determine if the infection will progress to clinical disease; demonstrated by the increased susceptibility of cattle with mutations in innate PRRs (Mucha et al. 2009; Koets et al. 2010). The pathogenesis of MAP is demonstrated in Figure 1-1.

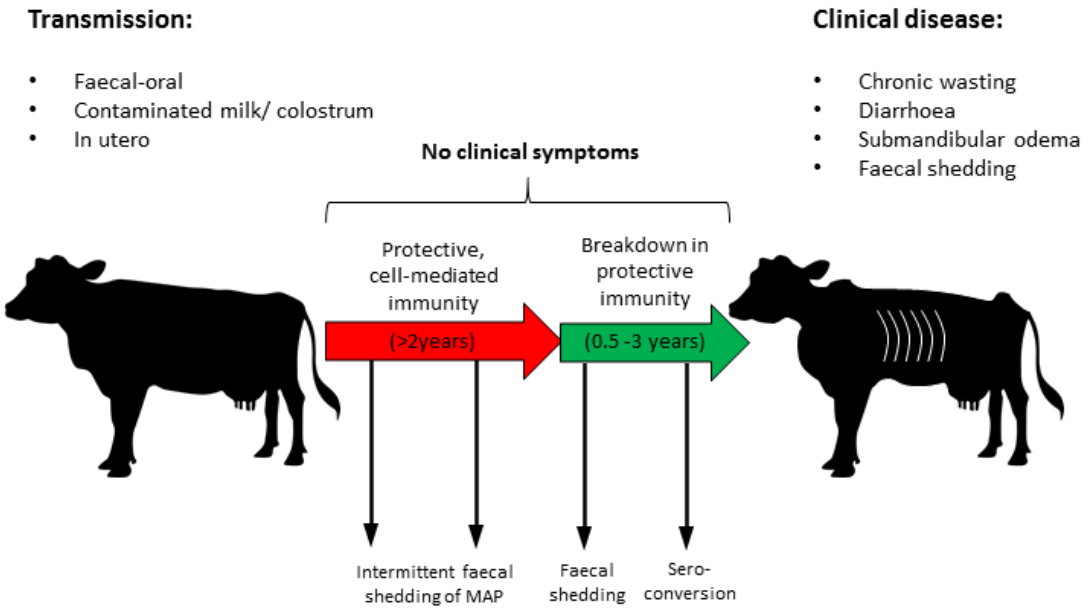

Figure 1-1 Johne's disease pathogenesis.

Cattle generally become infected with MAP as neonates via contaminated milk or colostrum from the mother, or directly through the faecal-oral route. A long subclinical stage to the infection then occurs, lasting 3-5 years, on average. During the subclinical period, the infection is initially well contained by granuloma formation and a protective Th-1 response. However, as time progresses, protective immunity wanes and shifts to a more Th-2 dominant response, causing consistent faecal shedding and, subsequently, seroconversion. Eventually clinical symptoms will develop, causing diarrhoea and chronic wasting.

1.6.4 Identifying, and improved characterisation of correlates of infection, disease, and protection will benefit disease control

Identifying correlates of protection, infection, and disease requires a robust understanding of the host-pathogen interaction, in any given context. However, the long subclinical period of paratuberculosis and the poor understanding of the immune response that leads to either clinical disease or protection (discussed in section 1.6.3), has meant that identifying correlates of protection, infection, and disease for paratuberculosis has been extremely challenging. Current understanding is summarised in Table 1

	Notes
<u>Correlates of Infection</u>	
• Antibody response	• An antibody response to MAP antigens is indicative of MAP infection; however the absence of an antibody response does not confirm the absence of infection. This is due to delayed seroconversion, and variation in the time take to seroconversion between individual animals (this remains incompletely understood)
• IFNγ response	• An IFNγ response (measured by IGRA) has been utilised as a method to identify infected animals at early time-points (discussed in section 1.3.1). While IFNγ is produced in response to MAP, there are issues with specificity as IFNγ is produced in response to a wide range of antigens expressed by various mycobacteria species
• Faecal shedding of bacteria	• Faecal shedding is indicative of infection, however absence of faecal shedding does not necessarily correlate to absence of infection. In addition, there is evidence that animals can be passive shedders of MAP (Kralik et al. 2014)
<u>Correlates of Disease</u>	
• Antibody response	• A switch from Th1 to Th2 immunity has traditionally been associated with disease progression; however, as discussed in section 1.6.3, this is an over-simplification and the nature of the immune events leading to clinical disease remain poorly understood. A positive antibody response does not guarantee an animal will present clinical disease.
• Faecal shedding of bacteria	• Faecal shedding can occur in subclinical animals that never go on to develop disease; however, there is a reported correlation between level of faecal shedding and development of clinical Johne's (Raizman et al. 2007)
<u>Correlates of Protection</u>	
• IFNγ response	• A Th-1 response (characterised by IFNγ production) is considered to be protective, particularly early in infection; however, animals producing high levels of IFNγ are not necessarily resistant and a change in immune status may occur at a later time-point of infection.

Table 1: Correlates of, infection, disease and protection in the context of Johne's disease.

This table summaries current understanding of correlates of infection, disease and protection associated with Johne's disease. A correlate of protection is defined as a measurable response indicating containment or clearance of infection. A correlate of infection is defined as a measurable response indicating that an animal is infected with the bacteria, but does not necessarily indicate that an animal will develop clinical Johne's disease; whereas, a correlate of disease refers to a measurable response during subclinical infection that would indicate the animal will go on to develop clinical disease.

Identifying correlates of infection is key to the development of sensitive and specific diagnostics, however it would also be of significant benefit to disease control to, not only identify infected animals, but identify those animals that will become 'super-shedders', or go on to develop clinical disease. As discussed in section 1.3.1, an antibody response to MAP antigens is commonly used to diagnose MAP infection, however, the ELISA tests that measure this response lack sensitivity, particularly at early time-points, due to delay in seroconversion. The majority of commercially available paratuberculosis ELISAs measure antibodies in serum or milk that bind to paratuberculosis protoplasmic antigen (PPA) (Gonza et al. 2009). PPA is a crude mixture of MAP-derived antigens, therefore the test does not necessarily measure an antibody response to a MAP-specific antigen, meaning the specificity of the ELISA test is lowered by the possibility of antibodies against other mycobacterial species cross-reacting with MAP antigens (Osterstock et al. 2007). An antibody response is, therefore, not a particularly reliable correlate of infection.

Work has been previously been carried out to utilise IFNγ as a correlate of MAP infection (discussed further in section 1.3.1). Unlike antibody, IFNγ can be produced at early time-points post infection, therefore an IGRA utilising MAP-specific antigens may benefit diagnosis of paratuberculosis. IGRA has previously been carried out using crude mixtures of antigens known as purified protein derivative (PPD). Johnin PPD (PPDj) (derived from MAP) has been utilised; in addition, a comparison between the IFNγ response to PPDa (derived from *M. avium*) and PPDb (derived from *M. bovis*) has also been as a method to detect MAP infection. The use of PPD for the IGRA test is disadvantaged by the fact that, being a crude mixture, PPD will share many common antigens with other mycobacteria species, causing a reduction in specificity(Jungersen et al. 2002; Souriau et al. 2017). Recently, research has been carried out to identify MAP-specific antigens that could be utilised as an alternative to PPD to improve the sensitivity and specificity of the IGRA (Dernivoix et al. 2017; Hughes et al. 2017). IFNγ was produced in response to certain candidate antigens, however further work to refine these tests and accurately interpret results needs to be carried out before the tests could be widely used.

Identifying correlates of protection both the *in vitro* and *in vivo* is critical to developing efficacious vaccines against Johne's disease. The Johne's disease integrated programme (JDIP) research consortium have highlighted the need to identify reliable *in vitro* correlates of protection in order to successfully screen MAP vaccine candidates, as attenuation or immunogenicity of any given vaccine candidate cannot be accurately assessed in the absence of correlates of protection (Bannantine et al. 2014). The study conducted by JDIP used only intracellular survival within MDM to assess *in vitro* attenuation in Phase I of their trial (Bannantine et al. 2014; Lamont et al. 2014). However, reduced survival in the macrophage does not necessarily translate to protection in vivo, as demonstrated in a study by Park et al (Park et al. 2011). Therefore, identifying early macrophage correlates of protection, such as gene expression, or cytokine secretion profiles, that translate to attenuation in the natural host is of paramount importance for the identification of novel vaccine strains.

1.7 The bovine immune system

The bovine immune system is functionally similar to that of other mammals, such as mice and humans. However, there are specific phenotypic differences that may be of importance when considering natural host-pathogen interactions in the context of bovine paratuberculosis. A study by Corripio-Miyar et al. highlighted that there are multiple subsets of bovine peripheral blood monocytes with unique functional properties, similar to monocyte subsets found in humans and mice; the bovine $CD14^{+}$ $CD16^{-}$ monocyte subset was functionally similar to 'classical' human monocytes, whereas the $CD14^{-}$ $CD16^{++}$ bovine monocyte subset was functionally similar to 'non-classical' human monocytes. However, the functional subsets are phenotypically different between species; human monocytes are also identified by CD14 and CD16 expression (although they have a slightly different expression pattern of these cell surface molecules compared to bovine monocytes), however, murine monocyte subsets are differentiated by the expression of Ly6C and CD43 (Corripio-Miyar et al. 2015). Cattle have higher levels of T-cells expressing the γδ T-cell receptor (TCR) compared to humans (10% of circulating lymphocytes are γδ TCR+ T-cells (γδ T cells) in adult cattle, compared to 5% in humans); ~60% of circulating lymphocytes are γδ T-cells in young calves, whereas γδ T-cells are a minority population in mice and humans (Price & Hope 2009). In addition, subsets of bovine γδ T-cells are identified by expression of the surface scavenger receptor workshop cluster-1 (WC1), which is absent from human or murine γδ T-cells. γδ T-cells are known to express IFNγ in response to mycobacterial antigens and likely play a significant role in defence against MAP, especially due to the elevated numbers of these cells in young calves, which are particularly susceptible to contracting MAP (Price & Hope 2009). Similarly, numbers of bovine NK cells are increased in neonates, likely to compensate for under-developed specific immunity. Numbers of bovine NK cells have been reported to be influenced by the age of the animal - similar to human NK cells which are reported to wane with age (Graham et al. 2009). In both cattle and humans, functionally distinct subsets of NK cells are present; these are identified in humans by their expression of CD56 and CD16, whereas bovine NK cell subsets are identified by differential expression of CD2 alongside NKp46. The cytolytic ability of bovine $NKp46^{+}$ NK cells was shown to be

dependent on the activity of perforin, whereas the activity of perforin has been reported to be redundant for the cytolytic activity of human NK cells (Berthou et al. 1995; Boysen et al. 2006).

1.8 Intestinal Macrophages

Macrophages are innate immune cells capable of phagocytosing and destroying invading pathogens, secreting pro- and anti-inflammatory cytokines and chemokines, (a major effect of which is the recruitment of other immune cells to the site of infection) and presenting antigen to T-cells (Murphey & Weaver 2016). However, resident gut macrophages play a unique role in immunity; they reside in the lamina propria and GALT, within close proximity of huge numbers of commensal bacteria and express an anti-inflammatory gene expression profile, under normal conditions, essential for maintaining tolerance to commensal bacteria and food antigens (Smith et al. 2011). Gut macrophages are a heterogeneous population; studies in mice have shown them to be derived from blood-circulating Ly6C^{hi} monocytes, and to consist of CX3CR1^{hi} and CX3CR1^{int} sub-populations (Joeris et al. 2017; Weber et al. 2011). CX3CR1^{hi} cells are the most abundant sub-population; these cells are non-inflammatory and are, therefore, important in maintaining tolerance. CX3CR1^{int} macrophages are derived from the same Ly6C^{hi} monocyte precursors as CX3CR1^{hi} macrophages. However, the presence of pathogenic bacteria (such as MAP) or inflammatory signals, halt their differentiation into steady-state, non-inflammatory CX3CR1^{hi} cells and they become capable of secreting pro-inflammatory cytokines, such as IL-1β, IL-6 and IL-12 (section 1.9.3), and producing antimicrobial products such as ROS and RNS (section 1.9.2.1) (Bain et al. 2013; Joeris et al. 2017). Currently, no studies have been carried out examining the origin and phenotype of resident gut macrophages in cattle. However, a recent study by Corripio-Miyar et al. demonstrated that monocyte subpopulations exist in the blood of cattle, that are functionally similar to populations found in mice and humans, despite having phenotypic differences (Corripio-Miyar et al. 2015). It is therefore reasonable to infer that bovine gut macrophages likely have a similar, function and origin to murine macrophages, although they may be identified by different phenotypic

markers. Future studies related to paratuberculosis could aim to identify and categorise subsets of bovine gut macrophages.

The phenotype and properties of various tissue-resident macrophages are summarised in Table 2:

	Anatomical location	Phenotype (murine)	Function	Phenotype (bovine)
Blood monocytes	Circulating blood	Ly6C^{lo}, CCR2^{-}, CX3CR1^{++} (Thomas et al. 2015)	Protection of vascular endothelium, resolution of inflammation, differentiation into M2 macrophage phenotype	CD14^{-}CD16^{++}CD163^{low-} (Corripio-Miyar et al. 2015)
Blood monocytes	Circulating blood	Ly6C^{hi}, CCR2^{+}, CX3CR1^{+} (Thomas et al. 2015)	Inflammatory response, differentiation into intestinal macrophages	CD14^{+}CD16$^{low/-}$CD163^{+} (Corripio-Miyar et al. 2015)
Alveolar macrophages	Lung	F4/80^{lo}, CD11b^{lo}, CD11c^{hi}, CD68^{+}, MARCO^{+}, CD206^{+}, Dectin-1$^{+,}$ CD80^{+}, MHCII^{+} (20-30%) (Fulton et al. 2004; Davies et al. 2013)	Immune surveillance and regulation of tissue function	CR3, $\alpha_V\beta_2$ integrin, CD40, CD80, CD86, MHCII (Sobotta et al. 2016)
Kupffer cells	Liver	F4/80^{hi}, CD11b^{lo}, CD169^{+}, CD68^{+}, Galectin-3^{+}, CD80$^{lo/-}$ (Klein et al. 2007; Davies et al. 2013)	Clearance of aged erythrocytes and micro-organisms	CD68^{+}, CD172a^{+}, Iba-1^{+} (Kitani et al. 2011)
Langerhans cells	Skin	F4/80^{+}, CD11b^{+}, CD11c^{+}, Langerin^{+}, MHCII^{+} (Chorro et al. 2009)	Immune surveillance and antigen presentation to T-cells (Doesbel et al)	MHCII^{+} (Bryan et al. 1988), CD172a^{+} (Ohmann 1988)

Intestinal macrophages	Gastrointestinal tract	CX3CR1^{hi}, MHCII^{hi}, F4/80^{+}, CD206^{+}, CD163^{+}, CD11b^{+} (Bain et al. 2013)	Surveillance and regulation of responses to commensal bacterial	Current understanding of the phenotype of bovine intestinal macrophages is limited. Macrophages present in bovine paratuberculosis intestinal lesions are known to express CD163, CD64 and MHC II, but the expression of these markers varies dependant on the number of bacilli present, and the structure of the lesion (i.e. focal or diffuse) (Fernández et al. 2017)
Intestinal macrophages	Gastrointestinal tract	CX3CR1^{int}, CD64^{+}, CD11b^{+} (Bain et al. 2013)	Production of pro-inflammatory cytokines	

Table 2 Phenotype and function of tissue-specific macrophages.

Table 2 describes the phenotype and function of monocytes or macrophages resident to the blood, lung, liver, skin, and gastrointestinal tract. The majority of studies on resident macrophages have been carried out in mice; however, where information is available for bovine equivalents, this has been included. It should be noted that this table is a simplification – the surface markers described are not exhaustive, additionally, heterogeneity of macrophage populations can be observed in many tissues. Table adapted from Davies et al. (Davies et al. 2013)

1.9 The immune response to MAP infection

1.9.1 MAP survives intracellularly within macrophages

Within the sub-mucosa, MAP is recognised by and bound to innate immune receptors expressed by macrophages, including scavenger receptors, CR, Toll-like receptors (TLR) and FcRs. Recognition of the pathogen leads to its phagocytosis by resident macrophages (see section 1.10). Macrophages are phagocytic cells capable of destroying invading pathogens and eliciting a protective inflammatory response in the context of infection. However, pathogenic mycobacteria (including MAP) have evolved to subvert the process of destruction within the phagosome and survive within the macrophage itself (Wong et al. 2011; Fratti et al. 1997; Arsenault et al. 2014). This is achieved through multiple mechanisms (discussed below) but is not yet fully understood.

1.9.2 Inhibition of phagosome maturation

The uptake of foreign material and apoptotic cells by macrophages occurs through a process known as phagocytosis. There are distinct mechanisms of phagocytosis (described in section 1.12) but all mechanisms result in engulfment of particulate matter within an intracellular vesicle known as the phagosome. Phagocytosed material is destroyed through a process known as 'phagosome maturation', which refers to a sequential decrease of the pH in intracellular phagosomes, through interaction with other intracellular vesicles known as endosomes and lysosomes. This interaction leads to the acquisition of endosomal and lysosomal components, such as vesicular-H^+-ATPase pumps (V-ATPase) , which pump protons into the phagosome to decrease the pH (Lukacs et al. 1990), and proteolytic enzymes (such as procathepsin D) (Sturgill-Koszycki, Schaible, and Russell, 1996). The production of reactive oxygen species (ROS) (see section 1.9.2.1) is also generated by this process, and contributes to bacterial degradation within the phagosome (Poirier & Av-Gay 2012). The process of phagosome acidification is demonstrated in Figure 1-2.

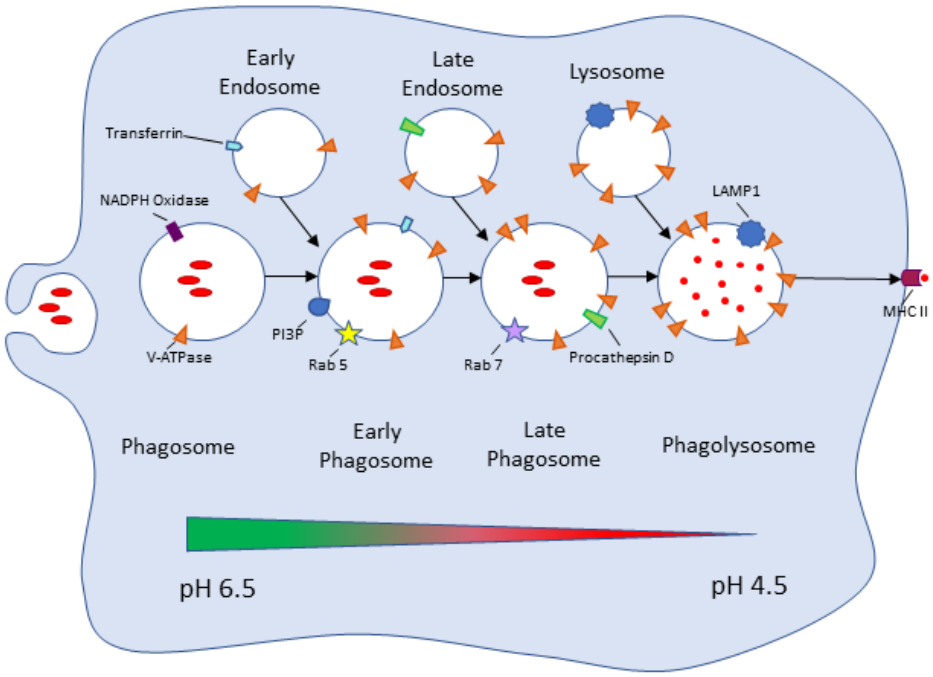

Figure 1-2 Phagosome maturation.

Bacteria are taken up by macrophages into intracellular phagosomes. Phagosomes mature and destroy phagocytosed pathogens by producing antimicrobial products such as ROS (via NADPH oxidase) and acquiring components of endosomes and lysosomes, causing the pH within the phagosome to decrease and degradation of the bacteria to occur. Early phagosomes acquire V-ATPase and transferrin from early endosomes; V-ATPase is a proton pump that pumps H+ into phagosomes in order to decrease pH, and transferrin transports iron into the phagosome (iron is necessary for bactericidal activity of macrophages). Late phagosomes express procathepsin D (acquired from late endosomes). Procathepsin D is the inactive form of a protease capable of degrading intracellular proteins and activating other enzymatic precursors (cathepsin D). Procathepsin D is activated at a reduced pH. Late phagosomes then fuse with lysosomes to form the phagolysosome. The phagolysosome expresses the late-endosomal marker LAMP1. Bacteria are fully degraded within the phagolysosome and bacterial antigens are then processed for presentation to T-cells. Image adapted from Poirier and Av-Gay, 2012.

Mycobacteria are capable of evading intracellular degradation, in part, through the ability to arrest phagosome maturation. This process is not yet fully understood, particularly in the context of MAP infection, however studies have shown mycobacteria can employ a variety of mechanisms to avoid degradation within phagosomes. For example, secretion of the acid phosphatase SapM, by intracellular *M. tb* can hydrolyse phosphatidylinositol 3-phosphate (PI3P), a membrane-trafficking lipid, and thereby blocks acquisition of lysosomal constituents by the phagosome (Puri et al. 2013; Vergne et al. 2005). In addition, *M. tb* secrete a tyrosine phosphatase, PtpA, which interacts with the proton pump V-ATPase, excluding it from the phagosome, thus inhibiting the reduction in phagosomal pH required for bacterial degradation (Wong et al. 2011). GTPases Rab5 and Rab7 regulate the fusion of phagosomes with early endosomes and late endosomes, respectively. Phagosomes positive for *M. avium* retain Rab5 and exclude Rab7 in order to prevent late endosome fusion to promote their intracellular survival (Kelley & Schorey 2003). A recent study by Danelishvili et al demonstrated that *M. avium* can bind to voltage-dependent anion channels (VDAC) on the vacuole membrane of phagosomes and that VDAC was used by the bacteria for the transport mycobacterial lipids into the cytoplasm (Danelishvili et al. 2017), likely as a method to disrupt intracellular trafficking essential for phagosome maturation. Interleukin 10 (IL-10) also plays a role in inhibiting phagosome maturation in the context of mycobacterial infection (O'Leary et al. 2011; Hussain et al. 2016); the role of IL-10 in mycobacterial infection is discussed in detail in section 1.9.3.7. The importance of restricting phagosome maturation for the intracellular survival of mycobacteria is highlighted by the redundancy of multiple mechanisms that interfere with the process of phagocytosis.

1.9.2.1 The role of antimicrobial products

In addition to interrupting phagosome maturation, as described in section 1.9.2, pathogenic mycobacteria can interfere with the production of antimicrobial products, such as ROS and RNS.

1.9.2.1.1 Reactive Oxygen Species

ROS are a toxic chemical species that are produced by macrophages and other immune cells, such as neutrophils (Cifani et al. 2013). Production of ROS, known as the respiratory burst, requires a transient increase in oxygen consumption by cells. Briefly, the multicomponent enzyme known as Nicotinamide Adenine Dinucleotide Phosphate Reduced (NADPH) oxidase, converts oxygen (O^2) to the toxic compound superoxide anion (O_2^-), by adding a single election to the O_2 molecule – this results in O_2^- having an unpaired electron, making it an oxygen radical. Superoxide is then further converted to hydrogen peroxide (H_2O_2) by the enzyme superoxide dismutase. Further chemical reactions, and action of peroxidase enzymes can then convert hydrogen peroxide into hypochlorite (OCl^-) and hydroxyl radicals (•OH), which have potent microbicidal activity (Bayr 2005) (Figure 1-3).

ROS rapidly and non-specifically cause damage to DNA, proteins, lipids and carbohydrates of microbes (and host cells), and play an important role in immune defence, as demonstrated by lack of functional NADPH oxidase in patients with chronic granulomatous disease (CGD) (Buvelot et al. 2016).

Decreased ROS production is associated with increased susceptibility to mycobacterial disease. For example, there is a higher risk of complication from BCG vaccination in patients with CGD (Sadeghi-Shanbestari et al. 2009; Li et al. 2010), likely due to impaired granuloma formation in the absence of ROS (Deffert et al. 2014). Surprising, although lack of ROS is clearly associated with poor outcome of mycobacterial infection, there is little evidence to demonstrate that ROS directly impact mycobacterial survival, therefore the role of ROS in mycobacterial infection is still incompletely understood (Bustamante et al. 2011). It is possible that ROS influence infection outcome by acting as signalling molecules, impacting cellular processes, such as apoptosis, autophagy or cytokine production (Huang & Brumell 2009; Deffert et al. 2014). Further studies will be necessary to definitively understand the role of ROS in mycobacterial diseases.

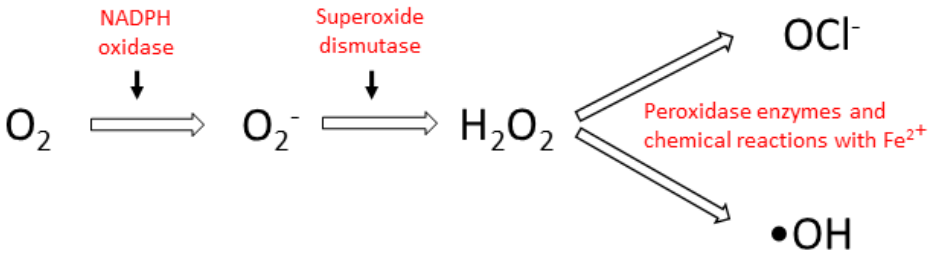

Figure 1-3: Reactive oxygen species production.

The enzyme NADPH oxidase converts oxygen to superoxide anion (O2-). A second enzyme, superoxide dismutase then converts superoxide anion to hydrogen peroxide (H_2O_2), which is toxic. Both superoxide anion and hydrogen peroxide are directly toxic to bacteria, but they can be further converted by peroxidase enzymes and chemical reactions to the microbicidal hypochlorite (OCl-) and hydroxyl radicals (•OH). Image adapted from Nathan and Shiloh, 2000.

1.9.2.1.2 Reactive Nitrogen Species

The term 'reactive nitrogen species' (RNS) refers to the nitrogenous products of nitric oxide synthase (NOS) enzymes, including: nitric oxide (NO), nitrogen dioxide ($\cdot NO_2$), nitrite (NO_2^-), nitrate (NO_3) and peroxynitrite (OONOH). There are three forms of NOS: endothelial NOS (eNOS), inducible NOS (iNOS), and neuronal NOS (nNOS), each with distinct biological functions. iNOS is upregulated by macrophages in response to infection and catalyses the oxidation of l-arginine to l-citruline and NO. Further RNS are then produced from NO through a series of oxidation reactions (Nathan & Shiloh 2000) (Figure 1-4).

RNS have a bactericidal effect by causing inactivation of key metabolic functions via damage to amino acid residues, and targeting pathogenic macromolecules essential for bacterial function, such as heme and ferritin. In addition, RNS can cause direct damage to DNA and lipids (Qu et al. 2011; Hughes 2008; Monteiro et al. 2016; Nathan 1992). Several studies have reported that NO is important for controlling growth of mycobacteria. For example, mice deficient in iNOS were highly susceptible to *M. tb* infection, with increased bacterial replication in the lungs (MacMicking et al. 1997). Additionally, NO production by bovine macrophages has been reported to control intracellular growth of *M. bovis* and *M. bovis* BCG (Esquivel-Solís et al. 2013). However, there are some conflicting reports; a study by Jung et al. demonstrated that NO produced by human macrophages in response to *M. tb* or BCG infection, had no bactericidal or bacteriostatic effects (Jung et al. 2013). However, it is worth noting that there are notable differences in iNOS activity between species, with bovine and murine macrophages expressing higher levels of iNOS in response to stimuli than human macrophages, *in vitro* (Jungi et al. 1996). Mycobacteria are known to have some resistance to RNS. For example, BCG can inhibit the recruitment of iNOS to phagosomes, where it can have bactericidal effects, by interfering with the scaffolding protein EBP50 (Guo et al. 2016; Davis et al. 2007). MAP infection is associated with iNOS expression in ileal lesions (Delgado et al. 2010). However, MAP has demonstrated a higher resistance to RNS, compared to *Mycobacterium avium* subsp. *avium* in bovine macrophages (Weiss et al. 2002). A study by Souza demonstrated that inhibition if MAPKp38 signalling in MAP-infected macrophages increased NO secretion (Souza 2015), suggesting that

MAP may directly target this pathway in order to limit intracellular degradation. The role of RNS in bactericidal responses of phagocytes to mycobacteria, and the way in which mycobacteria species may overcome the effects of RNS, require further investigation.

As with ROS, RNS have a diverse range of functions in addition to direct microbicidal activity. NO can regulate gene transcription by interfering with components of signalling cascades, such as the JAK/STAT pathway (Bogdan 2001; Mishra et al. 2012). It has also been demonstrated that NO can induce apoptosis in *M. tb* infected macrophages (Guo et al. 2016). Therefore, it is likely that RNS have important immunoregulatory roles that could potentially affect MAP infection outcome.

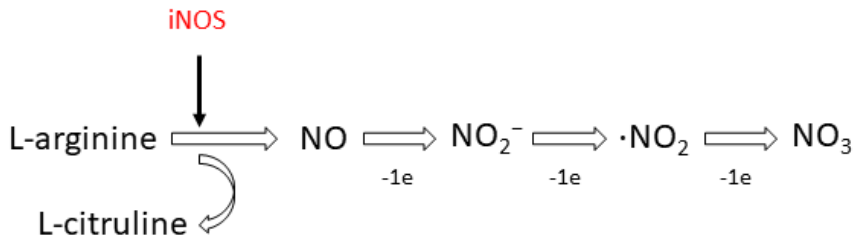

Figure 1-4 Reactive nitrogen species production.

Inducible nitric oxide synthase (iNOS) produces NO from the substrate L-arginine. Subsequent RNS, such as NO_2^- $\bullet NO_2$, and NO_3 form after a series of oxidation reactions (-1e). Image adapted from Nathan and Shiloh, 2000.

1.9.3 Roles of chemokines and cytokines in mycobacterial infection

Infected macrophages respond to mycobacterial infection by secreting multiple cytokines and chemokines with a wide range of biological activities. Some key cytokines and chemokines that significantly influence the pathogenesis and immune response to mycobacterial infection are described below:

1.9.3.1 Chemokines

Chemokines are cytokines that form a chemotactic gradient when produced by infected cells, including macrophages, guiding the recruitment of other immune cells (via chemokine receptors), to the site of infection. Granuloma formation is a key role of chemokines produced by macrophages in mycobacterial infection. Secretion of several chemokines is known to be elevated during mycobacterial infection; these chemokines are ligands for receptors expressed on several immune cells, including: macrophages, monocytes, DCs, neutrophils, T-cells, B-cells, NK cells and NKT-cells (Domingo-Gonzalez et al. 2016). A study by Khare et al demonstrated early upregulation of chemokines CCL2, CCL8, CXCL3, CXCL1, CXCL6, and CXCL8 in the ileal mucosa, in the context of MAP infection - suggesting that these chemokines are important for initial granuloma formation in paratuberculosis. (Khare et al. 2009)

1.9.3.2 Interferon-γ

Interferon-γ (IFNγ) plays a key role in the immune response to mycobacterial infection, and is secreted at early time-points by infected macrophages. IFNγ binds IFNγ receptors (IFNγRs) expressed on several cell-types, including macrophages, NK cells and T-cells. Interaction of IFNγ with the IFNγR initiates signalling through the Janus kinase (JAK)/Signal transducer and activator of transcription (STAT) pathway, to induce migratory and functional changes in IFNγR-expressing cells. Early IFNγ secretion by infected macrophages results in a pro-inflammatory response (Domingo-Gonzalez et al. 2016) An array of immune cells accumulate at the site of granuloma formation, including γδ T-cells, which are known to be capable of producing IFNγ in response to *M. bovis* antigens (Price & Hope 2009; Plattner et al. 2009). Effective production of IFNγ is known to be critical for protection against mycobacterial infection, as patients deficient in IFNγR are highly susceptible to

mycobacterial disease (Sologuren et al. 2011; Dorman & Holland 1998). In order to counter the protective effects of IFNγ, MAP can interfere with IFNγR signalling by preventing JAK/STAT phosphorylation. In addition, decreased expression of the IFNγR and increased expression of SOCS1 and SOCS3 (negative regulators of IFNγR signalling) have been observed in MAP infected monocytes (Arsenault et al. 2012).

1.9.3.3 Tumour necrosis factor α

Tumour necrosis factor α (TNFα) is a key pro-inflammatory cytokine, secreted primarily by macrophages. TNFα plays a significant role in mycobacterial infection by influencing granuloma formation and maintaining granuloma integrity. Neutralisation of TNFα leads to decreased secretion of chemokines CCL5, CXCL9 and CXCL10, which subsequently reduces migration of activated T-cells, macrophages and neutrophils to the site of infection (Domingo-Gonzalez et al. 2016). A study by Clay et al. demonstrated that absence of TNFα caused accelerated granuloma formation and accelerated bacterial growth, which led to necrotic death of infected macrophages, and breakdown of the granuloma structure, in zebrafish embryos infected with *M. marinum* (Clay et al. 2008). TNFα promotes phago-lysosomal fusion and apoptosis of infected cells, aiding presentation of antigen to T-cells. *M. tb* has, therefore, evolved to actively downregulate TNFα expression in infected macrophages, in order to aid its survival (Olsen et al. 2016). Although few functional studies have been carried out assessing the role of TNFα in paratuberculosis, it can be inferred that TNFα plays a similar role in all mycobacterial infections, and it has been demonstrated that MAP infection induces TNFα expression in bovine monocytes between 2 and 24 hours post infection (HPI) (Souza et al. 2007).

1.9.3.4 Transforming growth factor β

Transforming growth factor β (TGFβ) is a pleiotropic cytokine that has a largely regulatory role in immunity; it can modulate cell proliferation, differentiation, and migration, and is a key regulator of the inflammatory response (Domingo-Gonzalez et al. 2016). It has been demonstrated that MAP infected macrophages upregulate TGFβ expression within 6 HPI *in vitro* (Dudemaine et al. 2014). In addition,

histological analysis has demonstrated increased TGFβ expression in diffuse, compared to focal, paratuberculosis lesions in cattle; this increase in TGFβ expression is associated with increased bacterial numbers, possibly due to the inhibition of antimicrobial products, such as nitric oxide and reactive oxygen species (Muñoz et al. 2009).

1.9.3.5 Interleukin-17

IL-17 is a family of six cytokines, designated IL-17A – IL-17F. IL-17A and IL-17F are produced by Th-17 cells; these cytokines bind to IL-17RA, expressed on myeloid and epithelial cells. IL-17RA forms heterodimers with other IL-17Rs (i.e. IL-17RC) to initiate signalling in response to IL-17 cytokines (Ishigame et al. 2009; Zhang et al. 2015). IL-17A and IL-17F both induce the production of defensins (antimicrobial peptides), and the secretion of proinflammatory cytokines and chemokines that primarily promote neutrophil recruitment to the site of infection, among other functions. IL-17 expression has an important role in establishing protective immunity against virulent *M. tb*, as IL-17RA signalling induces production of the chemokine CXCL13 by non-haematopoietic cells, which is important for directing localisation of T-cells to infected macrophages (enabling optimal macrophage activation) (Gopal et al. 2014). However, enhanced neutrophil recruitment, associated with IL-17 secretion, may also contribute to immunopathology (Keller et al. 2006). Increased IL-17 levels have been reported in the blood of sub-clinical MAP-infected cattle that are ELISA positive and shedding MAP in faeces, which is indicative of increased inflammation in the intestinal mucosa (Dudemaine et al. 2014).

1.9.3.6 Interleukin-1β

Interleukin (IL)-1β is a potent pro-inflammatory cytokine that signals through IL-1 receptor 1 (IL-1R1) in a MyD88 dependent manner. There is a negative correlation between IL-1β secretion and intracellular survival and dissemination of mycobacteria (Sharon S Master et al. 2008). Mice deficient in IL-1R1 succumbed to *M. tb* infection within 4 weeks post infection, whereas IL-18R deficient, and wild-type mice, survived until the termination of the experiment at 90 days (Fremond et al. 2007). It is still not fully understood how IL-1β confers protection during

mycobacterial infection, but IL-1R1 deficient mice had functional CD4+ and CD8+ T-cell responses (Fremond et al. 2007), suggesting that IL-1β likely influences the innate immune response. A study by Juffermans et al., using an IL-1R knockout (KO) mouse model of *M. tb* infection, demonstrated that IL-1β may also play an important role in granuloma formation (Juffermans et al. 2000).

The gene encoding IL-1β was shown to be upregulated in bovine MDM in response to MAP infection in a micro-array study by MacHugh et al. (MacHugh et al. 2012). In addition, RNA-Seq analysis carried out by the Glass group (Roslin Institute) demonstrated upregulation of the IL-1β gene within the first 24 hours of infection by MAP infected MDM (unpublished data). Previous studies have also demonstrated that IL-1β is secreted in response to MAP or MAP proteins in bovine DCs and THP-1 cells (Lee et al. 2014; Borrmann et al. 2011a). The strain-type of MAP (see section 1.5) used for infection of these cells had an impact on the levels of IL-1β secretion during infection, with C-type strains inducing higher levels of secretion than S-type strains (Borrmann et al. 2011a). It can be inferred that IL-1β likely plays a similar role in MAP infection, compared to *M. tb* infection (likely impacting innate immune responses through influencing phagosome maturation and granuloma formation); however, the functional role of IL-1β in MAP infection needs to be further investigated.

Unlike other pro-inflammatory cytokines, IL-1β is produced by macrophages in a 2-step process. An inactive form of IL-1β (pro-IL-1β) is produced in response toPAMPs that signal through PRRs, such as TLRs. Pro-IL-1β is cleaved to active IL-1β by caspase-1; caspase-1 also exists in an inactive form (pro-caspase 1) within the cytoplasm, but is activated to cleave pro-IL-1β by a multi-protein structure known as the inflammasome. The inflammasome generally consists of the adaptor molecule ASC, pro-caspase-1, and a cytosolic PRR, and are induced to activate caspase 1 by the presence of PAMPs or danger associated molecular patterns (DAMPs) (Sahoo et al. 2011). The PRRs (described to date) capable of forming an inflammasome include: absent in melanoma 2 (AIM2), NACHT, LRR, pyrin, NOD-like receptor (NLR) family caspase activation and recruitment domain (CARD) containing protein 4 (NLRC4), and NLR pyrin domain-containing protein 1

(NLRP1), NLRP3, and NLRP6 (Próchnicki & Latz 2017). The NLRP3 inflammasome is the best characterised; the mechanism of action of the NLRP3 inflammasome is demonstrated in Figure 1-5.

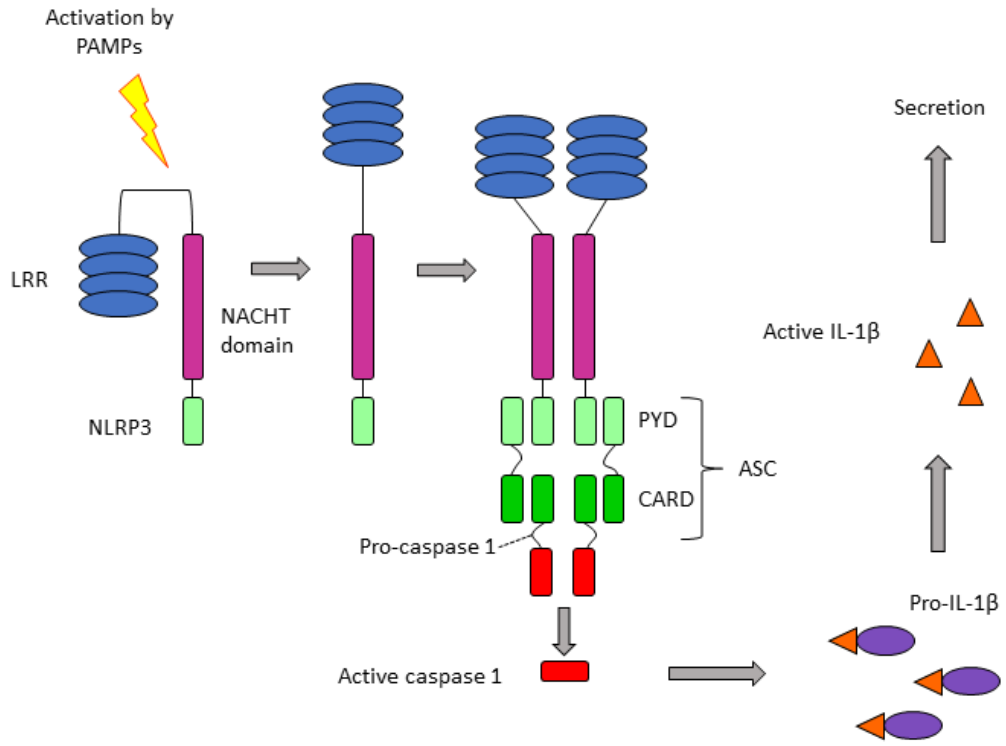

Figure 1-5 NLRP3 inflammasome activation.

The NLRP3 inflammasome is activated in response to PAMPS or DAMPs. The PYD domain (light green) of NLRP3 interacts with the pyrin domain (PYD) and CARD domain (dark green) of the adapter molecule ASC, which in turn, interacts with the CARD domain of pro-caspase 1, converting pro-caspase 1 to the active enzyme caspase 1.. Caspase 1 then cleaves pro-IL-1β, producing active IL-1β that can be secreted by the cell.

When examining the role of the inflammasome in MAP infection, this study focused on the role of the NLRP3 inflammasome, due to evidence in the literature that the NLRP3 inflammasome is important in the immune response against other mycobacterial species, such as *M. tb* (Mishra et al. 2010; Mishra et al. 2012). The *zmp1* gene expressed by *M. tb* is able to inhibit inflammasome activation within macrophages, as a virulence mechanism. A study by Master et al. demonstrated that macrophages infected with a *zmp1 M. tb* mutant increased secretion of IL-1β in response to infection, and demonstrated enhanced maturation of *M. tb* containing phagosomes, leading to increased clearance. In addition, *in vivo* experiments demonstrated that *zmp1 M. tb* mutants resulted in lower bacterial burden in the lungs of aerosol-infected mice, compared to wild-type *M. tb* infected mice (Sharon S Master et al. 2008). To date, the NLRP3 inflammasome has not been studied in the context of MAP infection. However, a microarray study by MacHugh et al. reported NLRP3 gene expression to be upregulated in MAP infected MDM at 2 HPI (MacHugh et al. 2012), suggesting that NLRP3 may be significant for the early immune response to MAP.

1.9.3.7 Interleukin-10

One of the PRRs that MAP is recognised by is TLR2 which activates MAPK-p38 to induce secretion of the anti-inflammatory cytokine IL-10 (Weiss et al. 2008; Souza et al. 2013). The anti-inflammatory properties of IL-10 could suggest that the purpose of high levels of IL-10 secretion by mycobacteria-infected macrophages is an attempt to limit inflammation-induced tissue damage, at the site of infection. However, there is much agreement in the literature that IL-10 secretion is beneficial to the intracellular survival of MAP (reviewed by Hussain et al.), and it is likely that mycobacteria promote the secretion of this cytokine as a virulence mechanism (Hussain et al. 2016).

IL-10 secretion is associated with a reduced protective response to *M. tb* infection in mouse models of infection (Beamer et al. 2008). In addition, a study by Weiss et al. demonstrated that neutralisation of IL-10 resulted in a >50% reduction in intracellular MAP survival by 96 HPI, *in vitro* (Weiss et al. 2005). IL-10 secretion likely enhances intracellular mycobacterial survival by inhibiting production of

antimicrobial products and phagosome acidification (Souza et al. 2006; Souza et al. 2013; Sullivan et al. 2005). It has also been demonstrated that IL-10 can downregulate the production of pro-inflammatory cytokines important for protective immunity in mycobacterial infection, including TNFα, IL-12 and IFNγ (Weiss et al. 2005; Riley et al. 1999; Buza et al. 2004; Khalifeh & Stabel 2004). In addition, increased secretion of IL-10 has been associated with the shift to Th-2 immunity that precedes the onset of clinical symptoms of Johne's disease (Magombedze et al. 2015)

1.9.3.8 Interleukin-6

IL-6 is a pro-inflammatory cytokine with varied biological functions and is known to be produced in response to mycobacterial infection. In addition, IL-6 is elevated in the serum of Crohn's disease patients. IL-6 can form complexes with soluble IL-6 receptors (sIL-6R); these complexes can bind to gp130 expressed by T-cells in the lamina propria, preventing apoptosis and perpetuating inflammation in inflammatory bowel disease (IBD) (Atreya et al. 2000)

IL-6 is known to be secreted in response to mycobacterial infection; it is correlated with protection against *M. avium* (Appelberg et al. 1994), and plays a critical role in induction of Th-1 responses, after vaccination with a subunit vaccine against *M. tb,* in mouse models of infection (Leal et al. 1999). In addition, a study by Martinez et al. showed *M. tb* to be capable of modulating macrophage IL-6 secretion, and that increased IL-6 production resulted in decreased *M. tb* survival (Martinez et al. 2013). It is possible that MAP have a similar mechanism for interfering with IL-6 production to promote their own survival. Previous studies investigating IL-6 in the context of MAP infection have demonstrated that IL-6 is upregulated in response to MAP antigens, however these studies investigated IL-6 production only at the mRNA level, and further investigations at the protein level are needed to fully appreciate the role of this cytokine in paratuberculosis (Alzuherri et al. 1996; Adams et al. 1996; Adams & Czuprynski 1995).

1.9.4 The Granuloma

The granuloma is an organised aggregate of immune cells that form a lesion that functions to contain mycobacterial infection. It is formed when infected macrophages secrete cytokines and chemokines (see section 1.9.3) that lead to an influx of immune cells, primarily macrophages, to the site of infection. Newly recruited macrophages essentially 'wall-off' infected cells and may fuse into giant multi-nucleated, lipid packed 'foam cells' or 'foamy macrophages' in response to mycobacterial lipids (Puissegur et al. 2007). These foam cells further contribute to the inflammatory response by producing prostaglandin E2 and leukotrienes, promoting the accumulation of immune cells at the site of infection (Silva et al. 2009; Russell et al. 2009). Cells that accumulate at the site of infection include: DCs, NK cells, neutrophils, CD4+ T-cells, CD8+ T-cells, B cells, and γδ T-cells (Figure 1-6 A).

Contrary to other mycobacterial diseases, such as bovine tuberculosis, paratuberculosis results a wide range of lesion-types, from focal granulomas within lymphoid tissue, to diffuse lesions, affecting large areas of the intestinal mucosa, that are associated with poor prognosis (Muñoz et al. 2009; Plattner et al. 2009). Well-organised, focal lesions contain higher numbers of WC1+ γδ T-cells early in infection, suggesting that these cells have a protective effect and are likely important in organising granuloma structure (Plattner et al. 2009).

As the centre of the granuloma loses a supply of blood, a fibrous cuff of collagen, and other extracellular matrix components, forms around the macrophage core, blocking the majority of lymphocytes from the centre of the structure (Russell et al. 2009). The lack of blood supply causes the centre of the granuloma to become hypoxic, however, mycobacteria can withstand this environment by entering into a dormant, non-replicative state, in which they can remain viable for several years. The majority of studies investigating dormancy have examined *M. tb* and BCG within hypoxic environments (Via et al. 2008; Leistikow et al. 2010). However, a recent study by Parrish et al. demonstrated that MAP enters a dormant state, in a similar manner to *M. tb*, *in vitro* (Parrish et al. 2017), suggesting that MAP likely

enters a dormant state to survive with granulomas for prolonged periods during the long subclinical stage of paratuberculosis. (Figure 1-6 B)

After an indeterminate period of time, a process known as caseation can occur, resulting in necrosis of infected macrophages at the centre of the granuloma (Lin et al. 2006) (Figure 1-6 C). Clinical disease occurs when a breakdown of cell-mediated immunity causes the structure of the granuloma to destabilise (Figure 1-6 D), causing bacilli to reactivate, facilitating the spread of infection. The cause of granuloma breakage is unclear; however it is associated with a shift from a Th-1 to a Th-2-type response, characterised by a decrease in IFNγ production and increased production of cytokines such as IL-4 and IL-10 (Sweeney et al. 1998). What leads to the change in immune response remains to be understood and it is possible that the early response of the macrophage, which effects formation of the granuloma, could directly influence these later events.

As discussed above, granuloma formation has long been considered a protective response that isolates infected macrophages from the rest of the host, preventing dissemination of infection. However, recent studies have demonstrated that mycobacteria encourage granuloma formation as it can also be beneficial to spread and replication of the bacteria (Clay et al. 2008). Therefore, this critical host-pathogen interaction remains to be fully understood.

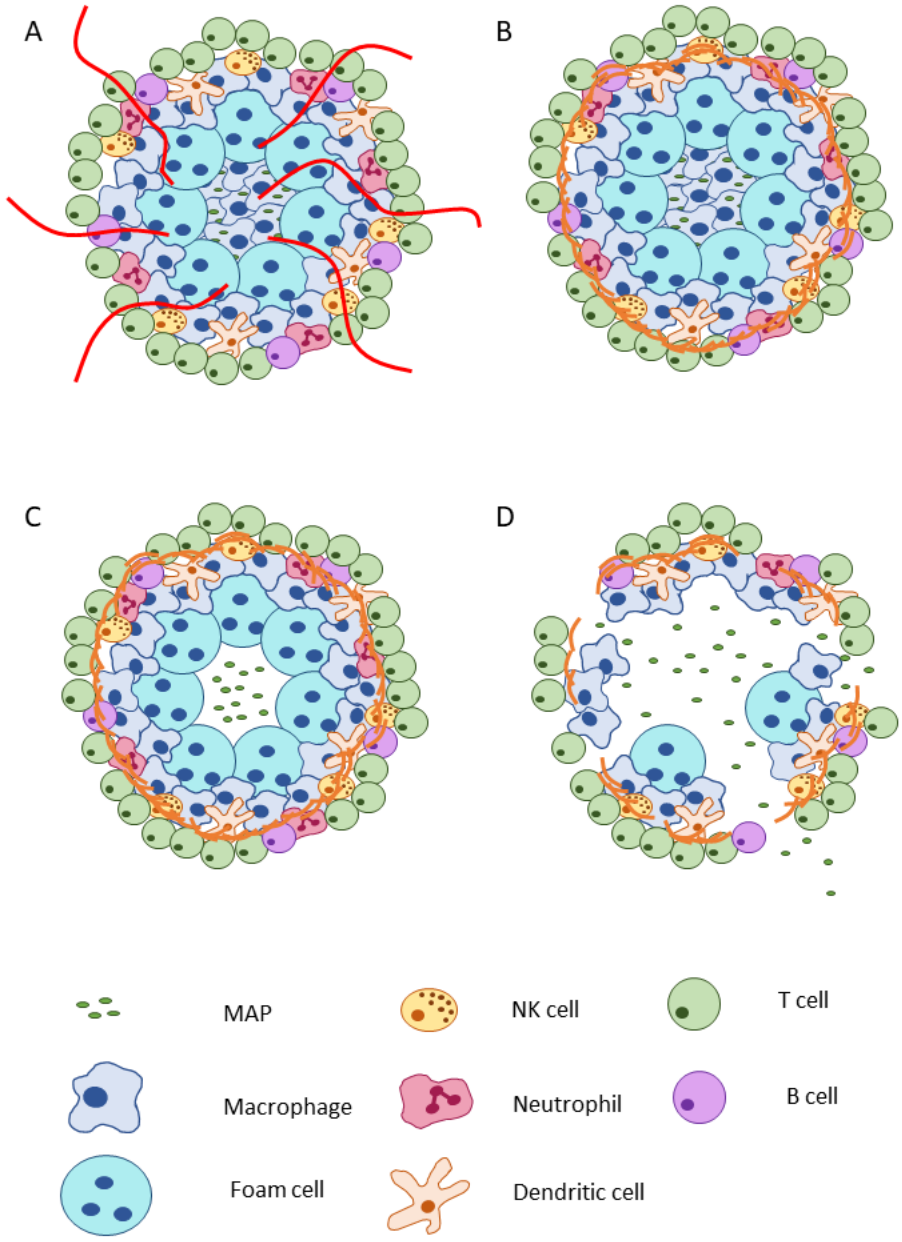

Figure 1-6 Granuloma formation

(A) Immune cells accumulate at the site of infected macrophages and form an organised structure, called a granuloma, around the infected cells. The early granuloma has access to a blood supply therefore the cells are surviving under aerobic conditions. (B) As the granuloma loses blood supply, a fibrous cuff forms, excluding the majority of lymphocytes from the centre, which contains infected cells. The centre of the granuloma becomes hypoxic and the bacteria enter a dormant state. (C) Caseation occurs and infected cells in the centre of the granuloma become necrotic. (D) A breakdown in Th-1-type immunity causes the granuloma to rupture and release bacteria, which then re-enter a metabolically active state. Image adapted from Russell, 2009.

1.10 Phagocytosis

Phagocytosis is a process by which macrophages (and other phagocytic cells) take up relatively large particulate material (>250nm), such as bacteria, into vesicles called phagosomes (Pieters 2008). Phagocytosis can occur through a diverse range of mechanisms, such as opsonic phagocytosis, in which foreign material is coated in proteins present in serum - namely complement proteins and antibodies - which subsequently bind to specific receptors on the surface of phagocytic cells, i.e. CRs or FcRs. In addition, non-opsonic phagocytosis can occur when phagocytes recognise and directly bind PAMPs on the surface of pathogens via phagocytic receptors (Murphey & Weaver 2016). Details of key phagocytic receptors expressed by macrophages are detailed in Table 3:

Receptor	Receptor class	Ligand
Dectin-1	Pattern recognition receptor	β1,3 glucans
CD14	Pattern recognition receptor	lipopolysaccharide-binding protein
Mannose Receptor (CD206)	Pattern recognition receptor	Mannan
DC-SIGN (CD209)	Pattern recognition receptor	Mannan
MARCO	Scavenger Receptor	Lipopolysaccharide, lipoteichoic acid
Scavenger receptor A (CD204)	Scavenger Receptor	Lipopolysaccharide, lipoteichoic acid + endogenous ligands
CD163	Scavenger Receptor	haemoglobin-haptoglobin complexes, bacterial ligands
FcγRI (CD64)	Fc Receptor	High affinity IgG1 = IgG3 >IgG4a
FcγRIIa (CD32a)	Fc Receptor	Low to medium affinity IgG1 >IgG2, IgG3, IgG4a
FcγRIIc (CD32c)	Fc Receptor	Low-affinity IgG1, IgG3, IgG4a
FcγRIIIa (CD16a)	Fc Receptor	High affinity IgG3, low to medium affinity IgG1 >IgG4a
FcαRI (CD89)	Fc Receptor	IgA1, IgA2
CR1 (CD35)	complement receptor	C1q, C4b, C3b, mannan-binding lectin
CR3 (αMβ2, CD11b/CD18, Mac-1)	complement receptor	iC3b, Factor X, factor H, fibrinogen, ICAM, denatured proteins
CR4 (αXβ2, CD11c/CD18, gp150/95)	complement receptor	iC3b, fibrinogen, ICAM, denatured proteins

Table 3: Phagocytic receptors expressed by macrophages.

The receptors described in this table are known to be phagocytic and to be expressed by macrophages in mice. However, it is unknown if all the receptors described are expressed by bovine MDM or intestinal macrophages. DC-SIGN = Dendritic Cell-Specific Intercellular adhesion molecule-3-Grabbing Non-integrin. MARCO = Macrophage receptor with collagenous structure. FcγR/FcαR = Fc gamma receptor/ Fc alpha receptor. CR= complement receptor.

All mechanisms of phagocytosis require rearrangement of the actin cytoskeleton to allow morphological changes in the macrophage essential for the phagocytic process; however, different mechanisms of actin polymerisation occur in response to engagement of different phagocytic receptors. For example, FcR-mediated phagocytosis induces the formation of pseudopods in a 'reaching' type of phagocytosis, whereas CR-mediated phagocytosis is a 'sinking' type of phagocytosis, whereby actin polymerisation allows the particle to sink into the cell, in a process somewhat similar to endocytosis. Details of different mechanism of phagocytosis are further described below.

1.10.1 Opsonic phagocytosis

1.10.1.1 The complement system

The complement system consists of multiple plasma proteins that can interact to opsonise pathogens for phagocytosis, elicit an inflammatory response, and directly destroy invading pathogens by formation of a 'Membrane Attack Complex' (MAC). Most complement proteins are proteases that exist in an inactive form, known as a zymogen, until cleaved into the active form in the presence of a pathogen. The complement system can be activated via three pathways: the classical pathway, the lectin pathway, and the alternative pathway. Briefly, the complement proteins react to form a C3 convertase, which will convert the complement protein C3 to C3b and C3a. C3b is an opsonin which will bind to the pathogen surface, targeting it for phagocytosis via CR. In addition, an 'inactive' form of C3b (iC3b) is proteolytically inactive but can act as an opsonin in its own right, binding to CR3, expressed on phagocytic cells (Bajic et al. 2013)

1.10.1.2 Complement Receptors

Phagocytosis of foreign particles coated in complement opsonins C3b or iC3b, is mediated by CRs expressed on phagocytic cells.

CR1 (CD35) is a glycoprotein expressed on macrophages and neutrophils and is a phagocytic receptor, important for the clearance of immune complexes. CR1 is able to bind with high affinity to C3b and C4b, and with lower affinity to iC3b and C3dg. C4b can act as an opsonin in its own right, however, most phagocytosis that occurs through CR1 occurs via C3b binding, due to higher levels of C3b being produced upon activation of the complement cascade. Binding of C3b to CR1 will not initiate phagocytosis alone, but requires the presence of an inflammatory mediator, such as the complement component C5a, to initiate phagocytosis of pathogens bound via CR1 (Murphey & Weaver 2016). In addition to its role as a phagocytic receptor CR1 can also act as a negative regulator of complement activation by preventing C3 convertase formation on host cells; CR1 also negatively regulates complement by directly cleaving C3b (Krych-Goldberg & Atkinson 2001).

CR2 (CD21) is expressed only on B cells and follicular DCs (Donius & Weis 2014). Like CR1, CR2 can bind to iC3b on pathogen surfaces. CR2 binds with high affinity to C3dg, and will augment B cell receptor signalling when the recognised pathogen is coated in C3dg (Murphey & Weaver 2016).

CR3 (CD11b/CD18) and CR4 (CD11c/CD18) are β2 integrins that have an important role in cell adherence and migration, in addition to phagocytosis; both receptors are expressed by macrophages (in addition to other immune cells), and bind to iC3b on the pathogen surface to initiate phagocytosis (Sándor et al. 2013). Unlike CR1, CR3 does not require the presence of C5a (or any other inflammatory mediator) to initiate phagocytosis when bound to iC3b.

1.10.1.3 The role of complement in paratuberculosis

Complement proteins C1-9 are present in adult bovine serum and, therefore, may play a role in opsonisation of MAP (Linscott & Triglia 1981), particularly in the later stages of infection. Several intracellular pathogens, primarily viruses, are known to target CRs to promote uptake (Lambris et al. 2008). CR-mediated phagocytosis is a non-inflammatory process; CR3 has been shown to inhibit MyD88 and TRIF signalling pathways, reducing secretion of proinflammatory cytokines by TLR stimulated monocytes (Han et al. 2010; Roberts et al. 2016), thereby uptake via CR may be promoted by pathogens as a way to dampen the inflammatory response. A

report by Shin et al demonstrated that genes associated with the complement system were upregulated in whole blood of MAP-infected cattle (Shin et al. 2015). Additionally, a microarray study by the Glass group identified upregulation of genes associated with complement at 24 and 48 HPI in MAP-infected macrophages (unpublished data). The results of these studies suggest that complement may play a significant role in MAP infection. An early study by Schorey et al. demonstrated that presence of the complement component C2a promoted uptake of pathogenic mycobacteria (but not non-pathogenic species) by human macrophages, even in the absence of C1 and C4. This suggests that pathogenic mycobacteria can actively salvage C2a from the serum, after dissociation from C4b, and can use it to cleave C3 (even in the absence of C3 convertase) in order to enhance uptake through the complement pathway. The fact that this feature is conserved among pathogenic mycobacteria (including *M. leprae* and *M. tb*) but is absent from the non-pathogenic species (i.e. *M. smegmatis*), suggests that it is important for mycobacterial virulence (Schorey et al. 1997; Bermudez et al. 1999).

1.10.1.4 Fc Receptor Mediated phagocytosis

The adaptive immune system can assist in the clearance of pathogens by innate immune cells by producing antibodies specific for pathogen surface antigens. As discussed above, surface bound antibody is capable of activating the classical complement system, marking the pathogen for phagocytosis; however, antibodies can also act as an opsonin in their own right, by binding to FcRs expressed on the surface of immune cells (Murphey & Weaver 2016). There are multiple types of FcR (i.e. FcγRs, FcαRs and FcεRs), which are expressed on different cell-types and can bind specific antibody isotypes. All classes of FcγRs (FcγRI, FcγRII, FcγRIII, and Fcγ2R) are expressed by bovine macrophages (Kacskovics 2004).

FcR-mediated phagocytosis requires clustering of FcRs by a pathogen coated in IgG; this clustering allows cross-linking of at least two FcRs, in order for down-stream signalling to initiate actin polymerisation, pseudopod extension and, thereby, phagocytosis (García-García & Rosales 2002) (Figure 1-7).

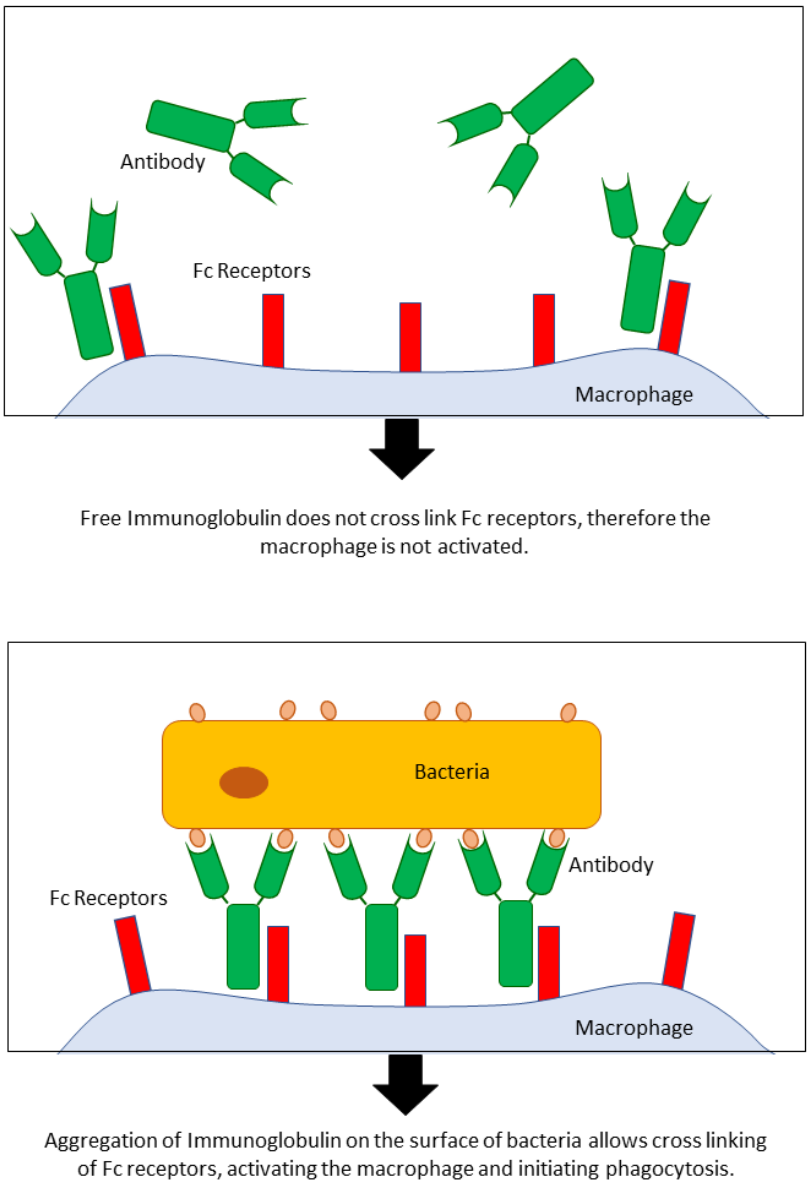

Figure 1-7 Fc receptor mediated phagocytosis.

Unbound antibody in serum or milk is unable to cross-link Fc receptors expressed on macrophages. However, when antibody is bound to antigen, it is able to bind Fc receptors on macrophages with high affinity. This is due to aggregates of pathogen-bound antibody binding multiple Fc receptors to causing cross-linking, which sends a signal to activate the macrophage for phagocytosis.

FcR-mediated phagocytosis may impact early MAP-macrophage interactions, due to the fact that MAP is often contracted by neonates through contaminated milk/colostrum, and there is potential for MAP-specific antibodies to be present in the milk of infected cows during faecal shedding (Arsenault et al. 2014; Nielsen & Toft 2008). It is therefore reasonable to infer that neonates could be exposed to IgG-coated MAP, via this infection route. Optimisation of MAP with MAP-specific antibody has previously been shown to enhance translocation across epithelial cells, and coincide with an increase in bacteria adherence/uptake, and a decrease in intracellular survival within macrophages, *in vitro* (Hostetter et al. 2005; Everman & Bermudez 2015). In addition, MAP opsonised in immune sera (containing MAP-specific antibodies) caused increased apoptosis and TNFα secretion in bovine MDM (Jolly et al. 2016). This suggests that, despite antibody traditionally being associated with disease progression of paratuberculosis at later time-points, the presence of antibody at early time-points likely has a protective effect, and FcR mediated phagocytosis may influence the ability of MAP to survive intracellularly and, ultimately, impact infection outcome.

1.10.2 Non-opsonic phagocytosis

Several PRRs expressed by macrophages are able to initiate phagocytosis upon direct binding to bacterial ligands (see Table 3). It is possible that signalling events initiated by specific phagocytic receptors could influence the downstream immune response of macrophages during mycobacterial infection, impacting the pro-inflammatory response and granuloma formation. Therefore, virulent mycobacteria species may target their uptake via specific phagocytic receptors in order to circumvent protective immunity. Macrophage phagocytic receptors that could potentially be important in macrophage-mycobacteria interactions are discussed below:

1.10.2.1 Macrophage receptor with collagenous structure

Phagocytosis by the macrophage receptor with collagenous structure (MARCO) significantly impacts the outcome of mycobacterial infection, as evidenced by studies using *M. marinum* infection of zebrafish to model tuberculosis *in vivo*. Zebrafish

embryos with morpholino knockdown (KD) of MARCO showed delayed phagocytosis of *M. marinum* as well as an impaired inflammatory response and increased intracellular growth of the bacteria (Benard et al. 2014), suggesting that uptake through MARCO is critical for early control of the infection. Additionally, SNPs in the gene encoding MARCO were associated with altered susceptibility to tuberculosis in a human study (Bowdish et al. 2013).

1.10.2.2 CD163

The scavenger receptor CD163 is differentially expressed by subsets of bovine monocytes (described in section 1.7), with higher expression associated with 'classical' monocytes that will enter tissues in response to infection or inflammatory stimuli and differentiate into macrophages (Corripio-Miyar et al. 2015). CD163 is capable of recognising ligands expressed by mycobacteria (Fabriek et al. 2009), and increased expression of CD163 is observed in diffuse multibacillary lesions, compared to focal lesions, in the intestines of MAP infected cattle (Fernández et al. 2017). In addition, CD163 expression was shown to be upregulated on monocytes of children with active tuberculosis compared to healthy children (Aktas Cetin et al. 2017), suggesting a link between this receptor and mycobacterial disease progression.

1.10.2.3 C-type lectins: DC-SIGN and the Mannose Receptor

C-type lectins bind to carbohydrates on the surface of mycobacteria (Cummings & McEver 2009), primarily Man-LAM. DC-SIGN is expressed on bovine MDM (Park et al. 2016) and is known to bind Man-LAM. Several studies have shown that mycobacteria binding to DC-SIGN can modulate the downstream immune response and that Mycobacteria likely target this receptor for their own advantage. For example, *M. tb* can modulate TLR signalling in primary human DCs, via Man-LAM binding to DC-SIGN, which results in increased secretion of the anti-inflammatory cytokine IL-10 in the presence of TLR ligands (Gringhuis et al. 2007; Gringhuis et al. 2009).

Uptake of Mycobacteria through the mannose receptor (MR) has also been shown to be beneficial for mycobacterial persistence within the host. A study by Sweet et al showed that knockdown of MR in human MDM increased phagosome maturation in

response to *M. avium* infection (Sweet et al. 2010), suggesting that *M. avium* may be targeting their uptake through this receptor to avoid degradation within lysosomes. Additionally, engagement of the mannose receptor on human DCs has been shown to promote IL-10 production and the production of anti-inflammatory mediators IL-1ra and IL-1RII (Chieppa et al. 2003), potentially affecting downstream responses by causing cells to reduce co-stimulatory molecule expression, and suppressing expression of cytokines.

1.11 Hypothesis, Aims and Objectives

Paratuberculosis is detrimental to the livestock industry and poses a potential threat to human health. Control of the disease is hindered by sub-optimal diagnostic tests and vaccines, and current control programmes are often deemed too expensive, due to the need for repeated testing.

Macrophages play a central role in directing the immune response to paratuberculosis. These innate immune cells have the potential to destroy invading bacteria; however, mycobacteria are often able to evade intracellular bactericidal mechanisms of macrophages (although the exact mechanism of this is still incompletely understood). In addition, macrophages can inform granuloma formation, and other downstream immune responses, via secretion of cytokines and chemokines, as well as present antigen to T-cells. It is clear, therefore, that gaining a better understanding of early MAP-macrophage interactions would likely benefit the design of more reliable diagnostics and efficacious vaccines.

The over-arching hypothesis of this thesis was that the early macrophage response to MAP infection is critical in influencing infection outcome, and that the strain of MAP may significantly influence this response.

This project aimed to further elucidate early MAP-macrophage interactions, and to assess if macrophages responded similarly to different strains of MAP, by comprising the following objectives:

1. Establish reliable methods to study MAP-macrophage interactions. (Chapter 3)
2. Identify early innate responses that are likely important for determining infection outcome. (Chapter 4)
3. Assess if the macrophage response to infection differs between a lab-adapted strain and a recent clinical isolate of MAP. (Chapter 4)
4. Assess how the mechanism of uptake impacts macrophage responses to infection and the ability of MAP to survive intracellularly. (Chapter 5)

2 Materials and Methods

2.1 Media, Buffers and Suppliers

Details of media, buffers and suppliers are detailed in appendix A, B and C, respectively.

2.2 Animals

Blood was obtained by jugular venepuncture from Holstein Friesian or Holstein - Norwegian Red cross heifers aged 6-15 months. Heifers were housed at either Dryden Farm or Langhill Farm, at the University of Edinburgh, according to Home Office guidelines and with approval from The Roslin Institute Local Ethics Committee. Both farms are considered to be Johne's-free, with no reported clinical cases.

2.3 Tissue Culture

2.3.1 Isolating peripheral blood mononuclear cells from whole blood

Large blood volumes (>100ml) were collected into blood bags containing citrate phosphate dextrose adenine (CPDA), before being aliquoted into 50ml falcon tubes. Blood was spun at 1200g for 15 minutes with no brake, in order to separate the buffy-coat (containing peripheral blood mononuclear cells (PBMC)) from other blood components. The thin buffy-coat layer was removed and diluted to 50ml in PBS; 25ml was then layered on top of 20ml Lymphoprep, a density gradient medium. The buffy coat was further purified by density gradient centrifugation at 1200g for 30 minutes, with no brake. The entire buffy-coat was collected, diluted to 50ml in PBSa and centrifuged at 650g for 15 minutes. If erythrocytes were observed in the cell pellet, 3ml RBC lysis buffer was added to the disrupted pellet and incubated at room temperature for 3 minutes. Cells were then washed 3x with PBSa by centrifugation at 400g for 10 minutes. Cells were re-suspended in a small volume of RPMI 1640 media and counted on a haemocytometer, using trypan blue exclusion of non-viable cells.

2.3.2 Generating monocyte derived macrophages (MDM)

First, PBMC were isolated as described above and adjusted to $1x10^7$/ml in RPMI 1640; $1x10^8$ PBMC were then seeded into $75cm^3$ tissue culture flasks and incubated at 37ºC, with 5% CO_2, for 2 hours. Non-adherent cells were removed and media replaced with 20ml Tissue Culture Media A (TCMa). Adherent cells were further incubated at 37°C with 5% CO_2 for 12 days, to allow differentiation of adherent cells into monocyte derived macrophages (MDM). On day 12 of culture, MDM monolayers were washed 3x in PBS and harvested from tissue culture flasks by addition of 4ml TrypLE Express and incubation at 37ºC for 10 minutes. MDM were washed from the plastic with Tissue Culture Media B (TCMb). Collected cells were centrifuged at 1200 RPM for 10 minutes and re-suspended in a small volume (5-10ml) of TCMb to be counted on a haemocytometer, using trypan blue exclusion of non-viable cells. $2.5x10^5$ cells were used to test purity by flow cytometry analysis of CD14 expression (see section 2.23); purity ranged from 90.8% to 99.5%. Depending on the experiment, MDM were seeded as follows: $2.5x10^5$/well of a 24 well plate, $4x10^5$ cells/well of a 12 well plate or $1x10^6$ cells/well of a 6 well plate. If microscopy was to be carried out, 13mm diameter sterile glass coverslips were added to the wells prior to seeding. Seeded MDM were incubated at 37˚C with 5% CO2 for a further 48 hours.

2.4 Bacterial Culture

2.4.1 Culture of MAP

MAP strain K10 was obtained from ATCC (BAA-968), and MAP strain C49 was isolated from the faeces of a cow with clinical Johne's, from a farm in Midlothian, Scotland. MAP strains K10 and C49 were grown on slopes of 7H10 agar supplemented with Mycobactin J, at 37ºC with 5% CO_2 until visible colonies appeared (roughly 4-6 weeks). A single colony was transferred into 5ml of 7H9 media supplemented with Mycobactin J. This was cultured with agitation by magnetic stir bar, at 37ºC with 5% CO_2, until it reached an OD_{600} of 0.5 (measured by

spectrophotometer), indicating mid-log growth phase. Cultures were aliquoted into 250µl, centrifuged at 3000g for 10 minutes, re-suspended in 250ul 7H9+glycerol and frozen at -80˚C. Further liquid cultures were made by thawing the glycerol stocks, diluting in 10ml 7H9 media and culturing with agitation at 37ºC with 5% CO_2. At mid-log growth (measured by OD_{600}), the cultures were passed several times through a 23-gauge needle, divided into 100µl aliquots and frozen at -80ºC. At least 24 hours after freezing, 3 separate aliquots were thawed in order to perform CFU counts, as described in section 2.6.

2.4.2 Culture of Mycobacterium smegmatis

Mycobacterium smegmatis (*M. smegmatis*) was a kind gift from Dr Benjamin Swift and Prof. Catherine Rees, from the University of Nottingham. A single colony of *M. smegmatis* was transferred into 5ml 7H9 media and cultured with agitation by magnetic stir bar at 37ºC with 5% CO_2, until mid-log growth phase (determined by an OD600 of 0.5 by spectrophotometer). Cultures were aliquoted into 100µl, centrifuged at 3000g for 10 minutes, re-suspended in 7H9+glycerol and frozen at -80ºC. 24 hours prior to any experiment requiring *M. smegmatis*, an aliquot was thawed, diluted into 12.5ml 7H9/2mM $CaCl_2$ media and cultured with agitation at 37ºC for 24 hours.

2.5 DNA extraction from MAP cultures

100µl of MAP culture was transferred to an Eppendorf tube and centrifuged at 3000g for 10 minutes. The supernatant was then removed, and pellets left to dry in a microbiological safety cabinet (MSC) for ~5 minutes. At this stage, pellets could be frozen at -20ºC until processing using the Qiagen DNeasy Blood and Tissue kit. Cell pellets were re-suspended in 180µl enzymatic lysis buffer and incubated at 37ºC for 2 hours. 25µl proteinase K and 200µl buffer AL (supplied with DNeasy Blood and Tissue kit) were added and the samples were vortexed then incubated at 50ºC for 1 hour. 200µl of 100% ethanol was added and samples mixed by vortexing. The rest of the process as carried out by following the Animal Tissue Spin Column Protocol,

provided the Qiagen DNeasy Blood and Tissue kit, from step 4. Briefly, the samples were transferred to DNeasy Mini spin columns, placed in a 2 ml collection tube, and centrifuged at 6000g for 1 minute. The flow-through was discarded and the spin columns placed into new collection tubes. 500 µl Buffer AW1 (supplied with the DNeasy kit) was added to the spin column and samples were centrifuged at 6000g for 1 minute. Flow-through was discarded and spin columns placed into new collection tubes. 500µl of buffer AW2 (supplied with DNeasy kit) was added to the spin column and centrifuged at 16,000g for 3 minutes. Spin columns were then transferred to sterile microcentrifuge tubes and DNA eluted in 50µl buffer AE (supplied with DNeasy kit) by centrifuging at 6000g for 1 minute. DNA concentration was measured using Nanodrop Spectrophotometer and DNA samples stored at -20ºC for up to 6 months.

2.6 Performing CFU counts

Serial dilutions of bacterial culture, or infected MDM lysate (see section 2.28), were carried out in PBS to 10^{-6}. 10µl of each dilution was plated on to 7H10 agar plates supplemented with Mycobactin J, in duplicate. Plates were incubated upside down at 37ºC with 5% CO_2 for 5 weeks or until visible colonies appeared.

2.7 Heat Inactivation of MAP

MAP strains were heat inactivated by incubation at 71°C for 10 minutes. Heat inactivated strains were then plated on 7H10 agar plates supplemented with 2µg/ml Mycobactin and incubated for 5 weeks at 37°C, to ensure effectiveness of heat treatment in killing bacteria.

2.8 Staining bacteria

2.8.1 SYTO 9 viability staining

The viability of MAP strains was assessed by analysing the fluorescence of SYTO9, a membrane permeant dye, versus the propidium iodide fluorescence, a membrane impermeant dye. 500µl samples were centrifuged at 3000g for 10 minutes and washed in 500µl 0.85% NaCl. Samples were centrifuged again, as above, and re-suspended in 97.5µl 0.85% NaCl. 0.5µl of SYTO 9 and 2µl propidium iodide were added to give final concentrations of 1µM and 30µM, respectively. Samples were mixed well and incubated in the dark for 15 minutes. 5µl was then pipetted on to a glass slide and allowed to dry in an MSC for ~5 minutes. 5µl Pro-Long Gold was added on top of each sample and a glass coverslip placed on top. Pro-Long gold was allowed to dry overnight at 4°C, and samples were imaged using a Leica DMLB fluorescent microscope. The amount of green fluorescence (SYTO9, indicating live cells) versus red fluorescence (propidium iodide, indicating dead cells) was assessed using ImageJ software.

2.8.2 Staining MAP with Fluorescein isothiocyanate (FITC)

As this method requires several wash steps, it was first determined how many bacteria were lost at each wash by performing CFU counts; the starting volume of MAP culture was then adjusted accordingly. A 0.2mg/ml Fluorescein isothiocyanate (FITC) solution was prepared to the same volume as the bacterial culture to be stained, and centrifuged at 16,000g for 2 minutes to avoid carry-over of particulate, undissolved FITC. The supernatant was then removed and added to the bacterial culture, to give a final concentration of 0.1mg/ml. Cultures were incubated in the dark for 1 hour, at room temperature, then washed 3x in PBS by centrifugation at 3000g for 10 minutes. Cultures were then re-suspended, to the desired concentration, in the appropriate media for downstream application.

2.9 Transforming C49 MAP stain to express GFP

A C49 MAP culture was grown to mid-log phase and separated into 4 Eppendorf tubes, each containing 1.5ml. Samples were pelleted by centrifugation at 3000g for 10 minutes and re-suspended in 1ml 300mM sucrose (filter sterilised). This was repeated twice and bacterial pellets re-suspended in a total volume of 1ml 300mM sucrose. This was separated into 5 200µl volumes and 5µl PWes4 plasmid (2µg), containing genes for GFP and kanamycin resistance, (Parker & Bermudez 1997) was added to each sample. Bacteria were electroporated with a single pulse, using the following settings: 25µF, 1000 Ω and 2.5kV. Bacteria were then immediately recovered into 10ml 7H9 media and incubated at 37ºC, with agitation, for 16 hours. 100µl of electroporated culture was then plated on 7H10 agar plates (supplemented with 2µg/ml Mycobactin J) with 25µg/ml kanamycin. 100µl non-transformed bacteria were plated on identical agar plates, as a control. Additionally, 100µl transformed culture was plated on 7H10 agar (supplemented with 2µg/ml Mycobactin J) without kanamycin, in order to calculate transformation efficiency.

2.10 Infection of MDM with MAP

2.10.1 Standard method

Aliquots of K10 and C49 MAP strains, frozen at -80ºC, were thawed at room temperature and diluted in TCMb to a concentration that would give a specific multiplicity of infection (MOI) per ml. Media was removed from MDM monolayers (in a 24, 12 or 6 well plate, depending on the application of the cells) and replaced with 1ml of the K10 or C49 suspension. Media was removed from uninfected control wells and replaced with 1ml TCMb. In certain experiments, additional controls were included; polystyrene beads were added at the same multiplicity as MAP, as a non-infectious control, *M. smegmatis* was added at the same MOI, as a non-pathogenic control and heat inactivated K10 or C49 were added at the same MOI as live bacteria, in order to draw comparison. If the experiment was carried out in 12 or 6 well plates, an additional 1ml or 2ml of sterile TCMb was added,

respectively. Plates were centrifuged at 400 RPM for 5 minutes, at room temperature, and incubated at 37ºC with 5% CO_2. At 0.5 hours post infection (HPI) media was removed from each well and MDM washed 3x with PBS to remove extra-cellular bacteria. All control wells were treated the same way. Media was replaced with sterile TCMb and plates returned to the incubator for the remainder of the infection time-course. Samples were taken for downstream processing at 2, 6 and 24 HPI.

2.10.2 Infecting MDM to measure nitrite secretion

For experiments involving the measurement of nitrite, the methodology was the same as the standard method (2.10.1) with the exception that DMEM without phenol red, supplemented with 20% FBS was used in place of TCMb.

2.10.3 Infecting MDM for live-cell imaging of infection

MAP strains were stained with FITC (see section 2.8.2) and diluted in Tissue Culture Media D (TCMd) so that 100µl would contain 5x more bacteria than there were MDM in each well of a 6 well plate. MDM were placed inside the CO_2 chamber of the Zeiss Live Cell Imager and regions of interest (specific areas of the monolayer to be analysed) were established up, along with an experimental time-course. Just prior to the start of the experiment, 100µl of bacteria diluted in TCMd was added to appropriate wells, to give an MOI of 5. MDM were kept at 37ºC with 5% CO_2 throughout.

2.11 Immunocytochemistry of MDM

Media was removed from infected MDM, and the monolayer washed 2x with PBS. Coverslips were then transferred to a new 24 well plate, fixed with 4% paraformaldehyde (PFA) and stored at 4°C for at least 1 hour. PFA was removed and coverslips were washed 3x with PBS. If staining intracellular bacteria or MDM expressed molecules, cells were permeabilised by addition of 150µl 0.5% TritonX-100 and incubated at room temperature for 15 minutes. Coverslips were washed 3x with PBS and non-specific binding blocked by addition of 200µl PBS/1%BSA/0.1% sodium azide for 30 minutes at room temperature. PBS/1%BSA/0.1% sodium azide

was then removed from wells and coverslips incubated in 150µl of appropriate primary antibody (see appendix E) for 30 minutes, at 37°C. The primary antibody was then removed from the wells and coverslips washed 3x in PBS. Coverslips were then incubated in 150µl of appropriate secondary antibody for 30 minutes at 37°C. For certain experiments, only cell surface molecules were stained; in this case there was no need for a permeabilisation step and therefore only the blocking step was carried out prior to addition of primary antibody and, subsequently, secondary antibody, as detailed above. Phalloidin 488 (2U/ml, diluted in PBS) was used to stain f-actin; 150µl was added to each well and incubated at room temperature for 15 minutes. Coverslips were then washed 3x in PBS and 200µl DAPI (477nM) was added to each well. Coverslips were washed 2x in distilled H_2O and excess moisture was removed prior to mounting on glass slides with 5µl ProLong Gold. Slides were stored flat at 4°C for at least 24 hours before being analysed by Leica DMLB fluorescent microscope or Zeiss LSM confocal microscope.

2.12 Image analysis

2.12.1 Quantification of intracellular MAP

Maximum Intensity Projections of confocal Z-stack images were saved as CZI files and opened on ZEN Blue software. The images were then exported as Tiffs and opened in ImageJ software. ImageJ was used to split the channels on the Tiff image and adjust the Threshold of the red channel (depicting MAP), using the Otsu method, until all areas positive for MAP staining were covered, with minimal background. The threshold was applied to the image, and background and debris eliminated by selecting '50-infinity' under the 'Analyse Particles' menu, in order to remove anything smaller than the size of 1 MAP bacterium. The number of pixels with a 255-grey value (representing positive staining for MAP) was then found under 'Histogram' and 'List', and copied to an excel spreadsheet. The total area (μm^2) covered by pixels with a 255-grey value was calculated for each image and then divided by the average size of MAP in μm^2 (Wu et al. 2009), to give the number of MAP/image. The average number of MAP/image was calculated in excel for each condition. Each image depicted an area of 18211.5025 μm^2 and a 24 well plate is

$1.9x10^8$ μm^2: an area 10439.6x greater than the area of an individual image. Therefore, the average number of MAP/image was multiplied by 10439.6, to give the average number of MAP/well of a 24 well plate.

2.12.2 Analysing co-localisation of MAP with LAMP1

Tiff virtual stacks were imported into ImageJ software and the channels split into red, green and blue channels (depicting MAP, LAMP1 and DAPI staining, respectively). To assess co-localisation of MAP with LAMP1, each clump of MAP was treated as an individual entity. Regions of interest (ROIs) were drawn around any areas positive for staining in the red channel and applied to green channel, under the 'Set Measurements' menu. The green channel image was opened and each ROI selected from the ROI manager, in order to observe if the ROIs associate with positive staining in the green channel; indicating co-localisation of MAP with LAMP1. For a diagrammatic description of the methodology, see Appendix F.

2.12.3 Analysing fluorescence intensity

Images were analysed using ImageJ software. Tiff virtual stack files were imported into ImageJ and the multi-channel image split into red, green and blue channels. The image of the channel depicting the staining to be analysed was duplicated and the Lookup Table (LUT) set to 'Fire'. Regions of interest (ROIs) were then applied to the image by either manually drawing, and adding to the ROI manager, or by subtracting the background (50-pixel rolling ball radius) and setting a threshold using the 'Triangle' method, to select cells. Area, Minimum Grey Value, Maximum Grey Value and Mean Grey Value were measured by selecting these under the 'Select Measurements' menu and redirecting the measurements to the original image. The results of each image were then exported to an excel spreadsheet and average minimum, maximum and mean grey values calculated for each treatment condition.

2.13 Preparing stocks of D29 bacteriophage

Dr Benjamin Swift and Professor Catherine Rees from the University of Nottingham kindly gifted original stock of mycobacteriophage D29. Further phage stocks were prepared by infecting a lawn of *M. smegmatis*, cultured on 7H10 agar plates, with

$1x10^7$ D29 plaque forming units (PFU) in 7H9/2mM CaCl2 and incubating overnight at 37°C with 5% CO_2, to produce lacy plates (plates with several plaques). 5ml SM buffer (see appendix B) was added to plates and incubated overnight at 4°C, in order for phage to be released into the buffer. The SM buffer was removed, centrifuged at 5000g for 1 minute to remove debris, and the supernatant collected. 100µl chloroform was added to the supernatant and left to incubate, uncovered, in a fume hood for 15 minutes. The phage suspension was then sterilised by filtration through a 0.45µm filter and stored at 4°C for up to 9 months.

2.14 Titration of D29 bacteriophage

Serial 10-fold dilutions of D29 phage stock were carried out to 10^{-7} in 1ml 7H9/2mM CaCl2. $1x10^8$ *M. smegmatis* (1ml of a culture grown in 7H9/2mM $CaCl_2$) was added to each dilution. Samples were poured into labelled petri dishes and 6ml of molten 7H10 agar was added. Plates were swirled, to mix and remove bubbles, left to set at room temperature for 1 hour, then incubated overnight at 37ºC. Plaques were counted on plates which contained between 10-100 plaques and multiplied by the dilution factor to give PFU/ml.

2.15 Phage assay for MAP Quantification

M. smegmatis was cultured for 24 hours, as described in 2.4.2. D29 phage stock was diluted in 7H9/2mM $CaCl_2$, to give an approximate MOI of 10, based on an estimate of MAP CFU present in the sample being tested. Serial 10-fold dilutions of samples containing MAP were carried out in 1ml 7H9/2mM $CaCl_2$, and 100µl D29 phage was added to the 10^{-4}, 10^{-5}, and 10^{-6} dilutions. A positive control (900µl 7H9/2mM $CaCl_2$ + 100µl *M. smegmatis* culture + 100µl D29 phage) and a negative control (1ml 7H9/2mM CaC_2 + 100µl D29 phage) were prepared. Samples and controls were incubated at 37°C with 5% CO_2 for 1 hour. 100µl of ferrous ammonium sulphate hexahydrate ((NH4)2Fe(SO4)2·6H2O), diluted to a range of concentrations in distilled H_2O, was then added to act as a virucide, and samples were rotated for 6 minutes at room temperature. The ferrous ammonium sulphate was then inactivated

by addition of 5ml 7H9/2mM $CaCl_2$. 1ml of *M. smegmatis* culture (approximately $1x10^8$ CFU) was then added to every sample and control, and the mixture subsequently poured into labelled petri dishes. 6ml molten 7H10 agar was poured into each dish and samples swirled to mix. Plates were left to set at room temperature for around 1 hour and then incubated at 37°C overnight.

2.16 DNA extraction from infected MDM

Infected MDM were removed from tissue culture plates by incubation in Tryple Express at 37°C for 10 minutes. Cells were then removed to Eppendorf tubes, spun down at 1200 RPM for 2 minutes and washed twice with PBS. After the final wash step, supernatants were removed and cell pellets frozen at -20°C until further processing. Several different methods were tested to determine the most reliable way to extract DNA from both MDM and MAP simultaneously:

2.16.1 Cetyltrimethyl Ammonium Bromide (CTAB) extraction of genomic DNA

Cell pellets were re-suspended in 567µl TE buffer and vortexed. 30µl 10% SDS and 3µl 20mg/ml Proteinase K were then added to each sample. Samples were mixed several times by inversion and incubated at 37°C for 2 hours. 100µl 5M NaCl and 80µl CTAB/NaCl solution (see appendix B) were then added and samples were incubated at 65˚C, on a heated block. DNA was extracted by adding 750µl phenol:chloroform:isoamyl alcohol to the samples and carrying out 3 sequential spins at 13,000 RPM, removing the supernatant to a fresh tube each time. The first 2 spins were for 30 minutes and the final spin for 15 minutes. The aqueous supernatant was then removed to a fresh tube, 450µl room temperature isopropanol was added and samples were spun at 13,000 RPM for 10 mins. The supernatant was removed and the pellet rinsed in 400µl 70% ethanol by spinning at 13,000 RPM for 5 minutes. The pellet was air-dried then re-suspended in 50ul distilled water. Finally, RNase was added at a final concentration of 10µg/ml. Samples were incubated at room temperature for 20 minutes before concentrations were determined by Nanodrop spectrophotometer.

2.16.2 Qiagen DNeasy Blood and Tissue kit

DNA extractions were carried out using the Qiagen DNeasy Blood and Tissue kit. Briefly, pellets were thawed at room temperature, re-suspended in 180µl enzymatic lysis buffer (see appendix B) and incubated at 37°C for 2 hours. 25µl Proteinase K and 200µl buffer AL (both supplied with Qiagen DNeasy Blood and Tissue kit) were then added and samples were vortexed before incubation at 56°C for 1 hour. 200µl 100% ethanol was added prior to vortexing and the remainder of the DNA extraction protocol carried out from step 4 of the 'Animal Tissues (spin column protocol)' supplied with the Qiagen DNeasy Blood and Tissue kit (see section 2.5). Concentration of DNA was measured by Nanodrop spectrophotometer.

2.16.3 Promega Wizard Genomic DNA Purification Kit

Genomic DNA extraction was carried out using the Promega Wizard Genomic DNA Purification Kit and following the manufacturer's instructions. Concentration of DNA was measured by Nanodrop spectrophotometer.

2.16.4 Genomic DNA extraction by TRIzol® Reagent

The method for isolating genomic DNA from MDM by TRIzol Reagent was adapted from the protocol supplied by the manufacturer. Briefly, 400µl TRIzol reagent was added to each well of a 24 well plate (containing $2.5x10^5$ MDM/well) and pipetted up and down several times, in order to lyse the cells and homogenize. Lysates were then removed to Eppendorf tubes and incubated at room temperature for 5 minutes. 80µl chloroform was added and samples shaken vigorously by hand for 15 seconds. Samples were incubated at room temperature for 2-3 minutes and then centrifuged at 12,000g for 15 minutes at 4˚C. This resulted in a separation of the sample into 3 phases. The aqueous phase (upper phase) was discarded and the entire interphase was removed to a new microcentrifuge tube. 120µl 100% ethanol was added to the interphase and the samples inverted several times, by hand. Samples were incubated at room temperature for 2-3 minutes, then centrifuged at 2000g for 5 minutes at 4ºC. The supernatant was removed from the DNA pellet and the pellet washed by adding 400µl 0.1M sodium citrate in 10% ethanol (pH 8.5), and incubating for 30 minutes (with occasional inversion by hand). Samples were then centrifuged at 2000g for 5 minutes at 4ºC, and the supernatant removed. 400µl 0.1M sodium citrate in 10%

ethanol (pH 8.5) was added to each sample and the previous wash step repeated. Pellets were resuspended in 500µl 75% ethanol and incubated for 15 minutes (with occasional inversion by hand). Samples were then centrifuged at 2000g for 5 minutes, at 4ºC and the supernatant discarded. Pellets were left to air dry for 5-10 minutes, re-suspended in 100µl distilled H_2O and centrifuged at 12,000g for 10 minutes at 4ºC, to remove insoluble materials. The supernatant was transferred to a new microcentrifuge tube and DNA concentrations were measured by Nanodrop spectrophotometer.

2.17 Quantifying genome copy number by qPCR

qPCRs were performed using the Agilent Brilliant III Ultra-Fast SYBR Green qPCR master mix. Master mixes were made up as follows: 5.0µl 2x master mix, 0.5µl forward primer (diluted to the pre-determined optimal concentration), 0.5µl reverse primer (diluted to the pre-determined optimal concentration), 0.15µl Rox reference dye (diluted 1:500 in nuclease-free H_2O) and 1.35µl nuclease-free H_2O. 7.5µl master mix was dispensed into each well of a 96 well plate, on ice, and 2.5µl of genomic DNA (diluted 1:10 in H_2O) or non-template control added to appropriate wells. Primers targeted the single-copy bovine gene SPAST (Fadista et al. 2010) and the single-copy F57 insertion sequence in the MAP genome. Each sample to be tested was represented in triplicate and a 5-point standard curve of 10-fold dilutions included, in order to calculate the efficiency of the reaction. Wells were sealed with Ultra Clear qPCR caps and the plate was centrifuged at 1200 RPM for 2 minutes. The reaction was run on a Stratagene Mx3000P qPCR machine under the following conditions:

95°C	3 minutes	
95°C	10 seconds	50 cycles
60°C	22 seconds	

A dissociation curve was included in the reaction set up to ensure that only a single product was generated. The data was analysed using MxPro software and Microsoft

Excel. Relative quantification of F57 copy number compared to SPAST copy number was calculated using the Pfaffl method (Pfaffl 2001).

2.18 RNA extraction from MDM

RNA was extracted using the Reliaprep RNA extraction kit from Promega. All buffers, reagents and equipment were supplied with the kit, unless otherwise stated. Prior to RNA extraction, a 1:100 dilution of 1-Thioglyercol was made in BL buffer (BL+TG buffer). 500µl of BL+TG buffer was added to $2x10^5$ – $1x10^5$ MDM and pipetted up and down several times. Samples were removed to RNase free plastic-ware and frozen at -80°C for up to 3 months. Once thawed, 170µl isopropanol was added to each sample and mixed by vortexing. Samples were then transferred to a mini-column in a collection tube and centrifuged at 14,000g for 30 seconds. 500µl RNA wash solution was added to the mini-column and centrifuged at 14,000g for 30 seconds. DNase I Solution was made up by combining 24µl Yellow core buffer, 3µl 0.09M MnCl2 and 3µl DNase I enzyme per sample. Samples were then incubated in DNase I solution for 15 minutes at room temperature, in order to remove residual DNA. 200µl Column Wash Solution was added to each mini-column and centrifuged at 14,000g for 15 seconds. 500µl RNA Wash Solution was added and samples centrifuged at 14,000g for 30 seconds. Flow through was discarded after each centrifugation step. At this stage, mini-columns were placed into clean collection tubes and 300µl RNA wash solution was added and centrifuged at maximum speed for 1 minute. Flow-through was discarded and mini-columns centrifuged again at maximum speed for 1 minute. RNA was eluted by placing mini-columns into clean elution tubes, adding 15µl nuclease-free H_2O directly onto the membrane and centrifuging at 14,000g for 1 minute. Eluted RNA was stored at -80°C.

2.19 Reverse Transcription

Frozen RNA samples were thawed on ice and the concentration of each sample measured by Nanodrop spectrophotometer. The volume of each sample to give

0.5µg RNA was calculated and dispensed into individual PCR tubes. The volume of each sample was made up to 11µl with DNAse and RNase-free H_2O. RNA was reverse transcribed to cDNA using the GoScript Reverse Transcription System (Promega) and following the manufacturers' instructions. A non-enzyme control was included for each sample to ensure no genomic DNA contamination.

2.20 Primer Design

The DNA sequence of the gene of interest was obtained from the NCBI nucleotide database and copied into the input window of the Primer3 website (http://primer3.ut.ee/). The product size range was then set depending on the application of the primers; for polymerase chain reaction (PCR) the size range was between 400 and 800 base pairs, and for quantitative PCR (qPCR) the size range was between 100 and 200 base pairs. Primer length, annealing temperature, GC content and polyX were adjusted to desired values. The number of primer pairs to be returned was set to 50 and the list was rigorously checked, in order to select only primers that would result in minimal complementarity (and therefore primer dimer formation). Complementarity of the primers was further examined by checking the ΔG values using the NetPrimer website (http://www.premierbiosoft.com/netprimer/) and only selecting primer pairs with a ΔG value greater than -4 kcal/mol. A BLAST search was run to ensure the primers would not anneal to any non-target DNA sequences. Details of all primers used are detailed in Appendix D.

2.21 Polymerase chain reaction

A master-mix containing: 2.5µl 10 x PCR buffer, 1.5µl 25 mM MgCl2, 0.5µl 10 mM dNTP mix, 0.25µl 25 pmol/µl oligonucleotide mix, 19.15µl H_2O and 0.1µl Taq polymerase, was prepared for each sample plus a positive control (cDNA/gDNA from a sample known to express the gene) and a negative control (nuclease free H_2O). 24µl master mix was added to 1µl cDNA/gDNA sample and the reaction run under the following conditions:

95°C	3 minutes	
95°C	30 seconds	30 cycles
60°C	30 seconds	
72°C	45 seconds	
72°C	5 minutes	

A heated lid was used to prevent evaporation of the PCR products.

2.22 Agarose gel electrophoresis

PCR products were run on a 1% or 2% agarose gel in order to determine the size and purity of the product. 1.5g or 3g of agarose powder was dissolved in 150ml TAE buffer (see appendix B) to make a 1% or 2% gel, respectively. 7.5µl of SYBR safe was added per 150ml gel. 1µl of each sample was mixed with 5µl loading dye and loaded into wells of the agarose gel. A 1kb or 100bp ladder (HyperLadder I or IV, respectively) was run along-side samples in order to determine size, and samples were run at 100 volts for 50 minutes. Gels were imaged on a G:BOX transilluminator.

2.23 Quantitative reverse transcription polymerase chain reaction (qRT-PCR)

qRT-PCRs were performed using the Agilent Brilliant III Ultra-Fast SYBR Green qPCR master mix. Master mixes were made up for each gene transcript, as follows: 5.0µl 2x master mix, 0.5µl forward primer (diluted to the pre-determined optimal concentration), 0.5µl reverse primer (diluted to the pre-determined optimal concentration), 0.15µl Rox reference dye (diluted 1:500 in nuclease-free H_2O) and 1.35µl nuclease-free H_2O. 7.5µl master mix was dispensed into each well of a 96 well plate, on ice, and 2.5µl of cDNA (diluted 1:10 in H_2O) or non-template control added to appropriate wells. The reference transcript used was Chromosome

Alignment Maintaining Phosphoprotein 1 (CHAMP1), which is constitutively expressed (Jensen et al. 2014). Each sample to be tested was represented in triplicate and a 5-point standard curve of 10-fold dilutions included, in order to calculate the efficiency of the reaction. Wells were sealed with Ultra Clear qPCR caps and the plate was centrifuged at 1200 RPM for 2 minutes. The reaction was run on a Stratagene Mx3000P qPCR machine under the following conditions:

95°C	3 minutes	
95°C	10 seconds	50 cycles
60°C	22 seconds	

A dissociation curve was included in the reaction set up to ensure that only a single product was generated. The data was analysed using MxPro software and Microsoft Excel. Relative quantification of the target transcript compared to the reference transcript was calculated using the Pfaffl method (Pfaffl 2001).

2.24 Flow cytometry

2.24.1 Single colour staining

MDM monolayers were dissociated from 24 well plates by addition of 100µl TrypLE Express and incubation at 37ºC for 10 minutes. Cells were then transferred into 96 well plates and washed 3x with PBS. All wash steps were carried out by centrifugation at 1200 RPM for 2 minutes. 100µl of a 1:200 dilution of Zombie Aqua viability stain was then added to each well (minus the unstained control) and incubated in the dark for 20 minutes. A wash step was carried out, as described above, prior to addition of 100µl 20% goat serum in PBS to each well. Cells were incubated at room temperature, in the dark, for 30 minutes, and centrifuged at 1200 RPM for 2 minutes. Cells were re-suspended in 20µl of appropriate primary antibody or isotype control (see appendix E), diluted to the optimal concentration in PBS/1%BSA/0.1% sodium azide, and incubated in the dark for 10 minutes. Cells

were then washed, re-suspended in 20µl goat anti-mouse IgG conjugated to PE (see appendix E) and incubated at room temperature in the dark for 10 minutes. A secondary antibody control (where secondary antibody was added to cells without primary antibody) was included to ensure there was no non-specific staining. Cells were washed in PBS/1%BSA/0.1% sodium azide, as described previously, re-suspended in 100µl 2% PFA and left at 4ºC for 30 minutes. A final wash step was carried out, as described above, and cells re-suspended in 100µl PBS/1%BSA/0.1% sodium azide. Analysis was carried out using the BD Fortessa flow cytometer and FlowJo software; 10,000 events were collected and an example of the gating strategy is demonstrated in Figure 3-3

2.24.2 Multi-colour staining

The method for multi-colour staining was essentially the same as for single-colour staining, except that several isotype mis-matched primary antibodies were added to each sample. Secondary antibodies were selected based on specificity for the species and isotype of the primary antibody, and the emission spectra of the conjugated fluorophores. Compensation controls (with only a single colour) were included, as were Fluorescence-minus-one controls and isotype controls.

2.25 Enzyme-linked Immunosorbent Assay (ELISA)

2.25.1 IL-1β and IL-6

Supernatants from MAP infected MDM (section 2.10) were frozen at -20˚C on the day of infection. Prior to running ELISAs, supernatants were thawed at room temperature and vortexed. ELISAs for IL-1β and IL-6 were carried out using kits supplied by Thermo Fisher Scientific and following the manufacturer's instructions. Absorbance was measured at 450nm subtracted from 550nm using the Synergy HT Multi-Mode Microplate Reader and Gen 5 software.

2.25.2 IL-10

Flat bottomed 96 well plates were coated with coating antibody (appendix E) diluted in carbonate/bicarbonate buffer and incubated over-night at room temperature. All wash steps were as follows: plates were washed 5x in PBS/ 0.05% Tween-20, using the Skan Washer 400 plate washer. Plates were washed and blocked for 1-2 hours using blocking buffer (Appendix B). Again, plates were washed, and 100µl samples were added to the plate, in duplicate. Recombinant IL-10 was serial diluted 1:3 (in duplicate) to achieve a standard curve, and the plate was incubated at room temperature for 1 hour. A wash step was carried out, and 100µl biotinylated detection antibody (Appendix E), was added to each well, and incubated at room temperature for 1 hour. Plates were washed and 100µl streptavidin HRP (diluted 1:400 in reagent diluent) was added to each well. Plates were incubated for 1 hour then washed 5x, as above. 100µl TMB substrate solution was added to each well and plates were incubated in the dark until colour appeared in the bottom standard. The reaction was stopped by addition of 50µl 1M H_2SO_4 per well. Absorbance was measured at 450nm subtracted from 550nm, using the Synergy HT Multi-Mode Microplate Reader and Gen 5 software.

2.26 Analysis of nitrite secretion by Griess reaction

On day 14 of culture, MDM were infected as described in section 2.7, with the exception that TCMc was used instead of TCMb; this was due to the high intrinsic levels of nitrate/nitrite found in RPMI media, also the presence of phenol red in TCMb would likely have interfered with the assay. The concentration of nitrite was measured in the supernatant after 24 hours of infection, using the Griess assay kit from Thermo Fisher Scientific and following the manufacturer's instructions. Absorbance was measured at 540nm, using the Synergy HT Multi-Mode Microplate Reader and Gen 5 software.

2.27 Analysis of intracellular reactive oxygen species production by flow cytometry

Intracellular reactive oxygen species production was assayed by flow cytometry, using the 'CellROX Deep Red Flow Cytometry Assay' kit from Molecular Probes and following the manufacturer's instructions. Data were analysed using the BD Fortessa flow cytometer and Flowjo software.

2.28 siRNA knockdown of NLRP3 gene expression

siRNA targeting bovine NLRP3 was obtained from Sigma-Aldrich (for sequence see appendix D). To introduce siRNA into MDM, RNAiMAX Lipofectamine was used. NLRP3 specific siRNA was diluted in 200µl Opti-MEM I serum free medium, to a final concentration of 2.9µM. In a separate tube, 6µl RNAiMAX was diluted in 200µM Opti-MEM I serum free medium then gently added to the siRNA dilution. The mixture was incubated for 20 minutes at room temperature to allow liposomes to form complexes with the siRNA. Media was removed from MDM monolayers (5 $x10^5$ cells/well of a 12 well plate) and replaced with 2ml fresh TCMb. 400µl RNAiMAX:siRNA mixture was gently added to each well and the plates swirled to mix. MDM were incubated with the siRNA:RNAiMAX mixture at 37°C for 24 hours. After 24 hours, media was replaced with 2ml fresh TCMb and the cells left to incubate at 37˚C for a further 24 hours before downstream experimental procedures. A negative control (no treatment), transfection control (cells treated only with RNAiMAX without siRNA) and non-template control (cells transfected with non-specific siRNA) were all included in the experimental set up. In addition, in order to be confident that a high proportion of MDM were successfully transfected, uptake of siRNA was assessed using flow cytometry to detect the intracellular presence of fluorescently labelled non-specific siRNA.

2.29 Inhibition of Nitric Oxide with NG-Monomethyl-L-arginine

MDM monolayers were infected, in duplicate, at an MOI of 5 with either heat-inactivated or live K10 or C49 diluted in TCMc, and incubated at 37°C for 30 minutes. At 30 minutes post infection, monolayers were washed 3x with PBS and media replaced with fresh, sterile media. NG-Monomethyl-L-arginine (L-NMMA) was then added to half the wells at a final concentration of 500µM. LPS was added to appropriate wells at a final concentration of 1µg/ml. Details of all treatment conditions are detailed in Table 4:

L-NMMA	No treatment
K10	K10
C49	C49
K10 stimulated with LPS	K10 stimulated with LPS
C49 stimulated with LPS	C49 stimulated with LPS
Heat killed K10	Heat killed K10
Heat killed C49	Heat killed C49
Uninfected	Uninfected

Table 4 Treatment conditions of MDM.

MDM were incubated at 37°C until 24 HPI. Supernatants were then removed and nitrite concentration measured by the Griess assay kit, as described in section 2.25.

In order to determine whether NO impacted the ability of MAP to survive intracellularly, 100µl 0.1% Triton-X 100 was added to each well to lyse the MDM and lysate plated on 7H10 agar plates supplemented with 2µg/ml Mycobactin J, in order to perform CFU counts, as detailed in section 2.6.

2.30 Blocking C-type lectin receptors

C-type lectin receptors on the surface of MDM were blocked by incubating in 2mg/ml Mannan from Saccharomyces cerevisiae (diluted in TCMb) at 37˚C for 30 minutes. The methodology and concentration was determined by preliminary

experiments comparing a range of concentrations of both D-mannose and Mannan. The efficiency of D-mannose and Mannan at blocking both DC-SIGN and the MR was measured by observing effects antibody binding by immunocytochemistry (see section 2.11)

2.31 Opsonisation of MAP strains in bovine serum

Pooled MAP-antibody positive cattle sera was a kind gift from Dr Lyanne McCallan at the Agri-food and Biosciences Institute, Belfast. Serum from uninfected cattle was obtained from Dryden farm, and pooled. Half of this sera was heat-inactivated at 56ºC for 30 minutes. All sera were frozen at -80ºC and thawed directly prior to use. In order to assess the role of serum components during MAP infection, MAP strains with incubated at 37ºC for 30 minutes in 10% MAP-antibody positive serum, 10% serum from uninfected cattle or 10% heat-inactivated serum (diluted in DMEM without phenol red, 2% L-glutamine). Immediately after this opsonisation step, MDM monolayers were infected, as described in section 2.10 and the effect of serum components on the ability of MAP to invade and survive intracellularly was measured by lysing MDM monolayers with 100µl 0.1% TritonX-100 and performing CFU counts, as described in section 2.6. Additionally, the impact on nitrite secretion was measured by Griess reaction (section 2.25).

2.32 Sequencing MAP strains

Sequencing of MAP strains used for this project was carried out by MicrobesNG. Single colonies of each MAP strain were obtained by plating serial dilutions of frozen stocks on 7H10 agar plates and incubating plates as described in section 2.6. A single colony of each strain was picked off the agar plates with a sterile loop and mixed in 100µl PBS by repeated pipetting and vortexing. The full 100µl volume of each MAP suspension was then streaked onto a 7H10 agar plate (covering about 1/3 of the plate) and left to incubate at 37ºC with 5% CO_2 for 5 weeks. Using a large sterile loop, all bacteria were removed from the plate and transferred into barcoded bead tubes supplied by MicrobesNG. Tubes were vortexed and as much liquid

removed from them as possible. Tubes were then sent to MicrobesNG for DNA extraction and sequencing, using the Illumina HiSeq 250 platform. Basic bioinformatics analysis, including variant calling, was carried out by MicrobesNG. Further bioinformatic analysis was then carried out by Rodrigo Bacigalupe. Sequencing reads of strains K10 and C49 were mapped to the reference genome of MAP (K10) (GenBank accession no: AE016958.1) using Burrows-Wheeler Aligner (BWA). Identification of single nucleotide polymorphism (SNPs) and short insertions and deletions (indels) was performed using SAMtools and Genome Analysis Toolkit (GATK). Only mutations that were common to all 3 replicates were included in results.

2.33 Data analysis

Data analysis was performed using Microsoft Excel 2016 and GraphPad Prism 6. Data is presented as the mean and standard deviation (SD) (number of biological and technical replicates are described in individual legends), unless otherwise stated. SD was selected, as opposed to the standard error of the mean (SEM), as SD represents the variability observed within the data-set, whereas the SEM does not estimate variability, but rather how precise the mean of the data-set is likely to be in relation to the true mean. Statistical analysis was completed using Minitab 17 Statistical Software. Statistical tests used are described in the figure legends and include 2-sample t-tests and general linear models, for normally distributed data, and Kruskal-Wallis and Mann-Whitney tests for non-normally distributed data. The Anderson Darling test was used to assess data distribution either directly or, when appropriate, applied to general linear model residuals ($p<0.05$ considered to be a non-normal distribution). Non-normal data were log transformed and distribution re-analysed. Any data set that remained non-normally distributed after log transformation was analysed by appropriate non-parametric test/tests. Significance was reported as $p<0.05$*, $p<0.01$** and $p<0.001$***.

3 Establishing experimental techniques to investigate the response of bovine monocyte derived macrophages to *Mycobacterium avium* subsp. *paratuberculosis* infection

3.1 Introduction

One of the key features of MAP infections is the ability of the bacteria to infect bovine macrophages and survive intracellularly for prolonged periods of time. This intricate host-pathogen interaction is still incompletely understood, and the over-arching aim of this project was to understand how host macrophages respond to MAP infection at early time-points. The early MAP-macrophage interaction is likely a pivotal point that determines whether the outcome of exposure to MAP results in immunity or infection that eventually progresses to disease.

In order to investigate MAP-macrophage interactions, this chapter focused of creating tools and optimising methods that would be used for MAP infection studies throughout this body of work. First, methods of culturing both MAP and MDM had to be established. The project aimed to analyse and compare the MDM response to two strains of MAP: the reference strain K10, that has likely undergone lab-adaptation, and a field strain, C49, isolated from a clinical case of Johne's disease. Therefore, both MAP strains had to be successfully cultured, and cultures accurately quantified prior to infection studies.

The accurate quantification of bacteria in liquid culture is crucial when studying the immune response to bacterial infection, so as to maintain consistency and understand dose effect. It is generally achieved by creating a growth curve comparing colony-forming units (CFU) with the optical density (OD) of the culture. This is done by measuring OD of a culture at a wavelength of light that is absorbed by the bacteria, at several time-points. At the same time-points used for OD measurements, serial dilutions of the culture are plated on agar plates to obtain a CFU count corresponding to each OD reading. This creates a growth curve that can be used to estimate the CFU within a culture, based on an OD reading. Mycobacteria absorb light at a wavelength of 600nm (OD_{600}) (Kralik et al. 2012) and OD_{600} has previously been used to quantify cultures of several mycobacteria species, including *M. tb, M. marinum,* and MAP (Peñuelas-Urquides et al. 2013; Kralik et al. 2012; Benard et al. 2012); therefore, growth curves were established to quantify liquid cultures of both K10 and C49 so that MDM could subsequently be infected at a known multiplicity of infection (MOI) and that the MOI would be consistent for both strains. In addition,

the viability of bacterial cultures was measured with the viability dyes SYTO9 and propidium iodide, prior to infection experiments, to ensure that both K10 and C49 cultures contained a majority of viable cells and results would not be compounded by a high proportion of dead cells within one or both cultures.

MAP also had to be quantified at several time-points post-infection; for many species of bacteria, quantification is a simple, cost effective and non-labour-intensive process, generally done by plating serial dilutions of a suspension on agar plates to perform CFU counts. Although CFU counting is used for quantification of MAP, there are significant drawbacks to the method; performing CFU counts to quantify MAP could be considered impractical, expensive and somewhat imprecise, due to the nature of the organism (Shin et al. 2007). For example, MAP has a particularly slow generation time of >24 hours (Elguezabal et al. 2011), meaning colonies take between 3-5 weeks to appear on solid agar. The slow growth rate, combined with the tendency of MAP to form clumps in liquid culture, make quantifying MAP by CFU counting somewhat challenging and inefficient. In addition, MAP can only be cultured under very specific growth conditions. Unlike most other species of mycobacteria, many MAP strains are unable to produce mycobactin, an iron chelator, and successful culture therefore depends on the exogenous addition of Mycobactin J (Francis et al. 1953). The addition of Mycobactin J significantly increases the cost of performing CFU counts as a method of quantification, compared to other species of mycobacteria. Therefore, alternative quantification methods have been assessed in this chapter.

The Phage Amplification Assay was tested as an alternative to counting CFU. This method has been used to detect the presence of MAP in bovine blood, infant formula and milk (Swift et al. 2016; Botsaris et al. 2016; Foddai & Grant 2017). The assay utilises the mycobacteriophage, D29, which is capable of infecting a broad spectrum of mycobacteria, including *M. smegmatis* and MAP. The principle of the assay is detailed in Figure 3-1. Briefly, D29 phage is added to serial dilutions of samples containing MAP. Samples are then incubated for 1 hour, to allow the phage to infect and replicate within the cell. After 1-hour of incubation, a virucide is added and samples mixed thoroughly, so that extracellular phage is inactivated and only

intracellular phage survive. The virucide is then inactivated by dilution and ~1x10^8 fast-growing *M. smegmatis* added, in order to form a lawn. Samples are poured into plates, along with 7H10 agar, and incubated over-night at 37ºC. Eventually newly formed phage will lyse the infected cell, infect nearby *M. smegmatis* cells, replicate, and the process will repeat several times, leading to plaque formation. Due to the inactivation of extracellular phage prior to addition of *M. smegmatis*, one plaque should represent the presence of one MAP bacterium.

The benefits of using a phage amplification assay to quantify MAP infection include the efficiency of the assay (results can be obtained after just 48 hours), and the fact that D29 is only capable of replicating in live, metabolically active cells, meaning that the assay informs on only the number of live cells within a sample. Drawbacks of the phage amplification assay include the fact that it cannot differentiate clumps from single cells or replicate within dormant cells (since they are not metabolically active), meaning that actual numbers of MAP could be under-represented. Theoretically, the results of the phage assay should correlate very well with CFU counts (since CFU counting also cannot differentiate between single cells and clumps, and will not account for dormant cells) but provide results more rapidly, potentially making it an effective alternative.

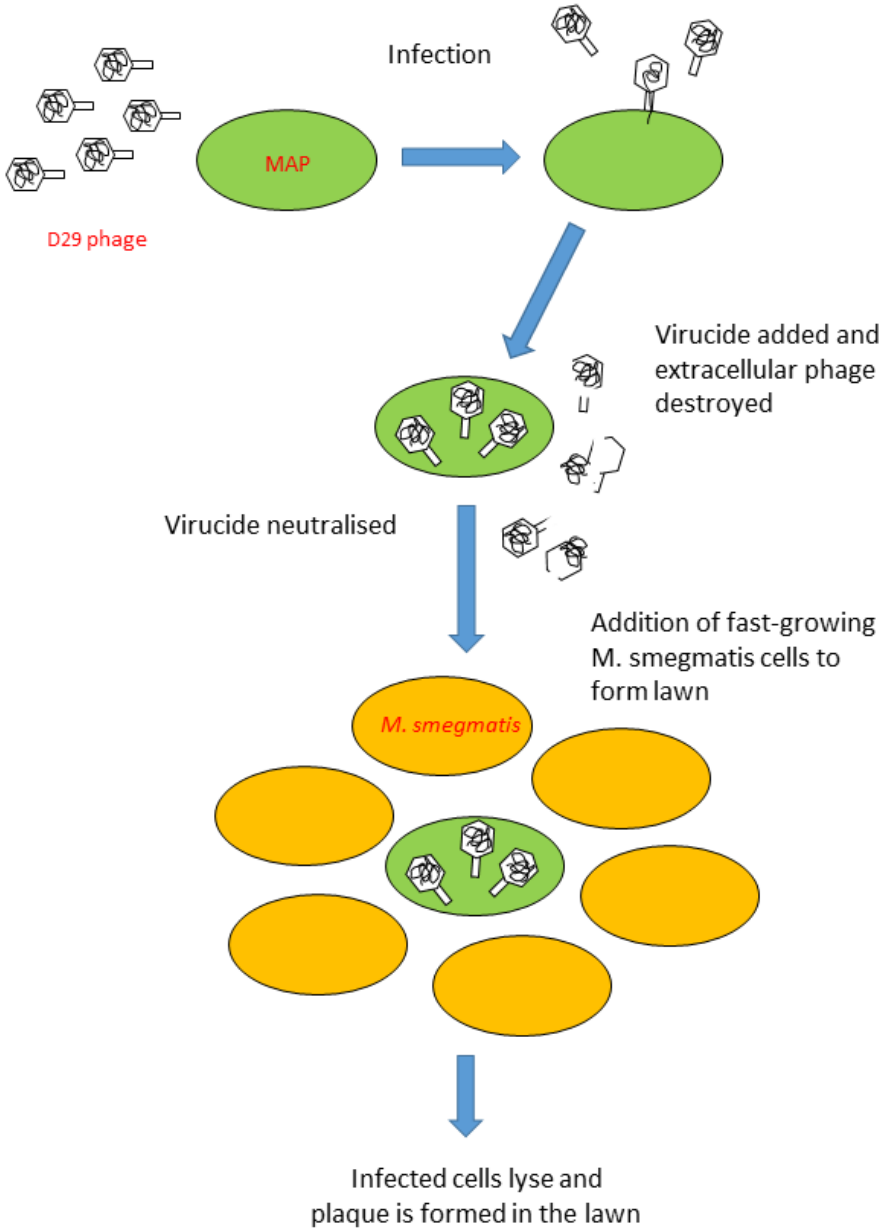

Figure 3-1 Phage Amplification Assay.

D29 bacteriophage and MAP are incubated together for 1 hour at 37°C, to allow D29 to infect MAP cells. After 1-hour of incubation, a virucide is added to destroy extracellular phage. The virucide is then inactivated by dilution, and fast-growing M. smegmatis are added. Samples are poured onto agar plates to allow M. smegmatis to form a lawn. D29 will lyse infected MAP cells and go on to infect surrounding M. smegmatis, forming a plaque in the lawn, marking the presence of each infected MAP cell.

Quantitative PCR (qPCR) is commonly used for detection of MAP and has been employed in several different sample types including water, milk and faeces (Beumer et al. 2010; Kruze et al. 2013; Kralik et al. 2011). qPCR can be employed to measure the number of genome copies of MAP by amplifying a target sequence specific to the MAP genome. The most commonly used genomic target is the IS900 insertion element, however this was not used in this study, as MAP can contain 14-18 copies of this sequence, which can increase sensitivity at low numbers but could also potentially lead to inaccuracy (Beumer et al. 2010). Instead, F57, a single-copy sequence specific to the MAP genome, was used to quantify MAP by qPCR throughout this PhD study. The F57 sequence is routinely used for qPCR- based quantification and has been demonstrated to have high specificity, sensitivity, and reproducibility (Sidoti et al. 2011; Slana et al. 2008; Fawzy et al. 2015). Use of F57 qPCR is advantageous over CFU counting when considering the slow generation time of MAP, as it can quantify genome copy number (GCN) in only a few hours. However, unlike quantifying by CFU counting, or phage amplification assay, qPCR cannot discriminate between live and dead bacteria, potentially making it an unsuitable method, particularly when investigating intracellular survival of MAP within MDM. Due to qPCR measuring numbers of both live and dead bacteria, there is often discrepancy between GCN and CFU counts from the same samples, as reported by Pathak et al., who showed a 10 – 100 fold difference between the two methods (Pathak et al. 2012). To combat this, it was investigated herein whether a direct correlation could be consistently drawn between GCN and CFU, in order to understand if qPCR could be used to quickly and accurately estimate CFU in a sample. qPCR could thereby be used as a method to quantify total number of MAP genomes and simultaneously estimate the number of live cells.

Confocal microscopy is a powerful imaging tool; laser scanning confocal microscopes are able to scan a series of optical slices through an object (without out-of-focus blur) to produce a 3D image stack. This method therefore allows the visualisation of a cell in its entirety, unlike wide-field fluorescent microscopy, which only allows the visualisation of single focal plane with out-of-focus blur reducing contrast (Jonkman & Brown 2015). The ability to create 3D image stacks with confocal microscopy makes it feasible to count the total number of bacteria in any

given cell (even if they fall in different focal planes), therefore confocal microscopy was employed as a method to both quantify the infection of MDM and determine the level of infection confluence. Confocal microscopy image analysis allowed the number of individual cells within a visible clump to be estimated and, as with qPCR, it provided no information about the viability of MAP cells. It was therefore hypothesised that bacterial numbers obtained by this method would correlate well with GCN. MAP numbers quantified by confocal microscopy were compared with numbers obtained using CFU count and qPCR, to assess the reliability of this method to inform on both total number of bacterial cells and accurately estimate the number of live cells.

Bacteria expressing GFP are considered a useful tool for infection studies, as they can be utilised to distinguish infected cells from bystander cells, and to analyse intracellular trafficking by methods such as flow cytometry and fluorescent microscopy. Parker and Bermudez developed a plasmid (pWES4) encoding both a GFP/hsp60 fusion gene and a kanamycin resistance gene (Figure 3-2), which they cloned in the fast-growing *E. coli* and successfully transfected into *M. avium* Incorporation of the plasmid did not alter the virulence of the bacteria (Parker & Bermudez 1997). For this study, a K10:GFP strain (transfected with pWES4) was kindly gifted by Dr Karen Stevenson from Moredun Research Institute and the C49 MAP strain was transformed to express GFP by electroporation with the pWES4 plasmid. K10 and C49 strains expressing GFP would be useful tools in imaging studies assessing and comparing the macrophage response to both strains.

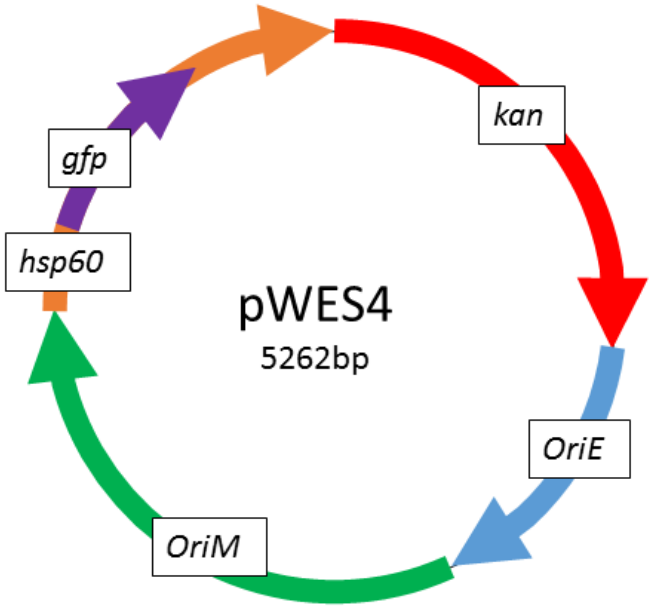

Figure 3-2 The pWES4 plasmid.

C49 was transformed to express GFP by electroporation with the pWES-4 plasmid. The pWES4 plasmid was made by ligating the GFP gene from pGFP into the hsp60 multi-cloning site of pMV261. The plasmid consists of origins of replication for both Escherichia coli (oriE) and M. avium (oriM), as well as a kanamycin resistance gene (kan). Image adapted from Parker and Bermudez, 1997

3.1.1 Aims

The aim of this chapter was to establish methods and tools that would be of use throughout this study as a whole. First, methods for culturing both MDM and MAP were established in order to carry out infection experiments. Understanding the number of bacteria within a culture is of great importance, so as to understand dose effect and maintain consistency in repeat experiments; therefore, work in this chapter aimed to establish a reliable method for growing both the K10 and C49 MAP strains, and for quantification of bacterial numbers in cultures prior to their use in infections. Accurate quantification of bacterial cultures allowed the MOIs used throughout this body of work to be established; it was important to know that the MOI used resulted in confluent and consistent infection, in order to gain meaningful results downstream.

As this study would focus on MAP infection of MDM *in vitro*, having fluorescent strains would be of great benefit when imaging infected cells or performing flow cytometry. Therefore, a further aim of this chapter was to establish and maintain K10:GFP and C49:GFP MAP strains, which would be used to carry out comparative studies of intracellular trafficking, and visually identify MAP infected cells, compared to bystander cells, during flow cytometric analysis of CSM expression.

In addition, it was necessary to investigate and develop methods for the quantification of intracellular bacteria post-infection. Quantification of MAP is notoriously difficult due to the characteristics of the bacteria described above, therefore a final aim of this chapter was to compare and contrast four quantification methods: the phage amplification assay, qPCR, confocal microscopy and CFU counting, in order to identify the most accurate and reliable method for quantifying MAP infection of MDM.

3.2 Results

3.2.1 Culture of monocyte derived macrophages (MDM)

MDM were isolated from PBMCs and cultured for 12 days in TCMa (appendix A), prior to being harvested, and seeded into 6, 12 or 24 well plates. Throughout the 12-day growth period, cell size and morphology was assessed by light microscopy in order to observe that the cultured cells were taking on the appearance of macrophages (data not shown). At day 12, the purity of the culture was assessed by analysing CD14 expression by flow cytometry. First, cells were gated on their Forward-Scatter-A/ Side-scatter-A (FSC-A/SSC-A) properties, in order to gate for cells with the expected size and granularity of macrophages, as detailed by Jensen et al (Jensen et al. 2016). Of 5 biological replicates, the mean percentage of events falling within this population was 64.4% However, debris accounted for 24% of events, with only 12.5% events ungated (Figure 3-3 A). Doublets were eliminated from the analysis by gating on FSC-A/FSC-H properties. Of 5 biological replicates, the mean proportion of single cells was 95% (Figure 3-3 B). CD14 expression was then analysed on cells falling within both the 'Macrophage' and 'single cells' gates. Gates were set using unstained controls and a mean of 95.58% cells were positive for CD14 expression (Figure 3-3 C).

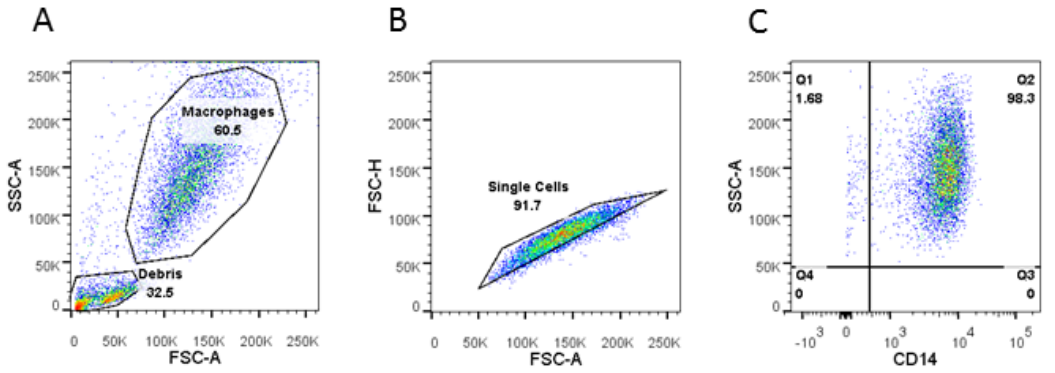

Population	Mean	SD
Macrophages	64.4	8.14
Debris	24	11.3
Ungated	12.5	6.89

Population	Mean	SD
Single Cells	95	2.9

Population	Mean	SD
CD14 +ve	95.58	5.24
CD14 -ve	4.43	5.23

Figure 3-3 Representative MDM gating strategy.

The purity of primary bovine MDM cultures was assessed by flow cytometry (A) Macrophages were gated on their FSC-A/SSC-A properties. (B) Doublets were excluded from the analysis by gating on FSC-A/FSC-H properties. (C) Expression of the macrophage marker CD14 was analysed. Gates were set using unstained controls. The tables presented under A, B, and C show the mean percentage of events falling into each gate from 5 biological replicates (N=5). SD= Standard deviation.

3.2.2 OD_{600} cannot accurately estimate CFU/ml of MAP cultures

K10 and C49 MAP cultures were grown from glycerol stocks as detailed in section 2.4.1. Briefly, a single 100µl aliquot of K10 or C49 glycerol stock was thawed, diluted in 10ml 7H9+Mycobactin J (Appendix A) and cultured with agitation by magnetic stir bar for several weeks. For the first culture (culture 1) of each strain, 1ml was sampled at day 7, 21, 28, and 35, in order to create growth curves comparing CFU to OD_{600} (Figure 3-4). The R^2 value of the K10 growth curve was 0.8095, meaning that there was no reliable correlation between OD_{600} and CFU (Figure 3-4 A). Whereas, the R^2 value for the C49 growth curve was 0.9994, suggesting that OD_{600} and CFU count correlated very well for C49 (Figure 3-4 B). These results indicate that OD_{600} could predict K10 CFU less reliably than C49 CFU (Figure 3-4 A). The growth curves demonstrated that ~OD_{600}: 0.6 was indicative of mid-log growth phase from both K10 and C49.

The length of time it took for 4 liquid cultures of each strain to grow to mid-log growth phase (OD_{600}: 0.6) was compared (Table 5). For culture 1, OD_{600} was measured every 7 days. On day 28, K10 OD_{600} was 0.41 and C49 OD_{600} was 0.44 (data not shown) therefore the cultures were incubated until day 35. However, by 35 days in culture OD_{600} had exceeded 0.6. To address this, an OD_{600} reading was made at day 31 for culture 2 of both strains. However, the OD_{600} of K10 culture 2 had already reached 0.8 by day 31 of culture (this OD_{600} equated to roughly 2.4 times as many CFU/ml as the same OD_{600} for culture 1), whereas the OD_{600} of C49 culture 2 was only 0.2. C49 culture 2 did not reach OD_{600}: 0.6 until day 62 of culture and, although the OD_{600} was lower than culture 1, the CFU/ml was higher (4.9×10^8 CFU/ml, compared to 3×10^8/ml) (Table 1). Culture 3 of both strains did not grow at all over a 7 week period (OD_{600} did not increase and no CFU were detected), whereas culture 4 of both strains grew considerably faster than previous cultures. K10 culture 4 OD_{600} reached 0.9 by 22 days in culture and C49 culture 4 OD_{600} reached 1.2 by 21 days in culture (Table 5). The variation in growth rates between cultures, and discrepancies in the number of CFU/ml correlating to specific OD_{600}

values, meant that calculation of CFU from actively growing cultures by OD_{600} was imprecise and impractical for establishing dose for infection experiments. Therefore, cultures were frozen in 100µl aliquots for use in infections to maintain consistency across multiple experiments.

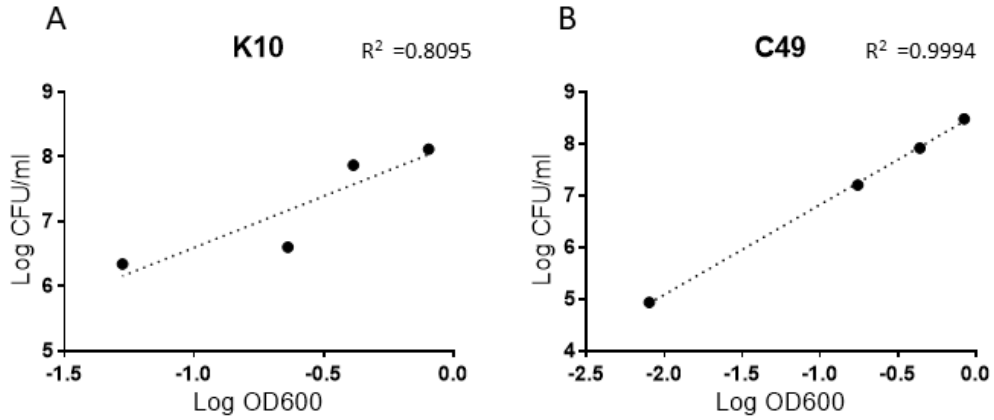

Figure 3-4 Growth of K10 and C49 MAP strains.

Growth curves were set up to assess the relationship between OD_{600} and CFU/ml for both K10 and C49 MAP strains(A) Growth curve comparing OD_{600} and CFU/ml for K10 culture 1. (B) Growth curve comparing OD_{600} and CFU/ml for C49 culture 1.

	K10			C49		
	Days in culture	OD600	CFU/ml	Days in culture	OD600	CFU/ml
Culture 1	35	0.8	1.30E+08	35	0.84	3.00E+08
Culture 2	31	0.8	3.10E+08	62	0.63	4.90E+08
Culture 3	didn't grow	N/A	N/A	didn't grow	N/A	N/A
Culture 4	22	0.9	2.00E+09	21	1.2	3.60E+09

Table 5: Comparison of the length of time required to grow K10 and C49 cultures to mid-log growth phase (OD_{600}: 0.6), and the correlation between observed OD_{600} readings and CFU/ml.

For K10 and C49 Culture 1, OD_{600} was measured at day 7, 21, 28 and 35, and reached 0.6 between days 28 and 35. Due to the OD_{600} exceeding 0.6 by day 35, the final measurement of K10 and C49 culture 2 was measured earlier, on day 31, however the OD_{600} of K10 Culture 2 had exceeded mid-log growth by this time-point. OD_{600} and CFU count of K10 and C49 Culture 3 did not increase over a 10-week period. The OD_{600} of K10 and C49 Culture 4 surpassed 0.6 by 22 and 21 days, respectively. The time taken to reach OD_{600}: 0.6 was, therefore, highly variable for both K10 and C49 MAP cultures. In addition, there was little correlation between OD_{600} reading and CFU/ml for either strain.

3.2.3 MAP strains remained viable post-freezing

As OD_{600} could not reliably predict CFU in actively growing cultures, 100µl aliquots of K10 and C49 cultures were frozen at -80ºC (as described in section 2.4.1). Qualitative analysis of the viability of these cultures, both before and after freezing, was carried out by staining with SYTO 9 and propidium iodide. SYTO9 is a cell-permeant nucleic acid stain; therefore, it is capable of staining both live and dead bacterial cells, whereas propidium iodide is a membrane impermeant nucleic acid stain, which will only stain cells with a damaged membrane. SYTO9 fluoresces green, however green fluorescence will be reduced in the presence of propidium iodide red fluorescence. A mixture of live (green fluorescence) and dead (red fluorescence) bacteria were observed in both cultures, both before and after freezing. There were increased numbers of dead cells in both cultures post freezing, however both K10 and C49 cultures presented a higher number of cells positive for green fluorescence, compared to red (Figure 3-5) suggesting the majority of bacteria remained viable.

Three aliquots of frozen cultures were thawed and plated on 7H10 agar plates in order to perform CFU counts. Formation of colonies confirmed that both K10 and C49 cultures remained viable post-freezing (data not shown). The mean CFU count obtained from each frozen culture was used to determine MOI for all downstream experiments.

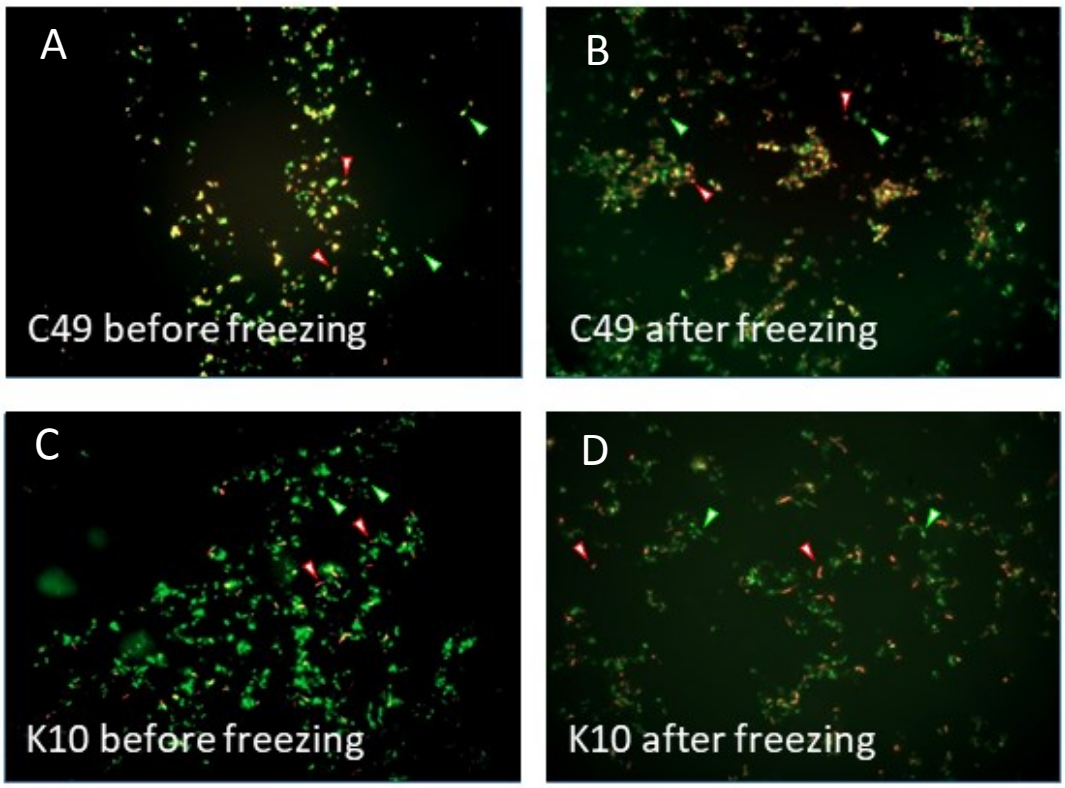

Figure 3-5 SYTO 9 and propidium iodide viability staining of MAP.

The viability of MAP cultures pre- and post-freezing was analysed using the viability stains SYTO9 and propidium iodide; results were analysed by fluorescence microscopy. Viable cells are depicted in green (SYTO9), whereas dead cells are shown in red (propidium iodide). (A) C49 viability before freezing. (B) C49 viability post-freezing. (C) K10 viability before freezing (D) K10 viability post-freezing. Examples of live bacteria are highlighted by green arrows and examples of dead bacteria are highlighted by red arrows.

3.2.4 Transforming C49 for GFP expression

GFP-expressing MAP strains would be a useful tool for this study, allowing differentiation between infected and bystander cells, as well as enabling analysis of intracellular trafficking. A K10 culture expressing GFP (K10:GFP) was kindly gifted by Dr Karen Stevenson, Moredun Research Institute. In order to obtain a C49 strain expressing GFP (C49:GFP), the C49 strain was transfected with the pWES4 plasmid, first constructed by Parker and Bermudez (Parker & Bermudez 1997) (Figure 3-2), and left to grow for 5 weeks, at 37ºC, on either 7H10 agar supplemented with 25µg/ml kanamycin or 7H10 agar without kanamycin (Figure 3-6 B). A lawn of C49 grew over the plate without kanamycin, whereas only 5 individual colonies appeared on the plate with kanamycin (Figure 3-6 B). These 5 colonies were positive for GFP expression, (determined by fluorescent microscopy) (Figure 3-6 C), making the transformation efficiency 5/1µg DNA. As a control for the transfection, C49 was electroporated in the absence of pWES4 and plated on to 7H10 agar plates either with or without 25µg/ml kanamycin. A lawn of C49 grew on the plate without kanamycin, whereas no colonies appeared on the plate with kanamycin (Figure 3-6 A), demonstrating that the transfection process did not affect bacterial viability and that in the absence of pWES4 MAP were susceptible to kanamycin. A sample of C49 electroporated in the absence of pWES4 was used as a negative control when determining GFP expression by fluorescent microscopy; no fluorescence was observed in these cells (Figure 3-6 D).

Individual colonies of C49-GFP were then transferred to 100µl volume of 7H9 supplemented with 25µg/ml kanamycin and broken up by vortexing and passing through a 21g needle. This was diluted into 5ml of the same media and incubated at 37ºC until mid-log growth phase ($OD_{600:}$ 0.6). Cultures were then aliquoted into 100µl volumes and frozen at -80ºC. The same procedure was carried out for the K10:GFP strain. MDM monolayers were infected with either K10:GFP or C49:GFP, at MOI 5, and uptake of bacteria measured by flow cytometry. MDM infected with K10:GFP or C49:GFP did not have increased percentages of cells positive for GFP, compared to uninfected controls (Figure 3-6 E-G). Therefore, 5µl volumes of

K10:GFP and C49:GFP frozen stocks were pipetted onto glass slides and visualised by fluorescence microscopy; no GFP fluorescence was observed (data not shown), demonstrating a loss of GFP expression from both K10 and C49 frozen liquid cultures.

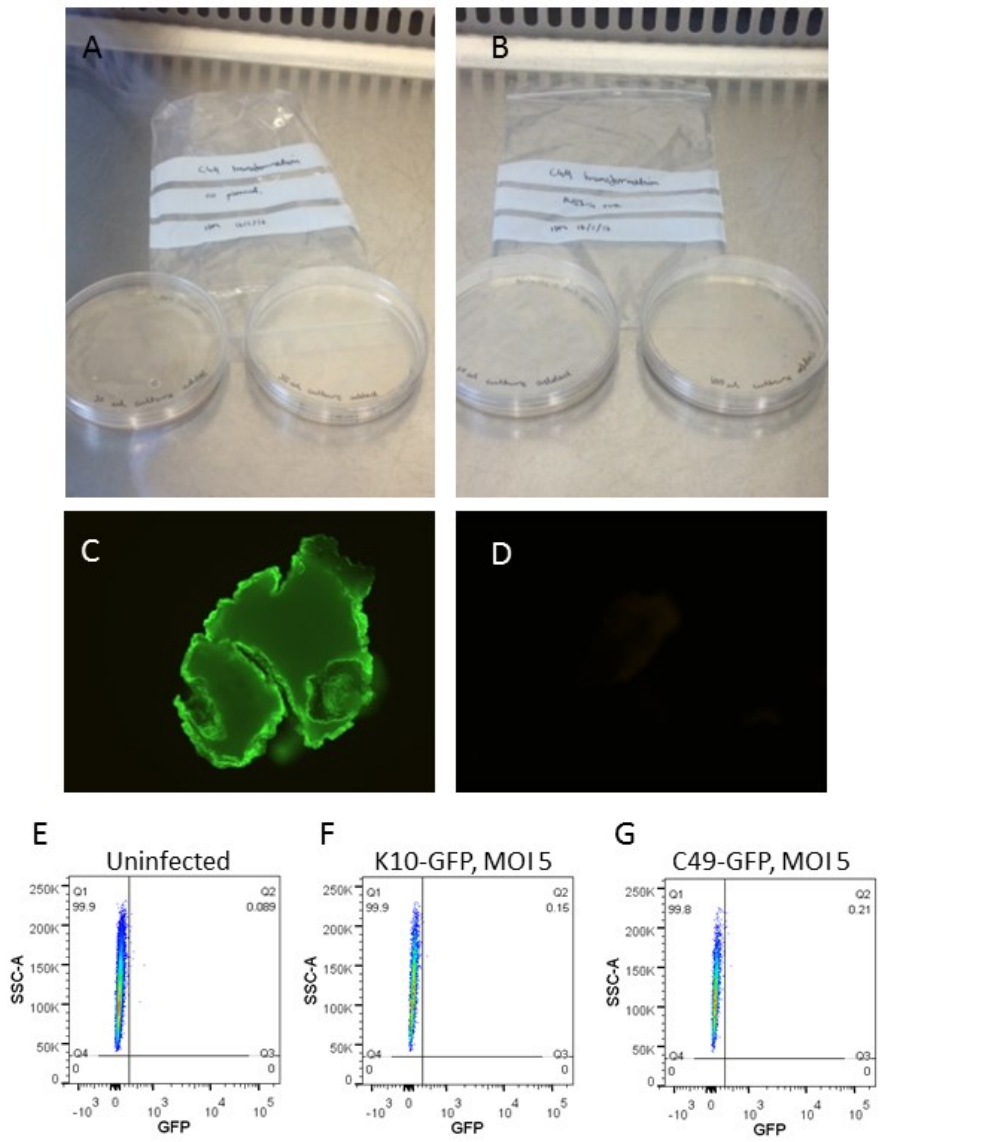

Figure 3-6 Transforming MAP strain C49 to express GFP.

C49 were transfected with the pWES-4 plasmid with the aim of obtaining a GFP-expressing strain. (A) C49 put through the transfection process in the absence of pWES-4 plasmid and plated on to 7H10 agar supplemented with kanamycin (right) or 7H10 agar without kanamycin (left). (B) C49 put through the transfection process in the presence of pWES-4 plasmid and plated on to 7H10 agar supplemented with kanamycin (right) or 7H10 agar without kanamycin (left). Together, A & B demonstrate that the transfection of the pWES-4 plasmid was successful and conferred specific resistance to kanamycin. (C) Fluorescence microscopy image of a C49 colony transfected with pWES4, excited at 490–520 nm (D) Fluorescence microscopy image of scraping of C49 cells electroporated in the absence of pWES-4, visualised at 490–520 nm. MDM were infected with transfected K10 and C49 MAP strains and bacterial uptake assessed by flow cytometry: (E) Uninfected MDM. (F) MDM infected with K10:GFP at MOI 5. (G) MDM infected with C49:GFP at MOI 5. Gating strategy is demonstrated in Figure 3-3. N =1

3.2.5 Determining confluence of infection

3.2.5.1 MAP infection of MDM visualised by confocal microscopy

Confocal microscopy was employed to visualise and quantify (see section 3.2.6.4) MAP infection of MDM. In order carry out confocal microscopy, DNA was stained with DAPI (blue), f-actin with phalloidin 488 (green) and MAP with an anti-mycobacteria polyclonal antibody raised in guinea pig, and an anti-guinea-pig secondary antibody conjugated to CF568 (red) (for details of antibodies see Appendix E). The use of this method to stain MAP gave positive and specific staining, demonstrated by the presence of red fluorescence in MAP infected monolayers (Figure 3-7A) and absence of red fluorescence in uninfected monolayers (Figure 3-7 B). In order to quantify the number of intracellular MAP in each image, a Z-stack was compiled by capturing images every 1μm vertically through the cell (Figure 3-7 C). Maximum Intensity Projections of each Z-stack were then created in order to perform quantitative analysis (Figure 3-7 D). For quantitative analysis, to determine infection confluence, MDM were infected with K10 at MOI 5, 20 or 50, washed at 0.5 HPI and multiple Z-stack images were captured at random areas across the infected monolayers (Figure 3-8 A, B and C, respectively). The total number of MDM, and the number of MDM positive for MAP, in each image was then counted. Percentage confluence was determined by counting a minimum of 50 MDM for each MOI. All 3 MOIs gave >70% confluence (representative images shown in Figure 3-8), with higher doses tending to increase the number of MAP per cell, as opposed to increasing the number of cells infected (Figure 3-8 A, B & C).

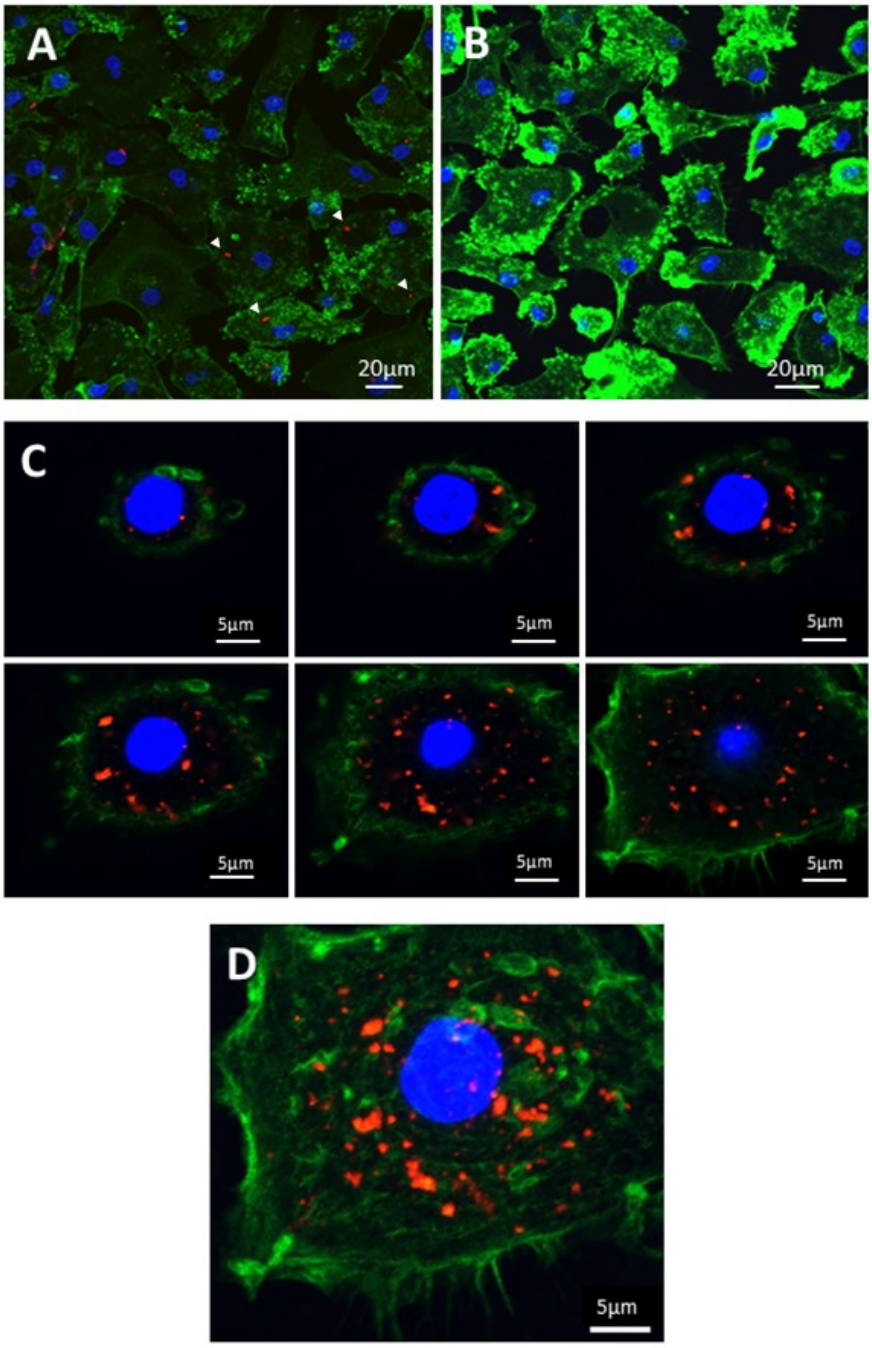

Figure 3-7 Confocal images of MDM infected with K10.

Confocal microscopy was employed as a method to visualise MAP infection of MDM. Infected MDM monolayers were stained by immunohistochemistry and visualised by creating a Z-stack, with images captured vertically every 1µm through the monolayer; these images were then compiled into Maximum Intensity Projections in order to visualise all bacteria present intracellularly. (A) Maximum Intensity Projection of a MAP infected MDM monolayer, examples of positive MAP staining are indicated by white arrows. (B) Maximum Intensity Projection of an uninfected

MDM monolayer (C) Z-stack of images taken at 1μm distances vertically through a cell. (D) Maximum Intensity Projection of all the images shown in C. Green = f-actin, Blue= nuclei, red =MAP.

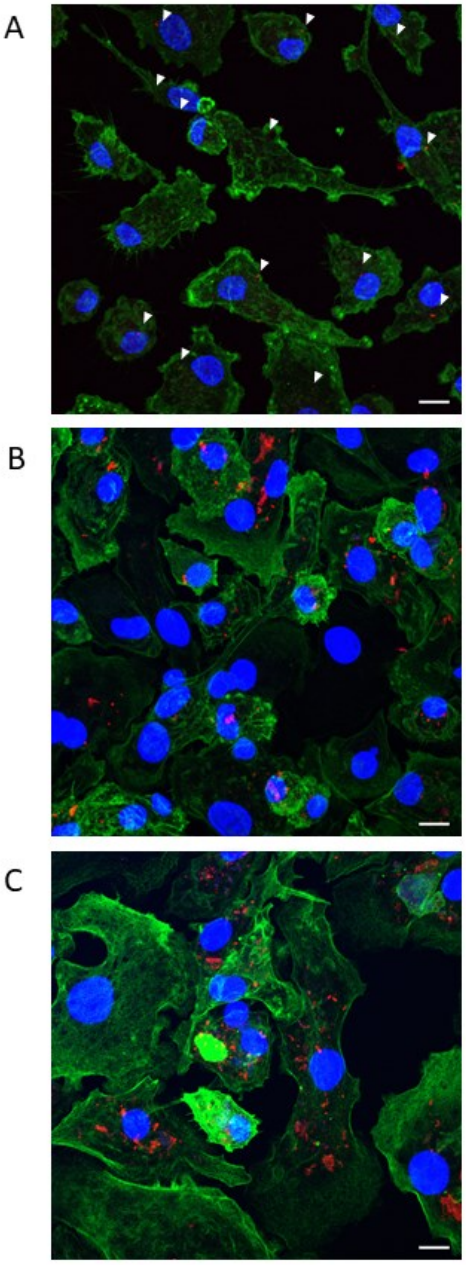

Figure 3-8 Determining infection confluence by confocal microscopy.

Confocal microscopy was employed as a method to determine the confluence of MAP infection. MDM monolayers were infected with K10 at MOI 5, 20 or 50, and Maximum Intensity Projections of infected monolayers were created as described in Figure 3.7 (A) Representative image of MDM monolayer infected with K10 at MOI 5. White arrows indicate the presence of MAP. (B) Representative image of MDM monolayer infected with K10 at MOI 20. (C) Representative image of MDM monolayer infected with K10 at MOI 50. A minimum of 50 MDM were assessed for each biological replicate (MOI 5 & MOI 20: N=3, MOI 50: N=1). Error bars = 10µm. Blue = nuclei, green = f-actin, red = MAP.

3.2.5.2 MDM uptake of FITC-labelled MAP by flow cytometry

Flow cytometry was investigated as a method to determine confluence of MAP infection, in comparison to confocal microscopy, as it is a highly efficient method that allows analysis of the entire sample. In order to analyse uptake by flow cytometry, MAP strains K10 and C49 were labelled with 0.2mg/ml FITC solution prior to infection. MDM monolayers were infected with either strain at MOI 5 and incubated at 37ºC until 0.5 HPI. Monolayers were then washed 3x with PBS and uptake of MAP was assessed by flow cytometry. Uptake of MAP by MDM grown from 2 animals were tested. MDM from animal 24 had very low levels of uptake, with 2.1% K10 infected MDM and 4.3% C49 infected MDM positive for FITC fluorescence (indicating the presence of intracellular MAP) (Figure 3-9 A & B). Higher levels of MAP uptake were observed in MDM from animal 17, with 11.1% and 13.1% MDM positive for K10 and C49, respectively (Figure 3-9 C& D).

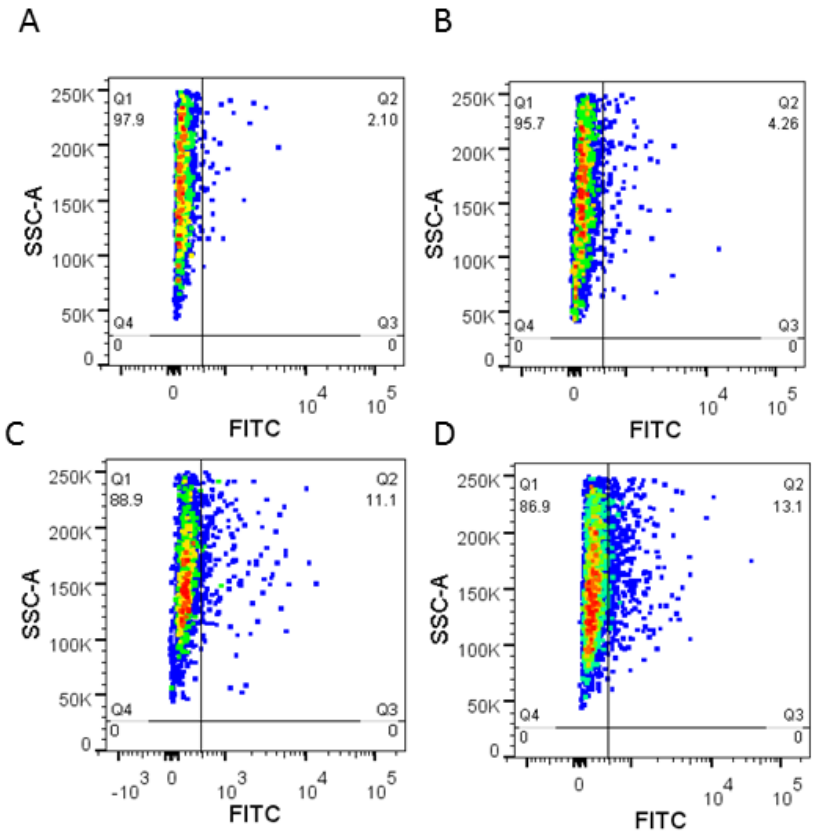

Figure 3-9 Uptake of FITC stained MAP by MDM.

The uptake of FITC-labelled K10 and C49 by MDM was determined by flow cytometry. MDM were obtained from 2 biological replicates, Animal 24 and Animal 17, and were gated as demonstrated in Figure 3-3 (A) Animal 24 infected with FITC labelled K10 at MOI 5. (B) Animal 24 infected with FITC labelled C49 at MOI 5. (C) Animal 17 infected with FITC labelled K10 at MOI 5. (D) Animal 17 infected with FITC labelled C49 at MOI 5. Numbers refer to the percentage events in each gate.

3.2.5.3 MDM uptake of FITC-labelled MAP assessed by live-cell imaging

In order to understand the low percentages of MDM positive for FITC fluorescence in Figure 3-9, uptake of FITC labelled MAP by MDM was visualised by live-cell imaging. Briefly, MDM were plated in 24 well plates at $2x10^5$ cells/well and cultured for 48 hours in 1ml TCMd (Appendix A). 24 hours after seeding MDM into 24 well plates Dextran Alexa Fluor 647 (AF647) was added to monolayers at a final concentration of 20µg/ml and monolayers were incubated at 37ºC overnight. Monolayers were then washed 3x and pHrodo Red Dextran added at final concentration of 40µg/ml. Regions of interest (ROIs) on the monolayer were set up on the Zeiss Live Cell Imager with the 40x objective lens prior to the addition of bacteria. ~$1x10^6$ CFU of FITC labelled K10 were suspended in 10µl TCMd and added to the MDM monolayer immediately prior to imaging. Images of the selected ROIs were captured every 3 minutes until 2 HPI. The imaging time-course demonstrated that MDM took up MAP rapidly, with one MDM positive for intracellular MAP at only 3 minutes post infection (MPI) (Figure 3-10 B). However, FITC fluorescence was rapidly quenched intracellularly; two MDM were positive for intracellular FITC fluorescence at 6 MPI but absent of FITC 12 MPI (Figure 3-10 C & E).

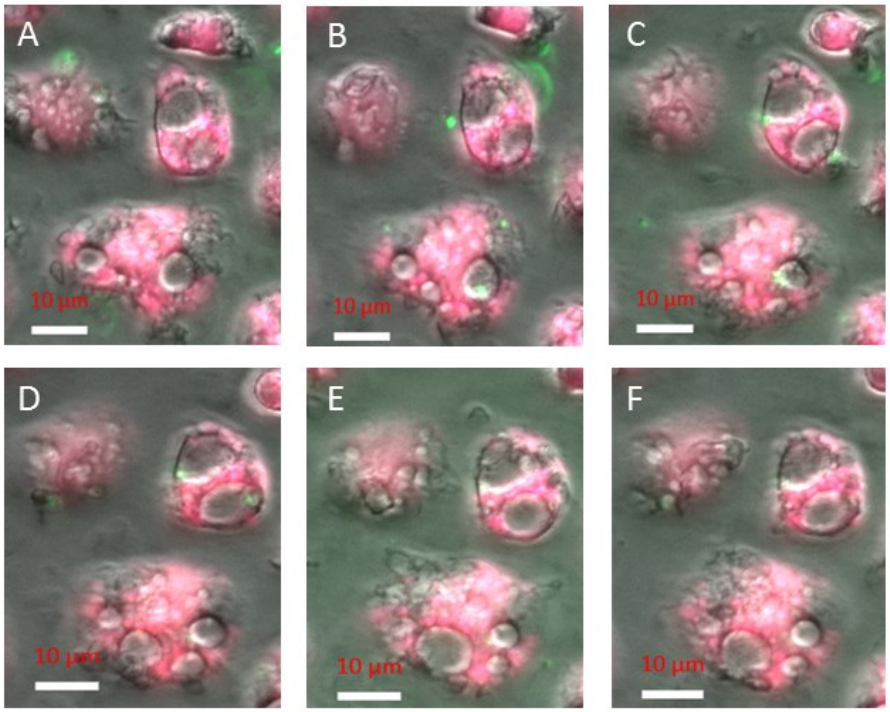

Figure 3-10 Live cell imaging time-course of MAP uptake by MDM.

The MDM monolayer was stained by incubation with fluorescent dextrans prior to imaging. In order to observe phagocytosis of MAP, an ROI on the MDM monolayer was set up on the Zeiss Live Cell Imager, prior to FITC-labelled K10 being added to the monolayer at MOI 5. An image of the ROI was captured every 3 minutes in order to observed the process of bacterial uptake by MDM (A) 0 minutes post infection. (B) 3 MPI. (C) 6 MPI. (D) 9 MPI. (E) 12 MPI. (F) 15 MPI. Green = K10 strain of MAP. Pink = AF647 dextran and pHrodo dextran.

3.2.6 Establishing and comparing different methods to quantify MAP infection of MDM

The long generation time of MAP makes quantifying bacterial numbers by traditional colony counting a slow process. An aim of this chapter was therefore to compare other quantification methods with colony counting, to determine the most reliable and efficient method of quantifying MAP infection of MDM. In order to address this, 3 quantification methods were tested and compared to colony counting: a bacteriophage amplification assay, qPCR and confocal microscopy.

3.2.6.1 Phage Amplification Assay

D29 phage and *M. smegmatis* were kindly provided by colleagues at the University of Nottingham. The virucide ferrous ammonium sulphate hexahydrate was bought in powder form and made up to 5mM in distilled H_2O. The efficacy of this virucide was first tested on control plates. The positive control contained both *M. smegmatis* and D29 phage; the positive control demonstrates that the phage is viable and able to infect and lyse bacteria; therefore, full lysis of the *M. smegmatis* lawn should occur. The negative control contained only D29 phage diluted in 7H9/2mM $CaCl_2$ and should result in an intact lawn of *M. smegmatis*, showing that the virucide effectively inactivates the phage and that plaques are formed only in the presence of MAP (see Figure 3-1).

Use of 5mM virucide resulted full lysis of both the positive control plate and the negative control plate (Figure 3-11 A). This result indicated that the concentration of virucide was too low to inactivate the phage. Virucide was therefore titrated to find the optimal concentration for the assay. 5, 10, 20, 40 and 50mM concentrations of ferrous ammonium sulphate were tested. At 5 and 10mM, the negative control plates were either fully lysed, or mostly lysed (plates that are mostly lysed are referred to as 'lacy' plates, and are highlighted by red arrows in Figure 3-11), whereas at 20-50mM no plaques were formed on the negative control plates and the positive control plates were lacy (Figure 3-11 B). A concentration of 20mM ferrous ammonium sulphate

was therefore considered sufficient for phage inactivation. However, in subsequent assays, plaques appeared in the negative control plates when virucide was included at 20mM (Figure 3-11 C). The concentration of virucide was again increased to achieve effective inactivation of the phage; however, plaques would sporadically appear on negative controls even with virucide concentration increased to 50mM (data not shown). Therefore, this method was not further investigated.

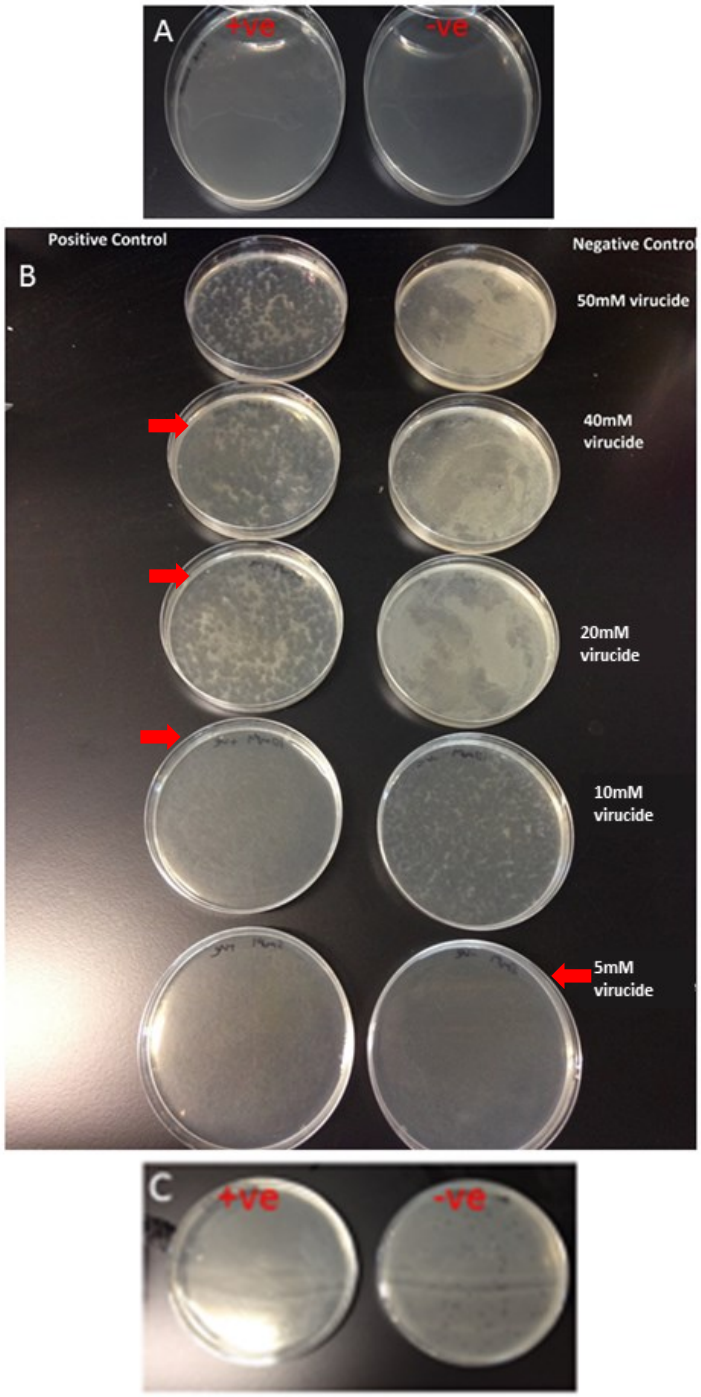

Figure 3-11 Optimisation of the Phage Amplification Assay.

The phage amplification assay was optimised by testing a range of concentrations of the virucide ferrous ammonium sulphate hexahydrate. The optimal concentration should result in no plaques forming on the negative control (demonstrating effective inactivation of the phage by the virucide prior to addition of an M. smegmatis lawn), and full lysis of the positive control plate (demonstrating the ability of the phage to lyse mycobacteria cells) (A) Positive and negative controls using virucide at 5Mm,

demonstrating full lysis of both. (N=2) (B) Titration of virucide, testing a range of concentrations from 5mM – 50mM. Positive controls are shown on the left and negative controls on the right (N=2) (C) Positive and negative controls using 20mM virucide, demonstrating a failed negative control at this concetration.(N = 5).

3.2.6.2 Optimising DNA extraction from MAP infected MDM

qPCR can be used to quantify MAP infection by comparing the number of MAP genomes to the number of bovine genomes. Therefore, in order to accurately use qPCR to quantify MAP infection, DNA extraction from bovine MDM had to be optimised. Four methods of extracting DNA from MDM monolayers were tested. The methods tested are detailed in Table 2 and include cetyl trimethylammonium bromide (CTAB), TRIzol reagent, Wizard® Genomic DNA Purification Kit by Promega, and the Qiagen DNeasy Blood and Tissue kit. Triplicate samples of MDM were removed from tissue culture plates for testing with each method (for details of methodology see section 2.16). DNA extraction by CTAB gave variable concentrations between technical replicates, with the 2nd replicate returning only ~1% of the DNA of the first replicate. DNA extraction by TRIzol reagent gave the lowest concentrations. The Promega kit gave less variable results than the CTAB method, however the concentrations were lower and the 260/230 ratios were highly irregular, potentially indicating the presence of salt contaminants. A 260/280 ratio ~1.8, and 260/230 ratio ~2 are indicative of a pure DNA sample, free from contaminants that absorb at either 280nm or 230nm, such as protein or phenol. The Qiagen DNeasy blood and tissue kit returned the highest concentrations of DNA (although there was variation between samples). DNA extraction with the Qiagen DNeasy kit also resulted in purer DNA samples, compared to the other methodologies, indicated by 260/280 ratios, although 260/230 ratios remained lower than ideal (Table 6). Collectively these results suggested that, of the 4 methods tested, the Qiagen DNeasy Blood and Tissue kit was the most reliable method for extracting DNA from MDM.

DNA extraction method	DNA conc. in ng/µl	260/280 ratio	260/230 ratio
cetyl trimethylammonium bromide (CTAB)	73.5	1.3	0.76
	0.71	0.86	0.65
	13.56	0.97	1.1
TRIzol Reagent	0.4	0.78	0
	-0.16	0.11	-0.02
	1.34	1.68	0.02
Promega Wizard kit (A1120)	9.6	2.4	-102.45
	10.4	2.44	123.06
	17.18	2.14	4.32
Qiagen Dneasy Blood and Tissue kit (ID:69504)	27.22	2.08	1.25
	111.38	1.51	0.73
	45.86	1.68	0.89

Table 6: Concentration of DNA extracted by several different methods from $2x10^5$ MDM.

260/280 and 260/230 ratios refer to the purity of the DNA sample. Optimal 260/280 ratio = 1.8, optimal 260/30 ratio = 2

Use of the Qiagen DNeasy kit was further optimised for MAP DNA extraction, in addition to bovine DNA extraction, using MDM infected with C49 at MOI 20, in order to extract high concentrations of DNA from both species simultaneously, and reduce variability between replicates. The concentration of DNA extracted from MAP infected MDM, was significantly increased by including an additional lysis step in the extraction process (Figure 3-12). Briefly, samples were incubated in 180µl enzymatic lysis buffer (containing lysozyme) (see Appendix B) at 37°C for 2 hours. 25µl proteinase K and 200µl buffer AL (supplied with DNeasy Blood and Tissue kit) were then added and incubated at 50ºC for 1 hour. Extraction was then carried out as detailed by the manufacturer's instructions. Further extractions, using this method, on MDM infected with K10 or C49 at MOI 5 or 20, demonstrated reduced variation between technical replicates (Table 7), compared to the first DNA extraction attempt using the Qiagen DNeasy kit alone (Table 6), although some variation was still present.

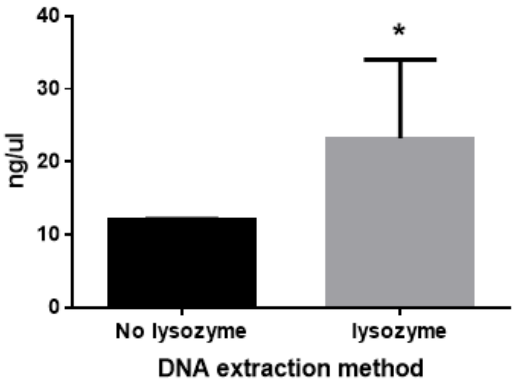

Figure 3-12 Optimisation of DNA extraction.

*Concentration of DNA extracted at 2 HPI from MDM infected with C49 at MOI 20, by Qiagen DNeasy Blood and Tissue Kit (black bar) (N-=3) and Qiagen DNeasy Blood and Tissue kit with additional lysis step (grey bar) (N=5). Bars represent mean and standard deviation of technical replicates. Data were normally distributed ($p>0.05$) and analysed by 2-sample t-test. $P<0.05$**

Sample	ng/ul	260/280	260/230
K10, MOI 5 a	21.99	1.86	1.05
K10, MOI 5 b	19.67	1.95	1.45
K10, MOI 5 c	33.88	1.59	0.85
K10, MOI 20 a	17.44	1.88	1.35
K10, MOI 20 b	34.4	1.66	0.87
K10, MOI 20 c	14.19	2.26	1.82
C49, MOI 5 a	15.79	2.1	1.7
C49, MOI 5 b	29.61	1.68	0.88
C49, MOI 5 c	21.12	1.65	1.1
C49, MOI 20 a	15.11	1.86	1.82
C49, MOI 20 b	18.64	2.03	1.27
C49, MOI 20 c	29.35	1.73	1.06
uninfected	14.52	1.99	0.73

Table 7: DNA concentrations and ratios using Qiagen DNeasy kit with additional lysis step.

MDM were infected with K10 or C49 at MOI 5 or 20 (as indicated), and DNA extracted at 2 HPI by use of Qiagen DNeasy Blood and Tissue kit, with additional lysis step. 260/280 and 260/230 ratios refer to the purity of the DNA sample. Optimal 260/280 ratio = 1.8, optimal 260/30 ratio = 2. a, b and c refer to technical replicates.

A PCR was run to test that both bovine and MAP DNA were present after DNA extraction by the Qiagen DNeasy kit with additional lysis step, from MDM infected with C49 at MOI 20. Primers targeting GAPDH in the bovine genome and F57 in the MAP genome were used. F57 is a sequence unique to MAP and present only once in the genome, making it an effective target for qPCR. F57 primers designed for qPCR (amplifying a 90bp product) were used in this PCR in order to test their specificity. PCR products were run on a 2% agarose gel and a band can be seen for both F57 and GAPDH, with no bands appearing in negative controls (PCR master mix + H_2O) (Figure 3-13)

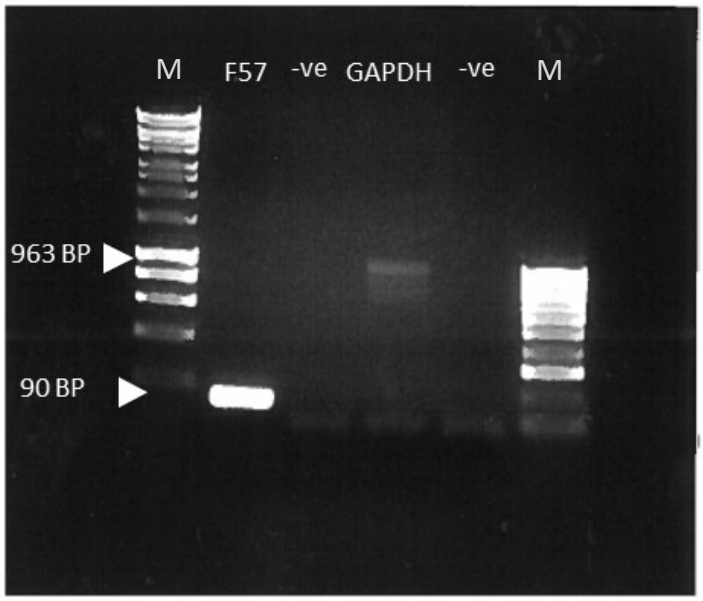

Figure 3-13: Agarose gel electrophoresis of F57 and GAPDH PCR products.

DNA was extracted from MDM infected with C49 at MOI 20 and a PCR run using primers targeting the MAP F57 insertion sequence and bovine GAPDH. PCR products were run on a 2% agarose gel, demonstrating that they were the correct size (F57=90bp, GAPDH = 963bp). Representative image (N=2).

3.2.6.3 Quantitative polymerase chain reaction

qPCR was used as a method to quantify MAP infection of MDM. Briefly, MDM were infected with either K10 or C49 at MOI 5 or 20. DNA was extracted from samples at 2 HPI, using the Qiagen DNeasy kit, with the additional lysis step, as described in section 3.2.6.2. Optimised concentrations of primers targeting the F57 insertion sequence of MAP, or the bovine gene SPAST, were added to Agilent Brilliant III Ultra-Fast SYBR Green qPCR master mix, along with ROX reference dye and H_2O. SPAST was selected for the qPCR as it is known to be single copy gene and has been previously utilised as a control gene in a published study (Fadista et al. 2010). 7.5µl master mix was added to 2.5µl genomic DNA sample and the qPCR reaction run as described in section 2.17. F57 and SPAST primers used for qPCR were designed to produce a product ~100bp in length. Serial dilutions of F57 and SPAST PCR products (400-1000bp in length), produced from primers that flank qPCR primers, were included in order to produce a standard curve to demonstrate the efficiency of the reaction. A dissociation curve was included in the reaction set up; Figure 3-14 A & B depict the dissociation curves of F57 and SPAST, respectively - the single peak indicates that a single product was produced for both F57 and SPAST, complementing the results for the F57 primers demonstrated in Figure 3-13. The efficiency of the reaction was calculated using the equation of the standard curves (Figure 3-14 C). R^2 values indicate the accuracy of the standard curves; $R^2=1$ indicates that 100% of values are predicted to fall on the equation of the line. R^2 values ranged between 0.9857 - 0.9997 for F57, and 0.998 – 0.9995 for SPAST. The efficiency of the reactions ranged from 1.9-2 for F57 and 1.98-2 for SPAST. The efficiency was used to calculate MAP GCN relative to bovine GCN, using the Pfaffl method (Pfaffl 2001). Bovine GCN was estimated based on cell counts prior to infection, and was relatively consistent when measured by qPCR, indicating little bovine cell death or growth (data not shown). A clear dose effect was observed for both K10 and C49 GCN, with MOI 20 returning a GCN an average of 5.3x and 4.6x higher than MOI 5, for K10 and C49, respectively. There were no significant differences between C49 and K10 GCN at either dose (Figure 3-14 D).

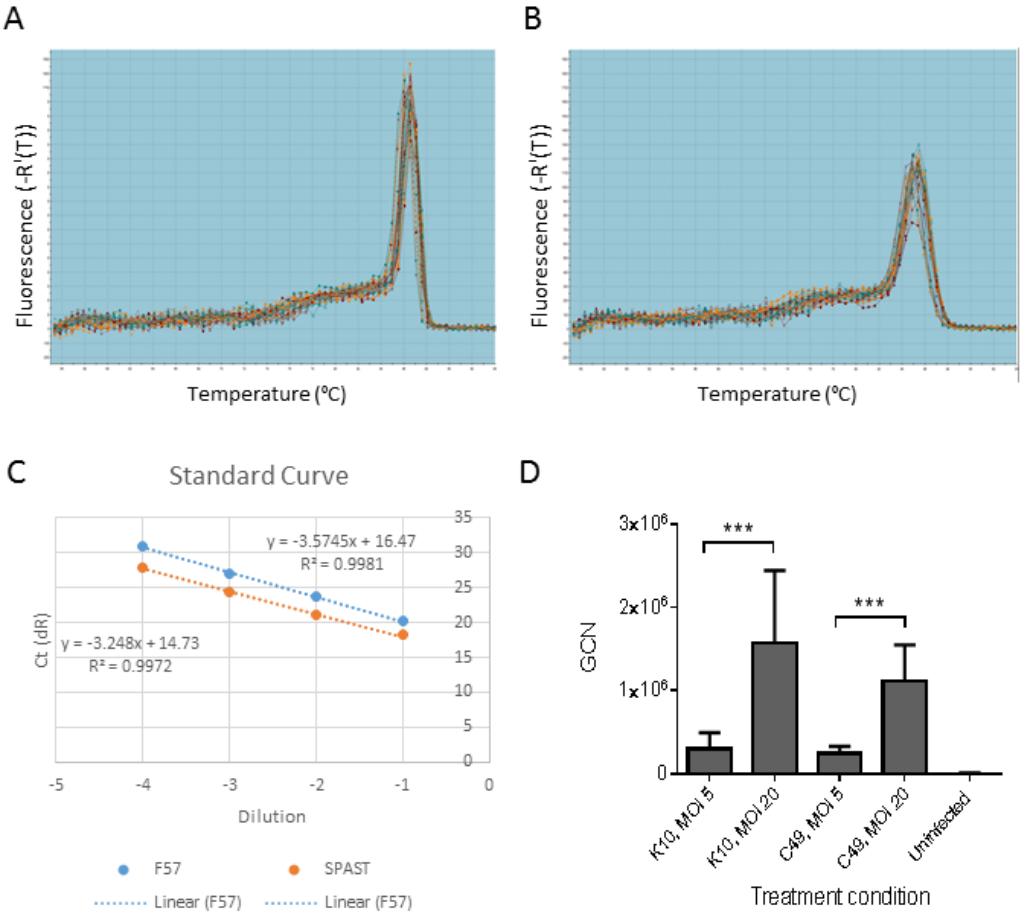

Figure 3-14 quantifying MAP infection of MDM by qPCR.

*The number of MAP genomes within an infected monolayer was calculated, relative to the number of bovine genomes, by qPCR. Primers targeting the MAP-specific F57 insertion sequence, and the single copy bovine SPAST gene were used, and MAP GCN calculated using the Pfaffl method. (A) Representative F57 dissociation curve, demonstrating specificity of F57 primers. (N=3) (B) Representative SPAST dissociation curve, demonstrating specificity of SPAST primers. (N=3) (C) Representative F57 and SPAST standard curves, produced from serial dilutions of F57 and SPAST PCR products. (N=3) (D) Mean MAP GCN at 2HPI. (N=3 biological replicates). Data were non-normally distributed ($p<0.05$) and analysed by Mann-Whitney tests. $p<0.001$****

3.2.6.4 Quantification by microscopy

Confocal microscopy was developed as a method to quantify the number of bacteria present in an infected sample. Bacterial numbers were presented as 'per well' instead of 'per cell' to allow for uneven infection and/or bovine cell death, and so that numbers could be easily compared to CFU count from simultaneously infected samples (see section 3.2.6.5). Briefly, MDM were infected with either K10 or C49 at MOI 5 or 20, until 2 HPI. The methodology of staining the monolayers and capturing the images was as described in section 3.2.5.1, and resulted in maximum intensity projections of Z-stacks, which were used for quantitative analysis. A minimum of 50 MDM, from random and varied regions of the coverslip, were visualised for each condition, and used to extrapolate the total number of bacteria within an infected sample; this methodology was used to limit inaccuracies caused by uneven infection or cell survival across the well. Image analysis was carried out using Zen Blue and ImageJ software. The number of pixels positive for MAP staining was calculated and converted into μm^2 positive for MAP staining (based on the area of 1 pixel). This was then divided by the average size of 1 MAP bacterium in μm^2 (Wu et al. 2009), to give the average number of MAP/image. The results were highly variable between technical replicates (i.e. there was high variability between individual images for each condition). There was also significant variation between biological replicates (general linear model: $p<0.05$; data not shown), however, this biological variation was not unique to the microscopy method of quantification, as variation between biological replicates was observed for all methodologies tested. Confocal microscopy analysis provided average bacterial numbers greater than CFU but lower than GCN for K10 infected MDM at either MOI 5 or 20 (Figure 3-15 A & C), and bacterial numbers higher than both CFU and GCN for C49 at MOI 5, but only higher than CFU for C49 at MOI 20 (Figure 3-15 E & G). No reliable correlation was observed between CFU and microscopy numbers or between GCN and microscopy numbers when looking at individual biological replicates (Figure 3-15 B, D, F and H). For example, for MDM infected with C49 at MOI 5, microscopy results in bacterial numbers higher than GCN number for one biological replicate (purple), but lower than CFU for another biological replicate (blue) (Figure 3-15 F).

3.2.6.5 Comparison of different methods to quantify infection of MDM

Once the quantitation methods had been developed and assessed, MDM were infected with MAP strains K10 or C49 at MOI 5 or 20 and a comparative study was carried out examining the number of bacteria per well, as determined by qPCR, microscopy, and CFU count at 2 HPI. The phage amplification assay was not included as this proved to be unreliable due to assay control failures (see section 3.2.6).

The mean GCN (measured by qPCR) was significantly higher than CFU count for all conditions (Figure 3-15 A, C, E & G). However, it should be noted that the difference between GCN and CFU was greater for MDM infected with the K10 strain versus the C49 strain, at both MOI 5 and 20. GCN gave an average of 42.7x more K10/well (MOI 5) and 56.8x more K10/well (MOI 20), compared to CFU count, whereas GCN gave an average of 4.9x more C49/well (MOI of 5) and 6.6x more C49/well (MOI 20), compared to CFU (Figure 3-15 E & G).

Quantification by microscopy gave significantly higher numbers of bacteria/well, for K10 infected MDM but not C49 infected MDM (MOI 5 and 20), compared to CFU counts. At MOI 5, K10 numbers were an average of 10.4x higher when quantified by microscopy compared to CFU, while C49 numbers were only slightly increased compared to CFU count, and the difference was not significant (Figure 3-15 A & E). At MOI 20, K10 numbers were an average of 16.4 times higher when quantified by microscopy compared to CFU ($p<0.001$), whereas C49 numbers were not significantly different when comparing the same methodologies (Figure 3-15 C & G).

Although microscopy returned increased K10 numbers compared to CFU, these numbers were significantly lower than GCN for K10 at MOI 5 ($p<0.05$) and 20 ($p<0.001$). However, the difference between K10 numbers determined by microscopy and GCN was not as pronounced as the differences between GCN and CFU; K10 numbers were, on average, 2.1 and 4.1 times higher (MOI of 5 and 20, respectively) when determined by qPCR, compared to microscopy (Figure 3-15 A &C). The same effect was not observed for C49 infected MDM; at MOI 5, C49 numbers were 3.7x higher when determined by microscopy compared to GCN

($p<0.05$), and at MOI 20, there was no significant difference between C49 numbers determined by microscopy and GCN. The increase in mean bacterial numbers determined by microscopy for C49 at MOI 5 can be attributed to a large degree of variation between biological replicates (Figure 3-15 F).

The mean number of bacteria/well for each biological replicate is shown for K10 MOI 5 (Fig 3.14 B), K10 MOI 20 (Fig. 3.14 D), C49 MOI 5 (Fig. 3.14 F) and C49 MOI 20 (Figure 3-15 H). There were statistically significant differences between biological replicates for each quantification method ($p<0.05$). Quantification by CFU count gave the least variation between biological replicates, whereas quantification by microscopy and qPCR demonstrated more variation between biological replicates for all treatment conditions. No reliable or reproducible correlation existed between the different methods of quantitation.

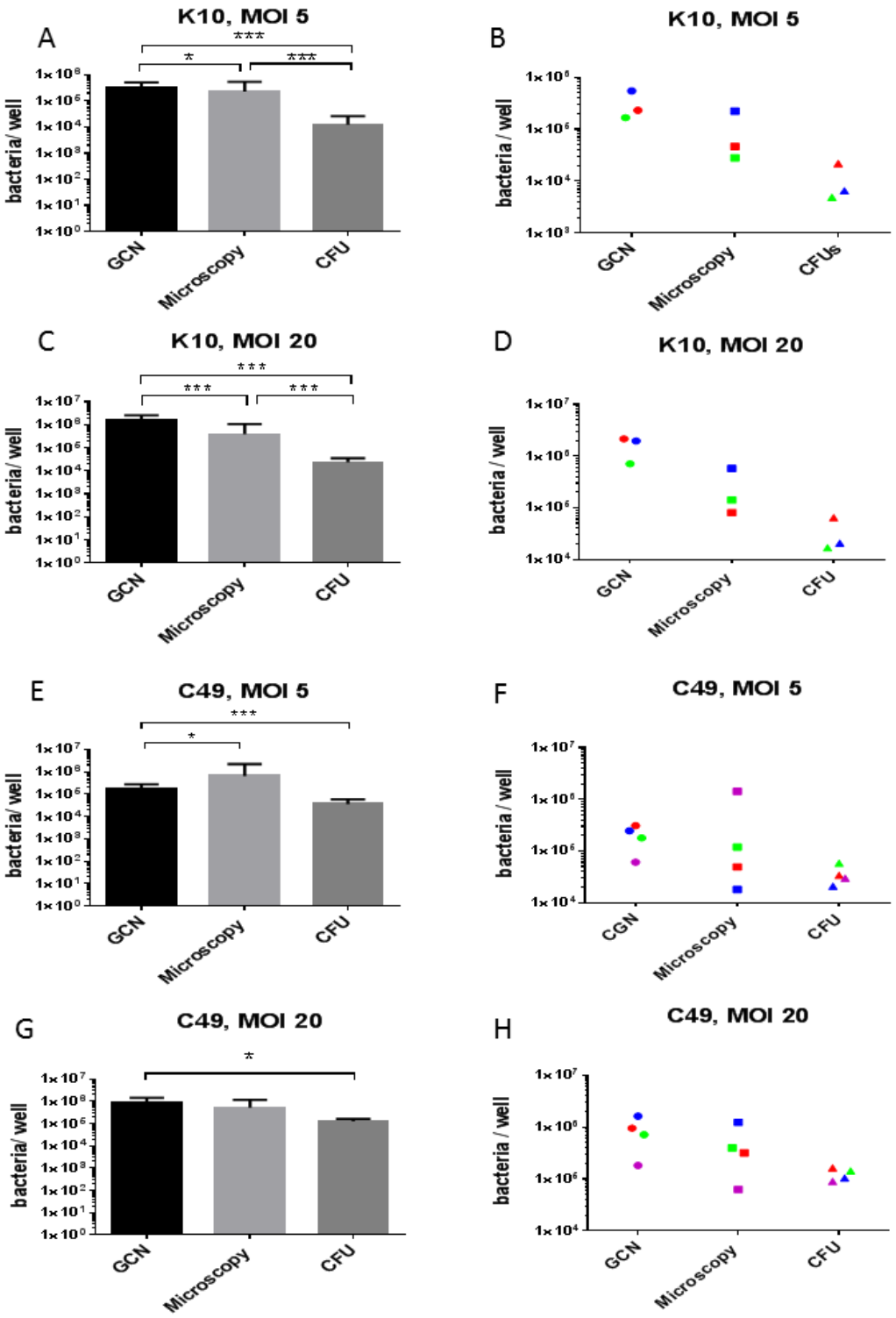

Figure 3-15 Comparison of different methods to quantify MAP infection of MDM.

The mean (±SD) number of bacteria/well as calculated by qPCR, confocal microscopy or performing CFU counts, is shown for MDM infected with K10 (MOI

5), K10 (MOI 20), C49 (MOI 5), and C49 (MOI 20)(A, C, E & G, respectively). The mean bacterial number per well for each biological replicate is demonstrated for MDM infected with K10 (MOI 5), K10 (MOI 20), C49 (MOI 5), C49 (MOI 20) (B, D, F & H, respectively). K10 infected MDM: N=3, C49 infected MDM: N=4. Colours represent individual biological replicates. Data were normally distributed ($p>0.05$) and analysed by GLM (A) or non-normally distributed ($p<0.05$) and analysed by Kruskal Wallis and Mann-Whitney tests (C, E and G). $p<0.05$, $p<0.01$**, $p<0.001$****

3.3 Discussion

This chapter established methodologies essential for the completion of this body of work.

The method used to culture MDM resulted in relatively pure MDM cultures, with a mean 95.58% cells positive for expression of the macrophage-associated cell surface molecule CD14. However, there was a high level of sub-cellular debris for all biological replicates (Figure 3-3), likely caused by the method of dissociation from the plastic (Volovitz et al. 2016). TrypLE Express and light scraping were used to dissociate cells; TrypLE express is a gentler alternative to Trypsin, however use of a non-enzymatic dissociation buffer without scraping may have reduced the percentage of debris further.

Throughout this project, MAP strains were cultured by diluting 100µl aliquots of a glycerol stock of each strain (grown from single colonies and frozen at -80ºC) into 10ml 7H9+Mycobactin J. Accurately quantifying the number of bacteria in a culture was crucial, so as to maintain consistency and understand dose-effect during infection experiments. It was originally hypothesised that numbers of MAP could be accurately estimated from actively growing cultures prior to infection experiments using OD_{600} spectrophotometer readings. OD_{600} readings measure the absorbance of light at a wavelength of 600nm, and as mycobacteria absorb light at 600nm (Kralik et al. 2012), the OD_{600} reading is indicative of the density of a mycobacterial culture. Measuring OD is a commonly used method to quantify bacteria and has previously been used to quantify liquid cultures of MAP and other mycobacterial species (Peñuelas-Urquides et al. 2013; Kralik et al. 2012; Janagama et al. 2006).

A simple linear regression model, comparing OD_{600} readings to CFU count for both K10 and C49 cultures, returned R^2 values of 0.8095 and 0.9994, respectively. The R^2 value is a statistical measure of how close data falls to a fitted regression line, and therefore how much variance is accounted for by the regression model. For example, if $R^2 = 1$, then 100% of data points would fall upon the regression line, whereas if $R^2 = 0.45$, then the fitted regression line would only account for 45% of the variance. The OD_{600} measurement for C49 could therefore accurately predict the number of

C49 CFU; however, it would provide a less accurate estimate for K10 CFU. This is likely due to the increased clumping of the K10 culture, compared to C49. Although care was taken to eliminate clumps as much as possible (for both strains) visible clumps were observed in the K10 liquid culture. Large clumps of bacteria can cause light to scatter differently, therefore cultures prone to clumping (such a mycobacterial cultures) can often provide unreliable OD_{600} readings.

Although linear regression showed that OD_{600} reading could accurately predict CFU for C49 culture 1, the linear regression line from this culture was not applicable to subsequent cultures. For example, OD_{600}: 0.84 correlated to $3x10^8$ CFU/ml for C49 culture 1 but OD_{600}: 0.63 correlated to $4.9x10^8$ CFU/ml for C49 culture 2. If the linear regression line from culture 1 had been used to estimate CFU in C49 culture 2, it would have predicted there to be ~$1.6x10^8$ CFU/ml – approximately 3x less than the actual number. This is somewhat in agreement with the literature, as there is much variation in the MAP CFU count correlating with specific OD_{600} readings between different studies. For example, Janagama et al. reported OD_{600}: 0.3 to correlate to ~$1x10^9$ CFU, whereas Kralik et al. reported an OD_{600}: 0.3 to correlate to ~$6x10^6$ CFU (Janagama et al. 2006; Kralik et al. 2012), suggesting there is much variation in OD_{600} readings between different cultures and results are likely influenced by strain, clumping, culture conditions etc.

The length of time in culture was also highly variable for both K10 and C49 cultures (Table 1). C49 culture 2 took roughly twice as long to grow as culture 1. The reason for this was unclear, as the method of culture was identical for C49 culture 1 and 2, and they were each grown from the same glycerol stock. In addition, K10 culture 2 (which was set up at the same time as C49 culture 2, with the same media) grew at a similar rate to K10 culture 1, therefore the slow growth in C49 culture 2 was unlikely to be caused by an issue with the media components, such as expired Mycobactin J or OADC. Culture 3 of both strains did not grow at all, likely due to out-of-date media components. The slow growth rate of MAP meant that it took at least 2 weeks to determine that no growth was occurring, which could be very problematic if trying to set up cultures with the aim of the mid-log growth phase coinciding with planned infection experiments. Culture 4 of both strains grew considerably faster than

previously cultures; it was suspected that this was due to contamination, however when plated on 7H10 agar plates it took 4-5 weeks for colonies to appear and no contaminating colonies formed, although it may have been worthwhile to run a PCR to confirm culture purity.

Taken together, this data suggested that it would be impractical to use actively growing cultures in infection experiments due to the variability in growth times and the difficulty in accurately estimating bacterial numbers from OD_{600} readings. It was therefore decided that the best way to maintain consistency between infection experiments was to grow C49 and K10 cultures to mid-log growth phase (~OD_{600}: 0.6), aliquot them into 100µl volumes and freeze them at -80ºC. The mean CFU post-freezing was then calculated from 3 random aliquots. This meant that CFU could be calculated prior to infection experiments and the same culture could be used for repeat experiments, reducing the variation by maintaining a consistent dose between biological replicates. Prior to using frozen aliquots, the viability of the cultures was tested both pre- and post-freezing by SYTO9 viability staining. Freezing did appear to increase the number of dead cells in both K10 and C49 cultures, however it was not observed that one strain had a higher ratio of dead:live cells than the other, and live cells remained predominant post-freezing (Figure 3-5), suggesting that frozen cultures were a suitable alternative to actively growing cultures for infection experiments. This method has been previously used for *M. bovis* BCG infection studies (Hope et al. 2002). A direct comparison between GCN and CFU was made in order to confirm that frozen cultures contained mainly viable MAP; however, GCN was significantly lower that CFU count (data not shown). It was later determined that this was due to the multiple spin steps carried out on samples prior to DNA extraction. Each spin reduced bacterial numbers (determined by CFU count) by 43-64% (data not shown), explaining how GCN appeared lower than CFU.

GFP expressing strains would be a useful tool for this project, as well as future studies, as they would allow the determination of infected cells from bystander cells, by flow cytometry and fluorescent microscopy, as well as allowing visualisation of bacterial intracellular trafficking by fluorescent microscopy. A K10:GFP strain was kindly gifted by Dr Karen Stevenson from Moredun Research Institute, and the C49

strain was successfully transfected to express GFP, using the pWES4 plasmid herein. The transfection efficiency was extremely low, at 5 transformants/1µg DNA, however mycobacteria, particularly *Mycobacterium avium* subsp., are notoriously difficult to transform, in part due to the composition of their cell wall (Parker & Bermudez 1997; Goude & Parish 2009). Although the transfection was successful, GFP expressing strains were not successfully maintained in liquid culture. When frozen K10:GFP and C49:GFP aliquots were used to infect MDM, no GFP fluorescence was observed (Figure 3-6 E, F &G). It was first thought that the loss of fluorescence was a consequence of freezing, therefore the infection was repeated with actively growing cultures, which also did not result in an increase in GFP fluorescence in MAP infected MDM compared to uninfected MDM (data not shown). Thus, it was likely that the GFP expression was lost prior to freezing. This may reflect a loss of activity of the selection antibiotic, kanamycin. As plasmids are a metabolic burden to host cells, they are often lost from the cell in the absence of a selective pressure (i.e. kanamycin). According to the manufacturers, kanamycin is stable at 37ºC for 5 days; therefore, it is feasible that kanamycin may lose its selective activity during the long generation time of MAP. Differential growth conditions between liquid and solid media may account for the fact that the plasmid was lost only during culture in liquid media, potentially explaining the successful growth of K10:GFP and C49:GFP on 7H10+kanamycin agar plates.

In order to determine an appropriate MOI of MAP for infection experiments, the confluence of infection was tested by two methods: confocal microscopy and flow cytometry. Establishing a confluent infection is necessary to obtain meaningful results from *in vitro* infection experiments, otherwise it is unlikely a significant effect would be observed. In addition, ensuring a confluent infection maintains consistency between experiments. Three doses (determined by CFU) were investigated by confocal microscopy (MOI 5, 20 and 50). This method utilised an anti-mycobacteria polyclonal antibody to stain MAP. Only the lowest dose (MOI 5) was tested by flow cytometry; in these experiments, MAP was labelled with FITC to enable visualisation. Ideally, GFP expressing MAP strains would have been used, but FITC was used as an alternative due to issues maintaining GFP positive MAP cultures. Confocal microscopy showed that greater than 70% of MDM were infected at all 3

MOIs, demonstrating that even at MOI 5, the majority of cells in the MDM monolayer were infected. Increased MOI appeared to increase the bacterial load per cell, as opposed to increasing the number of cells positive for MAP, suggesting that differences in MDM response observed between different MOIs (described in chapter 4) can be directly attributed to differences in bacterial burden of cells.

Surprisingly, similar results were not observed by flow cytometry. It was thought that flow cytometry would be a more practical and reliable methodology, as it is more efficient and measures fluorescence in the whole sample, as opposed to only a limited number of cells, and extrapolating data. However, percentages of FITC positive MDM at 0.5 HPI were markedly lower (<13.1%) than the percentage of MDM positive for MAP by confocal microscopy. This suggested that flow cytometry might lack sensitivity and reliability when used in this context. In addition, MOIs between 2 and 20 have been reported in the literature for *in vitro* studies (MacHugh et al. 2012; Agdestein et al. 2014; Lei & Hostetter 2007), suggesting that the MOIs used herein were suitable for infection studies with bovine MDM. In order to determine potential reasons for the poor detection of FITC-labelled MAP by flow cytometry, uptake of FITC stained MAP was visualised by live-cell imaging, which demonstrated that FITC fluorescence was rapidly quenched intracellularly. It is therefore likely that only MDM which had very recently taken up MAP were positive for FITC fluorescence when analysed by flow cytometry and the actual number of MAP-containing cells would be significantly higher than suggested by flow cytometry results. Due to the rapid quenching of FITC intracellularly, only the confocal microscopy results were used to determine that all three doses (MOI 5, MOI 20 and MOI 50) resulted in confluent infection.

Accurate quantification of bacteria is essential when carrying out infection experiments, in order to make experiments reproducible and to account for dose-effect. However, the nature of mycobacteria, particularly MAP, makes quantification challenging. MAP has a generation time >24 hours (Elguezabal et al. 2011), meaning that counting CFU takes ~5 weeks to generate results. Additionally, MAP has been shown to be capable of entering a state of dormancy in culture when subjected to stress, such as nutrient deprivation or hypoxia (Lamont et al. 2012); it is

therefore feasible that some MAP cells could be in a dormant state and unable to grow on agar, making the CFU count lower than the actual number of cells in a sample. Another issue regarding CFU counting is the fact that MAP will easily form clumps. It is likely that these clumps will develop as a single colony when grown on agar and therefore multiples of bacteria that have formed clumps could be mis-read as 1 CFU - resulting in the CFU count being lower than the actual number of MAP cells present. Therefore, an aim of the study was therefore to investigate if other methodologies could be used to quantify bacteria faster and more reliably than CFU count.

The phage amplification assay was developed from a protocol provided by Dr Ben Swift and Prof. Catherine Rees from the University of Nottingham. This protocol used the FastPlaqueTB kit (FPTB) and bacteriophage D29, which is known to be capable of infecting a wide range of mycobacteria (both pathogenic and non-pathogenic) and has been used as a tool to detect the presence of MAP in blood, infant formula and milk (Swift et al. 2016; Botsaris et al. 2016; Foddai & Grant 2017). As use of the FPTB kit was not practical in this context (due to cost and unnecessary components of the kit), adaptation and optimisation of the methodology was carried out. The FPTB kit provided the virucide ferrous ammonium sulphate in tablet form, which the original protocol stated should be diluted in 5ml H_2O to give a 5mM concentration. However, this concentration resulted in full lysis of the negative control plate, suggesting that 5mM virucide was insufficient to inactivate the phage. It seemed likely that 5mM should have been the final concentration, instead of the starting concentration. In order to test this, a virucide titration was carried out, demonstrating that 20mM virucide was sufficient to inactivate the phage, although 20-50mM concentrations all resulted in lacy positive controls instead of the expected complete lysis. A potential reason for this could have been low phage titre; a titration of the phage stock showed the titre to be ~$2x10^7$ pfu/ml, whereas *M. smegmatis* concentration was ~ $1x10^8$ CFU/ml. This finding was in agreement with the theory that low viral titre was the cause of lacy positive controls, as phage should be added at MOI 10 to efficiently infect *M. smegmatis* and achieve full lysis. The *M. smegmatis* lawns appeared irregular in the negative controls at 20-50mM virucide; the lawns were whole, with no plaques present but appeared uneven. The cause of

this is unknown but could perhaps be a problem with mixing when setting up the lawns. The issue likely did not affect the ability of the phage to infect cells and create plaques, as it is reasonable to assume the 5mM and 10mM virucide negative control lawns would have looked similar, and full lysis occurred on those plates; however, it may have made interpretation of assay results problematic. A 20mM concentration of virucide was used in subsequent phage assays; however, issues with control plates continued to occur, with plaques sporadically appearing on negative controls. Increasing the virucide concentration to 50mM did not improve reliability (data not shown) and controls routinely failed. The phage amplification assay would be a quicker alternative to CFU count, as results are available after 48 hours, as opposed to 5 weeks in culture. In addition, this method quantifies only live cells, making it advantageous over methods such as qPCR and microscopy that cannot differentiate between live and dead cells. However, the methodology itself was more laborious than performing CFU counts and required a large area of lab and incubator space in order to test several samples at once, which was impractical for this project. Optimisation of the phage amplification assay was therefore discontinued, as the method did not offer significant benefit when compared to performing CFU counts.

The use of confocal microscopy to quantify MAP infection yielded significantly higher bacterial counts than CFU from MDM infected with K10 (MOI 5 or 20), but differences in bacterial number were not observed between the two methods for MDM infected with C49. This was somewhat expected, as microscopy will not discriminate between live and dead MAP, and the quantification method was designed to estimate the number of individual bacteria even when clumps were present, using a calculation that incorporated the average size of 1 MAP bacterium. The fact that the K10 culture contained more clumps visible to the naked eye when compared to the C49 culture, could potentially explain why a significant increase in bacterial number determined by microscopy (compared to CFU) was only observed for K10 and not C49. The drawback of measuring bacterial numbers using confocal microscopy was that obtaining results was time-consuming and expensive. In addition, only a small fraction (minimum 50) of MDM were visualised for each condition and the results of these select images applied to the monolayer as a whole. This could introduce error, as it was observed that even at the high dose (MOI 50),

not all MDM became infected; instead, certain cells became heavily infected, while others did not contain bacteria or contained only a small number. This variation could potentially lead to error, as it is possible that the images collected displayed a number of highly infected cells that was not representative of the coverslip as a whole. This issue is highlighted by the fact that more variation between technical replicates was observed when quantifying by microscopy, compared to calculating GCN by qPCR or performing CFU counts (data not shown).

qPCR is commonly used as a method of detection of MAP (Beumer et al. 2010; Kruze et al. 2013; Kralik et al. 2011). It is an extremely efficient method of quantification as it can provide results in <24 hours - a vast improvement on the time required to perform CFU counts. qPCR essentially measures the number of genomes in any given sample, thus if DNA extraction is inefficient, qPCR results will be negatively impacted. DNA extraction from MAP was therefore optimised to obtain the highest concentrations and purity (indicated by 260/280 and 260/230 ratios). The Qiagen DNeasy kit gave the highest DNA concentrations and best 260/280 ratios, when compared to other DNA extraction methods. However, results were variable between technical replicates. As the technical replicates in Table 7 represent individual wells of MDM infected with MAP, as opposed to one sample split in three, it is possible that differences in cell numbers between the wells were the cause of the variation.

Mycobacteria are notoriously difficult to extract DNA from, as lipids in the cell wall (such as mycolic acid) are resistant to lysis by strong acids or alkali (Nakatani et al. 2004). As the Qiagen kit protocol was designed for mammalian cells, it was assumed that the DNA successfully extracted from infected MDM was likely mostly bovine, and that an additional lysis step may be necessary to efficiently extract MAP DNA. An additional lysis step involving the use of lysozyme and proteinase K was therefore included in the DNA extraction protocol. The concentration of DNA extracted from MDM infected with C49 (MOI 20) by the Qiagen kit, plus the additional lysis step, was found to be higher than the concentration of DNA extracted from the same samples by the Qiagen kit alone. This result suggested that incorporation of additional lysis during DNA extraction was necessary for reliable

extraction of MAP DNA. A PCR was run on DNA extracted with the additional lysis step, using bovine GAPDH primers and primers targeting the F57 sequence of MAP, in order to determine that both bovine DNA and MAP DNA were present in the DNA samples. Both GAPDH and F57 were successfully amplified by PCR. The F57 band was noticeably brighter that the GAPDH band. Although this was somewhat expected, as more MAP cells were added to the sample than bovine cells, it is possible that the additional lysis step during the extraction, caused degradation of bovine DNA. In hindsight, qPCR should have been carried out on DNA extracted from MAP cultures and uninfected MDM using the Qiagen kit both with and without the additional lysis step. This would have informed how the lysis step was likely to affect the sensitivity of qPCR for bacterial quantitation and demonstrated if additional lysis was degrading bovine DNA. MAP GCN was calculated relative to the reference gene (i.e. GADPH), the GCN of which was calculated prior to the experiment by performing cell counts, therefore degradation of bovine DNA could cause a false result.

Primers targeting F57 and SPAST were designed to quantify MAP infection by qPCR, as F57 is a single-copy insertion sequence, known to be specific to MAP (Sidoti et al. 2011). Dissociation curves included in the reaction set-up demonstrated that both primer sets were specific and produced only a single product. A clear increase in GCN was observed for MOI 20, compared to MOI 5, however, the difference was greater than expected, with GCN 5.3x and 4.6x greater at MOI 20, compared to MOI 5, for K10 and C49 respectively. This could potentially be explained by reduced intracellular survival of MAP at MOI 5, compared to MOI 20, at 2 HPI; this effect is described in detail in chapter 4.

GCN, as determined by qPCR, was significantly higher than CFU, for all conditions (MDM infected with K10 or C49 at MOI 5 or 20), and significantly higher than bacterial numbers determined by microscopy for K10 infected MDM. The differences between GCN and CFU were more pronounced for K10 than C49, likely due to the increased clumping of K10 already described, or to decreased viability of K10. SYTO9 viability staining was carried out on both cultures prior to infection and as there was no noticeable increase in cells positive for propidium iodide

(indicating dead cells) in the K10 culture, compared to the C49 culture, it can be inferred that higher levels of intracellular killing of K10 may be occurring over the 2 hour infection time-course. It should be noted, however, that SYTO9 viability staining did indicate the presence of dead cells in both cultures, which could (at least in part) account for the increased GCN, compared to CFU for both K10 and C49. Significant differences between GCN and numbers determined by microscopy was surprising, as both methodologies returned results for both live and dead bacteria and should be minimally affected by the presence of clumps. The differences between these two methodologies further suggests that the DNA extraction method could possibly be detrimental to bovine DNA; as MAP GCN was calculated relative to bovine GCN, an unknown reduction in bovine DNA would result in the overrepresentation of MAP GCN.

qPCR would be a significantly more efficient method of quantifying MAP than counting CFU; however, the fact that it cannot discriminate live from dead bacteria is a major drawback of this method. Infection studies in chapters 4 and 5 analyse intracellular survival of both C49 and K10 under different experimental conditions, therefore these experiments required a quantification method that could determine the number of live bacteria present. Additionally, no reproducible direct correlation was observed between GCN and CFU that would allow accurate estimation of CFU from GCN, due to variation observed between biological replicates, as well as between treatment conditions. It is likely the variation issue was compounded by the design of this experiment. With hindsight, it may have been more effective to quantify intracellular bacteria at 0.5 HPI, subsequent to washing off extracellular bacteria, as experiments referenced in chapter 4 and 5 detail differences in the ability of K10 and C49 to survive intracellularly, as well as significant biological variation in the ability of MDM to clear MAP over a 24-hour time-course. This could account for the increased K10 GCN, compared to CFU, as well as the variation observed between biological replicates in this chapter. Additional technical replicates should have been included to gain a better understanding of the reproducibility of each quantification method for individual biological replicates.

Due to the drawbacks of qPCR and microscopy (described above), primarily the inability to determine the viability of MAP, it was decided that CFU count would be used to quantify MAP for all subsequent experiments, despite the disadvantages of this method. Frozen stocks of both K10 and C49 MAP cultures were also quantified by CFU count prior to use in infection studies, therefore CFU counting over the infection time-course would allow a direct comparison to bacterial numbers at 0 HPI.

4 Monocyte-derived macrophages respond differently to the reference strain of *Mycobacterium avium* subspecies *paratuberculosis* (K10), compared to a recent clinical isolate (C49)

4.1 Introduction

MAP is generally contracted by neonates via the faecal-oral route and, subsequent to entering the gut, will cross the gut epithelium and enter its preferred niche – resident gut macrophages found within the lamina propria and Peyer's patches (see Introduction section 1.7). Resident gut macrophages are derived from monocytes which, in the presence of pathogenic bacteria (such as MAP), are known to be induced to differentiate into pro-inflammatory macrophages capable of secreting pro-inflammatory cytokines and producing antimicrobial products, such as ROS and RNS (Bain et al. 2013; Joeris et al. 2017) (see Introduction section 1.11). MDM were therefore selected as an appropriate *in vitro* model for MAP infection, and were used to investigate the macrophage response to MAP throughout this study. As with other pathogenic species of mycobacteria, such as *M. tb* and *M. bovis*, MAP is capable of subverting the host immune response and surviving within the macrophage itself. Infected macrophages respond to the infection by producing pro-inflammatory cytokines and chemokines, ultimately driving the formation of a granulomatous lesion (Plattner et al. 2009) (See Introduction section 1.11.3). It is therefore clear that the early host-pathogen interaction between MAP and macrophages likely plays a key role in determining the downstream immune response and outcome of MAP infection. However, the mechanisms of this intricate host-pathogen interaction are still incompletely understood,

In order to further understand MAP-macrophage interactions, the MDM response to two strains of MAP - the reference strain, K10, and the recent clinical isolate, C49, was assessed and compared. Several studies have previously utilised K10 to study features of the early host-pathogen interaction (Kugadas et al. 2016; Bannantine et al. 2015; Ghosh et al. 2014; Lamont et al. 2013). However, recent findings suggest that the strain of MAP can have a profound impact on infection outcome (Fernández et al. 2014) and that the K10 strain exhibits differences, compared to recent field isolates, at both the genome (Bryant et al. 2016) and protein level (Radosevich et al. 2007), likely due to lab-adaptation. It was, therefore, hypothesised that the recent clinical isolate, C49, would be better adapted to survive intracellularly, and would likely

induce an altered response in MDM, compared to K10. Thus, this chapter aimed to elucidate the early MDM response to both MAP strains, in order to determine the reliability of using K10 to model MAP infection *in vitro*. In addition, the genome of both strains was sequenced in order to gain an understanding of the genetic relationship between the two strains and identify MAP genes that potentially influence the macrophage response to infection and/or impact the ability of MAP to survive intracellularly.

In order to define the early macrophage response to MAP, several parameters were investigated within a 24-hour time-course, including: cell surface molecule (CSM) expression, cytokine secretion, phagosome maturation, the production of antimicrobial products, including ROS and RNS, and the ability of MAP to survive intracellularly.

The effect of MAP infection on the expression of MHC II, CD40, DC-SIGN, MR and CD11b by MDM was investigated by flow cytometry. MHC II is necessary for the presentation of antigen to CD4+ T-cells within lymph nodes. Previous studies have demonstrated that *M. tb* is capable of inhibiting MHC II expression (Noss et al. 2001; Harding & Boom 2010), therefore it was hypothesised that MAP may have a similar effect upon MDM. Interaction between the co-stimulatory molecule CD40, expressed on macrophages, and CD40 ligand (CD40L), expressed on T-cells, is essential in order to maintain activation of macrophages and induce a protective Th-1 response. CD40 signalling is known to be impaired in MAP infected MDM, compared to uninfected MDM (Sommer et al. 2009). It was therefore hypothesised that MAP may interfere with CD40 expression in order to prevent the induction of protective immunity. DC-SIGN, MR and CD11b are phagocytic receptors capable of inducing the phagocytosis of MAP; therefore, expression of these molecules could significantly affect the route of phagocytosis and downstream immune response of macrophages. The role of phagocytic receptors in MAP infection is discussed in detail in Chapter 5.

Infected macrophages are known to respond to mycobacterial infection by secreting multiple cytokines with a wide range of biological activities. This study focused on the expression of IL-1β, IL-6 and, IL-10 by MAP infected MDM, as the genes

encoding these cytokines were previously reported to be highly upregulated in bovine MDM infected with MAP in an RNA-Seq study performed by the Glass group (Roslin Institute, unpublished data), as well as a microarray study by MacHugh et al. (MacHugh et al. 2012).

IL-1β is a potent pro-inflammatory cytokine that has previously been reported to have protective effects against *M. tb* infection in mice both *in vitro* and *in vivo* (Sharon S. Master et al. 2008). The mechanism by which IL-1β confers protection against mycobacterial infection is still incompletely understood, however mice deficient in the receptor for IL-1β, IL-1R1, displayed functional CD4+ and CD8+ T-cell responses, suggesting that IL-1β likely confers protection against mycobacteria via the innate response (Fremond et al. 2007). For example, IL-1R1 signalling via MyD88 in macrophages can induce NO production (via enhanced NOS2 gene expression) sufficient to restrict intracellular growth of *Leishmania* within murine bone marrow derived macrophages (Lima-Junior et al. 2013); it is possible that IL-1β functions through a similar mechanism to restrict intracellular growth of MAP. Additionally, IL-1R1 KO mice had impaired granuloma formation in the context of *M. tb* infection, suggesting that IL-1β signalling likely plays an important role in granuloma formation (Juffermans et al. 2000). Relatively few studies have been carried out examining the role of IL-1β in MAP infection. However, evidence that IL-1β may have a role in granuloma formation in the context of paratuberculosis was reported by Lamont et al.; bovine epithelial cells infected with MAP secreted IL-1β that had a direct chemotactic effect on MDM, *in vitro* (Lamont et al. 2012). As stated above, expression of the IL-1β gene was shown to be upregulated in response to MAP infection (MacHugh et al. 2012) and increased IL-1β secretion was observed in DC treated with MAP-derived protein (Lee et al. 2014). It can be inferred that IL-1β has a similar role in bovine MAP infection compared to *M. tb* infection in other mammalian hosts.

Unlike most pro-inflammatory cytokines, secretion of IL-1β does not occur at the transcription level. Instead, the IL-1β gene encodes an inactive form of IL-1β known as pro-IL-1β. Secretion of IL-1β is a 2-step process that involves both transcriptional regulation of the IL-1β gene and inflammasome activation to catalyse the processing

of pro-IL-1β into active IL-1β (Sahoo et al. 2011) (See Introduction section 1.11.2.6). There are several different types of inflammasome; however, this chapter examined the role of the NLRP3 inflammasome in response to MAP infection due to the known role of this inflammasome in other mycobacterial infections. For example, the NLRP3 inflammasome is essential for the secretion of IL-1β in the context of *M. tb* infection *in vitro* (Mishra et al. 2010). To date, the NLRP3 inflammasome has not been studied in the context of MAP infection. However, NLRP3 gene expression was found to be upregulated in MAP infected MDM at 2 HPI in a microarray study by MacHugh et al (MacHugh et al. 2012), and also in an RNA-Seq study by members of the Glass group (Roslin Institute, unpublished data), suggesting it is likely important for IL-1β production by MAP infected cells.

IL-6 is a pro-inflammatory cytokine with varied biological functions and is known to be produced in response to mycobacterial infection. A study by Martinez et al. reported that increased IL-6 production resulted in decreased *M. tb* survival within murine macrophages and that *M. tb* are capable of modulating macrophage IL-6 secretion to promote their intracellular survival (Martinez et al. 2013). Previous studies investigating IL-6 in the context of MAP infection have demonstrated that IL-6 gene expression was upregulated in response to MAP antigens (Alzuherri et al. 1996; Adams et al. 1996; Adams & Czuprynski 1995). However, there are currently no published studies reporting the IL-6 response to MAP at the protein level, and it is possible that MAP are capable of modulating macrophage IL-6 secretion through post-transcriptional modification in a manner similar to that observed for *M. tb* (Martinez et al. 2013).

IL-10 is an anti-inflammatory cytokine known to be upregulated by macrophages in response to mycobacterial infection. A number of studies have demonstrated that IL-10 secretion is beneficial to the intracellular survival of MAP and it is likely that MAP promote the secretion of this cytokine as a virulence mechanism to promote survival, as reviewed by Hussain et al. (Hussain et al. 2016). A study by Weiss et al. demonstrated that neutralisation of IL-10 resulted in a >50% reduction in intracellular MAP survival by 96 HPI, *in vitro* (Weiss et al. 2005). IL-10 secretion likely enhances intracellular mycobacterial survival by inhibiting production of

antimicrobial products and phagosome acidification (Souza et al. 2006; Souza et al. 2013; Sullivan et al. 2005). In addition, increased secretion of IL-10 has been associated with the shift from Th-1 to Th-2 immunity that precedes the onset of clinical symptoms of Johne's disease (Magombedze et al. 2015). It has been demonstrated that IL-10 can downregulate the production of pro-inflammatory cytokines, including TNFα, IL-12 and IFNγ (Weiss et al. 2005; Riley et al. 1999; Buza et al. 2004; Khalifeh & Stabel 2004). While pro-inflammatory cytokines such as TNFα, IL-12 and IFNγ have protective effects against mycobacterial infection, it should be noted that IL-10 secretion might also be somewhat protective, as it is capable of limiting inflammation-induced damage at the site of infection.

The role of antimicrobial products such as ROS and RNS in MAP infection of MDM was investigated in order to understand if these chemical products impacted intracellular survival of MAP. The production and action of antimicrobial products is detailed fully in section 1.11.2.1 of the Introduction. ROS and RNS destroy invading pathogens by targeting pathogenic macromolecules essential for their function, such as heme and ferritin, as well as directly destroying DNA by targeting enzymes involved in DNA replication, and oxidising to form mutagens capable of directly damaging DNA (Nathan 1992). Decreased ROS production is associated with increased susceptibility to mycobacterial disease. For example, there is a higher risk of complication from BCG vaccination in patients lacking NADPH oxidase and therefore ROS (Sadeghi-Shanbestari et al. 2009; Li et al. 2010). However it remains unclear how ROS confers protection against mycobacteria; it likely enhances the bactericidal activity of macrophages but may also affect signalling pathways of important cellular processes, such as apoptosis and chemokine production (Schieber & Chandel 2014)

There are conflicting reports regarding the role of RNS in MAP infection. For example, NO has been reported to control intracellular growth of *M. bovis* BCG within bovine macrophages (Esquivel-Solís et al. 2013); whereas NO produced by human macrophages in response to *M. tb* or *M. bovis* BCG has been reported not to have a bactericidal effect (Jung et al. 2013). This chapter therefore aimed to further elucidate the role of RNS in MAP infection of bovine macrophages.

Pathogenic mycobacteria are known to be capable of arresting phagosome maturation, in order to evade degradation within macrophages (Wong et al. 2011; Kugadas et al. 2016). The process of phagosome maturation involves the interaction of phagosomes with endosomes and lysosomes, resulting in a gradual decrease in phagosome pH and the acquirement of proteolytic enzymes which degrade intracellular bacteria (Poirier & Av-Gay 2012) (see Introduction section 1.9.2). However, the mechanisms by which mycobacteria interfere with the process of phagosome maturation, and the downstream implications, remain incompletely understood; particularly in the case of MAP infection as the majority of studies have focused on *M. tb* and *M. bovis* BCG. In order to further understand the early MAP-macrophage interaction, *in vitro* phagosome maturation of MAP infected macrophages was investigated in this chapter.

This chapter hypothesised that the macrophage response to MAP would differ for the K10 strain compared to the recent clinical isolate, C49, and that K10 would likely be less adept at intracellular survival due to lab-adaptation.

The study aimed to compare and contrast the macrophage response to K10 and C49, in order to elucidate differences that may have important implications for intracellular survival and downstream immune responses. In order to achieve this aim, several parameters of the macrophage response to MAP were investigated, including CSM expression, cytokine secretion, phagosome maturation and production of antimicrobial products. A clear understanding of how MDM respond to both MAP strains will inform on the reliability of using the K10 to model MAP infection, and elucidate key pathways in the macrophage response to MAP that will be of benefit for the design of more reliable diagnostic tests and vaccines.

4.2 Results

4.2.1 Intracellular survival of MAP and impact of MAP infection of MDM survival

In order to understand the effect of strain and dose on the ability of MAP to survive intracellularly, MDM were infected with the K10 or C49 strain at MOI 5, 20, or 50. Infected MDM were washed twice at 0.5 HPI, in order to remove extracellular bacteria from the cell monolayer. At 0.5, 2, 6 and 24 HPI, infected MDM were lysed, and serial dilutions of the lysate plated on 7H10 agar plates, in order to perform colony counts to determine intracellular survival at these time points. Survival was expressed as a percentage of the number of CFU counted at the 0.5 HPI time-point (indicating the number of intracellular bacteria taken up by macrophages). At all 3 doses, percentage survival of C49 remained around 100%, by 24 HPI (Figure 4-1 A, C & E), however, the intracellular survival of K10 appeared to be dose dependent; at MOI 5 there was significantly less intracellular survival of K10, compared to C49 at 24 HPI (Figure 4-1 A). At MOI 20, there was an initial dip in K10 CFU at 2HPI, that appeared to recover by 6 HPI and remained constant until 24 HPI, at a similar survival rate to the C49 strain (Figure 4-1 C). At MOI 50, the number of K10 CFU approximately tripled by 24 HPI, whereas C49 CFUs remained constant (Figure 4-1 E). The effect of MAP strain and dose on the ability of MDM to survive MAP infection over a 24 hour time-course was also assessed, using the Zombie Aqua Viability marker and analysing survival of MDM at 24 HPI by flow cytometry (for gating strategy see Figure 4-2 A). At MOI 5, infection with the K10 strain and the C49 strain significantly increased MDM survival, compared to uninfected controls (Figure 4-1 B). A significant increase in survival was only observed for C49 infected MDM, and not K10 infected MDM, at MOI 20 (Figure 4-1 D). Whereas, at MOI 50 there was a subtle decrease in survival of MDM infected with C49 (that did not reach statistical significance) and a significant decrease in survival of K10 infected MDM, compared to uninfected controls (Figure 4-1 F).

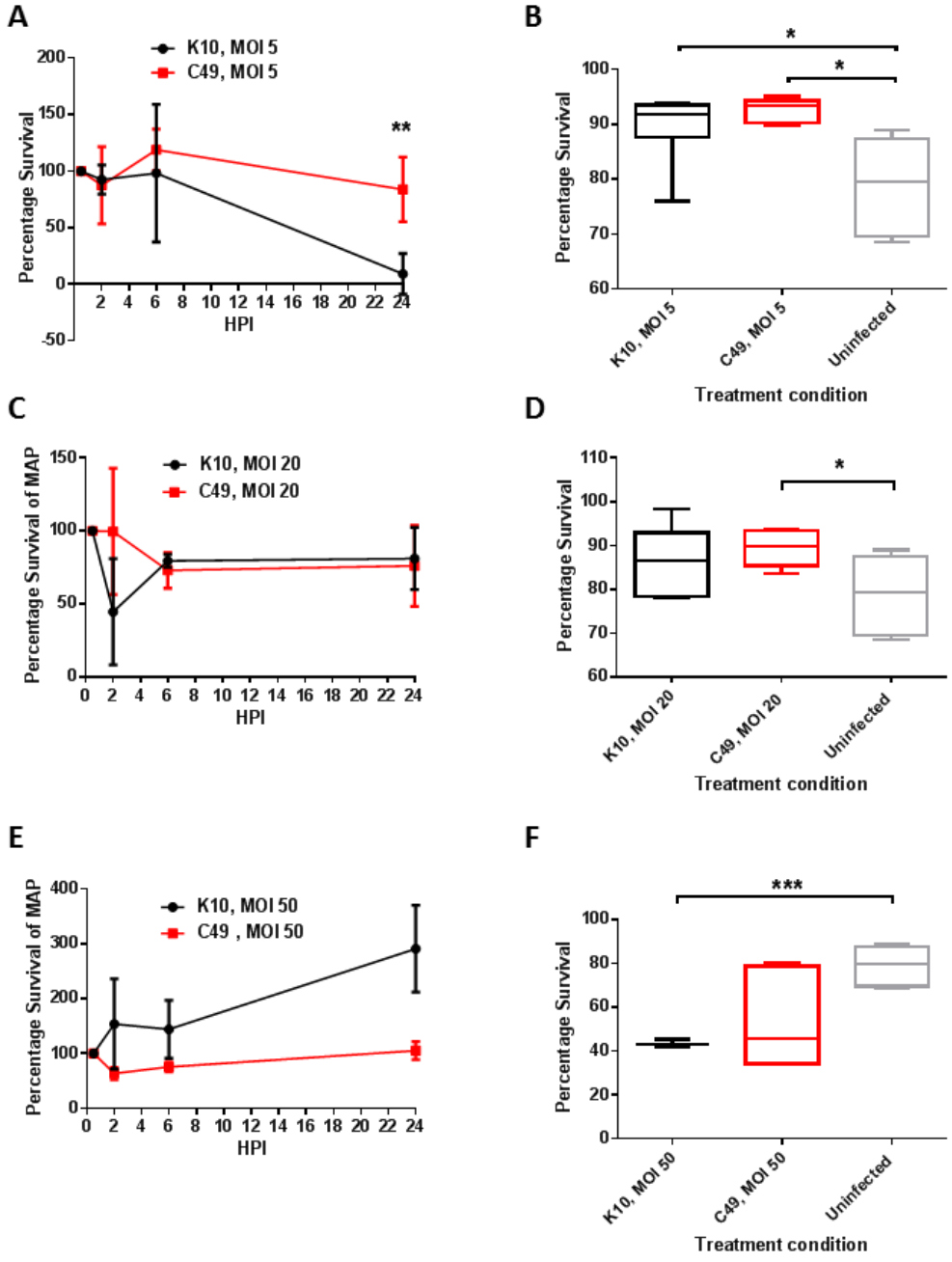

Figure 4-1 Percentage Intracellular survival of MAP throughout infection time-course and impact of infection on MDM survival

MDM were infected with either the K10 or C49 strain of MAP at MOI 5, 20, or 50, in order to assess if the strain and/or dose affected intracellular survival of MAP, or the survival of MAP-infected MDM, over an infection time-course of 24 hours. Intracellular survival of both the K10 and C49 strain is presented as a percentage of the number of intracellular CFU present at 0.5 HPI, (when infected monolayers were washed). Intracellular survival of MAP was measured by lysing infected monolayers and plating serial dilutions of the lysate at 2, 6 and 24 HPI, for MDM infected at MOI 5, 20 and 50 (A, C and E, respectively). Each symbol represents the mean of 3

biological replicates and error bars show the standard deviation. The effect of MAP infection on MDM survival at 24 HPI was measured by assessing the presence of the viability stain Zombie Aqua by flow cytometry for MDM infected at MOI 5, 20 and 50 (B, D, and F, respectively). Box plots represent the median, 25th and 75th percentile, and error bars represent the range of 6 biological replicates (B & D) or 3 biological replicates (F). HPI = Hours post infection, MOI = multiplicity of infection. Data were normally distributed ($p>0.05$) and analysed by 2 sample t-tests. $p<0.05$, $p<0.01$**, $p<0.001$***.*

4.2.2 Cell surface molecule expression of MAP infected MDM

The effect of MAP strain and dose on CSM expression by infected MDM was investigated by flow cytometry. MDM were infected with the K10 or C49 strain at MOI 5 or 20. Polystyrene beads were added as non-infectious controls, at the same multiplicity as the MAP strains, to account for non-specific effects of phagocytosis. The higher MOI 50 was not used here due to the high level of MDM death observed at this dose (Figure 4-1). At 2, 6 and 24 HPI, MDM monolayers were dissociated from 24 well plates and incubated with the viability stain Zombie Aqua. Multi-colour staining was then carried out, prior to fixation of the cells in 2% paraformaldehyde, in order to measure the expression of the cell surface molecules MHCII, CD11b, CD40, DC-SIGN, and the macrophage Mannose Receptor (MR). Results were analysed using a BD Fortessa flow cytometer and FlowJo software. Gating strategies are demonstrated in Figure 4-2.

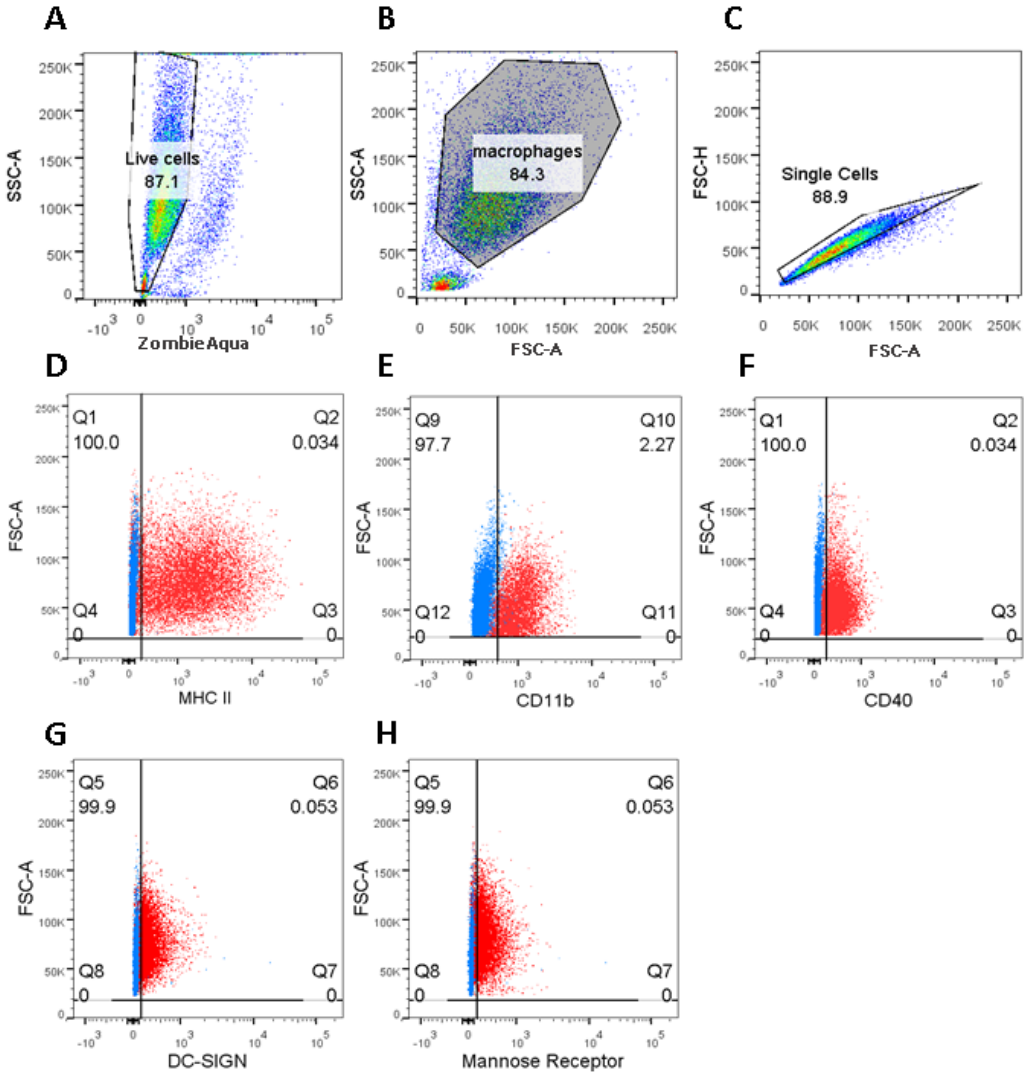

Figure 4-2 Gating strategy for analysis of flow cytometry data.

The gating strategy used to identify MDM positive for specific CSM is demonstrated. Cells were first gated for: (A) Expression of Zombie Aqua Viability stain in order to exclude non-viable cells from analysis. (B) The FSC-A/SSC-A properties of the cells, to determine that cultured cells had the expected size and granularity of MDM, and (C) FSC-A/FSC-H properties, so as to exclude doublets from analysis. Gates were then set for the CSMs MHC II (D), CD11b (E), CD40 (F), DC-SIGN (G), and the Mannose Receptor (H) FMO controls were used to establish gates for each CSM. Blue = unstained cells, Red = cells stained for each individual molecule. Numbers within each quadrant refer to percentage of FMO control cells within the quadrant.

The Geometric Mean Fluorescence intensity was calculated for each CSM, as an indicator of the level of expression of each marker on the cell surface. When measuring DC-SIGN and CD11b expression, only MOI 5 was used. It should be noted that at no time point or multiplicity were the results with polystyrene beads significantly different from the uninfected controls. There was significant down-regulation of DC-SIGN expression in K10 and C49 infected cells between 2 HPI and 6 HPI. Decreased expression of DC-SIGN was also observed over this time in uninfected MDM and therefore, there was no difference between infected cells and uninfected controls or non-infectious controls (MDM given polystyrene beads) (Figure 4-3 A). CD11b expression significantly reduced between 2 HPI and 24 HPI, however, again, there was no difference between infected cells and uninfected controls (no beads were used in this experiment and the 6-hour time point was missed out, due to a shortage of cells) (Figure 4-3 B). At MOI 5, there was a significant decrease in MHC II expression between 2 HPI and 6 HPI, by MDM infected with C49 but there were no differences between infected cells and controls at any time-point (Figure 4-3 C). At MOI 20, MHC II expression was significantly higher in K10 and C49 infected MDM, compared to uninfected controls, at 2 HPI, although a similar effect was not observed between infected cells and non-infectious controls. There was also a significant decrease in MHC II expression by K10 and C49 infected cells by 6 HPI and 24 HPI (Figure 4-3 D). No significant differences in CD40 expression were seen at MOI 5 (Figure 4-3 E); however, at MOI 20 there was a significant decrease in CD40 expression by K10 and C49 infected cells between 2 HPI and 6 HPI (although there were no differences in CD40 expression by MAP infected cells compared to either control at any time-point) (Figure 4-3 F). No significant differences in MR expression were observed in MDM infected at MOI 5 (Figure 4-3 G). At MOI 20, there were differences between MR expression in K10 and C49 infected MDM, compared to uninfected MDM but not compared to non-infectious controls. Mannose receptor expression in K10 and C49 infected cells was significantly higher at 2 HPI compared to 6 HPI (Figure 4-3 H). Of note, significant differences in the expression of CSMs, between MAP infected MDM and MDM exposed to polystyrene beads were not observed for any CSM, at any time point or at

either dose. Additionally, there were no significant differences in the expression of any CSM by MDM infected with K10, compared to MDM infected with C49.

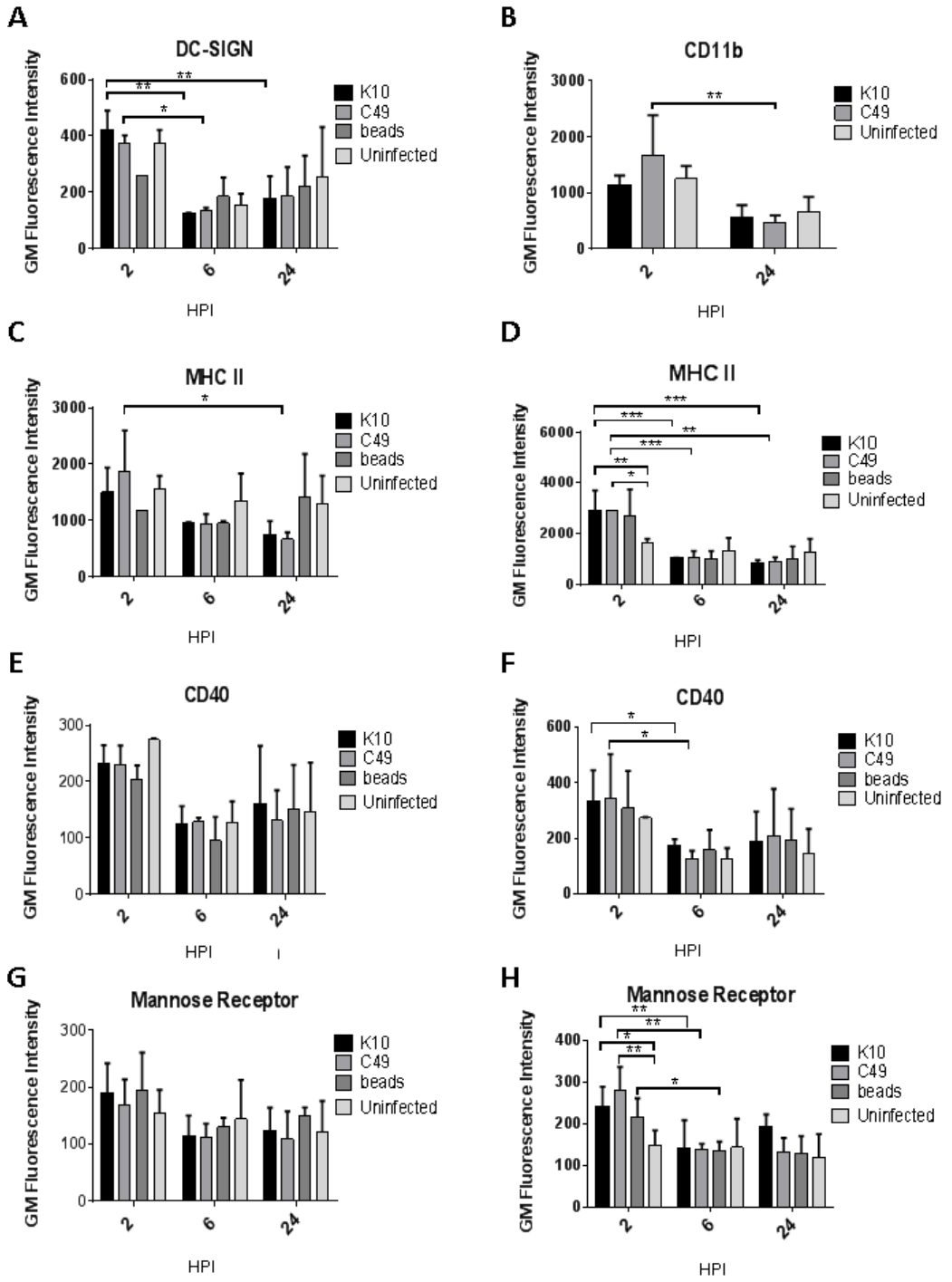

Figure 4-3 CSM expression by MAP infected MDM at MOI 5 or 20.

The expression of CSMs by MAP infected MDM was measured by flow cytometry. MDM were infected with MAP at MOI 5 and the Geometric Mean Fluorescence Intensity of DC-SIGN, CD11b, MHC II, CD40 and the Mannose Receptor, over a 24-hour time-course, is presented in A, B, C, E, and G, respectively. Additionally, MDM were infected with MAP at MOI 20 and the Geometric Mean Fluorescence Intensity of MHC II, CD40 and the Mannose Receptor over a 24-hour time-course is presented in D, F and H, respectively. CSM expression on infected cells was

compared to both uninfected controls and non-infectious controls, given polystyrene beads at the same multiplicity (labelled 'beads'). Graphs depict the mean and standard deviation of 4 biological replicates. Data were normally distributed ($p>0.05$) and analysed by general linear model. $P<0.05$, $P<0.01$***

4.2.3 Cytokine secretion of MAP infected MDM

The aim of this study was to examine how the dose and strain of MAP affected production of the cytokines IL-1β, IL-6, and IL-10 by infected MDM.

4.2.3.1 qPCR assessing cytokine gene expression

Expression of the genes encoding IL-1β, IL-6 and IL-10 was analysed by qRT-PCR. Briefly, MDM were infected with either K10 or C49 at MOI 5 or 20; polystyrene beads were given at the same multiplicity, to act as a non-infectious control. RNA was extracted from MDM at 2, 6 and 24 HPI, and reverse transcribed prior to gene expression analysis by qRT-PCR.. At MOI 5, K10 infected MDM significantly upregulated IL-1β gene expression, compared to non-infectious controls, at 2, 6 and 24 HPI. Additionally, at 2 and 24 HPI, IL-1β gene expression was upregulated in K10 infected MDM compared to uninfected controls (Figure 4-4 A).At 2 HPI IL-1β gene expression was significantly lower in non-infectious controls, compared to uninfected controls; this was likely due to very little variation observed between replicates in these samples, and the difference is unlikely to be biologically significant. When MDM were infected with K10 at MOI 20, IL-1β gene expression was significantly upregulated, compared to both uninfected controls and non-infectious controls, at 2 HPI and 24 HPI. An increase in IL-1β secretion by K10 infected cells at 6 HPI was observed, however the difference was not significant compared to any other treatment conditions (Figure 4-4 B). At an MOI of 20, C49 infected MDM significantly upregulated IL-1β expression compared to uninfected and non-infectious controls at 24 HPI. There was no significant difference in IL-1β gene expression in MDM infected with C49 at MOI 5, compared to uninfected controls or non-infectious controls, at at any time point post infection (Figure 4-4 A & B).

At MOI 5, IL-6 gene expression was significantly upregulated in K10 and C49 infected MDM, compared to both uninfected and non-infectious controls at 6 HPI and 24 HPI (Figure 4-4 C). In addition, the upregulation of IL-6 gene expression was significantly higher in K10 infected MDM, compared to C49 infected MDM at 6 HPI and 24 HPI (Figure 4-4 C). It should be noted that IL-6 gene expression was significantly lower in non-infectious controls, compared to uninfected controls at

2HPI and 6 HPI, however it is unlikely that these differences would be biologically relevant (Figure 4-4 C). . At MOI 20, K10 infected MDM had significantly higher levels of IL-6 gene expression, compared to non-infectious controls at 2 HPI and 24 HPI, and compared to uninfected controls at 6 HPI and 24 HPI. Additionally, C49 infected MDM had increased IL-6 gene expression, compared to uninfected controls, at 6 HPI and 24 HPI. K10 infected MDM IL-6 gene expression was slightly increased, compared to C49 infected MDM at 6 HPI and 24 HPI, however the difference was not significant (Figure 4-4 D).

At MOI 5, IL-10 gene expression was significantly upregulated by K10 infected MDM, compared to uninfected controls and non-infectious controls, at6 HPI and 24 HPI. C49 infected MDM also significantly upregulated IL-10 gene expression, compared to uninfected controls and non-infectious controls, at 24 HPI. However, IL-10 gene expression in C49 infected MDM was significantly lower than K10 infected MDM at 24 HPI (Figure 4-4 E). At MOI 20, IL-10 gene expression was significantly upregulated by both K10 and C49 infected MDM at 2 HPI, compared to non-infectious controls. However, by 24 HPI, there was a reduction in IL-10 gene expression, although it was still significantly increased in K10 infected cells, compared to non-infectious controls at the 24 HPI time point. . (Figure 4-4 F)

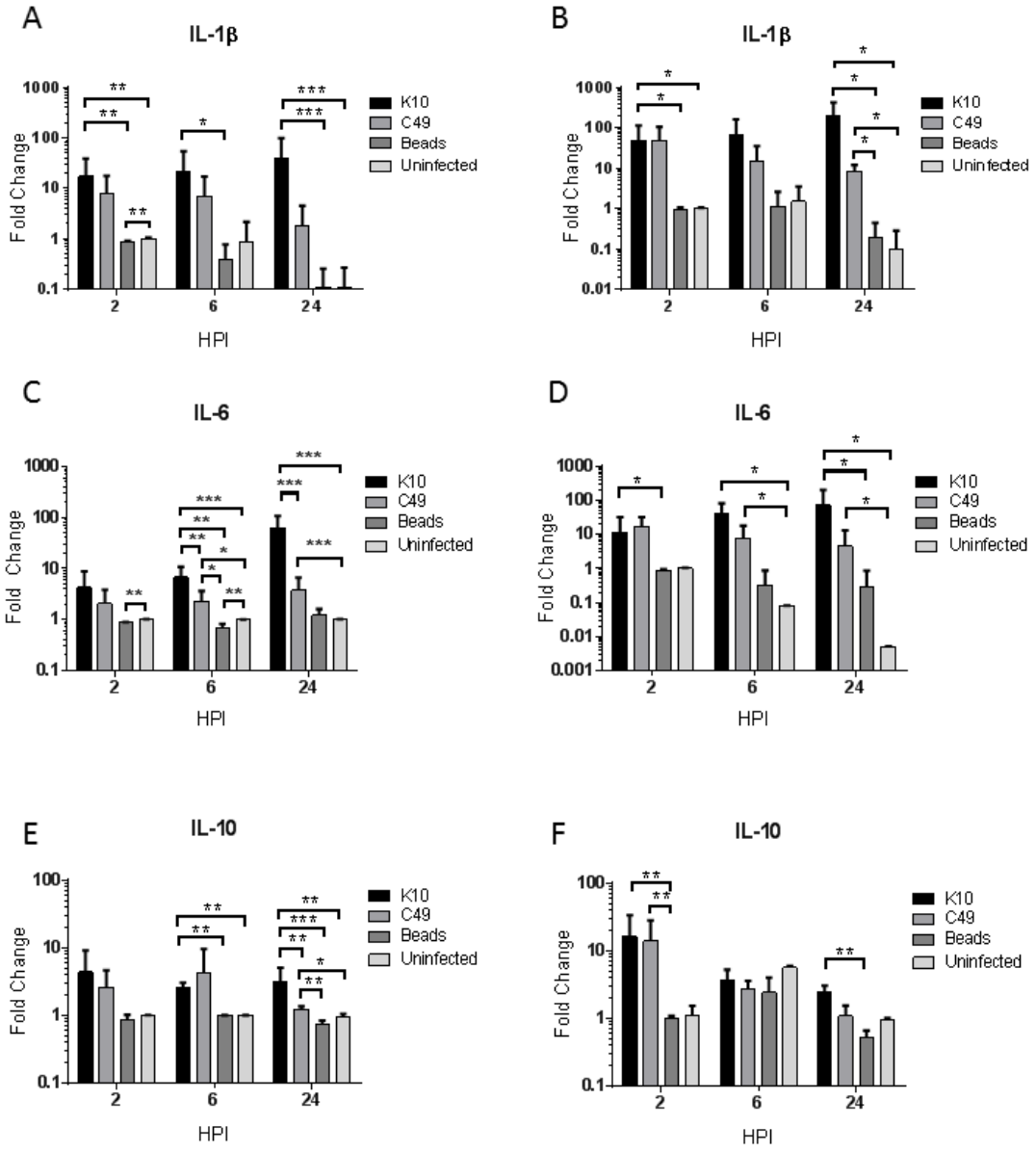

Figure 4-4 qRT-PCR analysis of genes encoding IL-1β, IL-6 and IL-10.

Expression of the genes encoding IL-1β, IL-6, and IL-10 by MAP infected MDM was analysed by qRT-PCR at 2, 6, and 24 HPI. Results are expressed as fold change in gene expression, compared to uninfected controls at 2 HPI. MDM were infected with K10 or C49 at MOI 5 and fold change in IL-1β (A), IL-6 (C)) and IL-10 (E) Gene expression was analysed at 2, 6 and 24 HPI by qRT-PCR. Additionally, MDM were infected with K10 or C49 at MOI 20 and fold change in Il-1β (B), IL-6 (D), and IL-10 (F) gene expression was analysed at 2, 6, and 24 HPI by qRT-PCR. Polystyrene beads were added at the same multiplicities as a non-infectious controls. Bars represent the mean and SD of 3 biological replicates (A, C, and E) or 2 biological replicates (B, D, and F) Each biological replicate incorporated 3 technical replicates, which were included in statistical analysis. Uninfected controls

in fig D consist of only one biological replicate due to shortage of cells. 1 technical replicate was missing for MDM infected with C49 at 2HPI in fig. D.. Data were non-normally distributed ($p<0.05$) and analysed by Kruskal Wallis and Mann-Whitney tests (A-E), or normally distributed ($p>0.05$) and analysed by general linear model (F). $p<0.05$, $p<0.01$**, $p<0.001$****

4.2.3.2 Cytokine secretion by MAP infected MDM

Analysing gene expression alone does not inform on the actual level of protein produced by cells, as it does not account for post-translational modification. Therefore, in order to confirm the qRT-PCR results presented in Figure 4-4, IL-1β, IL-10 and IL-6 protein secretion into the supernatant of infected cells was measured. Briefly, MDM were infected with K10 or C49 at MOI 5 or 20 and supernatants collected at 24 HPI. Supernatants were frozen at -20°C until further processing and IL-1β, IL-6 and IL-10 concentration measured by ELISA. No significant differences were observed between uninfected controls and non-infectious controls (given polystyrene beads) at either multiplicity for any cytokine measured.

At MOI 5 and 20, K10 infected MDM upregulated IL-10 secretion, compared to uninfected controls. At the higher MOI 20, K10 infected MDM upregulated IL-10 secretion compared to non-infectious controls, in addition to uninfected controls. No significant differences were seen between C49 infected MDM (at both MOIs) and controls (Figure 4-5 A). IL-1β secretion was upregulated in K10 infected cells, but not C49 infected cells, at both MOI 5 and MOI 20, compared to both uninfected controls and non-infectious controls. The results of the IL-6 ELISA were somewhat surprising, as despite upregulation at the gene expression level, no differences were observed between infected samples and controls by ELISA (Figure 4-5 C). However, there was significant variation between biological replicates, with 2 replicates secreting no IL-6 at all, and the other biological replicate, animal 27, producing levels above 700pg/ml, when infected with K10 at MOI 20 (Figure 4-5 D). Animal 27 is not one of the biological replicates included in the qRT-PCR data in Figure 4-4, but all other biological replicates were the same between the two experiments.

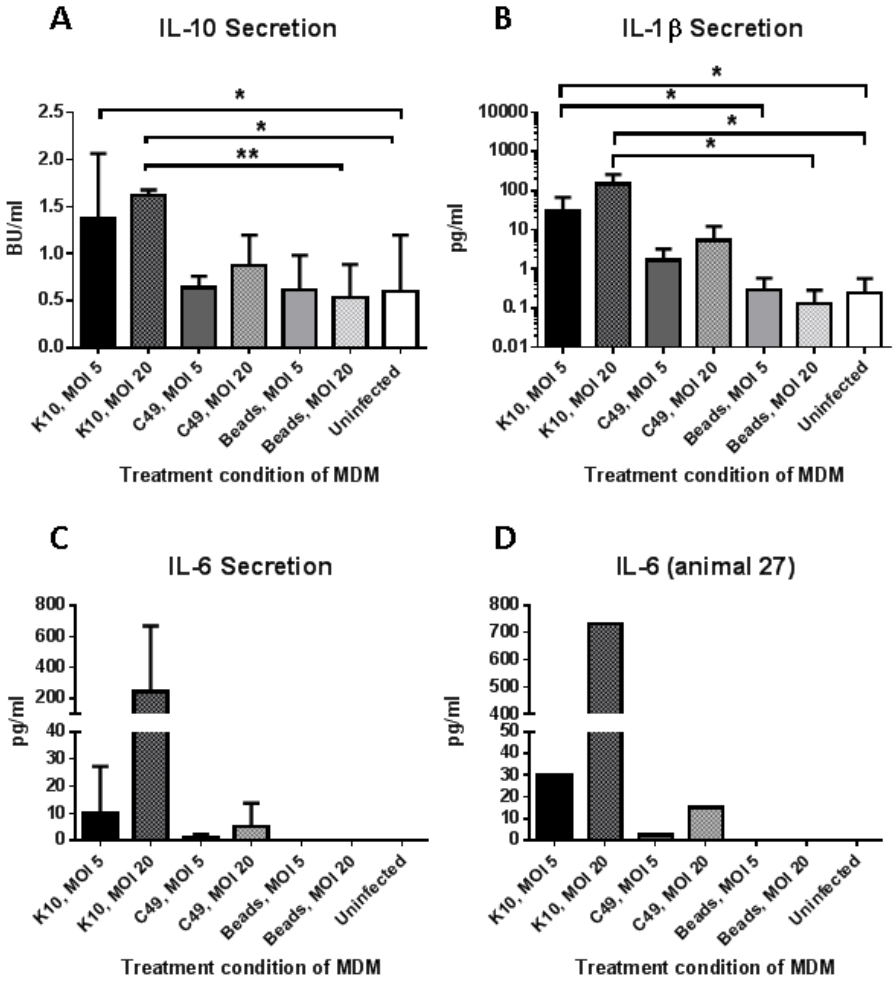

Figure 4-5 Cytokine secretion of MAP infected MDM at 24 HPI.

The concentration of IL-10 (A), IL-1β (B) and IL-6 (C), in the supernatant of MDM infected with C49 or K10 at MOI 5 or 20 was measured by ELISA at 24 HPI. Polystyrene beads were included at the same multiplicities as non-infectious controls. Graphs represent the mean and standard deviation of 4 biological replicates (A & B) or 3 biological replicates (including Animal 27) (C) IL-6 ELISA results from animal 27 are also shown individually (D). Data were normally distributed ($p>0.05$) and 2-sample t-tests used to determine dose-effect. A General Linear Model was used to determine treatment effect. $p<0.05$, $p<0.01$** (IL-10 and IL-1β: N=4, IL-6: N =3)*

4.2.4 siRNA knockdown of NLRP3 inhibited IL-1β secretion by MAP infected MDM

As described in section 4.2.3, IL-1β production was significantly upregulated by K10, but not C49 infected MDM. However, the mechanism by which IL-1β was produced in response to K10 was unknown. IL-1β is produced via a two-step process - an inactive form (pro-IL-1β) is produced in response to PAMPs that signal through PRRs, and pro-IL-1β is subsequently cleaved to active IL-1β by a multi-protein structure known as the inflammasome. Several PRRs are capable of forming an inflammasome, however this study focused on the role of the NLRP3 inflammasome in MAP infection, as NLRP3 gene expression was upregulated by bovine MDM in response to MAP infection in previous RNA-Seq (Glass group, Roslin Institute (unpublished data)) and microarray studies (MacHugh et al. 2012). siRNA was used to knock down NLRP3 gene expression, in order to determine the role of the NLRP3 inflammasome in IL-1β secretion by MAP-infected MDM, and demonstrate if NLRP3 affects intracellular survival of MAP strains K10 and C49. For full detail of the method used, refer to Materials and Methods section 2.28. Briefly, NLRP3 was knocked down on day 14 of culture, by incubating MDM with siRNA and Lipofectamine RNAiMAX transfection reagent, at 37ºC, for 24 hours. After 24 hours, the media was replaced with fresh, sterile TCMb (Appendix A) and cells were incubated for a further 24 hours at 37°C. Several controls were included in the experimental set up: Negative Controls (NC) were untreated and incubated in TCMb only; Non-Template Controls (NTC) were treated with Lipofectamine and non-specific siRNA; and Transfection Controls (TC) were treated with Lipofectamine only. NTCs and TCs were included to demonstrate the non-specific effects of siRNA treatment and Lipofectamine, respectively. The most relevant control to assess the specific effect of NLRP3 siRNA treatment on a sample is, therefore, the NTC control. qRT-PCR was run to determine the level of gene KD by 48 hours post treatment; siRNA targeting NLRP3 achieved significant KD of NLRP3 gene expression, compared to all controls (an average of 39.3%, 54.2% and 46.5% gene KD, compared to NC, NTC and TC, respectively) (Figure 4-6).

Infection experiments were carried out at 48 hours post treatment, in order to understand how NLRP3 KD impacted IL-1β production by MAP infected MDM. Briefly, MDM treated with siRNA targeting NLRP3 were infected with K10 or C49 at MOI 5 (untreated MDM were also infected at MOI 5 for comparison). NC, NTC and TC were included as controls. At 24 HPI, RNA was extracted and reverse transcribed, in order to determine the level of NLRP3, OAS1 and IL-1β gene expression by qRT-PCR. Somewhat in agreement with the RNA-Seq and microarray studies described previously (Glass group, unpublished data), (MacHugh et al. 2012), NLRP3 gene expression was upregulated by K10 infected MDM, but not C49 infected MDM, compared to NC. There were no significant differences between NC, NTC and TC (Figure 4-6 A). NLRP3 gene expression was significantly reduced in K10 and C49 infected MDM treated with siRNA targeting NLRP3, in comparison to untreated K10 and C49 infected MDM (Figure 4-7 A). Expression of OAS1 was measured to assess off-target effects of NLRP3 KD. OAS1 gene expression is induced by interferons and type 1 interferon production is a potential off-target effect of siRNA delivery, as it is naturally produced by mammalian cells in response to nucleic acids in the cytosol (McNab et al. 2015). Additionally, cationic liposomes (i.e. Lipofectamine RNAiMAX transfection reagent) are known to induce an immune response *in vitro*, in the absence of siRNA, through the extracellular-signal-regulated kinase (ERK) pathway (Karlsen & Brinchmann 2013; Yan et al. 2007). OAS1 gene expression was significantly increased in NTCs and TCs, as well as MDM treated with NLRP3 siRNA (Figure 4-7 B), however the upregulation was reduced compared to initial experiments by amending the protocol of NLRP3 KD to incorporate a wash step at 24 HPI, as detailed by Jensen et al (data not shown) (Jensen et al. 2014). It is unlikely that the interferon response could have been reduced further, without impairing target gene KD. NLRP3 KD had no impact on IL-1β gene expression. Somewhat in agreement with the findings presented in Figure 4-4, IL-1β gene expression was increased in K10 compared to C49 infected MDM. However, this increase did not reach significance, likely due to the large degree of biological variation observed (Figure 4-7 C).

In order to confirm that KD of NLRP3 reduced IL-1β production, thereby demonstrating that IL-1β is produced via the NLRP3 inflammasome in the context of

MAP infection, IL-1β secretion was measured by ELISA. Briefly, MDM were treated with siRNA, as described above, and NTCs were included in the experimental set-up. MDM treated with siRNA targeting NLRP3 were either left uninfected or infected with K10 or C49 at MOI 5. NTCs and untreated MDM were also infected with either K10 or C49 at MOI 5, for comparison. As observed in Figure 4-5, IL-1β secretion was significantly increased by K10, but not C49, infected MDM by 24 HPI, compared to uninfected controls. The concentration of IL-1β in the supernatant of K10 infected MDM was significantly reduced by NLRP3 KD, suggesting that MAP-induced IL-1β production was dependent on the NLRP3 inflammasome. Of note, the difference between K10 infected NTCs and K10 infected NLRP3 KD was not significant, however this was likely due to a reduced number of K10 infected NTC replicates(Figure 4-7.)

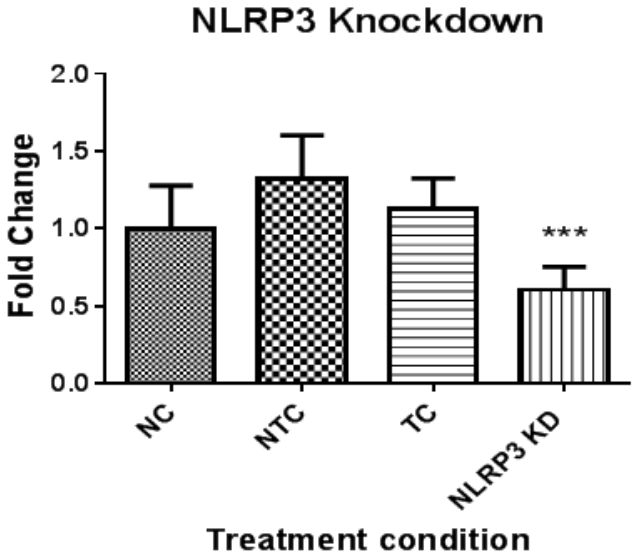

Figure 4-6 qRT-PCR measuring knockdown of NLRP3 gene expression

*On day 14 of culture MDM were treated with siRNA targeting NLRP3 for 48 hours and NLRP3 gene expression was measured by qRT-PCR. Bars represent the mean and SD of 3 biological replicates. NC = negative control, NTC = non-template control, TC = transfection control, NLRP3 KD = NLRP3 knockdown. Data were normally distributed and analysed by general linear model. P<0.001****

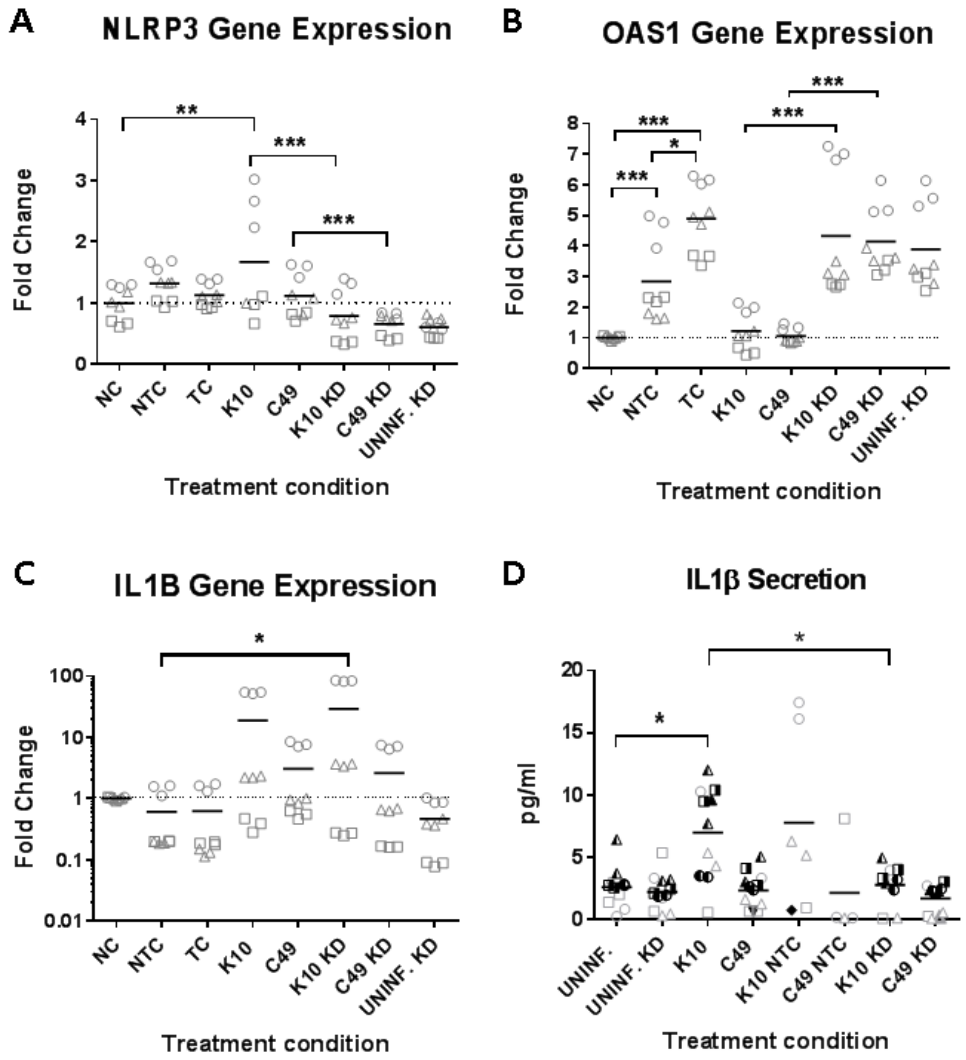

Figure 4-7 The effect of NLRP3 knockdown on IL-1β secretion and gene expression of MDM.

On day 14 of culture MDM were treated with siRNA targeting NLRP3 for 48 hours prior to infection with K10 or C49 at MOI 5. Gene expression of NLRP3, OAS1 and IL-1β was assessed at 24 HPI by qRT-PCR, and IL-1β secretion measured by ELISA at 24 HPI. (A) qRT-PCR measuring NLRP3 gene expression by MDM at 24 HPI. (B) qRT-PCR measuring OAS1 gene expression by MDM at 24 HPI. (C) qRT-PCR measuring IL-1β gene expression by MDM at 24 HPI. (D) ELISA measuring the concentration of IL-1β in the supernatant of MDM at 24 HPI. NC= negative control, NTC = non-template control, TC = transfection control, KD = knockdown. Horizontal lines represent the mean of 3 (A-C) or 6 (D) biological replicates. Shapes represent individual biological replicates (data-points of the same shape represent qRT-PCR technical replicates). Data in A were normally distributed ($p>0.05$) and analysed by general linear model. Data in B, C, and D were non-normally distributed ($p<0.05$) and analysed by Kruskal Wallis and Mann-Whitney

tests ($p<0.05$, $p<0.01$**, $p<0.001$***). Variance between biological replicates was also assessed and significant differences were found for A ($p<0.001$***), B ($p<0.01$**), C ($p<0.001$***), D ($p<0.001$***), E ($p<0.001$***) and F ($p<0.001$***).*

4.2.4.1 NLRP3 knockdown did not impact intracellular survival of MAP within MDM

The effect of NLRP3 knockdown (as described above) on intracellular survival of MAP was assessed by lysing infected cells at 0.5 HPI and 24 HPI, and plating serial dilutions of the lysate, in order to calculate the percentage survival at 24 HPI, compared to 0.5 HPI. In addition to the siRNA knockdown, MDM stimulated with 1µg/ml LPS, at the point of infection, were included in order to draw comparison; LPS stimulates MDM (through TLR4 signalling) to produce cytokines and antimicrobial products, and it was hypothesised that LPS stimulation of MDM may reduce intracellular survival of MAP.

There was no significant difference in the intracellular survival of K10 in untreated MDM, compared to MDM stimulated with LPS and MDM treated with NLRP3 siRNA (Figure 4-8 A). Surprisingly, higher levels of K10 intracellular survival were observed in untreated cells, compared with the earlier experiment presented in Figure 4-1 A. NLRP3 knockdown also had no impact on the intracellular survival of C49 by 24 HPI, compared to intracellular survival in untreated MDM or MDM treated with 1µg/ml LPS (Figure 4-8 B). It initially appeared that NLRP3 knockdown may have impacted intracellular bacterial survival (of K10 and C49) for some individual biological replicates, however the rate of intracellular survival was compared between biological replicates and no statistical differences were observed (Figure 4-8).

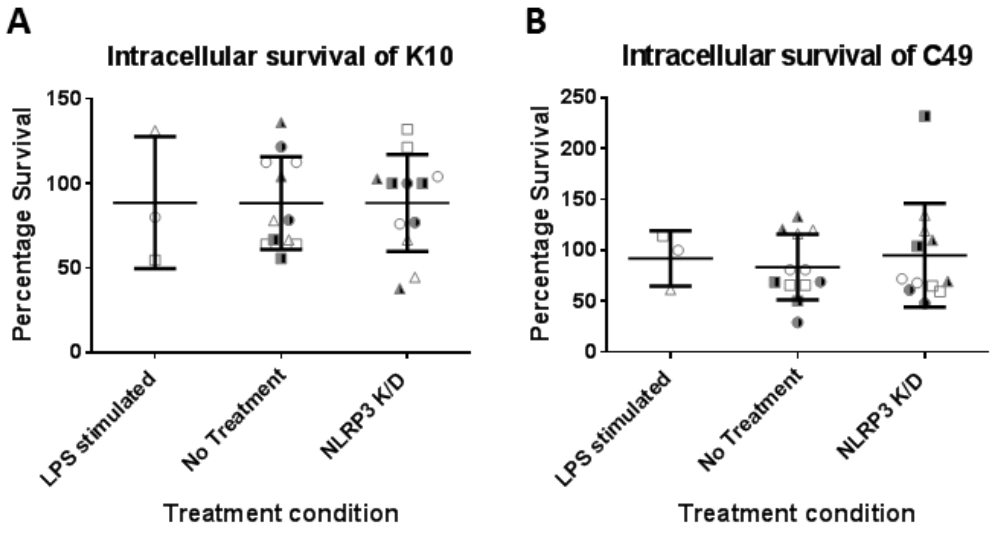

Figure 4-8 The impact of NLRP3 knockdown on intracellular survival of MAP infected MDM.

MDM were treated with siRNA targeting NLRP3 prior to infection with K10 or C49 at MOI 5, in order to assess if NLRP3 knockdown impacted intracellular survival of MAP. (A) The effect of NLRP3 gene knockdown on intracellular survival of K10 at MOI 5. (B) The effect of NLRP3 gene knockdown on intracellular survival of C49 at MOI 5. Horizontal lines represent the mean, error bars represent the SD and the shape and fill of symbols represent individual biological replicates (N=6). Data were normally distributed ($p>0.05$) and analysed by general linear model. There were no significant differences. Variation between biological replicates was assessed by Kruskal Wallis; there were no significant differences.

4.2.5 Phagosome maturation in MAP infected MDM

The aim of this experiment was to understand if K10 and C49 differ in ability to arrest phagosome maturation at MOI 5, which could account for differences in percentage survival observed between the two strains (as shown in Figure 4-1 A). CD71 is an early endosomal marker, whereas LAMP1 is a late endosomal marker. MDM were infected with K10 or C49 at MOI 5 (beads were given at the same multiplicity as a non-infectious control, in addition to uninfected controls) and expression of the genes encoding CD71 and LAMP1 was analysed by qRT-PCR at 2, 6, and 24 HPI. MDM infected with K10 at MOI 5, significantly upregulated CD71 gene expression, compared to uninfected controls, at 2, 6 and 24 HPI and compared to non-infectious controls (beads) at 6 and 24 HPI. C49 infected MDM upregulated CD71 gene expression compared to non-infectious controls, at 6 and 24 HPI; however, not to the same extent as K10 infected cells, which had significantly higher levels of CD71 gene expression (compared to C49 infected MDM) at the same time-points. Gene expression of CD71 was highest at 6 HPI (Figure 4-9 A). LAMP1 gene expression was upregulated by C49 infected MDM compared to non-infectious controls, at 6 HPI. At 24 HPI, K10 infected MDM had significantly higher LAMP1 gene expression compared to C49 infected MDM, non-infectious controls, and uninfected controls (Figure 4-9 B).

Since gene expression analysis cannot inform on co-localisation of MAP with endosomal markers, confocal microscopy was employed to determine if MAP was co-localising with LAMP1 intracellularly, thereby demonstrating the ability of both MAP strains to inhibit phagosome maturation. MDM were infected with either live or heat inactivated (H/in) K10 or C49 at MOI 5. Infected MDM were fixed in 2% paraformaldehyde at 2 and 6 HPI and stained with antibodies targeting mycobacteria (red) LAMP1 (green) and DAPI to visualise nuclei (blue) (Figure 4-10). Z-stacks of infected MDM were created, with images captured at 1μm intervals. Both light microscopy (in order to observe the outline of the cells) and fluorescent microscopy (demonstrating fluorescent labelling of MAP, LAMP1, and nuclei) were included to create Z-stacks, demonstrating MAP to be intracellular (Figure 4-10 A). Maximum intensity projections of Z-stacks were then created and used to carry out image analysis using ImageJ software. Light microscopy was removed from Maximum

Intensity Projections to improve image clarity (Figure 4-10 B). Further details of the methodology are presented in Appendix F.

H/in forms of both strains were incorporated, in order to compare co-localisation of LAMP1 with live MAP versus killed MAP; it was hypothesised that live bacteria may interfere with phagosome maturation through an active process and that LAMP1 co-localisation with H/in MAP would be increased, compared to LAMP1 co-localisation with live MAP. A minimum of 70 MAP were included in the image analysis for each condition. K10 co-localisation with LAMP1 was significantly reduced for live bacteria, compared to H/in bacteria, at both 2 HPI and 6 HPI (Figure 4-11 A). Co-localisation of C49 with LAMP1 was also reduced in live cells compared to H/in cells at 2 and 6 HPI. However, there was a significantly higher percentage live C49 co-localising with LAMP1 at 2 HPI, compared to 6 HPI (Figure 4-11 B) - a result which was not observed for K10. The study was blinded, so as to avoid bias during image analysis.

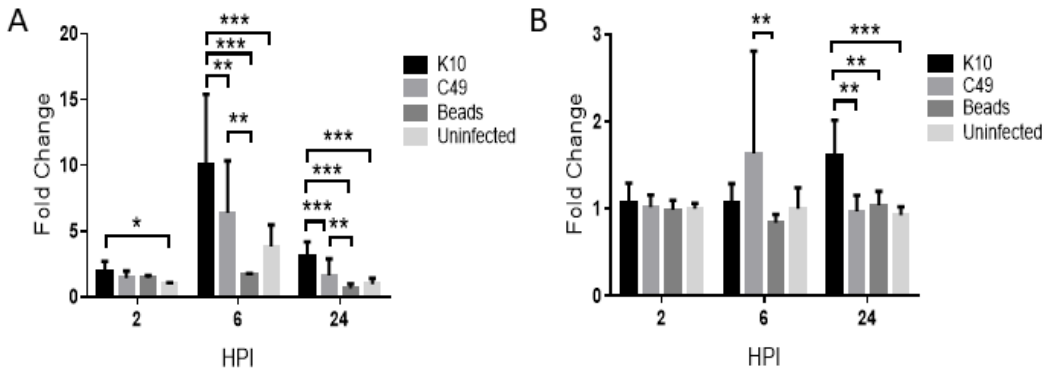

Figure 4-9 Expression of genes associated with phagosome maturation, by MAP infected MDM.

CD71 and LAMP1 gene expression by MDM infected with K10 or C49 at MOI 5 was measured by qRT-PCR at 2, 6 and 24 HPI. (A) qRT-PCR measuring CD71 gene expression (B) qRT-PCR measuring LAMP1 gene expression. Polystyrene beads (labelled 'Beads') were included as non-infectious controls. Results are expressed as fold change in relation to uninfected controls at 2 HPI. Bars represent the mean of 3 biological replicates and error bars represent SD. Data in A were normally distributed ($p>0.05$) and measured by general linear model. Data in B were non-normally distributed and measured by Kruskal Wallis and Mann-Whitney tests. $p<0.05$, $p<0.01$**, $p<0.001$****

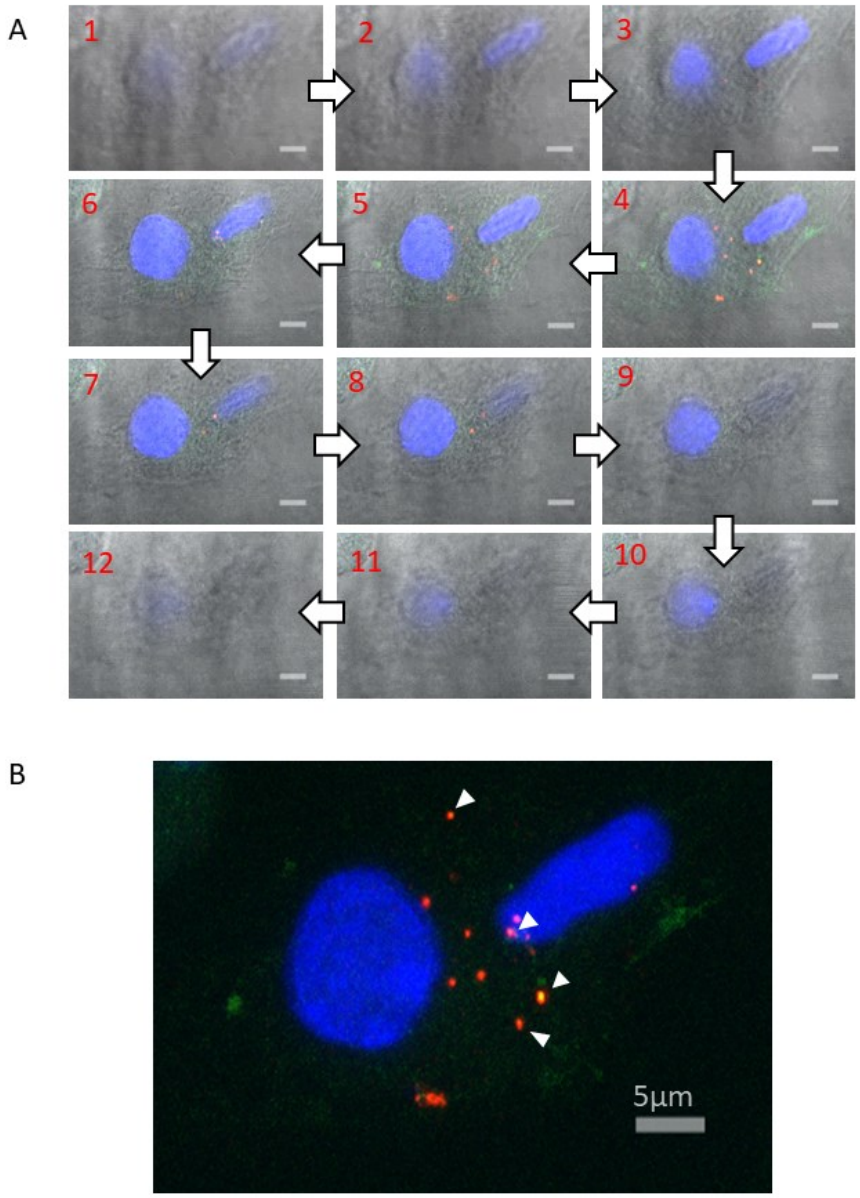

Figure 4-10 Confocal microscopy analysing co-localisation of MAP with the late endosomal marker LAMP1

MAP-infected MDM monolayers were stained by immunocytochemistry and visualised by confocal microscopy, in order to assess if MAP co-localised with LAMP-1 intracellularly. (A) Example of the Z-stack images collected to demonstrate that MAP were present only intracellularly. Images were taken at 1µm intervals vertically through cells; numbers represent an individual image at each interval and demonstrate the order in which the images were captured. A light microscopy image was included so as to observe the outline of the cells. (B) A maximum intensity projection of all Z-stack images presented in A. The light microscopy image was removed for clarity. Arrows indicate MAP positive for co-localisation with LAMP1. Maximum intensity projections were utilised for image analysis. All error bars represent 5µm. Green = LAMP1, red = MAP, blue = nuclei

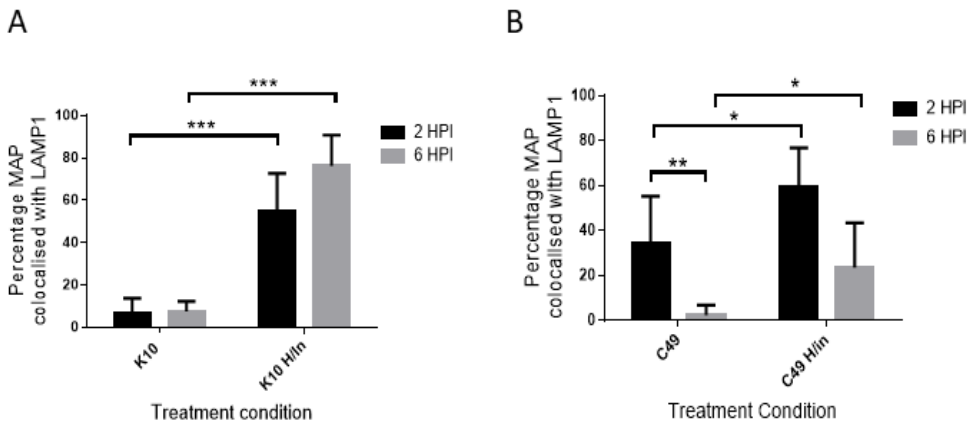

Figure 4-11 Co-localisation of MAP strains with the late endosomal marker LAMP1 at 6 and 24 HPI.

MDM monolayers were infected with either viable or H/in K10 or C49 at MOI 5, fixed at 2 and 6 HPI, stained by immunocytochemistry and visualised by confocal microscopy, in order to assess if MAP co-localised with LAMP-1 intracellularly. (A) Percentage of K10 and H/in K10 co-localised with LAMP1. (B) Percentage of C49 and H/in C49 co-localised with LAMP1. Bars represent the mean and standard deviation of ≥ 70 technical replicates (N=1 biological replicate). Data were normally distributed (p>0.05) and analysed by general linear model. P<0.05, p<0.01**, p<0.001****

4.2.6 MAP infection does not significantly increase production of Reactive Oxygen Species by MDM

The aim of this experiment was to investigate if MDM produced differential levels of ROS when infected with K10, compared to C49 at MOI 5. It was hypothesised that K10 infected MDM would produce higher levels of ROS than C49 infected MDM, potentially explaining the decreased intracellular survival of K10 at MOI 5 presented in Figure 4-1. To investigate the role of ROS in MAP infection, fold change of NOX2 gene expression was analysed by qRT-PCR at 2, 6 and 24 HPI. NOX2 (also known as gp91-phox or CYBB) is a gene encoding a subunit of NADPH oxidase, an enzyme important for the production of superoxide (Murphey & Weaver 2016). At 24 HPI, K10 infected MDM had significantly higher NOX2 gene expression, compared to C49 infected MDM and uninfected controls (Figure 4-12 A). The CellROX Deep Red Flow Cytometry Assay (Thermo Fisher Scientific) was then used to measure intracellular ROS within live cells at 2 HPI. The CellROX reagent is a membrane permeable dye that fluoresces upon oxidation. Flow cytometric analysis demonstrated that GM fluorescence intensity did not increase in infected cells, compared to uninfected. However, there was a significant increase in GM fluorescence intensity in MDM stimulated with LPS, compared to uninfected controls, demonstrating the reliability of the assay and that MDM are capable of producing ROS (Figure 4-12 B).

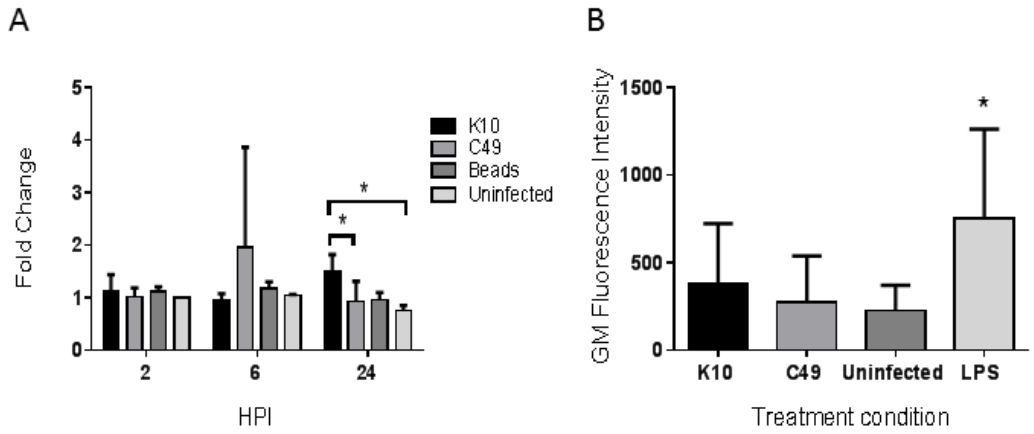

Figure 4-12 Reactive oxygen species production by MAP infected MDM.

The role of ROS in MAP infection was investigated by assessing NOX2 gene expression by MDM infected with K10 or C49 at MOI 5 at 2, 6 and 24 HPI, by qRT-PCR. In addition, ROS production by MDM infected with K10 or C49 at MOI 5 was analysed by flow cytometry (A) Fold change in NOX2 gene expression, measured by qRT-PCR. Results are expressed as fold change in relation to uninfected controls at 2 HPI. Polystyrene beads were included at the same multiplicity as a non-infectious control. (B) GM fluorescence intensity of MDM treated with fluorogenic CellROX deep red reagent at 2 HPI. Increased GM fluorescence intensity indicates increased ROS production. Bars represent the mean and standard deviation of 3 biological replicates (A &B). Data were non-normally distributed ($p<0.05$) and analysed by Kruskal Wallis and Mann-Whitney tests. $P<0.05$ (N=3)*

4.2.7 MAP infection causes MDM to significantly increase Reactive Nitrogen Species production

This experiment aimed to understand if MDM respond to MAP infection by producing RNS. MDM were infected with K10 or C49 at MOI 5 and polystyrene beads were added at the same multiplicity as non-infectious controls, in addition to uninfected controls. Expression of NOS2 (the gene encoding iNOS) by infected MDM, compared to controls, was analysed at 2, 6 and 24 HPI by qRT-PCR. K10 and C49 infected MDM expressed higher levels of NOS2, compared to both uninfected and non-infectious controls, at 2, 6 and 24 HPI. In addition, at 6 and 24 HPI, NOS2 gene expression was significantly higher in K10 infected MDM, compared to C49 infected MDM (Figure 4-13A).

In addition to analysing NOS2 gene expression, secretion of nitrite (a metabolite of NO) into the supernatant of infected cells was measured by the Griess assay, at 24 HPI. Supernatants from both K10 and C49 infected MDM contained a significantly higher concentration of nitrite, compared to non-infectious controls. Furthermore, the supernatants of K10 infected MDM contained a significantly higher concentration of nitrite than supernatants from C49 infected MDM (Figure 4-13 B).

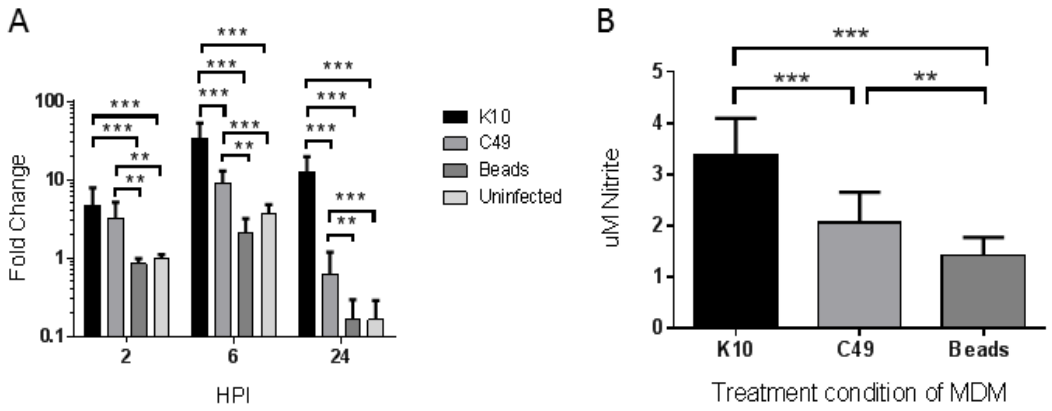

Figure 4-13 Production of NO by MAP infected MDM.

The role of RNS in MAP infection was investigated by assessing NOS2 gene expression by MDM infected with K10 or C49 (at MOI 5) at 2, 6 and 24 HPI, by qRT-PCR. In addition, nitrite secretion into the supernatant of infected MDM was measured at 24 HPI by Griess assay. (A) Fold change in NOS2 gene expression, measured by qRT-PCR. Results are expressed as fold change compared to uninfected controls at 2 HPI. Polystyrene beads were added at the same multiplicity as a non-infectious control and are labelled 'Beads'. Bars represent the mean and standard deviation of 3 biological replicates. (B) Concentration of nitrite in the supernatant of MDM infected with K10 or C49 at MOI 5 , at 24 HPI, measured by Griess assay. 'Beads' refers to MDM given polystyrene beads at the same multiplicity as a non-infectious control. Bars represent the mean and standard deviation of 3 biological replicates. Data presented in A were normally distributed ($p>0.05$) and measured by general linear model. Data presented in B were non-normally distributed ($p<0.05$) and measured by Kruskal Wallis and Mann-Whitney tests. $p<0.05$, $p<0.01$**, $p<0.001$****

4.2.8 Inhibition of Inducible Nitric Oxide Synthase

Work presented in this chapter demonstrates an association between increased NOS2 gene expression, increased nitrite secretion, and reduced intracellular survival of K10 compared to C49, at MOI 5 (Figure 4-1 & Figure 4-13). However, this association alone did not prove that reduced intracellular survival of K10 was directly caused by increased production of RNS by infected MDM. In order to investigate this further, the non-selective NOS inhibitor L-NMMA was utilised to prevent RNS production and assess the impact of reduced RNS on intracellular survival of MAP. LPS is known to stimulate MDM to produce nitrite, therefore 1μg/ml LPS was added to K10 or C49 infected MDM as a positive control. H/in forms of K10 and C49 were also included in the experiment, as non-infectious controls, in order to understand if nitrite secretion was in direct response to the presence of live MAP, or simply in response to PAMPs on the bacterial cell surface. The concentration of nitrite in the supernatant of MDM monolayers was measured by Griess assay at 24 HPI; L-NMMA successfully inhibited the secretion of nitrite by K10 and C49 infected cells stimulated with LPS (Figure 4-14 A). However, the results of the previous experiment, presented in Figure 4-13 were not repeated, as MAP infected MDM did not secrete significantly higher concentrations of nitrite when compared to uninfected controls. The concentration of nitrite was slightly lower in the supernatant of MDM infected with H/in K10 or C49; however, this difference did not reach significance.

The effect of NOS inhibition by L-NMMA on intracellular survival of MAP was also assessed. MDM were infected with K10 or C49 at MOI 5 and either stimulated with 1μg/ml LPS or unstimulated. Monolayers were lysed at 0.5 HPI and 24 HPI and serial dilutions of the lysate plated in order to count CFU. Percentage survival at 24 HPI was calculated relative to the number of intracellular CFU at 0.5 HPI. Despite there being little nitrite produced by K10 infected MDM (in the absence of LPS stimulation) (Figure 4-14 A), a significant decrease in K10 intracellular survival at 24 HPI was observed – an effect that was absent in the presence of L-NMMA. Therefore, the reduction in K10 survival may be directly attributed to the activity of iNOS. However, it is interesting to note that the increased secretion of nitrite

observed in LPS stimulated MDM (Figure 4-14 A) did not result in a decrease in intracellular survival of either K10 or C49 (Figure 4-14 B)

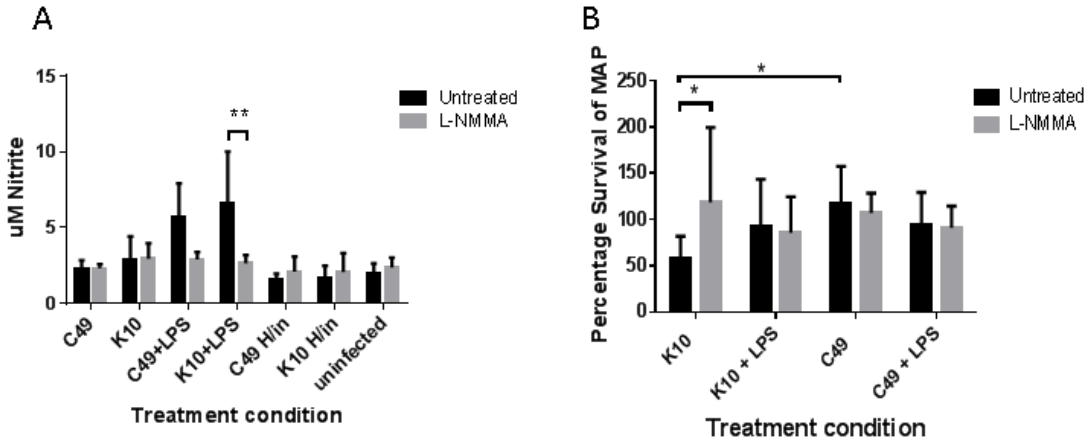

Figure 4-14 Inhibition of iNOS by L-NMMA.

iNOS was inhibited by L-NMMA, in order to understand if RNS production directly impacted the ability of MAP strains to survive intracellularly .(A) Griess assay measuring the concentration of nitrite in the supernatant of MAP-infected MDM treated, or untreated, with L-NMMA, at 24 HPI. MDM were infected at MOI 5. H/in refers to heat-inactivated MAP. MAP infected MDM treated with 1μg/ml LPS were included as positive controls. (B) Percentage intracellular survival of MAP strains at 24 HPI, measured by CFU count. Bars in both A & B represent the mean and standard deviation of 3 biological replicates. Data were normally distributed ($p>0.05$) and analysed by general linear model. $P<0.05$, $p<0.01$***

4.2.9 Sequencing of MAP strains

In order to further understand differences observed between the macrophage response to K10 and C49, and potential causes of these differences, genome sequencing of both strains was carried out by MicrobesNG. DNA was extracted from 3 technical replicate samples of both K10 and C49 according to the instructions provided by MicrobesNG. Although the MAP reference genome is the K10 strain (accession number NC_002944), analysis of the K10 strain used throughout this study was included, so as to determine any divergence between this and the reference genome. Sequencing was performed using Illumina HiSeq 2500 and initial bioinformatic analysis, including variant calling, was carried out by MicrobesNG. Further bioinformatic analysis was carried out by Rodrigo Bacigalupe. Briefly, sequencing reads of strains K10 and C49 were mapped to the reference genome of MAP, strain K10, using Burrows-Wheeler Aligner (BWA). Identification of single nucleotide polymorphism (SNPs) and short insertions and deletions (indels) was performed using SAMtools and Genome Analysis Toolkit (GATK). Only mutations that were common to all 3 replicates are presented.

Bioinformatic analysis identified 72 mutations that were common to both the K10 and C49 strains but absent from the reference genome. 17 of these mutations were frame shift mutations with a high-effect (meaning that the protein encoded by the gene is disrupted), and are detailed in Table 8. Of these 17 mutations, 9 are associated with either hypothetical proteins, or conserved hypothetical proteins. Two mutations occur on a locus that is associated with virulence (mce2 and MAP3603). Other mutations were present in genes encoding a membrane protein (MAP3788), an efflux protein (MAP2081), serine threonine protein kinase (pknA), fatty acids (echA3), energy metabolism (MAP3956), and a glycosyltransferase (MAP4156).

Position	Ref	Alt	Locus
19072	A	AC	pknA
148110	TC	T	MAP0142c
1348418	CG	C	MAP1266c
1847089	TC	T	MAP1687
1864323	AC	A	MAP1705c
1886935	GC	G	MAP1726c
1914846	TG	T	MAP1751
2300420	GC	G	MAP2081
3607486	C	CT	MAP3250
3999142	TG	T	MAP3603
4235461	GA	G	MAP3788
4417540	G	GA	MAP3956
4553473	AC	A	mce2
4577679	AC	A	echA3
4634485	CG	C	MAP4156
4691109	CG	C	MAP4221c
4827081	AC	A	MAP4346c

Table 8. High-effect mutations common between both K10 and C49 strains but absent from the reference strain. *'High-effect' refers to mutations that disrupt the protein encoded by the gene.*

Only four mutations were specific to the K10 strain used throughout this study, and of these four mutations only 1 (an indel mutation) had a high-effect (Table 9). The mutated gene was associated with respiration (Li et al. 2005); therefore, this mutation could potentially account for the reduced ability of the K10 used in this study to survive within an intracellular environment.

Position	Ref	Alt	Locus
2115910	TC	T	MAP1915

Table 9. High-effect mutations specific to the K10 MAP strain used in this study (in comparison to the reference K10 genome). *'High-effect' refers to mutations that disrupt the protein encoded by the gene.*

247 mutations (237 SNPS and 10 indels) were specific to the C49 strain. Of these mutations, 10 had a high effect (

Table 10). Of these high effect mutations, 2 occurred on a locus with unknown function, 1 affected an insertion sequence, and 2 were conserved hypotheticals. Processes affected by C49 high effect mutations include: the modification of fatty acids (MAP0097c), amino acid biosynthesis (gshA), respiration (MAP0445c), detoxification (MAP3682), and polyketide and non-ribosomal peptide synthesis (MAP3721) (Li et al. 2005).

Position	Ref	Alt	Type	Locus
104639	CG	C	FRAME_SHIFT	MAP0097c
326891	C	CG	FRAME_SHIFT	gshA
470098	G	A	STOP_GAINED	MAP0442
473112	G	T	STOP_GAINED	MAP0445c
685570	A	C	STOP_LOST+SPLICE_SITE_REGION	MAP0663
989614	G	GA	FRAME_SHIFT	MAP0955
2893583	GC	G	FRAME_SHIFT	MAP2573
3300014	TC	T	FRAME_SHIFT	MAP2963c
4090458	G	GC	FRAME_SHIFT	MAP3682
4140707	GC	G	FRAME_SHIFT	MAP3721

Table 10 High-effect mutations specific to the C49 MAP strain. *'High-effect' refers to mutations that disrupt the protein encoded by the gene.*

4.3 Discussion

The K10 strain of MAP used throughout this study (ATCC no: BAA968) was isolated in Wisconsin in July 1990 and is likely to have undergone lab-adaptation (Radosevich et al. 2007). It was hypothesised that K10 may have lost virulence (due to lab-adaptation) and that MDM may be more efficient at responding to, and potentially clearing infection with K10, compared to a clinical isolate of MAP. Therefore, a key aim of this chapter was to assess the nature of the MDM response to K10, compared to the recent clinical isolate C49, and determine if intracellular survival, within MDM, differed between the two strains. Observed differences in the MDM response to K10 compared to C49 could significantly impact the field, as the K10 strain has previously been extensively used to study the early host response to MAP infection. (Kugadas et al. 2016; Bannantine et al. 2015; Ghosh et al. 2014; Lamont et al. 2013; Lamont et al. 2012). Significant differences were observed between the macrophage response to K10, compared to a clinical isolate, could therefore call into question the clinical relevance of using K10 to model the infection *in vitro*.

In addition to analysing strain effect, an MOI 5, 20 and 50 of K10 and C49 were selected in order to analyse the dose effect of MAP infection. At MOI 50, intracellular survival of K10 approximately tripled by 24 HPI and survival of MDM was reduced compared to uninfected controls; this suggested that at MOI 50 K10 could rapidly multiply intracellularly, likely directly causing cytotoxicity. MOI 50 was therefore excluded from future experiments, and only MOI 5 and 20 were further investigated. C49 survival remained fairly constant (~100% survival by 24 HPI) at either MOI 5 or 20, however K10 survival was significantly decreased at MOI 5, compared to C49, suggesting that the lab-adapted K10 strain is less robust than the clinical isolate C49, at low doses. This could be due to a loss of genes associated with virulence from the K10 strain, suggesting its use may not accurately represent clinical host-pathogen interactions. MAP infection at MOI 5 or 20 (with either strain) appeared to promote MDM survival, compared to uninfected controls; this is likely a survival strategy of MAP, as the macrophage is its preferred niche; it

has previously been demonstrated that MAP can promote the survival of primary bovine macrophages by suppressing apoptosis (Kabara & Coussens 2012).

The effect of strain and dose on CSM expression of infected MDM was analysed by flow cytometry. The CSM analysed included the MR (CD206), DC-SIGN (CD209), and CD11b, which are all phagocytic receptors. Phagocytic receptors facilitate the uptake of foreign material by MDM, and uptake of mycobacteria through the different receptors can lead to differential downstream responses by infected cells. Expression of these particular receptors was measured due to evidence in the literature showing that mycobacteria can interact with each of them. For example, *M. tb* has been shown to target its uptake through the MR, in order to arrest phago-lysosome fusion (Kang et al. 2005; Sweet et al. 2010). CD11b is a complement receptor and complement likely plays an important role in the uptake of MAP; Schorey et al first demonstrated that pathogenic mycobacteria (but not non-pathogenic species) actively promote their uptake through this pathway (Schorey et al. 1997). In addition, *M. bovis* BCG, *M. tb* and MAP have all been reported to bind to DC-SIGN *in vitro*, and uptake of the mycobacterial cell surface glycolipid, Man-LAM, through DC-SIGN led to increased IL-10 production in DCs *in vitro* (Geijtenbeek et al. 2003). It is, therefore, reasonable to infer that MAP infection may have altered the level of expression of these phagocytic receptors. Surprisingly, no differences were observed in the expression of the MR, DC-SIGN or CD11b in MDM infected with either strain of MAP at MOI 5, compared to either uninfected controls or non-infectious controls given polystyrene beads at the same multiplicity. Although MR expression was significantly increased at 2 HPI on MDM infected with K10 or C49 at MOI 20 (compared to uninfected controls), there was no significant difference in MR expression on infected cells, compared to non-infectious controls. This suggests that the increase in expression was a transient effect of a high level of phagocytosis, as opposed to a specific response to MAP infection. The role of phagocytic receptors in MAP infection is further discussed in Chapter 5.

MHC II and CD40 expression were also analysed by flow cytometry in the context of MAP infection. MHC II expression, together with expression of co-stimulatory molecules, such as CD40, are essential for effective antigen presentation and

activation of T-helper cells, and driving the critical Th-1 response necessary to control mycobacterial infection. Several species of pathogenic mycobacteria, are known to cause the upregulation of co-stimulatory molecules, including CD40, by infected macrophages (Kumar et al. 2014; Wang et al. 2015). In addition, there is much evidence in the literature demonstrating that several mycobacteria species are capable of downregulating MHC II expression, allowing them to prevent the activation of T-cells and evade the immune response (Noss et al. 2001; Wojciechowski et al. 1999; Weiss et al. 2001). It was therefore, hypothesised that MAP infection may alter the level of expression of these molecules. Contrary to previous studies analysing the CSM expression macrophages infected with MAP and other pathogenic mycobacterial species, no differences were observed in CD40 or MHC II expression between infected cells and non-infectious controls, at either MOI 5 or 20. MHC II expression was upregulated at 2 HPI in K10 and C49 infected MDM, compared to uninfected controls, however, as there was no difference between the non-infectious controls, this is likely to be a non-specific effect. The differences between the results of this study and the results of the 2001 study by Weiss et al (Weiss et al. 2001) could potentially be explained by dose effect, as Weiss et al used MOI 10 as opposed to MOI 5 or 20. In addition, different strains were used, suggesting these reported differences could be a strain-specific effect. It should be noted however, that a similar pattern of downregulation of MHC II expression at 24 HPI (MOI 5) was observed between MAP infected MDM in this study and in the study by Weiss et al (Weiss et al. 2001) , except that the results of this study did not reach significance. It is therefore possible that the addition of more biological replicates would have produced a significant result.

Several studies have reported that mycobacterial infection induces macrophages to secrete both pro-inflammatory and anti-inflammatory cytokines (Abendaño, Juste, et al. 2013; Dudemaine et al. 2014; Cooper et al. 2011). As macrophage cytokine production can have a profound effect on infection outcome, differences in cytokine secretion by macrophages infected with K10 versus C49 were investigated. The cytokines IL-1β, IL-10 and IL-6 were selected for this study, as they have functional relevance during mycobacterial infection, as described below. In addition, the genes encoding these cytokines were previously reported to be among the highest

upregulated genes in bovine MDM infected with MAP in an microarray study (MacHugh et al. 2012). Furthermore, previous RNA-Seq analysis by the Glass group showed these genes to be highly upregulated within the first 24 hours of infection. Both studies were performed using clinical isolates of MAP; there have been no previous studies assessing differences in the transcriptomic profile of MDM infected with a clinical isolate of MAP, compared to the K10 strain.

At the gene expression level, all three cytokines were significantly upregulated in K10 infected MDM, compared to either uninfected or non-infectious controls, particularly at the later 24 HPI time-point; this effect was observed at both MOI 5 and 20. Upregulation of IL-6 and IL-10 (compared to either non-infectious or uninfected controls) was observed in MDM infected with C49 at MOI 5, and upregulation of IL-1β, and IL-6 (compared to either non-infectious or uninfected controls) was observed in MDM infected with C49 at MOI 20; however the upregulation of the genes encoding these cytokines was observed to a lesser extent in C49 infected MDM, compared to K10 infected MDM It is interesting to note that, at the protein level IL-1β and IL-10 were upregulated in K10 infected MDM, however IL-6 was not secreted (except in 1 biological replicate, which secreted IL-6 at very high levels), suggesting that post-translational modification could be taking place. It is possible that MAP directly interfere with IL-6 secretion as a virulence mechanism. IL-6 has varied biological functions but has been shown to play a critical role in induction of Th-1 responses after vaccination with a subunit vaccine against *M. tb* in a mouse model (Leal et al. 1999) and secretion is correlated with protection against *M. avium* in mouse models of infection (Appelberg et al. 1994). Previous studies investigating IL-6 in MAP infection have looked only at the mRNA level (Alzuherri et al. 1996; Adams & Czuprynski 1995; Adams et al. 1996). However, a study by Martinez et al reported *M. tb* to be capable of modulating macrophage IL-6 secretion and that increased IL-6 production resulted in decreased *M. tb* survival (Martinez et al. 2013); it is possible that MAP have a similar mechanism for interfering with IL-6 production to promote their own survival. It is interesting to note that sequencing analysis of the two strains identified a mutation common to K10 and C49 in a locus encoding serine threonine protein kinase, an enzyme involved in post-translational modification. IL-6 is important for inhibiting

the differentiation of T_{reg} cells and (together with TGF-β) plays an important role in the differentiation of Th-17 cells (Bettelli et al. 2006; Mangan et al. 2006), meaning that over production of IL-6 is associated with several inflammatory and autoimmune diseases, including Crohn's disease (see Introduction section 1.4) (Ito et al. 2004). Th-17 responses have been reported to correlate with protection against mycobacterial infection (Bull et al. 2014; Vordermeier et al. 2009; Khader et al. 2007), but likely contribute to inflammation-induced damage to the gut during Johne's disease.

IL-1β is a potent pro-inflammatory cytokine and has been reported to have important protective effects against *M. tb* infection in mouse models deficient of IL-1R1 (Fremond et al. 2007; Mayer-Barber et al. 2010). IL-1β has also been shown to have chemoattractant effects on bovine macrophages in an *in vitro* model of MAP infection (Lamont et al. 2012), which could promote further uptake of MAP. Therefore, increased levels of IL-1β secretion by K10, but not C49, infected MDM observed in this study could be an indicator of altered virulence in the K10 strain. Few studies have investigated IL-1β in the context of MAP infection, however a study by Borrman et al. demonstrated that a clinically isolated C-type strain induced significantly less IL-1β secretion than the K10 strain in THP-1 cells (a human monocytic cell line) (Borrmann et al. 2011b), further confirming that IL-1β production by MAP infected cells is strain-dependant.

IL-1β is produced by macrophages in a 2-step process involving inflammasome activation. Inflammasomes are multiprotein complexes that contain a PRR (primarily NLRs). This study focused on the role of the NLRP3 inflammasome in IL-1β production of MAP infected MDM, as NLRP3 gene expression was found to be upregulated in MAP infected MDM at 2 HPI in a an RNA-Seq study by members of the Glass research group (unpublished data) and a microarray study by MacHugh et al (MacHugh et al. 2012).

NLRP3 gene expression was upregulated by K10, but not C49 infected cells. This result was somewhat surprising, as a microarray study had previously reported up-regulation of NLRP3 gene expression in MDM infected with clinical isolates of MAP (MacHugh et al. 2012). However, C49 infection of MDM also did not induce

secretion of IL-1β in this study, suggesting that the lack of IL-1β secretion could be a result of reduced NLRP3 expression, as IL-1β is not being produced by through any other mechanism in response to C49 infection. As expected, based on previous ELISA results, K10 infected MDM increased secretion of IL-1β compared to NC. This increase in IL-1β secretion was reversed by NLRP3 knockdown, demonstrating that the NLRP3 inflammasome is the mechanism by which K10 infected MDM produce IL-1β. The role of the NLRP3 inflammasome in MAP infection has not been previously reported, however the finding that IL-1β production by MAP infected MDM is dependent on the NLRP3, is in agreement with studies involving other species of mycobacteria, as reviewed by Briken et al. (Briken et al. 2013). The finding that IL-1β secretion by MDM, in the context of MAP infection, is dependent on NLRP3 could be of significance for this field, as understanding molecular pathways involved in cytokine signalling by MAP infected MDM could benefit the design of novel vaccines against paratuberculosis. However, it should be noted that there was a high level of biological variation in this experiment and K10 infected MDM from some biological replicates did not secrete IL-1β at all. This could potentially have implications for how each of these biological replicates would respond to MAP infection *in vivo,* as there have been correlations between IL-1β and infection outcome. For example, IL-1R1 knockout mice have been reported to be highly susceptible to acute *M. tb* infection *in vivo* (Fremond et al. 2007),

The role of IL-1β and the NLRP3 inflammasome in intracellular survival of MAP was studied due to the association previously observed between reduced K10 intracellular survival and increased Il-1β secretion in K10 infected MDM. IL-1β binding to IL-1R1 results in MyD88 dependent signalling, NFκB activation and, subsequently, the production of proinflammatory cytokines and antimicrobial products (Dinarello 2009). It was therefore hypothesised that IL-1β secretion might have directly impacted the intracellular survival of MAP, perhaps through the production of ROS or RNS. However, NLRP3 knockdown had no effect on the ability of MAP to survive intracellularly. This finding is in agreement with a study by Fremond et al, investigating the role in IL-1R1 in *M. tb* infection in mice. The study demonstrated that IL-1R1 knockout mice were more susceptible to acute disease in the context of *M. tb* infection, but macrophages from IL-1R1 knockout

mice displayed no increased ability to control intracellular survival of *M. tb, in vitro* (Fremond et al. 2007). The protective role of IL-1β during infection is therefore not due to increasing bactericidal activity of macrophages.

The expression of OAS1 was assessed alongside NLRP3 and IL-1β during NLRP3 knockdown experiments, in order to assess the non-specific Type-1 IFN response induced by siRNA treatment. It is known that lipofectamine can induce Type-1 IFN production (Li et al. 1998) and an increase in OAS1 gene expression was observed for all cells treated with lipofectamine, therefore the role of Type-IFN must be included when drawing conclusions from knockdown studies. It has previously been demonstrated that Type-1 IFN can inhibit IL-1β secretion by *M. tb* infected primary human macrophages (Novikov et al. 2011), suggesting that non-specific Type-1 IFN, produced in response to lipofectamine, could potentially reduce IL-1β secretion by MAP infected MDM, compounding the results of this study. However, no reduction in IL-1β secretion was observed in K10 infected NTC, compared to untreated K10 infected cells, suggesting that inhibition of IL-1β was due to reduced NLRP3 expression only, and not to non-specific Type-1 IFN production. In addition, Type-1 IFN has been shown to have no impact of intracellular survival of *M. tb*. in mice (Desvignes et al. 2012), suggesting it is unlikely to compound the results of the NLRP3 knockdown intracellular survival assay. The effect of Type-1 IFN on intracellular MAP survival *in vitro* could be further investigated in future by directly treating MAP infected MDM with a range of concentrations of IFN-α and IFN-β to assess if these cytokines affect intracellular CFU count at early time-points post infection.

NLRP3 knockdown did not affect IL-1β gene expression; this result was expected as IL-1β gene expression is primarily induced by NFκB via TLR signalling, and should not be affected by NLRP3 expression (Poeck et al. 2010). In addition, IL-1β gene expression was not significantly reduced in the NTC or TC, suggesting that Type-1 IFN secretion did not negatively impact IL-1β gene expression.

IL-10 has been reported to reduce the protective response to *M. tb* in mouse models (Beamer et al. 2008; Hussain et al. 2016). IL-10 likely also has a non-protective effect during MAP infection; a mathematical model suggests that IL-10 expression

suppresses the Th-1 response and enhances the Th-2 response in MAP infected cattle (Magombedze et al. 2015). In addition, a study by Weiss et al. demonstrated IL-10 to have non-protective effects in an *in vitro* model of MAP infection, with neutralisation of IL-10 resulting in a >50% reduction in intracellular MAP survival by 96 HPI (Weiss et al. 2005). It was therefore surprising that both IL-10 and IL-1β were upregulated in K10 infected MDM. It should be noted, however, that in addition to having non-protective effects in mycobacterial infection, IL-10 is known to be critical in controlling levels of inflammation (Redford et al. 2010; Higgins et al. 2009) which could potentially result in tissue damage. It is therefore possible that IL-10 gene expression is increased in K10 infected MDM, in response to high levels of IL-1β secretion. Indeed, biological replicates with high levels of IL-1β secretion, simultaneously had high levels of IL-10 secretion.

It is well established that a common feature of pathogenic mycobacteria is the ability to arrest phagosome maturation (Via et al. 1997; Pieters 2008), and previous studies have reported MAP to be capable of arresting phagosome maturation in a mouse macrophage cell line and human polymorphonuclear cells (Rumsey et al. 2006; Purdie et al. 2012; Kuehnel et al. 2001). The process of phagosome maturation is described in detail in the Introduction (section 1.8.1) and involves acidification of phagosomes via accumulation of V-ATPase molecules on the membrane, and the fusion of the phagosome with the lysosome, which contains several degradative, hydrolytic enzymes capable of degrading protein, DNA, RNA, lipids and polysaccharides (Rosales & Uribe-Quero 2017; Cooper 2000). It was hypothesised that K10 may have reduced ability to arrest phagosome maturation compared to C49, which could account for the decreased intracellular survival observed at MOI 5.

CD71 is an early endosomal marker, expressed on the surface of phagosomes before maturation has occurred, whereas LAMP1 is a late endosomal marker, expressed on the surface of lysosomes; co-localisation of bacteria with LAMP1 demonstrates that phagosome maturation has occurred and that phago-lysosome fusion has taken place.

Gene expression of CD71 was increased in K10 and C49 infected MDM at 6 and 24 HPI, compared to non-infectious controls, although K10 infected MDM also had increased expression compared to C49 infected MDM at 6 and 24 HPI. Increased

CD71 expression complements the results of the RNA-Seq carried out by the Glass group, which showed that macrophages infected with two different strains of MAP upregulated CD71 gene expression at 2, 6 and 24 HPI, with the highest expression at 6 HPI. Up-regulation of CD71, compared to non-infectious controls in this experiment, was somewhat surprising, as it was hypothesised that CD71 would be upregulated in non-infectious controls in response to the process of phagocytosis. However, the lack of PAMPs on polystyrene beads may account for the reduced upregulation of CD71 in non-infectious controls, compared to infected cells. The CD71 gene encodes a transferrin receptor, which transports iron into cells. Although iron is required for bacterial growth, it is also required for bactericidal responses in host cells. An early study by Alford et al showed that intracellular killing of *Listeria monocytogenes* was inhibited in macrophages in the presence of a blocking antibody against transferrin (the ligand for CD71) (Alford et al. 1991). It is possible that increased intracellular iron in K10 infected MDM, due to increased CD71 expression, could account for the decrease in intracellular survival of K10, compared to C49.

Gene expression of LAMP1, was upregulated by C49 infected cells at 6 HPI and by K10 infected cells at 24 HPI (compared to non-infectious controls) potentially indicating an increase in phago-lysosome fusion. However, the upregulation was less pronounced than CD71 upregulation and was contrary to the results of the RNA-Seq experiment, described earlier, which did not show up-regulation of the gene encoding LAMP1 in MAP infected macrophages. It should be noted that LAMP1 is continuously present on the lysosomal membrane, and is trafficked to late phagosomes upon maturation; therefore, up-regulation of LAMP1 gene expression may not occur in direct response to phagocytosis, and gene expression analysis alone is insufficient to demonstrate if phagosome maturation has occurred. In order to address this question further, LAMP1 and MAP were detected within infected cells using fluorescent antibodies and co-localisation was assessed by immunocytochemistry. H/in forms of both K10 and C49 were included in the experimental design for comparison; it was expected that if arrest of phagosome maturation occurred, it would be as a result of an active process directed by a virulence mechanism of MAP, and that phagosomes containing H/in forms of the

bacteria would go through maturation and co-localise with LAMP1. However, both strains of live bacteria showed reduced co-localisation with LAMP1, compared to H/in strains at 2 and 6 HPI, and live C49 had significantly higher levels of co-localisation with LAMP1 at 2 HPI, compared to live K10 ($p<0.01$), suggesting that both K10 and C49 are capable of arresting phagosome maturation through an active virulence mechanism, and therefore decreased ability to arrest phagosome maturation was not the cause of the reduced intracellular survival of K10 observed at MOI 5.

Since arrest of phagosome maturation did not account for differences in survival observed between the two MAP strains, the role of antimicrobial products, such as ROS and RNS, in the intracellular killing of MAP was investigated. ROS can be produced by all mammalian cells but is primarily produced in polymorphonuclear cells and macrophages. Macrophages produce significantly higher levels of RNS than any other cell type and are capable of producing nearly equal amounts of both RNS and ROS, resulting in the generation of the potently destructive peroxynitrite (OONO2) (Nathan & Shiloh 2000). It was hypothesised that RNS and ROS might be produced at higher levels in K10 infected MDM than C49 infected MDM, which could account for the decreased intracellular survival of K10. Surprisingly, this study found that MAP infection had no effect on intracellular ROS production by infected MDM. However, NOS2 gene expression and nitrite secretion were significantly increased in both K10 and C49 infected MDM, compared to controls; additionally, there was significantly higher NOS2 gene expression and nitrite secretion in K10 infected cells, compared to C49 infected cells. These results suggest that RNS, but not ROS, may play a significant role in bactericidal activity of macrophages towards MAP. iNOS expression has previously been reported to be increased in granulomatous lesion in ileum and ileocaecal lymph nodes of MAP infected cattle, suggesting a role for iNOS and RNS in the pathogenesis of MAP (Delgado et al. 2010). This study investigated the role of RNS in MAP infection *in vitro* by use of the NOS inhibitor L-NMMA. Surprisingly, no increase in nitrite secretion by K10 infected MDM compared to uninfected controls was observed in untreated cells - contrary to the results previously demonstrated in Figure 4-13. This could potentially be explained by the use of a different set of biological replicates between the two experiments. Despite the lack of nitrite secretion by K10 infected

cells, the inclusion of LPS stimulation alongside MAP infection induced nitrite secretion and clearly demonstrated that treatment with L-NMMA effectively inhibited nitrite production. Despite no increase in nitrite secretion by K10 infected MDM, treatment with L-NMMA significantly increased K10 intracellular survival, compared to K10 survival within untreated cells. The same result was not observed for C49, or intracellular survival of either strain within LPS stimulated cells. This could possibly be explained by the fact that L-NMMA is an inhibitor of NOS, meaning that it will inhibit the production of NO, NO metabolites and RNS; since the Griess assay measures only nitrite secretion, it is possible that concentration of nitrite does not represent the full activity of iNOS and there could be high concentrations of other NO metabolites, such as nitrate, that are going unmeasured. The fact that nitrate has a significantly increased half-life compared to nitrite supports this theory (Dejam et al. 2007; Vavra et al. 2011; Bryan & Grisham 2007). Undetected high concentrations of nitrate produced by K10 infected cells could account for the increased K10 survival in the presence of L-NMMA. The experimental design could have been improved by incubating samples in nitrate reductase prior to performing the Griess assay, in order to convert nitrate to nitrite and thereby more accurately estimate the level of NO produced.

The genome sequence of both the K10 and C49 MAP strains used throughout this study were sequenced in order to understand MAP genomic differences that may have caused MDM to respond differently to infection with K10 versus C49, and effect the ability of the strains to survive intracellularly. It has previously been established that strain-type (i.e. C-type versus S-type) can impact the intracellular survival of MAP within bovine MDM, suggesting that the genetics of a specific strain could have a significant effect on its ability to survive within bovine macrophages (Abendaño, Sevilla, et al. 2013). A substantially higher number of specific mutations were observed for C49 (249) compared to K10 (4), demonstrating that there are genetic differences between these two MAP strains. Of the mutations present in C49, 10 were predicted to have a high effect. Notably, one of the high effect mutations specific to C49 (MAP0097c) is involved in the modification of fatty acids. A recent paper by Alonso-Hearn et al. identified differences in the fatty acid composition between the K10 MAP strain and a MAP isolate from sheep. The fatty

acids Palmitic acid and Tuberculostearic acid (TBSA) are essential for the binding of Man-LAM to the MR and it was suggested that fatty acid composition may alter the amount of Man-LAM on the cell surface or perhaps alter the spatial conformation, thereby affecting recognition by the MR, and uptake via this receptor (Alonso-Hearn et al. 2017). It should be noted that 72 common mutations were observed in both K10 and C49 compared to the reference strain (K10). This result suggests that either the K10 strain used throughout this project has mutated from the reference strain (possibly due to freeze-thaw cycles or passage – although passage number was low), or that there were sequencing errors or some inaccuracies with the alignment with the reference strain.

Infection of bovine MDM with MAP was selected as a model for this infection as previous studies comparing bovine MDM and a bovine peritoneal macrophage cell line (BoMac), have shown significant differences between the 2 cell types in their response to MAP infection (Woo et al. 2006; Abendaño, Sevilla, et al. 2013); suggesting that the use of this cell line may not reliably model the response of primary cells. However, a drawback of using primary MDM for this study was the introduction of biological variation, as individual animals appeared to have unique responses to MAP. Biological variation between samples can be caused by several factors, including environmental factors such as diet, climate, and previous exposure to infection, as well as age, sex, lactation, and genotype. Although, biological variation was somewhat controlled for, as all cattle used throughout the study were approximately age-matched heifers housed under the same conditions, animal 27, which produced higher levels of cytokine and nitrite secretion in response to K10, was a Norwegian Red-Holstein cross, whereas all other animals were Holstein-Friesians – potentially explaining (at least in part) the differential response of this animal to MAP infection. There is a known genetic association with susceptibility to paratuberculosis (Pritchard et al. 2017; Attalla et al. 2010; Küpper et al. 2012), however there have currently not been any studies directly comparing susceptibility between different breeds of cattle. The difference in the genotype of this replicate was unknown until after experiments had been carried out, and care was subsequently taken to ensure MDM were derived from Holstein-Friesians only. Host genetic factors undoubtedly impact the outcome of infection, as not all infected

animals go on to develop clinical disease. It would have been interesting, although out-with the scope of this project, to carry out *in vivo* infection experiments on the cattle that donated PBMCs for this study, in order to gain an understanding of how differential responses between biological replicates to would correlate to the development of clinical disease. Despite the high level of biological variation, MDM undoubtedly respond differently to the K10 and C49 strain of MAP, with decreased intracellular survival of K10, compared to C49, and significantly higher levels of IL-1β, IL-10 and nitrite secretion from K10 infected MDM. Since these observed differences occurred in pure macrophage cultures *in vitro*, it was clear that the differences in gene expression, cytokine secretion and bactericidal activity between K10 and C49 infected MDM occurred purely as a result of MAP-macrophage interactions, without the interaction of other immune cells. The binding of specific ligands to phagocytic receptors, alongside the binding of PAMPS to PRRs, likely significantly influences how a phagocytic cell responds to a pathogen, by inducing appropriate signalling cascades. It was therefore hypothesised that the route of entry may impact the response of MDM to MAP infection and thereby intracellular survival of the bacteria; this was further investigated in chapter 5 of this thesis.

5 The route of uptake impacts the monocyte derived macrophage response to *Mycobacterium avium* subsp. *paratuberculosis* infection.

5.1 Introduction

The primary role of the macrophage is uptake and destruction of foreign pathogens (and damaged host cells) through a process known as endocytosis. The uptake of bacteria, including mycobacteria, occurs through a type of endocytosis known as phagocytosis (Introduction section 1.12), which allows macrophages (and other phagocytic cells) to take up relatively large particulate material (>250nm) into vesicles called phagosomes (Pieters 2008). Phagocytosis can occur through a diverse range of mechanisms, such as opsonic phagocytosis, in which foreign material is coated in proteins present in serum - namely complement proteins and antibodies - which subsequently bind to specific receptors on the surface of phagocytic cells (CR or FcR). In addition, non-opsonic phagocytosis can occur when phagocytes directly recognise and bind PAMPs on the surface of pathogens via phagocytic receptors (Murphey & Weaver 2016)

Macrophages express several different phagocytic receptors (refer to Introduction, Table 1) that can induce phagocytosis of particulate matter via different mechanisms, influenced by engagement of these receptors. For example, 'reaching' phagocytosis involves the extension of pseudopods around the targeted object, whereas 'sinking' phagocytosis does not involve pseudopod extension, instead the targeted object appears to sink into the cell. Each process occurs through actin polymerisation but the differences between them arise via specific signalling cascades elicited by engagement of specific receptors. For example, it is well-established that phagocytosis via FcRs is a 'reaching' form of phagocytosis that results in an inflammatory response and a respiratory burst (Rosales 2017); whereas uptake via CR is a 'sinking' form of phagocytosis that does not directly induce a respiratory burst and is considered non-inflammatory (Wright & Silverstein 1983; Reed et al. 2013; Roberts et al. 2016).

For this chapter, the expression of eight phagocytic receptors by bovine MDM was analysed by flow cytometry. The receptors studied included: the scavenger receptors 'macrophage receptor with collagenous structure' (MARCO), and CD163; the C-

type lectins, ‘macrophage Mannose Receptor’ (MR) (CD206), and Dendritic Cell-Specific Intercellular adhesion molecule-3-Grabbing Non-integrin (DC-SIGN) (CD209); the complement receptor subunits, Integrin Subunit Alpha M (CD11b), and Integrin Subunit Alpha X (CD11c), which make up complement receptor 3 (CR3) and complement receptor 4 (CR4), respectively, when in conjunction with CD18; and the Fc Receptors (FcRs), Fc Gamma Receptor IIa (CD32), and Fc Gamma Receptor IIIa (CD16).

Expression of the scavenger receptor MARCO was analysed as it was hypothesised that this receptor might significantly affect the ability of MDM to phagocytose and respond to MAP, due an association between expression of MARCO and a protective response against other species of mycobacteria. For example, SNPs in the gene encoding MARCO were associated with altered susceptibility to pulmonary tuberculosis in humans (Bowdish et al. 2013). In addition, zebrafish embryos with morpholino knockdown of MARCO showed delayed phagocytosis of *M. marinum* alongside an impaired inflammatory response and increased intracellular growth of the bacteria (Benard et al. 2014). These studies suggested that uptake through MARCO could significantly affect the outcome of infection. MARCO is known to be expressed only by distinct subsets of both mouse and human macrophages, including alveolar macrophages, making it relevant for pulmonary tuberculosis (van der Laan et al. 1997; Sun & Metzger 2008). However, it was unknown if this receptor was expressed by bovine MDM, or tissue resident macrophages.

Expression of the scavenger receptor CD163 was also investigated. CD163 is expressed exclusively on monocytes and macrophages and is a receptor for haemoglobin-haptoglobin complexes, in addition to bacterial ligands (Fabriek et al. 2009). Increased CD163 expression is associated with an M2 macrophage phenotype (induced by IL-4 and IL-13) and is observed in diffuse multibacillary lesions, compared to focal lesions, in the intestines of MAP infected cattle (Fernández et al. 2017). In addition, CD163 expression was shown to be upregulated on monocytes of children with primary pulmonary tuberculosis compared to healthy children (Aktas Cetin et al. 2017), suggesting a link between this receptor and disease progression.

This chapter looked in detail at the interaction of MAP with C-type lectin phagocytic receptors, specifically the MR and DC-SIGN. C-type lectins bind to carbohydrates on the surface of mycobacteria (Cummings & McEver 2009), primarily mannose-capped lipoarobinomannan (Man-LAM). DC-SIGN is expressed on bovine MDM (Park et al. 2016) and is known to bind Man-LAM. Several studies have shown that Mycobacteria binding to DC-SIGN can modulate the downstream immune response and that Mycobacteria likely target this receptor for their own advantage. For example, *M. tb* can modulate TLR signalling in primary human dendritic cells, via Man-LAM binding to DC-SIGN, which results in increased secretion of the anti-inflammatory cytokine IL-10 in the presence of TLR ligands (Gringhuis et al. 2007; Gringhuis et al. 2009).

Uptake of Mycobacteria through the MR has also been shown to be beneficial for mycobacterial persistence within the host. A study by Sweet et al. demonstrated that knockdown of the MR in human MDM increased phagosome maturation in response to *M. avium* infection (Sweet et al. 2010) suggesting that *M. avium* may target their uptake through this receptor in order to avoid degradation within lysosomes. Additionally, engagement of the MR on human DC has been shown to promote IL-10 production and the production of anti-inflammatory mediators IL-1ra and IL-1RII (Chieppa et al. 2003), potentially affecting downstream responses by causing cells to reduce co-stimulatory molecule expression and suppressing expression of cytokines that promote protective Th-1 immunity.

The role of heat-labile serum components in the uptake and intracellular survival of MAP was also investigated in this chapter. The main class of heat-labile serum components that are likely to play an important role in phagocytosis, are complement proteins, which are known to facilitate phagocytosis, in addition to destroying pathogens directly via the 'membrane attack complex' (MAC), and inducing an inflammatory response (Murphey & Weaver 2016). The complement system promotes phagocytosis by a process known as opsonisation, whereby invading pathogens are coated in proteins known as C3b, C4b and inactivated-C3b (iC3b). Surface-bound complement proteins will subsequently bind to CR on phagocytic cells, such as CR1 (CD35), CR3 (CD11b:CD18) and CR4 (CD11c:CD18) to initiate

phagocytosis. The complement system can be activated via three pathways, all of which could potentially contribute to the opsonisation of mycobacteria. The pathways are the classical pathway, the lectin pathway and the alternative pathway. For an explanation of all three complement pathways, see Introduction, section 1.12.1.

Complement proteins C1-C9 are present in adult bovine serum. Foetal bovine serum (FBS), which is present at 20% in TCMb (Appendix A), has been reported to contain only 1-3% C1 and C6, negligible levels of C3 and 5-50% of all other complement components, compared to adult bovine serum (Linscott & Triglia 1981). Therefore, in order to study the role of heat-labile serum components, such as complement, herein, sera was obtained from adult MAP-negative cattle (naïve sera; NS). A proportion of the NS was heat-inactivated at 56°C for at least 30 minutes (heat inactivated naïve sera; HNS), prior to use – a standard method that is known to inactivate complement proteins (Schlesinger et al. 1990; Lesniak et al. 2010). NS and HNS were used to pre-treat MAP prior to infection studies and the effect of opsonisation on bacterial uptake and survival was assessed by performing CFU counts.

The role of antibody in the phagocytosis of MAP was also investigated. MAP can be commonly contracted by neonates through contaminated milk and colostrum from the mother (Arsenault et al. 2014) and MAP-specific antibodies may be present in the milk of infected cows (Nielsen & Toft 2014). The likelihood of MAP specific antibodies being present in milk is increased during periods of time when the mother could be shedding MAP, as bacterial shedding coincides with a switch from Th-1 to Th-2-type immunity. It is therefore reasonable to infer that neonates could be contracting MAP that is opsonised with antibody, via this infection route. Antibody can contribute to uptake of mycobacteria through the classical complement pathway or through FcR-mediated phagocytosis (see Introduction, section 1.12.1).

This study hypothesised that the route of entry of MAP into MDM would affect the early response of MDM to infection and, therefore, the ability of MAP to survive intracellularly.

The aims of the chapter included establishing the percentage of MDM positive for a range of phagocytic receptors, and analysing the relative level of expression of these receptors on the MDM surface. Additionally, this chapter aimed to assess the impact of specific families of phagocytic receptors on bacterial uptake and intracellular survival, as well as analysing the response of MDM to MAP infection by measuring phagosome maturation, cytokine production, antigen presentation, intracellular survival and the production of anti-microbial products by infected MDM, under specific inhibitory conditions for certain groups of receptors.

5.2 Results

5.2.1 MDM express several phagocytic receptors

This experiment aimed to understand which phagocytic receptors were being expressed on bovine MDM, and thereby which of the receptors could potentially play a role in the uptake of MAP *in vitro*. The phagocytic receptors investigated were as follows: DC-SIGN, CD32, CD163, CD16, MARCO, MR, CD11b and CD11c. The gating strategy for each receptor is demonstrated in Figure 5-1. At least a proportion of MDM expressed every phagocytic receptor, except the scavenger receptor MARCO. All antibodies were optimised prior to use and a range of dilutions (1:1000 – 1:100) of anti-MARCO were tested, none of which yielded positive staining on MDM (Figure 5-2 A). To assess if MDM were genuinely not expressing MARCO or if the lack of positive staining was a technical issue with the antibody used, or lack of cross-reactivity, a PCR using two sets of primers targeted to bovine MARCO, was carried out on cDNA from K10, C49 and uninfected MDM. Primer-set 1 was designed to produce a 405bp product, whereas primer-set 2 was designed to produce a 145bp product. PCR products were run on a 2% agarose gel along with two ladders – Hyperladder I and Hyperladder IV. However, no product was amplified with either primer set, in any of the cDNA samples (Figure 5-2 B), suggesting that bovine MDM do not express the receptor, however no positive controls were included, therefore a false negative result due to an issue with the PCR reaction cannot be ruled out. It was noted that Hyperladder I produced bands of the incorrect size, when compared to Hyperladder IV.

The mean percentage of MDM positive for each phagocytic receptor is demonstrated in Figure 5-2 C. >90% MDM were positive for CD32 (mean = 97.8% positive), CD163 (mean = 96.6% positive), CD16 (mean = 96% positive), and CD11c (mean = 96.7% positive), whereas the expression of DC-SIGN, MR, and CD11b was more varied within the population, with > 60% MDM positive for DC-SIGN (mean = 71.6% positive), > 77% MDM positive for MR (mean = 81% positive), and >56% MDM positive for CD11b (mean= 75.6% positive) (Figure 5-2. C). The expression of DC-SIGN and CD11b also varied between animals. For example, MDM from

animals 41 and 77 were 57-67.4% positive for DC-SIGN expression, whereas MDM from animals 49 and 83 were 79.4-82.1% positive for DC-SIGN expression. Additionally, MDM from animals 89, 86 and 76 were 61.1%, 85.8% and 79.8% positive for CD11b expression, respectively (data not shown).

The Geometric Mean Fluorescence Intensity was measured to determine the relative level of expression of each receptor, on each cell. CD32, CD163, CD16, CD11c and CD11b were all highly expressed, whereas DC-SIGN and the MR were expressed at lower levels on bovine MDM (Figure 5-2 D).

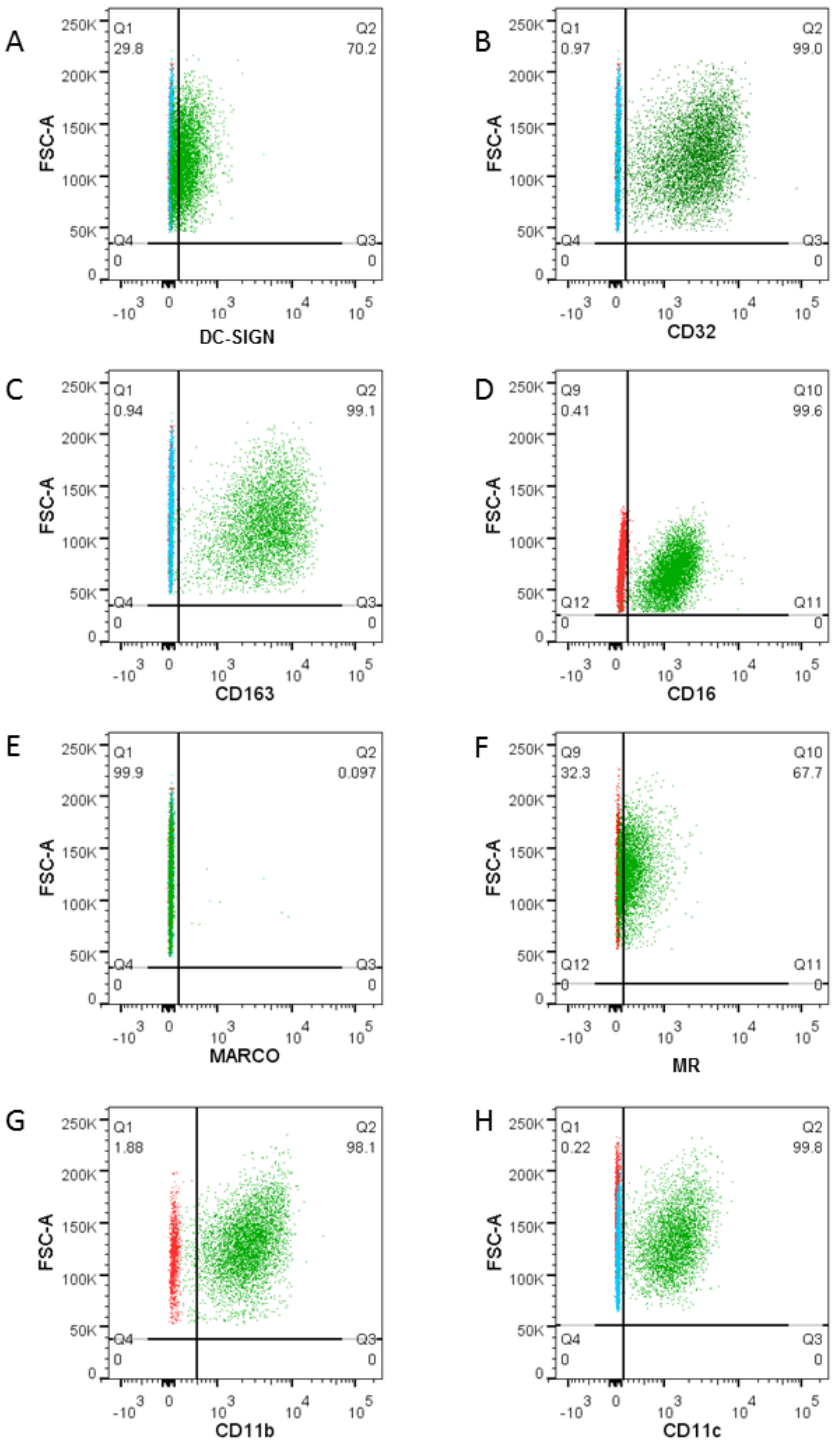

Figure 5-1 Gating Strategy for analysis of phagocytic receptor expression

In order to analyse the expression of phagocytic receptors on MDM by flow cytometry, gates had to established to determine cells positive for each molecule. Cells were first gated by viability, size and granularity, and exclusion of doublets, as described in Figure 4.2 Gates were then established for the phagocytic receptors (A) DC-SIGN (B) CD32 (FcγR2a) (C) CD163 (D) CD16 (E) MARCO (F) MR (G) CD11b (H) CD11c. Gates were set using secondary antibody controls (indirect

single staining) or unstained controls (direct staining with conjugated antibodies). Red =unstained controls, Blue = secondary antibody controls, green = cells treated with specific monoclonal antibodies against the specified molecule. Numbers represenent the percentage of cells within each gate. Representative of N= 5 (DC-SIGN, CD32, CD163), N=4 (CD16, MR, CD11b, CD11c), N=2 (MARCO).

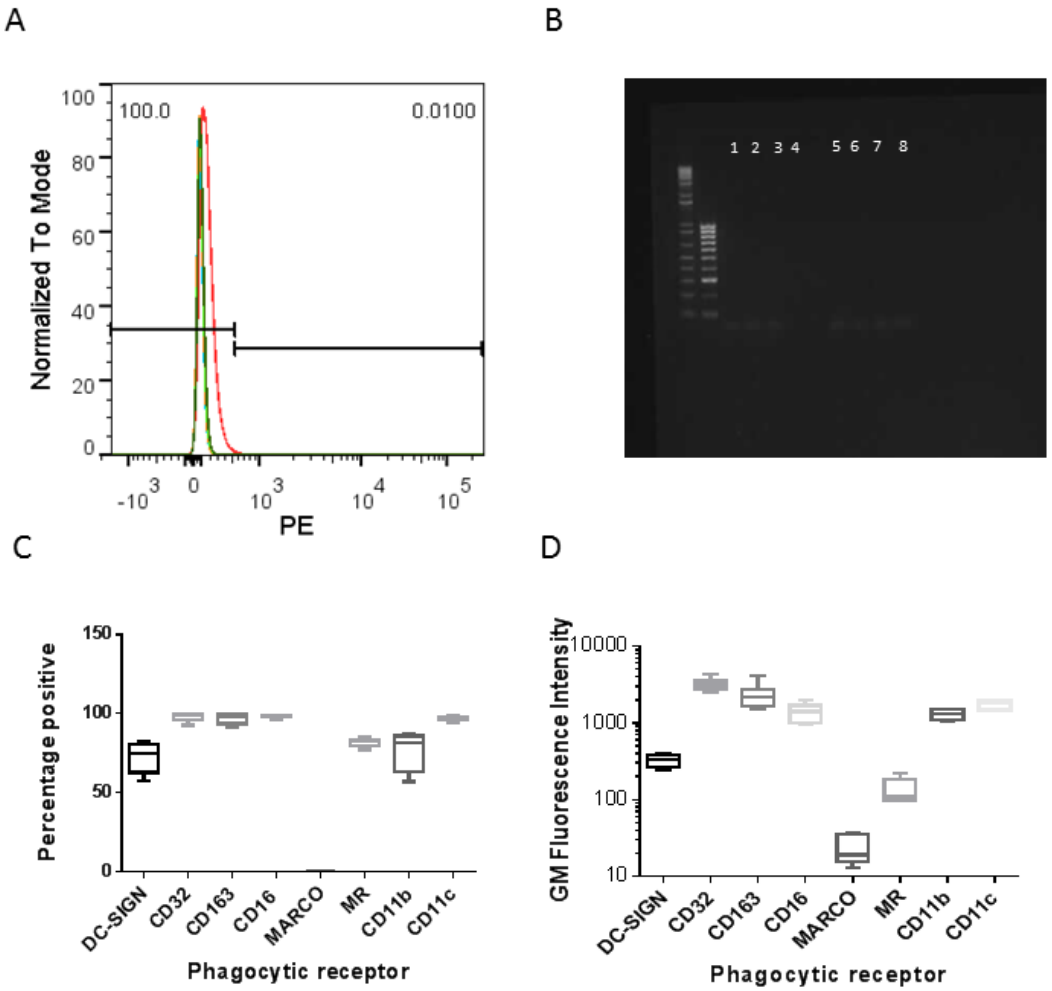

Figure 5-2 Expression of phagocytic receptors by MDM

The expression of the phagocytic receptors DC-SIGN, CD32, CD163, CD16, MARCO, MR, CD11b, and CD11c, by MDM was analysed by flow cytometry. (A) The concentration of anti-MARCO antibody was optimised. Red= IgG3 isotype control, blue= 1:1000 antibody dilution, orange = 1:500 antibody dilution, light green = 1:250 antibody dilution, dark green = 1:100 antibody dilution. Numbers within gates refer to the percentage of events within each gate. (B) Agarose gel electrophoresis of MARCO PCR product: 1= primer-set 1, K10 infected MDM; 2 = primer-set 1, C49 infected MDM; 3 = primer-set 1, uninfected MDM; 4 = primer-set 1, negative control; 5 = primer-set 2, K10 infected MDM; 6 = primer-set 2, C49 infected MDM; 7 = primer-set 2, uninfected MDM; 8 = primer-set 2 negative control. Two ladders were used: Hyperladder I, ranging from 10,000bp to 200bp, and Hyperladder IV, ranging from 1000bp to 100bp (C) Percentage of MDM positive for each phagocytic receptor. Gates determining expression of each molecule are described in Figure 5.2 (D) The GM fluorescence intensity of each phagocytic receptor. (DC-SIGN, CD32, CD16: N=5; MARCO: N= 2; MR, CD11b, CD11c: N=3)

5.2.2 Inhibiting bacterial uptake through MR and DC-SIGN.

Despite DC-SIGN and MR being expressed at lower levels than other phagocytic receptors (Figure 5-2 C&D), the role of these receptors in MAP infection was further investigated due to evidence in the literature that they play a significant role in the uptake and downstream immune response of macrophages to mycobacteria species (Gringhuis et al. 2007; Gringhuis et al. 2009; Sweet et al. 2010)

This experiment aimed to block MR and DC-SIGN with a polysaccharide-blocking agent, in order to carry out downstream experiments examining the role of these receptors. Two blocking agents were tested: Mannan from *Saccharomyces cerevisiae* (mannan), and D-Mannose. A range of concentrations were tested by incubating MDM in blocking agent for 30 minutes at 37°C, subsequently adding antibodies specific for MR (at a pre-determined optimal concentration) and analysing binding of the antibodies by fluorescent microscopy. Five technical replicate images of each MDM monolayer were captured, in order to quantify the relative fluorescence intensity, compared to controls. It was observed that 2mg/ml mannan resulted in a significant decrease in binding of anti-MR, demonstrated by a 16.9% decrease in fluorescence intensity, whereas the highest concentration of D-mannose tested (0.25M) caused a 7.4% increase in fluorescence intensity, compared to MDM treated with anti-MR, alone Figure 5-3A). Representative images of unstained control MDM, MDM treated only with anti-MR, and MDM treated with 2mg/ml mannan and anti-MR, are presented in Figure 5-3 B, C & D, respectively. Figure 5-3-D clearly demonstrates that mannan, used at 2mg/ml, significantly reduced the binding of anti-MR to MDM; therefore, this concentration of mannan was used as a blocking agent for downstream experiments. In order to be certain that treatment of MDM with 2mg/ml mannan would prevent uptake through DC-SIGN and the MR, and not simply prevent antibody binding, MDM monolayers were treated with 20µg/ml dextran conjugated to AF467 (dextran-AF647). As dextran-AF647 is a polysaccharide, it is phagocytosed via interaction with C-type lectin receptors, and it has been previously demonstrated that afferent lymph dendritic cells expressing MR take up significantly higher levels of dextran, compared to those absent of MR expression (Hope et al. 2012). MDM untreated with mannan showed strong intracellular AF647 fluorescence, demonstrating that MDM efficiently phagocytosed

dextran-AF647 in the absence of the blocking agent E). However, intracellular AF647 fluorescence was absent from MDM pre-treated with mannan, indicating that treatment with 2mg/ml mannan effectively inhibited phagocytosis through C-type lectin receptors. (Figure 3-5 E&F)

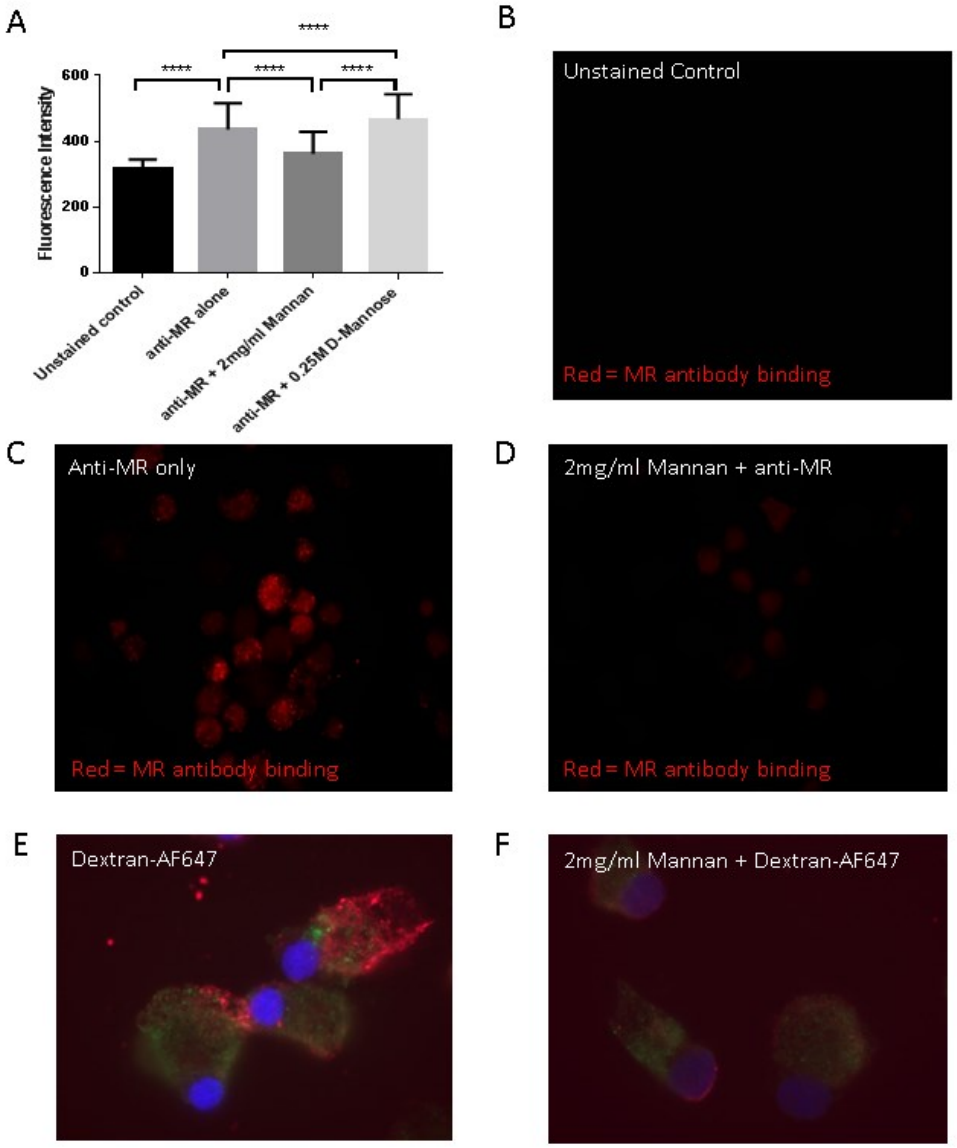

Figure 5-3 Blocking the Mannose Receptor.

Different methods of blocking the MR were investigated by immunocytochemistry and fluorescence microscopy. The blocking agents D-mannose and mannan were tested for their ability to block specific binding of anti-MR antibody to the surface of MDM. The effect of mannan treatment on the ability of MDM to take up fluorescent dextran was also investigated. (A) Fluorescence intensity of MDM monolayers under different treatment conditions. Bars represent the mean and standard deviation of >190 ROIs (cells) observed across 5 technical replicate images (20x objective). B-D were taken at 20x objective and depict MDM monolayers treated with an anti-MR antibody conjugated to PE; positive staining is shown in red. (B) Representative image (N=5) of an unstained MDM monolayer (C) Representative image (N=5) of MDM monolayer treated with anti-MR antibody only. (D) Representative image

*(N=5) of an MDM monolayer pre-treated with 2mg/ml mannan and then incubated with anti-MR antibody. Images E & F were taken at 100x objective and depict MDM monolayers treated with 20µg/ml dextran conjugated to AF647 (Dextran-AF647). (E) Representative image (N=10) of MDM monolayer incubated with 20µg/ml dextran-AF647 only. (F) Representative image (N=10) of MDM monolayer pre-treated with 2mg/ml mannan, prior to incubation with 20µg/ml dextran-AF647. Green = LAMP1, Blue = nuclei, Red = Dextran-AF647. Statistics were calculated using ROIs; Data were normally distributed ($p>0.05$) and measured by general linear model. $p<0.0001$*****

To be certain that 2mg/ml mannan was also sufficient to block DC-SIGN, fluorescent microscopy was carried out using an anti-DC-SIGN antibody. The same microscope settings were used to visualise MR and DC-SIGN, however, anti-DC-SIGN produced only very faint positive staining, in contrast to the bright positive staining observed with anti-MR (Figure 5-4 B & Figure 5-3 C). This faint positive staining was inhibited in samples pre-treated with mannan (Figure 5-4), suggesting that the blocking agent was able to inhibit the limited binding of anti-DC-SIGN. This result was surprising as the GM fluorescence intensity was largely similar between these two antigens when measured by flow cytometry (Figure 5-2 D). A key difference between preparation of the samples used in this experiment, compared to flow cytometry, was fixation in 2% paraformadehyde prior to staining. The anti-DC-SIGN antibody has been approved for flow cytometry but not immunocytochemistry, by the manufacturers (Kingfisher Biotech Inc.), suggesting it may not work on fixed samples. The apparent difference in fluorescence intensity between flow cytometry and immunocytochemistry could therefore be explained by epitope masking on DC-SIGN caused by fixation, which limits antibody binding. It is also possible that there was non-specific binding of the antibody to live cells, measured by flow cytometry, which was then lost upon fixation.

In order to understand the cause of the discrepancy between DC-SIGN expression measured by flow cytometry, compared to fluorescent microscopy, non-specific binding of anti-DC-SIGN was investigated by incorporating isotype controls into flow cytometry analysis. The isotypes of the primary or conjugated antibodies used for analysis of phagocytic receptor expression (Figure 5-1) were as follows: anti-CD163, CD32, CD11c & MR = IgG1, anti-DC-SIGN & anti-CD16 = IgG2a, anti-CD11b = IgG2b, and anti-MARCO = IgG3. Isotype controls were concentration-matched with primary antibodies. Binding of each isotype control in relation to unstained controls, is demonstrated in Appendix G. IgG1 and IgG3 isotype controls resulted in negligible non-specific binding, whereas 78.4% and 52% of MDM stained positive when treated with IgG2a and IgG2b isotype controls, respectively. This demonstrated that antibodies of IgG2a and IgG2b isotypes could bind non-specifically to MDM. IgG2a isotype controls were subsequently used to set gates for anti-DC-SIGN staining; with gates set by isotype controls 99.8% of events were

negative for DC-SIGN (Figure 5-4 D). This suggests that the DC-SIGN staining observed in Figure 5-1 & Figure 5-2, was a result of non-specific, rather than specific, binding of anti-DC-SIGN. Little non-specific binding was observed for IgG1, the isotype of anti-MR, therefore results presented in sections 5.2.2 - 5.2.7 refer to the effect of blocking the MR only.

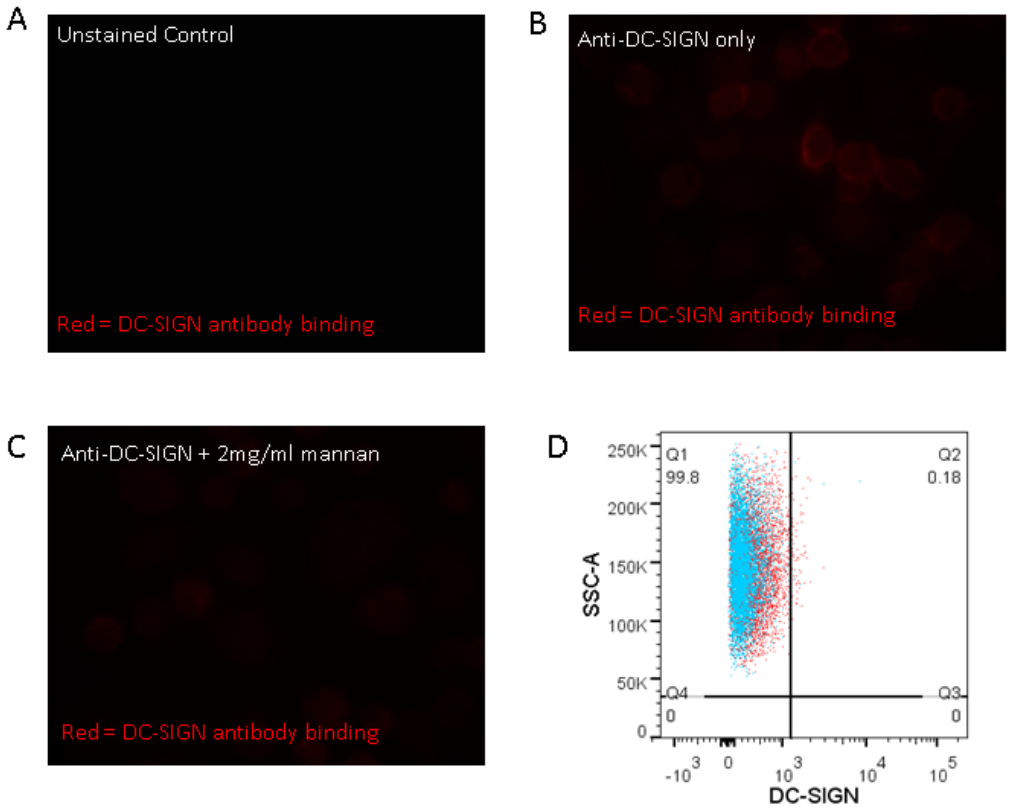

Figure 5-4 Staining MDM with an antibody targeting DC-SIGN.

The effect of mannan treatment on blocking the phagocytic receptor DC-SIGN was investigated by immunocytochemistry and fluorescence microscopy. Specific binding of anti-DC-SIGN antibody to the surface of MDM pre-treated with 2mg/ml mannan was compared to specific anti-DC-SIGN binding to untreated MDM. (A) Representative image (N=5) of MDM monolayer unstained control. (B) Representative image (N=5) of MDM monolayer treated with anti-DC-SIGN only. (C) Representative image (N=6) of MDM monolayer treated with 2mg/ml mannan + anti-DC-SIGN. Anti-DC-SIGN antibody binding to MDM was subsequently investigated by flow cytometry with the incorporation of an isotype control. (D) Representative flow cytometry scatter plot depicting MDM treated with anti-DC-SIGN (blue) and MDM treated with IgG2a isotype control antibody (red) at the same concentration (N=3 biological replicates).

5.2.3 Inhibiting MR does not impact phagocytosis of MAP

As the MR is a phagocytic receptor known to be of importance for the phagocytosis of mycobacteria species, the effect of MR inhibition on the ability of MDM to phagocytose MAP was investigated. MDM were treated with 2mg/ml mannan at 37ºC for 30 minutes prior to infection, and MDM monolayers were then infected with K10 or C49 at MOI 5. Infected MDM were incubated at 37ºC until 0.5 HPI, and washed 3x with PBS. Subsequent to washing at 0.5 HPI, monolayers were lysed and serial dilutions of the lysate plated on 7H10 agar plates in order to perform colony counts, to assess the level of uptake by MDM at 0.5 HPI. No significant differences were observed between numbers of intracellular CFU from MDM pre-treated with 2mg/ml mannan, compared to untreated MDM, for either K10 or C49 (Figure 5-5 A), suggesting that inhibiting MR does not impact the rate of phagocytosis of MAP by MDM. It was observed that there was slightly less uptake of C49, compared to K10, for both mannan-treated and untreated MDM, however the difference was not significant.

To further investigate the effect of MR inhibition on uptake of MAP by MDM. MDM monolayers were treated with 2mg/ml mannan, as described above, and infected with either heat inactivated (H/in) or viable K10 or C49. H/in strains were included in order to evaluate if MAP actively promote their own uptake through either the MR or another phagocytic receptor. The infected MDM monolayers were not washed at 0.5 HPI, to allow phagocytosis to continue over a 24- hour time-course. Infected monolayers were fixed in 2% paraformaldehyde at 0.5 HPI and 24 HPI, and uptake of MAP assessed by fluorescent microscopy, using a Leica DMLB fluorescent microscope. Percentage uptake was calculated by dividing the number of MAP observed by the number of MDM within each image.

There were no significant differences in the uptake of H/in forms of K10 or C49, compared to viable forms, either in the presence or absence of 2mg/ml mannan, at 0.5 HPI or 24 HPI, suggesting that viable bacteria were not actively promoting their uptake through the MR or any other pathway *in vitro* (Figure 5-5 B &C). Therefore, uptake is likely driven by the host in response to antigens present on the bacterial surface.

Somewhat in agreement with the CFU results described in Figure 5-5 A, the percentage uptake of C49 (viable and H/in) was low (<50%) compared to K10 (live and H/in) at 0.5 HPI, when determined by microscopy (Figure 5-5 B). However, pre-treatment of MDM with mannan significantly increased uptake of C49 and H/in K10 at 0.5 HPI (Figure 5-5 B), an effect that was not observed for C49 by counting CFU. It is likely that the discrepancies observed between microscopy and CFU in determining percentage uptake at 0.5 HPI can be accounted for by a relatively small number of technical replicate images, which may have introduced error. As the CFU count calculates the total number of CFU within an infected monolayer, it is likely a more accurate measurement.

At 24 HPI, no significant differences were observed between the uptake of either K10 or C49 (live or H/in) by MDM treated with 2mg/ml mannan, compared to untreated MDM (Figure 5-5 C). Taken collectively, these results suggest that MR inhibition is not detrimental to the ability of MDM to phagocytose MAP, and that MDM are capable of phagocytosing MAP via another pathway.

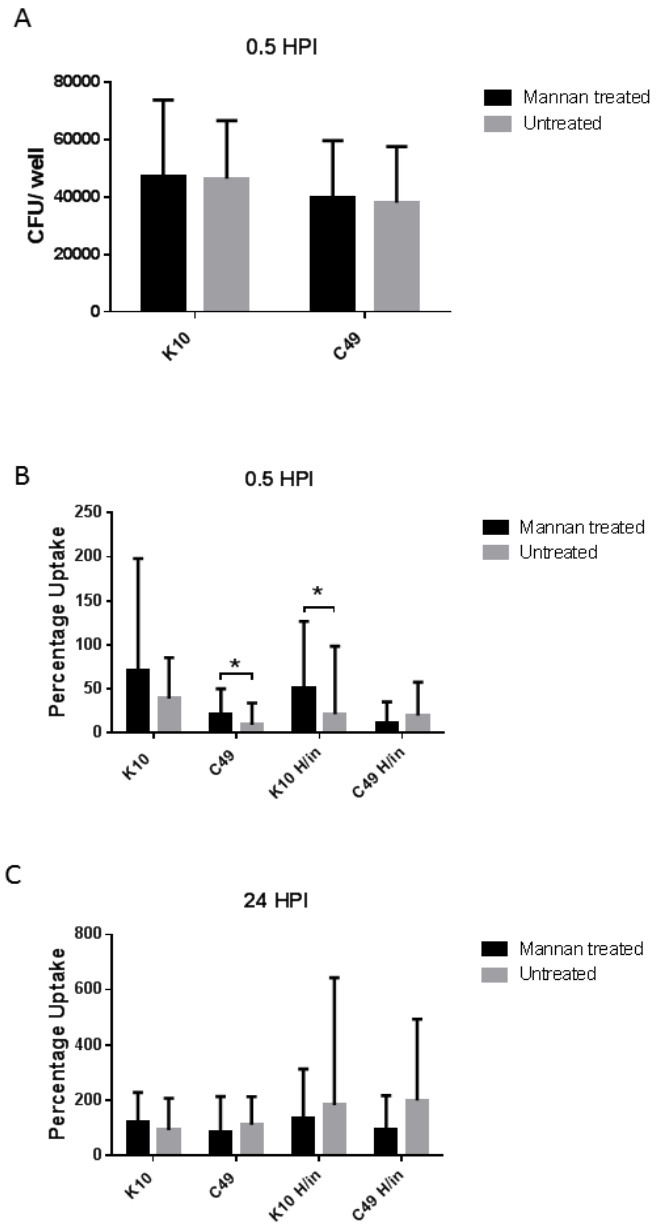

Figure 5-5 Uptake of MAP by MDM in the presence or absence of 2mg/ml mannan, a MR blocking agent.

*Percentage uptake of MAP by MDM treated with the MR blocking agent 2mg/ml mannan was assessed at 0.5 and 24 HPI by fluorescence microscopy. The number of intracellular bacteria at 0.5 HPI was also calculated by performing CFU counts. (A) CFU count at 0.5 HPI. Bars represent the mean and SD of 4 biological replicates. (B) Percentage uptake of MAP by MDM at 0.5 HPI, assessed by fluorescence microscopy. Bars represent the mean and SD of 3 biological replicates. (C) Percentage uptake of MAP by MDM at 24 HPI (without wash step at 0.5 HPI), assessed by fluorescent microscopy. Bars represent the mean and SD of 3 biological replicates. Data depicted in A was normally distributed ($p>0.05$) and analysed by general linear model. Data depicted in B & C were non-normally distributed ($p<0.05$) and analysed by Mann-Whitney tests. $p<0.05$**

5.2.4 Inhibiting the uptake of MAP by MR decreased intracellular survival of MAP by 24 HPI

The aim of this experiment was to assess if blocking the MR with 2mg/ml mannan affected the ability of MAP to survive, intracellularly, within MDM. In order to measure this, MDM were pre-treated with 2mg/ml mannan for 30 minutes at 37°C (as described in Section 5.2.2) and infected with either K10 or C49 at an MOI of 5. At 0.5 HPI, monolayers were washed 3x with PBS and the media replaced with fresh sterile media. At 0.5 HPI, a technical replicate for each condition was lysed, and serial dilutions of the lysate plated, so as to calculate the initial uptake of bacteria – CFU count at 0.5 HPI is demonstrated in Figure 5-5 A. At 2, 6 and 24 HPI, infected MDM monolayers were lysed and serial dilutions of the lysate plated on 7H10 agar plates, in order to count CFU to calculate the percentage intracellular survival, relative to the CFU count at 0.5 HPI.

As described in section 5.2.3, there was no difference in the number of K10 or C49 CFU taken up by MDM pre-treated with mannan, compared to untreated MDM, by 0.5 HPI (Figure 5-5A). At the earlier time-points of 2 HPI and 6 HPI, there was no difference in the percentage intracellular survival of K10 or C49, within MDM pre-treated with mannan, compared to intracellular survival within untreated MDM (Figure 5-6 B & C, respectively). However, by 24 HPI, the percentage intracellular survival of both K10 and C49 was significantly decreased in MDM pre-treated with mannan, compared to untreated controls (Figure 5-6 D).

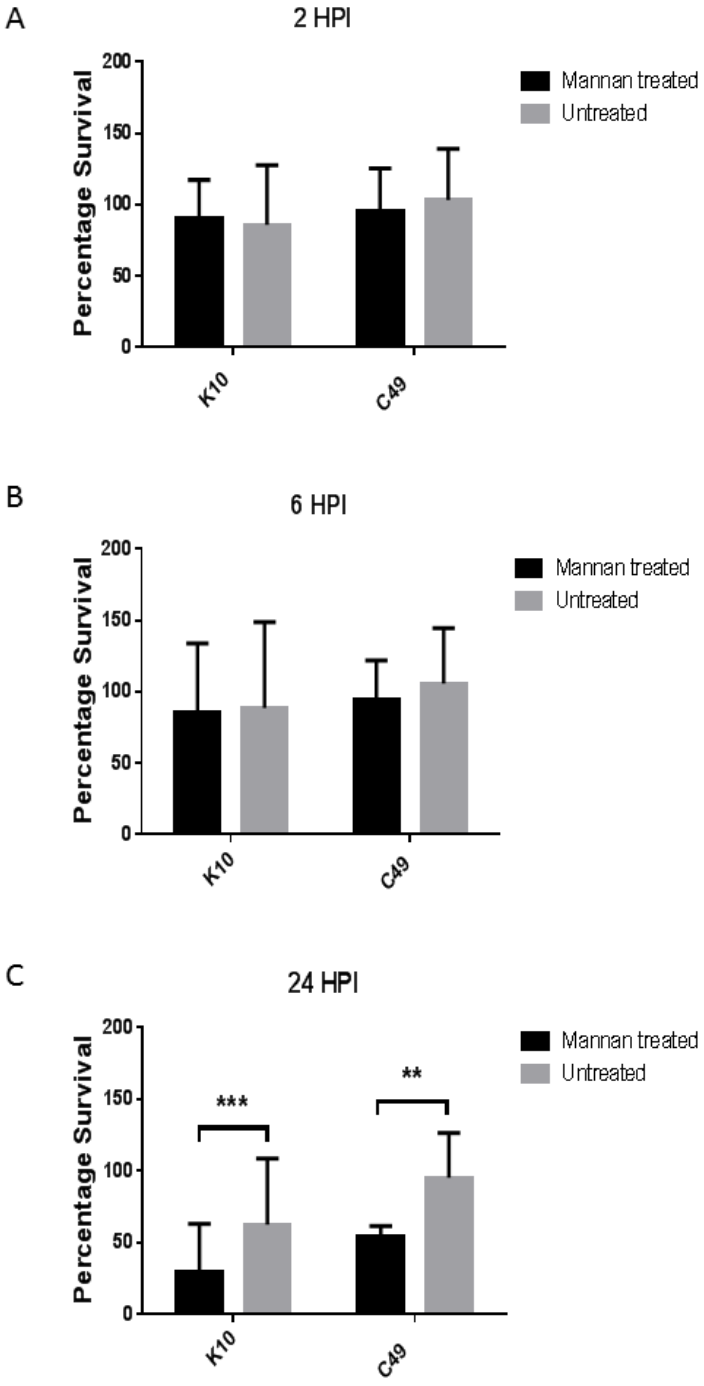

Figure 5-6 Percentage intracellular survival of MAP within MDM pre-treated with 2mg/ml Mannan.

MDM lysate was plated at 2, 6 and 24 HPI, and CFU counted in order to calculate percentage survival relative to CFU count at 0.5 HPI. (A) Percentage survival at 2 HPI (B) Percentage survival 6 HPI (C) Percentage survival at 24 HPI. Graphs represent the mean and SD of 4 biological replicates. Data were normally distributed ($p>0.05$) and analysed by general linear model. $p<0.05$, $p<0.01$**, $p<0.001$****

5.2.5 Co-localisation with LAMP1

Co-localisation of MAP with the late endosomal marker LAMP1 was investigated, in order to understand if the decrease in MAP intracellular survival observed when uptake through the MR was inhibited (Figure 5-6) was attributable to increased phago-lysosome fusion. Briefly, MDM were treated with 2mg/ml mannan for 30 minutes at 37°C (MDM untreated with mannan were included as controls), and subsequently infected with either live or H/in K10 or C49 at MOI 5. Infected MDM monolayers were not washed and a 24-hour infection time-course was carried out. At 0.5 HPI and 24 HPI samples were fixed in 2% paraformaldehyde and stained using antibodies targeting LAMP1 and mycobacteria. DAPI was used to visualise nuclei. Co-localisation of MAP with LAMP1 was visualised by fluorescent microscopy using a Leica DMLB fluorescent microscope, and images analysed using Image J, as described in Appendix F.

The percentage of MAP co-localising with LAMP1 was low at 0.5 HPI; C49 had the highest percentage co-localisation at ~20%, however there was much variation between technical replicates. No significant differences were observed for LAMP1 co-localisation between any of the treatment conditions at 0.5 HPI, demonstrating that MR inhibition did not impact phagosome maturation at this time-point. These results, combined with the results described in chapter 4 section 4.2.6, suggest that phagosome maturation occurs later in the infection time-course, explaining why little or no LAMP1co-localisation was observed for H/in MAP strains at 0.5 HPI.

Treatment of MDM with 2mg/ml mannan significantly reduced the percentage co-localisation of K10 with LAMP1 at 24 HPI, however the same effect was not observed for C49. Surprisingly no increase in LAMP1 co-localisation was observed for H/in K10, compared to live K10, within either mannan-treated or untreated MDM, at 24 HPI. In contrast, H/in C49 had significantly increased LAMP1 co-localisation, compared to live C49, within untreated MDM, but not mannan-treated MDM. In addition, a significant increase in LAMP1 co-localisation was observed for H/in C49 within MDM treated with 2mg/ml mannan, compared to untreated MDM (Figure 5-7 B).

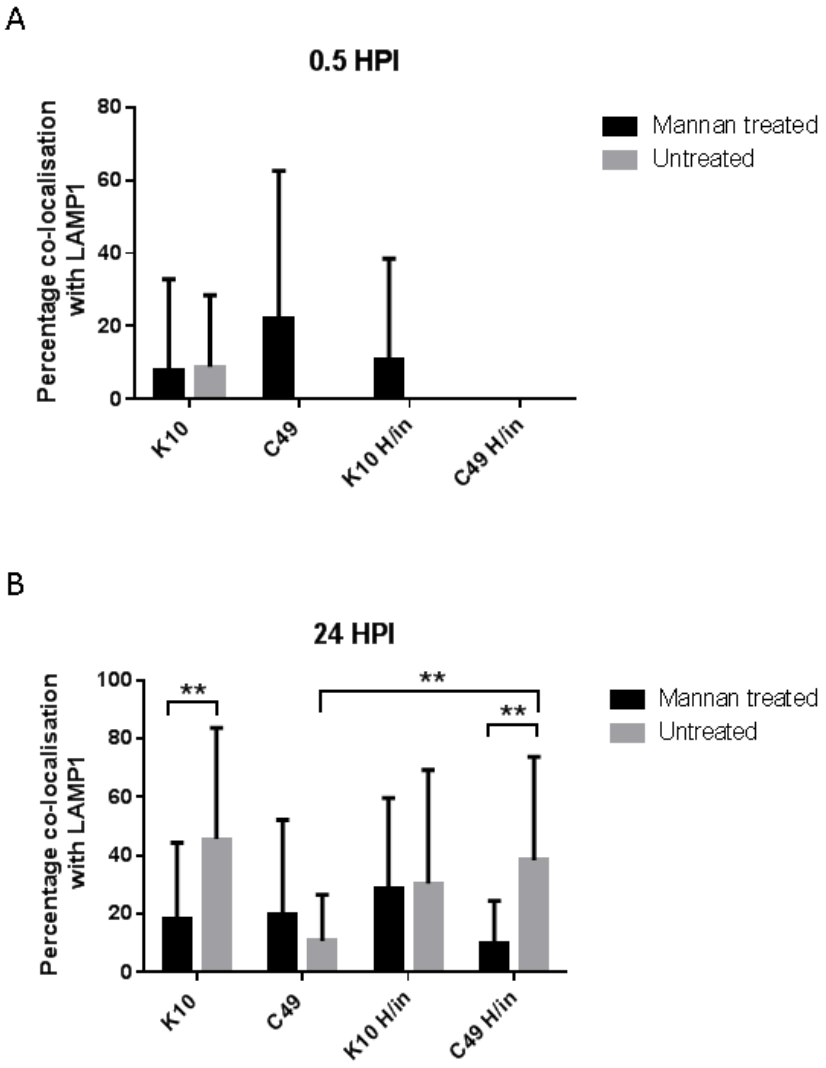

Figure 5-7 The effect of inhibiting MR on co-localisation of intracellular MAP with LAMP1.

MDM were pre-treated with 2mg/ml mannan prior to infection and the effect of MR inhibition on intracellular co-localisation of K10 and C49 with LAMP1 assessed by fluorescence microscopy at 0.5 and 24 HPI. H/in forms of K10 and C49 were included or comparison (A) Percentage co-localisation of MAP with LAMP1 at 0.5 HPI. (B) Percentage co-localisation of MAP with LAMP1 at 24 HPI. Bars represent the mean and SD of 30 technical replicates (3 biological replicates). Data were non-normally distributed ($p<0.05$) and analysed by Mann-Whitney tests. $p<0.05$, $p<0.01$***

5.2.6 The effect of blocking the mannose receptor on cytokine secretion

To understand if inhibiting the MR with 2mg/ml mannan, as described in section 5.2.2, affected the secretion of cytokines by infected cells, levels of IL-10 and IL-1β were measured. MDM were either treated with 2mg/ml mannan, or left untreated, prior to infection with K10 or C49 at an MOI of 5. MDM were also infected with H/in forms of K10 or C49, for comparison. Treatment of MDM monolayers with the blocking agent, mannan, caused increased IL-10 secretion in all samples, including uninfected controls, suggesting that engagement of the MR with mannan caused MDM to elicit an anti-inflammatory response. MDM infected with live K10 secreted significantly higher levels of IL-10 than MDM infected with H/in forms of the bacteria, regardless of treatment condition ($p<0.05$*). Whereas only untreated MDM infected with live C49 secreted significantly higher levels of IL-10, compared to untreated MDM infected with H/in C49; MDM treated with mannan prior to infection, did have increased IL-10 secretion when infected with live C49 compared to H/in C49, however it did not reach significance (Figure 5-8 A).

The level of IL-1β secreted by MDM pre-treated with mannan was also measured in the context of MAP infection. IL-1β secretion was slightly higher in MDM treated with mannan, compared to cells that were untreated (regardless of infection status); however, this increase did not reach significance. Surprisingly, the concentration of IL-1β was not increased in the supernatant of untreated K10 infected MDM, compared to untreated uninfected controls (or MDM infected with H/in K10) (Figure 5-8 B). This was contrary to previous findings detailed in chapter 4, which demonstrated MDM infected with K10 (at the same MOI) to have significantly elevated concentrations of IL-1β in the supernatant (30.8pg/ml (Figure 4-6 B) and 7pg/ml (Figure 4-7 B)), compared to C49 infected and uninfected MDM at the same time-point. However, there has been a large degree of variation in IL-1β secretion between biological replicates throughout this thesis, which likely accounts for the low level of IL-1β secretion observed from untreated K10 infected MDM in Figure 5-8 B.

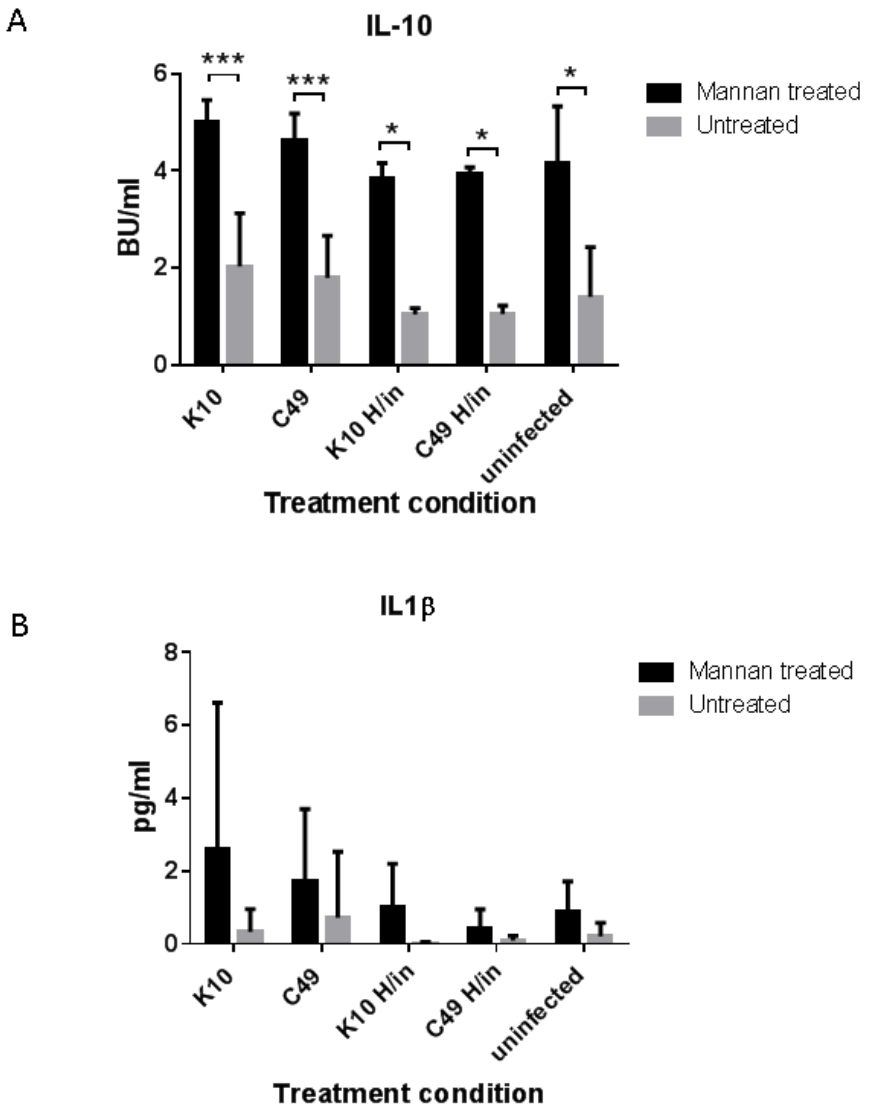

Figure 5-8 Cytokine secretion from MDM treated or untreated with 2mg/ml mannan, in the context of MAP infection.

The impact of blocking the MR, by pre-treating cells with 2mg/ml mannan prior to infection, on cytokine secretion by K10 and C49 infected MDM was investigated by ELISA at 24 HPI. H/in forms of K10 and C49 were included for comparison. (A) Concentration of IL-10 in the supernatant of MDM at 24 HPI. (B) Concentration of IL-1β in the supernatant of MDM at 24 HPI. Bars represent the mean and SD of 4 biological replicates (K10, C49 & uninfected) or 2 biological replicates (K10 H/in & C49 H/in). Data were non-normally distributed ($p<0.05$) and analysed by Mann-Whitney tests. $p<0.05$, $p<0.01$**, $p<0.001$****

5.2.7 Blocking the Mannose Receptor did not impact the expression of MHC II

In order to understand if treating MDM with 2mg/ml mannan (and therefore likely driving phagocytosis through receptors other than the MR) affected the ability of MDM to present antigen, the expression of MHC II was measured by flow cytometry. MDM were either treated with 2mg/ml mannan, or left untreated prior to infection. Monolayers were then infected with either K10 or C49 at MOI 5, and washed 3x at 0.5 HPI. MHC II expression was measured at 6 HPI and 24 HPI. Uninfected cells, either treated with mannan, or untreated, were included as controls. The gating strategy used to assess expression of MHC II is demonstrated in Chapter 4, Figure 4.2. No significant differences in MHC II expression were observed between treatment conditions at 6 HPI. At 24 HPI, untreated K10 infected cells, had significantly higher MHC II expression than untreated C49 infected and untreated uninfected cells ($p<0.05$*). However, no significant differences were observed between mannan-treated cells and untreated cells, for K10 infected MDM, C49 infected MDM or uninfected MDM, suggesting that inhibition of the MR had no effect on MHC II expression.

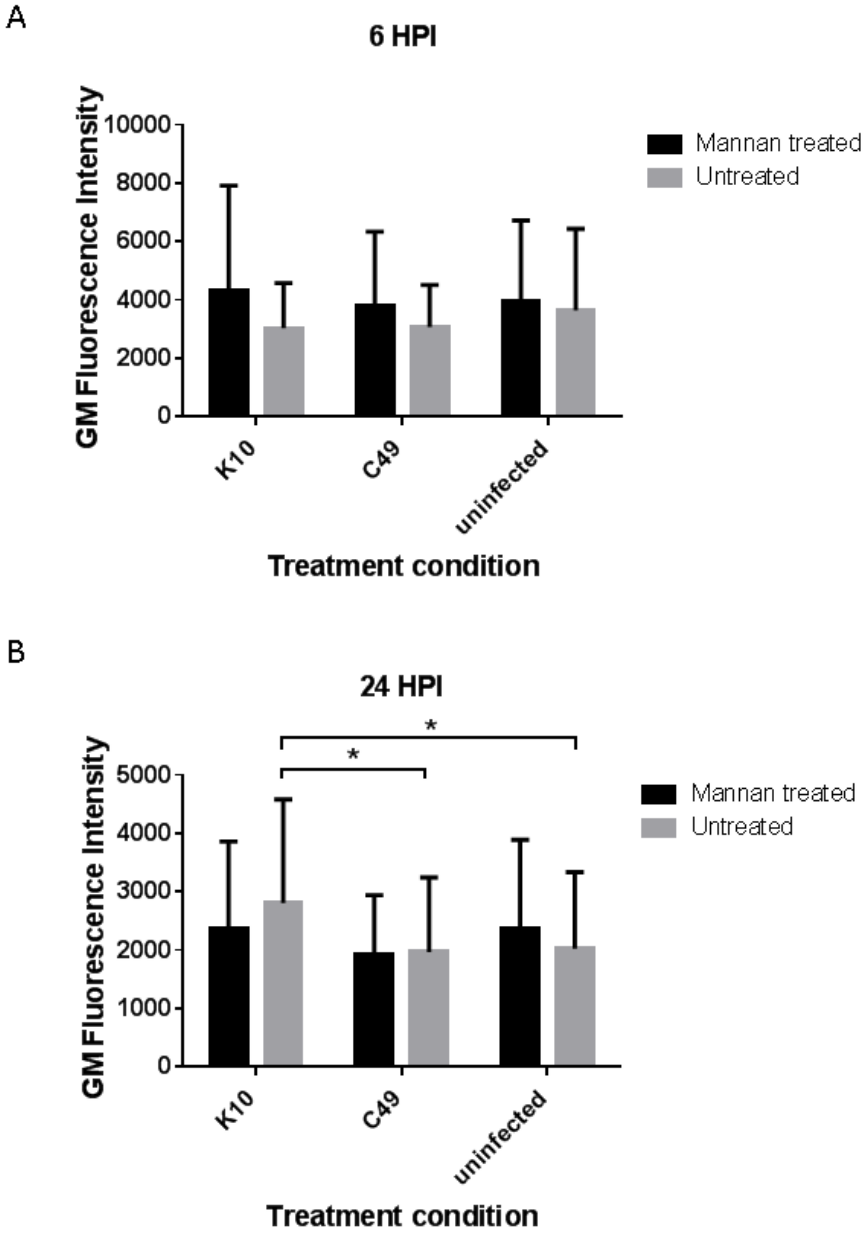

Figure 5-9 The effect of blocking uptake through the MR of expression of MHC II in the context of MAP infection.

MDM were pre-treated with 2mg/ml mannan prior to infection with K10 or C49, and the expression of MHC II was measured by flow cytometry at 6 and 24 HPI. (A) MDM MHC II expression at 6 HPI. (B) MDM MHC II expression at 24 HPI. Gating strategy is demonstrated in Chapter 4, Figure 4.3. Data were normally distributed ($p>0.05$) and analysed by general linear model (N=3).

5.2.8 The presence of heat-labile serum components increased the uptake of C49 by MDM.

The aim of this experiment was to understand if the presence of heat-labile components in the serum of cattle, could influence both the rate of phagocytosis of MAP by MDM, and, subsequently, intracellular survival. In order to study this, only the C49 strain of MAP was used, as this strain was likely the most relevant model of natural infection.

Prior to carrying out infection experiments, the effect of heat-labile serum components on C49 survival was tested, in order to understand if any differences observed in intracellular survival, could be attributed to direct effects of the sera on MAP cells. Briefly, 10µl of a C49 culture frozen at -80°C, and 10µl of an actively growing C49 culture, were incubated in RPMI 1640 containing 10% pooled NS, or 10% HNS, for 30 minutes at 37°C. Serial dilutions were then carried out and plated on 7H10 agar plates to perform colony counts. Only one measurement for each culture was made, therefore no statistics could be carried out; however it appeared there was no difference in C49 CFU between the two treatment conditions (Figure 5-10).

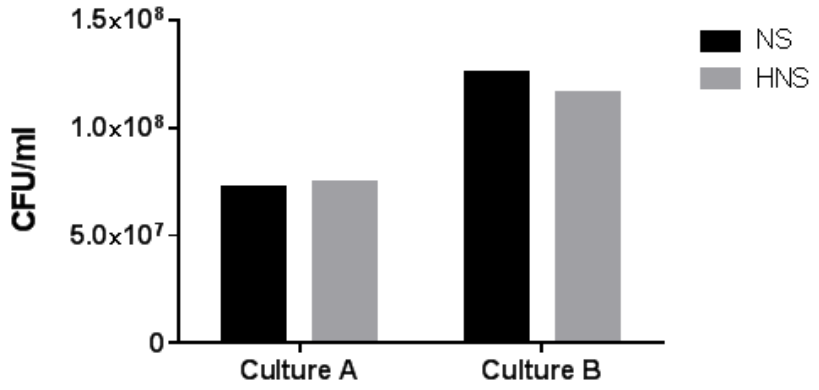

Figure 5-10 The effect of heat-labile serum components on extracellular C49 survival

The effect of heat-labile serum components on MAP extracellular survival was measured by incubating C49 in 10% NS or 10% HNS for 30 minutes at 37ºC, then immediately plating serial dilutions of cultures on 7H10 agar plates. CFU were counted after 5 weeks incubation at 37ºC.Culture A = C49 frozen at -80°C and thawed prior to assay. Culture B = actively growing culture of C49. NS= Naïve sera, HNS = Heat-inactive Naïve sera. (N=1)

To carry out infection experiments, C49 was incubated in NS or HNS, as described above, and then added to MDM monolayers at MOI 5. To calculate the percentage uptake, serial dilutions of both the inoculum and cell lysate at 0.5 HPI, were plated in order to perform colony counts; the percentage uptake refers to the number of intracellular CFU at 0.5 HPI divided by the number of CFU in the original inoculum. Percentage uptake was significantly higher for C49 pre-incubated in NS prior to infection, compared to HNS (Figure 5-11 A), indicating that the presence of heat-labile serum components increased phagocytosis of MAP by MDM.

Infected MDM monolayers were washed 3x at 0.5 HPI and a 24-hour infection time-course run. At 2, 6 and 24 HPI, MDM were lysed and serial dilutions of the lysates plated, in order to calculate percentage survival of C49 relevant to the number of intracellular CFU at 0.5 HPI. No significant differences were observed between intracellular survival of C49 incubated in NS prior to infection, compared to C49 incubated in HNS prior to infection, at 2, 6 or 24 HPI (despite the differences in original number of phagocytosed C49 at 0.5 HPI) (Figure 5-11 B). Additionally, intracellular survival of C49 pre-treated in either NS or HNS was not significantly different from the intracellular survival of C49 without any pre-treatment, as detailed in Chapter 4, Figure 4.2.

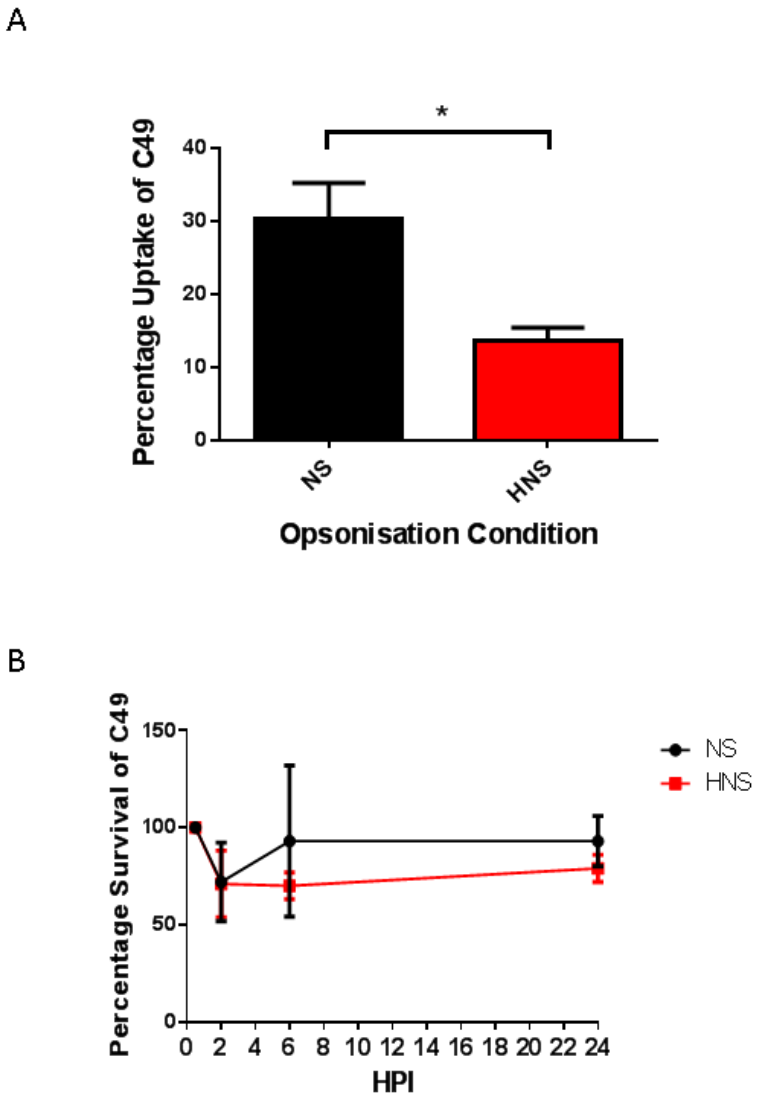

Figure 5-11 Percentage uptake and intracellular survival of C49 treated under different opsonisation conditions.

*C49 were incubated in 10% NS or 10% HNS prior to infection of MDM at MOI 5. Infected monolayers were lysed at 0.5, 2, 6, and 24 HPI and plated in order to perform CFU counts to calculate uptake and intracellular survival. (A) The percentage uptake of C49 by MDM by 0.5 HPI (calculated relative to number of bacteria in original inoculum). (B) The percentage intracellular survival of C49 over a 24-hour time-course (calculated relative to intracellular CFU at 0.5 HPI). Data were normally distributed ($p>0.05$) and analysed by general linear model (N=3 biological replicates). $p<0.05$**

5.2.9 The presence of MAP-specific antibody impacted uptake and intracellular survival of C49

In order to understand if the presence of MAP-specific antibody impacted the uptake and intracellular survival of C49, a third treatment condition was added to the experiment described in Section 5.2.7; C49 were incubated in pooled sera from MAP-antibody positive cattle (Immune Sera; IS) at 37°C, for 30 minutes, prior to infection. Percentage uptake and intracellular survival was measured as described in Section 5.2.7, and the results were directly compared with the percentage uptake and intracellular survival of C49 incubated in NS and HNS (Figure 5-12).

Surprisingly, the percentage uptake of C49 incubated in IS was significantly lower than the percentage uptake of C49 incubated in NS, with no significant difference between the percentage uptake of C49 incubated in IS, compared to HNS (Figure 5-12 A). However, the percentage intracellular survival of C49 incubated in IS was already decreased by 2 HPI, compared to C49 incubated in NS or HNS, and by 24 HPI intracellular survival of C49 incubated in IS was significantly lower than that of C49 incubated in NS or HNS (in addition to C49 not pre-treated with sera, as demonstrated in Chapter 4, Figure 4.1) ($p<0.05$) (Figure 5-12 B)

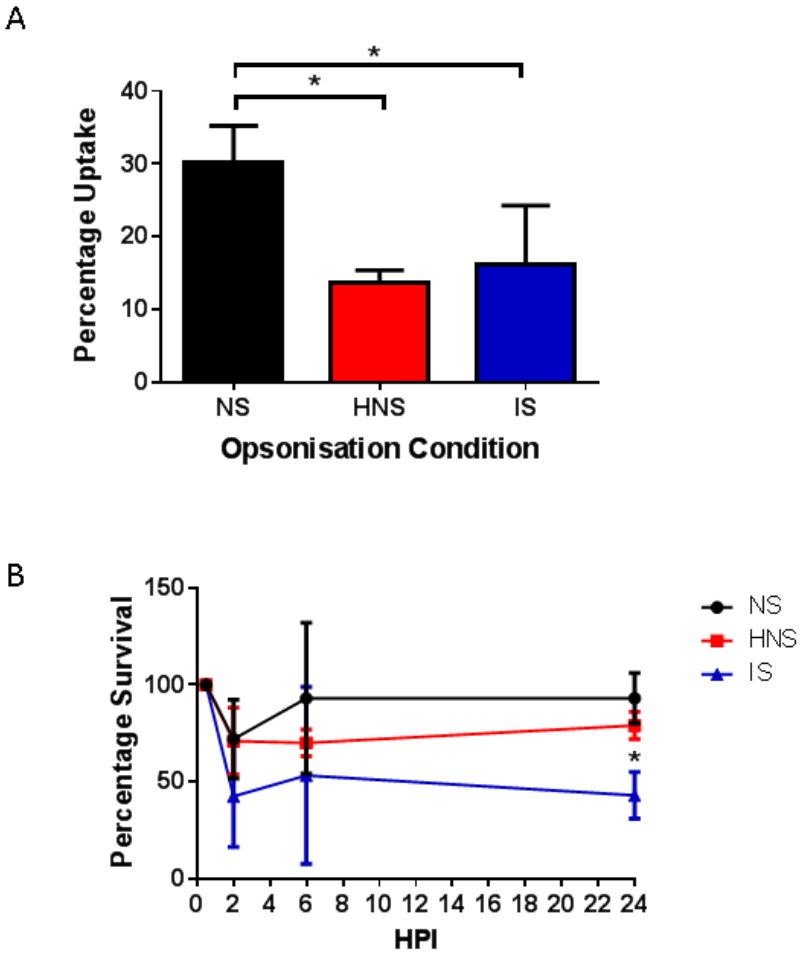

Figure 5-12 Percentage uptake and intracellular survival of C49 treated under different opsonisation conditions.

*C49 were incubated in 10% NS, 10% HNS, or 10% IS prior to infection of MDM at MOI 5. Infected monolayers were lysed at 0.5, 2, 6, and 24 HPI and plated in order to perform CFU counts to calculate uptake and intracellular survival. (A) The percentage uptake of C49 by MDM at 0.5 HPI (calculated relative to number of bacteria in original inoculum). (B) The percentage intracellular survival of C49 over a 24-hour time-course, relative to number of intracellular CFU at 0.5 HPI. Data were normally distributed ($p>0.05$) and analysed by general linear model (N=3). $p<0.05$**

5.2.10 The effect of serum components on the production of RNS by macrophages

In order to understand if increased production of RNS was responsible for the decreased intracellular survival of C49 incubated in IS (Figure 5-12 D), secretion of nitrite from MDM infected for 24 hours with C49 pre-treated in NS, HNS or IS, at MOI 5, was measured by Griess assay. Polystyrene beads were added at the same multiplicity as a non-infectious control.

C49 pre-treated in all three treatment conditions (NS, HNS and IS) resulted in increased nitrite concentrations in the supernatant of infected MDM, compared to MDM given polystyrene beads. However, it should be noted that despite significant differences, concentrations were low (particularly for C49 pre-treated with HNS or IS) and are unlikely to be biologically significant.

C49 incubated in NS caused MDM to secrete significantly higher levels of nitrite than C49 incubated in either HNS or IS (Figure 5-13 A) - an effect which correlates with increased uptake of MAP but not decreased intracellular survival. However, it should be noted that there was significant variation between biological replicates, and each replicate has been graphed individually in Figure 5-13 B, C & D, in order to demonstrate this. MDM derived from Animal 27 secreted higher levels of nitrite when infected with C49, but not polystyrene beads, (particularly when C49 was pre-treated in NS) (Figure 5-13 B), in comparison to MDM derived from Animal 30 and Animal 35 (Figure 5-13 C & D, respectively). Additionally, MDM from Animal 27 were the only cells to have an increased concentration of nitrite in the supernatant when infected with C49 incubated in NS, compared to HNS and IS. The increased nitrite secretion from MDM derived from animal 27 cannot be attributed to increased uptake of C49, as uptake by 0.5 HPI was similar for all three biological replicates; therefore, the cause of the increased nitrite secretion from this biological replicate is unknown. Since nitrite secretion from MDM infected with C49 pre-treated in IS was lower compared to C49 pre-treated in NS or HNS, it is unlikely that increased nitrite secretion is responsible for the decreased intracellular survival observed in Figure 5-12.

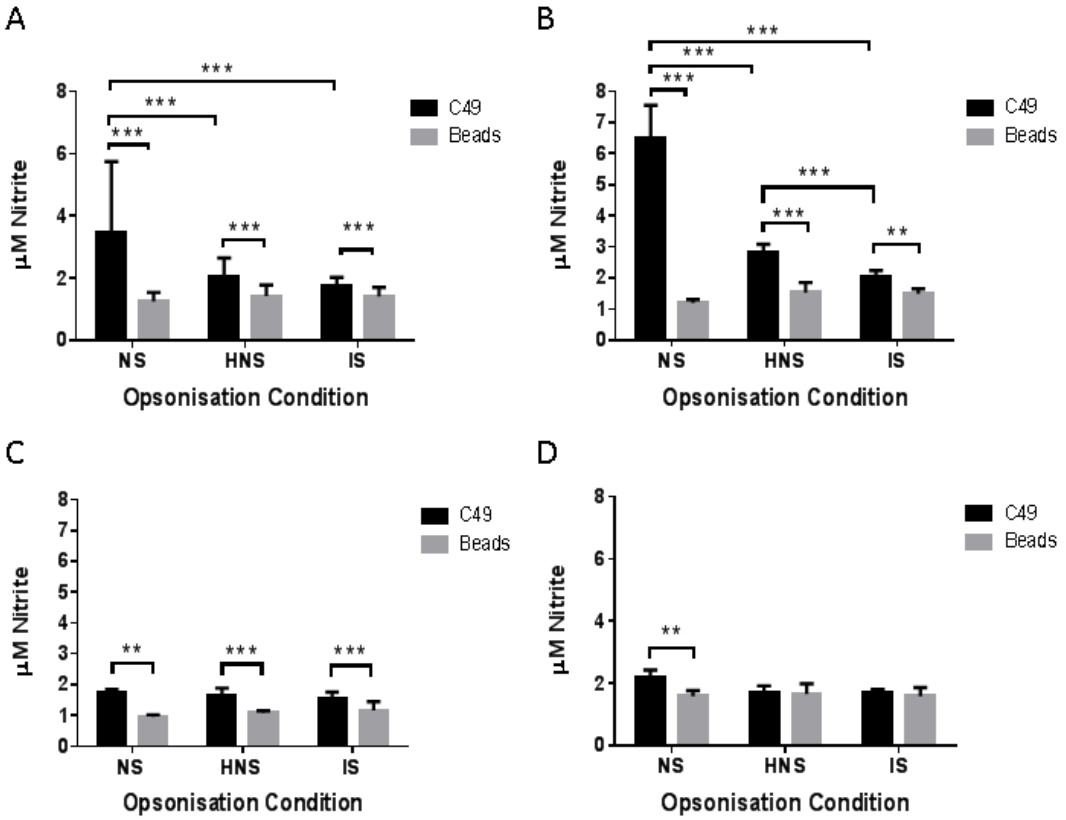

Figure 5-13 Secretion of nitrite into the supernatant of MDM infected with C49 treated under different opsonisation conditions.

C49 was incubated in 10% NS, 10% HNS, or 10% IS prior to infection of MDM monolayers at MOI 5. Polystyrene beads (labelled 'Beads') were included at the same multiplicity, as a non-infectious control. Secretion of nitrite into the supernatant of infected monolayers was then measured by Griess assay. (A) Secretion of nitrite from MDM infected with MAP pre-treated in NS, HNS or IS. Bars represent the mean and SD of 3 biological replicates. Due to variation between biological replicates, each replicate is depicted individually in B-D. (B) Nitrite secretion from MDM derived from animal 27. (C) Nitrite secretion from MDM derived from animal 30. (D) Nitrite secretion from MDM derived from animal 35. Bars represent the mean and SD of 6 technical replicates. NS= Naïve sera, HNS = Heat-inactive Naïve Sera. IS = Immune sera. Data was normally distributed ($p>0.05$) and analysed by general linear model. $p<0.05$, $p<0.01$**, $p<0.001$****

5.3 Discussion

Analysis of the presence of phagocytic receptors on the cell surface of MDM, revealed MDM to be a heterogeneous population regarding the expression of the MR, DC-SIGN and CD11b. The observed differential expression of the MR, DC-SIGN and CD11b could represent distinct subsets of MDM and could potentially impact the ability of these cells to take up and destroy invading pathogens, such as MAP. It would therefore be interesting to perform cell sorting to analyse the response of MDM either positive or negative for these receptors to MAP infection, in the future. In addition, it would be useful characterise bovine gut macrophages to aid the study of MAP infection. Although absent from steady-state gut macrophages in mice and humans, the MR, DC-SIGN and CD11b are known to be expressed by inflammatory gut macrophages in conditions such as Crohn's disease and colitis (Smythies et al. 2005; Kamada et al. 2008; Heinsbroek et al. 2016). As it is currently unknown if they are expressed within the bovine gut, it would be a useful future study to assess the expression of phagocytic receptors on bovine gut-derived macrophages from both healthy cattle and cattle displaying clinical Johne's disease, in order to understand if specific receptors play a role in the immune response and pathogenesis of bovine paratuberculosis.

It is known that several subsets of monocytes and macrophages exist simultaneously, and can respond differently to infection. Corripio-Miyar et al. demonstrated the presence of three distinct sub-populations of monocytes in the circulation of cattle; these monocyte subpopulations were identified by differential expression of CD14, CD16 and CD163, with $CD14^{-}$ $CD16^{++}$ monocytes secreting significantly less IL-10 and significantly more IL-12, than $CD14^{+}$ $CD16^{low/-}$ monocytes, in response to LPS, demonstrating that the two subsets are functionally distinct (Corripio-Miyar et al. 2015). In the current study, the percentage of MDM expressing DC-SIGN and CD11b varied between animals, with higher percentages of MDM from some animals, expressing these receptors, compared to others. Differential expression of these receptors could be indicative of differences in the functional properties of cell; therefore, differential expression of phagocytic receptors could be a potential

explanation as to the inter-animal variation in infection outcome, observed within a herd (Mortier et al. 2015), as well as the variation in response of biological replicates observed throughout this body of work.

The expression of the scavenger receptor MARCO was analysed due to its association with mycobacterial infection in other species. A study by Bowdish et al demonstrated that MARCO binds the mycobacterial cell wall glycolipid trehalose 6,6′-dimycolate (TDM/cord factor), which is also expressed on the surface of MAP (Sung et al. 2004), and is required for TDM-mediated signalling via TLR-2 (Bowdish et al. 2009), with the inflammatory response of transfected cells lacking MARCO significantly reduced. In addition, an *in vivo* study of *M. marinum* infection in zebrafish demonstrated that knockdown of MARCO delayed phagocytosis of *M. marinum* and that MARCO was required for an early pro-inflammatory response. Alongside this, MARCO knockdown caused increased bacterial burden (Benard et al. 2014), showing that MARCO significantly impacted early immune events and, therefore, infection outcome in an *in vivo* model of tuberculosis. Despite evidence in the literature describing the significant role of MARCO in mycobacterial infection in other species, there have not been any studies to date examining the role of MARCO in bovine MAP infection. It should be noted that MARCO gene expression was not upregulated in a microarray studied carried out by the Glass group (Roslin Institute) examining the response of MDM to MAP, suggesting that although significant for mycobacterial infection in other species, MARCO may not be significant in the context of bovine MAP infection.

Staining of MDM with an anti-human MARCO antibody showed MDM to be negative for MARCO expression. This antibody should be cross-reactive with bovine samples, according to the supplier (GeneTex Inc. 2013); however, the predicted sequence of bovine MARCO mRNA shared only 78% sequence identity with human MARCO mRNA (National Center for Biotechnology Information 2017), suggesting that the lack of anti-human MARCO binding to bovine MDM could potentially be due to lack of cross-reactivity between species. In order to understand if MDM truly did not express MARCO, or if the lack of staining was due to a technical issue with the antibody, a PCR was carried out using cDNA from infected and uninfected

MDM. Two sets of primers were used for the PCR, and were based on a sequence common to both transcript variants, X1 and X2. No product was amplified during the PCR reaction. cDNA from MAP infected MDM, as well as uninfected MDM, was used for the PCR, due to evidence that MARCO expression can be induced by TLR signalling, in the context of infection (Doyle et al. 2004; van der Laan et al. 1997; Sun & Metzger 2008). However, the fact that neither infection with K10 or C49 induced expression of the gene encoding MARCO (together with the absence of positive antibody staining of the receptor) suggested that bovine MDM do not express this receptor. It should be noted, however, that as a positive control was not included in the experimental set-up, due to the absence of genetic material known to encode the MARCO gene, the presence of this receptor on bovine MDM cannot be definitively ruled out. In the future, a positive control could be included by cloning and expressing the bovine MARCO gene in a cell-type known to be negative for MARCO expression.

Despite being expressed at lower levels, compared to other phagocytic receptors, the role of the C-type lectins DC-SIGN and MR, in MAP infection, were further analysed due to evidence in the literature that they may be important in the immune response to mycobacterial infection (Gringhuis et al. 2009; Gringhuis et al. 2007; Chieppa et al. 2003; Sweet et al. 2010). As both these receptors are C-type lectins, capable of binding carbohydrates, (primarily Man-LAM) on the surface of mycobacterial cells, these experiments aimed to block both receptors simultaneously, with a polysaccharide blocking agent.

The bovine orthologue of human DC-SIGN was first reported by Yamakawa et al. in a study which demonstrated that blocking of this receptor inhibited the uptake of *M. bovis* BCG by bovine dendritic cells (DC) (Yamakawa et al. 2008). This work complemented the results of an earlier study, in which DC-SIGN on human DC was shown to bind and internalise *M. bovis* BCG, and that binding of Man-LAM to DC-SIGN prevented DC maturation (Geijtenbeek et al. 2003), suggesting that mycobacteria could be deliberately targeting this receptor to prevent T-cell activation. In addition to bovine DC, bovine MDM have previously been shown to express DC-SIGN using the monoclonal antibody clone used in this study

(209MD26A) (Park et al. 2016). Although the results of this chapter initially demonstrated that 71.6% of MDM were positive for DC-SIGN expression, later inclusion of an isotype control demonstrated a large amount of non-specific binding by the isotype of 209MD26A, IgG2a, (which is able to bind all FcγRs (Nimmerjahn & Ravetch 2005)); this non-specific binding completely masked the positive DC-SIGN staining previously observed. The original study demonstrating DC-SIGN to be expressed on bovine MDM did not include isotype controls (Park et al. 2016), which may account for the difference between the results of that study and the work described herein. The development and characterisation of anti-DC-SIGN antibody (209MD26A) did include an isotype control (ColiS205A), however these experiments were carried out on PBMC, as opposed to MDM (Park et al. 2015). In contrast to PBMC, MDM are highly positive for FcγRs, meaning that non-specific binding of isotype-matched control antibodies is more likely in a pure population of MDM compared to PBMC. There was very little DC-SIGN fluorescence observed by immunocytochemistry, potentially indicating that either DC-SIGN or non-specific receptors (responsible for the isotype control binding observed by flow cytometry) was impacted by fixation in 2% paraformaldehyde. However, a previous study has demonstrated that DC-SIGN (expressed on monocyte derived DC) can withstand fixation in 2% paraformaldehyde; in contrast, fixation alone was sufficient to prevent non-specific binding of antibody in immunohistochemistry (Buchwalow et al. 2011). This suggests that the effect of reduced fluorescence observed by immunocytochemistry, compared to flow cytometry, is the effect of the elimination of off-target binding to FcR, and DC-SIGN is possibly not truly expressed on bovine MDM. Upregulation of the gene encoding DC-SIGN was not observed in an RNA-Seq of MAP infected MDM performed by the Glass group (Roslin Institute) (unpublished data). Future experiments comparing anti-DC-SIGN and isotype control binding pre- and post-fixation, by flow cytometry, could clarify if DC-SIGN is expressed by bovine MDM.

The MR was successfully blocked by 2mg/ml mannan and the effect of blocking on bacterial uptake and intracellular survival was assessed. It was hypothesised that MR inhibition would reduce phagocytosis of MAP by bovine MDM, as phagocytosis of mycobacterial species has previously been reported to be reduced in the presence of

MR ligands. For example, phagocytosis of *M. avium* by human MDM (and rat alveolar macrophages) was inhibited in the presence of mannan (Kudo et al. 2004), and phagocytosis of *M. kansasii, M. phlei* and *M. smegmatis* has been reported to be reduced by 43%, 45% and 34%, respectively, in human MDM treated with the MR ligand Man-BSA (Astarie-Dequeker et al. 1999). However, the results of this study demonstrated that inhibition of the MR had no impact of the rate of phagocytosis of MAP; no differences were observed between the number of intracellular CFU at 0.5 HPI within MDM pre-treated with 2mg/ml mannan, compared to untreated MDM (for either K10 or C49). Fluorescent microscopy was also employed to measure uptake of MAP in the presence of an MR inhibitor, and revealed percentage uptake of C49 to be particularly low at 0.5 HPI, regardless of MDM treatment condition. It should be noted that the low percentage uptake at 0.5 HPI is in contradiction to results presented in Chapter 3 of this thesis, which measured confluence by confocal microscopy and demonstrated that confluent infection was achieved at MOI 5. The low percentage uptake observed in this chapter can therefore be partly explained by reduced sensitivity of fluorescent microscopy, compared to confocal microscopy; it is possible that C49 numbers were under-represented when analysed by fluorescent microscopy due to the fact that only bacteria present within a single focal plane were included in this analysis. CFU count confirmed that there were lower numbers of C49 compared to K10; however, the difference was not significant. Low percentage uptake of C49 at 0.5 HPI measured by fluorescent microscopy can also be explained by the fact that a centrifugation step was not included in this immunocytochemistry experiment. Centrifugation allowed the bacteria to efficiently come into contact with the MDM monolayer during infection experiments and was not included in this individual experiment, as uptake was being measured over an extended time-course (24 hours). In hindsight, a centrifugation step should have been included for the 0.5 HPI time-point, to allow the results of the fluorescent microscopy to be directly comparable with the CFU count; the CFU count is therefore more representative of the level of uptake at this time-point. There were no significant differences in the uptake of K10 or C49 between any treatment conditions at 24 HPI when measured by fluorescent microscopy. Taken together, the CFU count at 0.5 HPI and fluorescent microscopy results at 24 HPI suggest that inhibition of the MR does not

significantly impact phagocytosis of MAP, suggesting that MAP is readily phagocytosed via interaction with other receptors, in the absence of MR. Fluorescent microscopy was employed to analyse bacterial uptake in this context due to the increased costs and time-constraints associated with confocal microscopy.

The impact of MR inhibition on intracellular survival of K10 and C49 was assessed by calculating percentage survival at 2, 6 and 24 HPI, in relation to intracellular CFU at 0.5 HPI (subsequent to washing). No differences were observed between the intracellular survival of K10 or C49 in MDM treated with 2mg/ml mannan, compared to untreated MDM, at 2 or 6 HPI. However, at 24 HPI, K10 and C49 intracellular survival was significantly decreased in mannan-treated MDM, compared to untreated controls, suggesting that uptake through the MR is beneficial for intracellular MAP survival. This finding is in agreement with studies examining the role of the MR in the response to other species of mycobacteria. A recent study by Rajaram et al. demonstrated that recruitment and activation of the protein tyrosine phosphatase SHP-1 on *M. tb* phagosomes was dependant on MR signalling, and inhibited phago-lysosome fusion; inhibition of SHP-1 increased phago-lysosome fusion and decreased intracellular growth and survival of *M. tb* (Rajaram et al. 2017). In addition, knockdown of the MR increased phago-lysosome fusion and decreased intracellular survival of *M. avium* in human macrophages (Sweet et al. 2010). It is likely that the MR has a similar influence on the outcome of MAP infection in bovine MDM. Therefore, co-localisation of MAP with the late endosomal marker LAMP1 was assessed, in order to understand if MR inhibition reduced MAP intracellular survival by causing increased phagosome maturation.

The ability of mycobacteria to avoid degradation within lysosomes by interfering with phagosome maturation is well established in the literature (Via et al. 1997; Pieters 2008; Sundaramurthy & Pieters 2007), and results from chapter 4 of this thesis demonstrated that both K10 and C49 were able to inhibit phago-lysosome fusion, by showing reduced co-localisation of LAMP1 with live MAP versus H/in MAP. In order to understand if uptake through the MR influenced the ability of MAP to avoid degradation within lysosomes, co-localisation of MAP with LAMP1 under different treatment conditions, was assessed by immunocytochemistry. No

significant differences in LAMP1 co-localisation were observed between any of the treatment conditions at 0.5 HPI. This was somewhat expected as it was unlikely that phagosome maturation would occur within 0.5 HPI (Canton et al. 2014), however this time point was included as the same samples used to assess uptake by fluorescent microscopy were used to assess LAMP1 co-localisation. There was limited uptake of bacteria at this time-point, as described above; meaning results at 0.5 HPI are somewhat unreliable due to limited technical replicates. Surprisingly, inhibition of the MR at 24 HPI significantly decreased co-localisation of live K10 with LAMP1, contrary to the hypothesis that MR inhibition would increase co-localisation. This discrepancy may be explained by the late time-point (24 HPI) analysed in this study - previous studies examined phagosome maturation within a 2-hour time course (Rajaram et al. 2017; Sweet et al. 2010; Kang et al. 2005). Since intracellular K10 and C49 CFU count is reduced in mannan-treated MDM at 24 HPI, it is likely that the results of this assay are not biologically significant. In hindsight, a single 2 HPI time-point would likely have been more informative on phago-lysosome fusion in this context than the 0.5 HPI and 24 HPI time-points.

In order to understand the effect of MR block on the inflammatory response of MDM, IL-10 and IL-1β secretion was measured. Both infected and uninfected cells increased IL-10 secretion when treated with 2mg/ml mannan, compared to untreated cells. This finding was in contrast to the results of Chieppa et al. who did not observe an increase in IL-10 secretion in monocyte-derived DCs treated with mannan. However, it should be noted that mannan was used at a lower concentration (30µg/ml) which could account for the differences between the two studies. In addition, Chieppa et al tested other methods of blocking the MR which did result in increased IL-10 secretion; immature monocyte-derived DCs treated with a monoclonal antibody targeting the MR (PAM-1), or Man-LAM, underwent functional maturation (by increasing expression of co-stimulatory molecules) and increased secretion of IL-10 and other anti-inflammatory mediators (Chieppa et al. 2003). It is possible that monocyte derived DCs may respond differently to treatment with mannan, compared to MDM, although this is somewhat unlikely, due to shared PRRs and signalling pathways of these two cell types (Park et al. 2016). As mannan is an agonist of the MR, the increase in IL-10 secretion suggests that

engagement of the MR with its ligand induces an anti-inflammatory response by MDM, and that MAP could actively target their uptake through this pathway, in order to prevent the secretion of protective, pro-inflammatory cytokines, promote a Th-2 type response and increase their intracellular survival within MDM (Weiss et al. 2005; Hussain et al. 2016; Magombedze et al. 2015), as discussed in chapter 4.

There were no significant differences in IL-1β secretion from MAP infected or uninfected MDM treated with mannan, compared to untreated controls. Surprisingly, while concentrations of IL-1β were slightly higher from both K10 and C49 infected MDM, compared to MDM treated with H/in K10 or C49, or uninfected cells, there were no significant differences between infection conditions, which is contrary to the results presented in Chapter 4 (see section 4.2.3.2). IL-1β secretion was not significantly upregulated in response to mannan, a finding in agreement with the study by Chieppa et al (Chieppa et al. 2003) which agrees with the hypothesis that signalling through the MR produces an anti-inflammatory phenotype in MDM. As with the results from chapter 4, there was a great deal of animal-animal variation. The reason for the animal-animal variation is unknown but could perhaps be due to the genotype of the animals from which the MDM are derived. It is known that host genotype can significantly affect mycobacterial infection outcome *in vivo*. For example, a polymorphism in the IL-1β gene is associated with protection against tuberculosis in humans (Gomez et al. 2006).

The effect of blocking the MR on MHC II expression, by uninfected and MAP infected MDM, was investigated due to the known effect of increased co-stimulatory molecule expression by monocyte derived DCs upon cross-linking of the MR (Chieppa et al. 2003). In addition, mycobacteria are known to be capable of manipulating MHC II expression (Weiss et al. 2001). Although results in Chapter 4 of this thesis did not show a significant difference between MHC II expression of MAP infected MDM and controls at 24 HPI, there was a trend towards decreased MHC II expression in infected cells. It was therefore hypothesised that inhibiting uptake via the MR (and forcing phagocytosis of MAP via receptors other than C-type lectins) may either exaggerate the reduction in MHC II expression observed in Chapter 4, or counter it, thereby impacting the ability of MDM to present Ag to T-

cells. However, the same reduction of MHC II expression at 24 HPI in MAP infected (untreated) MDM was not observed in this experiment. MHC II expression was significantly increased by K10 infected MDM compared to uninfected MDM at 24 HPI, whereas no differences were observed between C49 infected MDM and uninfected MDM, suggesting that MAP infection does not have an effect on MHC II expression at this time point. No differences were observed between MHC II expression of mannan-treated MDM and untreated controls, suggesting that MR inhibition during phagocytosis had no effect on the ability of MDM to present antigen to T-cells via MHC II. It would be interesting to expand on this finding by assessing co-stimulatory molecule expression upon MAP infection, in this context.

It is important to note that there are other C-type lectin receptors, in addition to DC-SIGN and MR, such as Dectin-1. A study by Willcocks et al. demonstrated that Dectin-1 is expressed at the mRNA level in bovine monocytes, macrophages, dendritic cells and NK cells (Willcocks et al. 2006). The development of antibodies targeting bovine Dectin-1 will allow the expression of this receptor at the protein level to be studied in future, and could provide insight into the role of this receptor in MAP infection.

The role of opsonic phagocytosis in determining the response of MDM to MAP, and determining the ability of MAP to survive intracellularly, was investigated by pre-treating C49 cultures in 10% NS, 10% HNS, or 10% IS. Serum contains heat-labile proteins capable of binding to the surface of pathogens for opsonisation (primarily complement proteins), therefore heat inactivation allowed the role of these serum components in MAP pathogenesis to be assessed. Only C49 was used for this experiment, as it is likely a better model of natural infection, as determined by the results of chapter 4. It was found that the presence of heat-labile components, such as complement in NS, significantly increased the uptake of C49 into MDM but did not negatively affect their ability to survive intracellularly. This finding is in agreement with the findings of Hostetter et al, who demonstrated increased uptake of fluorescently labelled MAP that had been pre-treated in sera from uninfected cattle, by flow cytometry (Hostetter et al. 2005). The fact that, despite increased uptake, there was no decrease in intracellular survival could be due to the poor pro-

inflammatory response and respiratory burst induced by complement receptor mediated phagocytosis (in comparison to FcγR-mediated phagocytosis) (Aderem et al. 1985; Aderem & Underhill 1999; Wright & Silverstein 1983; Roberts et al. 2016). These findings suggest that MAP could possibly target its uptake through CR, as a way to enter its preferred niche, the macrophage, but suppress the inflammatory response and avoid degradation. In future, CR could be blocked or knocked-down in order to assess if the increased phagocytosis observed in the presence of heat-labile serum components is directly attributable to complement. In addition, this use of serum depleted of certain components unique to a specific pathway complement pathways (such as MBL) could inform upon the precise mechanism by which the observed increased phagocytosis occurs.

Several intracellular pathogens, primarily viruses, have been reported to target CR to promote uptake (Lambris et al. 2008). An early study by Schorey et al. demonstrated that presence of the complement component C2a promoted uptake of pathogenic mycobacteria, but not non-pathogenic species, by human macrophages, suggesting that pathogenic mycobacteria salvage C2a, after dissociation from C4b. The enhanced uptake was shown to be dependent on C3 and occur through CR1 and not CR3 or CR4 (Schorey et al. 1997; Bermudez et al. 1999). Unfortunately, no anti-bovine CD35 (CR1) antibody was available to assess the expression of this receptor, alongside CR3 and CR4, on MDM for this study. The fact that the mechanism of utilising C2a to enhance uptake, is highly conserved in pathogenic mycobacteria (including *M. tuberculosis*, *M. avium* and *M. leprae*) but absent from non-pathogenic mycobacteria, such as *M. smegmatis*, suggests that enhanced uptake through CR1 may be an important virulence mechanism.

M. bovis BCG is known to activate all three complement pathways: the classical pathway, (in both an antibody dependent and independent manner), the lectin pathway and the alternative pathway (Carroll et al. 2009; Bartlomiejczyk et al. 2014). However, the inhibitory protein Factor H is also known to bind to mycobacteria and inhibit uptake of BCG by THP-1 macrophages in a dose-dependent manner (Abdul-Aziz et al. 2016). The binding of Factor H could explain why extracellular survival was not affected by the presence of complement proteins in this study. Factor H

binding also demonstrates that some regulation of the complement pathway occurs during mycobacterial infection, whether driven by the host or the pathogen.

The effect of opsonising MAP in sera containing MAP-specific antibody (IS) was also analysed in this study. Ideally, a fourth treatment condition of C49 incubated in 10% heat-inactivated IS (HIS), would have been included in the study in order to understand the role of antibody in the absence of complement proteins; however, this condition was not included due to having a limited supply of IS. It was found that C49 incubated in 10% IS prior to infection had significantly reduced bacterial uptake compared to MAP opsonised in NS, and uptake was at a similar level to MAP treated with HNS. This effect could potentially be explained by loss of complement activity through freeze-thaw cycles of IS (Lachmann 2010). Although the complement activity was not measured in IS, it is likely that active complement was not present. This suggests that complement alone is responsible for the observed increase in phagocytosis of MAP by MDM, and that effects of antibody opsonisation can be directly attributed to FcR-mediated phagocytosis, as opposed to antibody-mediated complement activation. A haemolytic assay could be carried out in future, in order to confirm the absence of complement activity in IS. Although there was no increase in phagocytosis of C49 opsonised in IS, MDM were able to destroy C49 opsonised in IS more efficiently than C49 opsonised with NS or HNS. This suggests that uptake through FcRs is detrimental to intracellular mycobacterial survival. Increased bactericidal activity is another potential explanation for the reduced CFU count of C49 opsonised in IS compared to C49 opsonised in NS at 0.5 HPI, as it is possible that intracellular killing is occurring rapidly upon phagocytosis therefore the reduced intracellular CFU at 0.5 HPI could be accounted for by increased killing as opposed to decreased uptake. This could be investigated by comparing CFU to GCN at this time-point, to assess if MAP GCN is significantly higher than CFU in samples treated with IS. Additionally, it would be interesting to observe the uptake of MAP pre-treated with the different sera by live-cell imaging.

An antibody response is often associated with poor protection and a decline into clinical disease in the context of mycobacterial infection (Nielsen et al. 2009; Nielsen et al. 2013; Jacobs et al. 2016; Stabel 2000), but the role of antibody is rarely

considered in the initial encounter between MAP and innate immune cells. The presence of antibody at the point of infection (without subsequent exposure) is entirely possible, due to the potential for infected animals to secrete antibody alongside the shedding of viable MAP in milk (Arsenault et al. 2014). This study hypothesised that the presence of MAP-specific antibody would be detrimental to the intracellular survival of MAP, within the first 24 hours of infection, due to the inflammatory response induced by FcR mediated phagocytosis (Aderem & Underhill 1999). This hypothesis was upheld. However, the results of this study differed from the study by Hostetter et al, which showed increased intracellular growth of MAP in macrophages activated with LPS, after 1 hour incubation in IS, and no significant differences in the intracellular growth/survival of MAP incubated in IS, compared to MAP incubated in NS, in the absence of LPS activation. This difference could possibly be accounted for by the fact that percentage survival was measured between 4-48 HPI, as opposed to 0.5- 24 HPI; also, MAP strain ATCC® 19698™ was used in the study by Hostetter et al (Hostetter et al. 2005), which has lost Mycobactin dependence, and likely has different characteristics to C49.

The presence of antibodies can augment Th-1 immunity and reduce intracellular survival of pathogens via FcR-mediated phagocytosis (Guilliams et al. 2014). A potentially significant role of FcR-mediated phagocytosis in mycobacterial infection was reported by de Vallière et al.; sera containing anti-LAM antibodies from patients vaccinated with BCG significantly increased uptake of BCG by macrophages and enhanced IFNγ production by CD4+ and CD8+ T-cells (de Vallière et al. 2005). However, there have been conflicting reports regarding the effect of antibody and FcR-mediated phagocytosis on intracellular survival of mycobacteria. An early paper by Oh and Straubinger demonstrated that restriction of phagosome maturation by *M. avium* occurred in both the presence and absence of antibody, suggesting that FcR-mediated phagocytosis did not impact the bactericidal activity of J774 cells (Oh & Straubinger 1996). However, a more recent study by Kumar et al. demonstrated that opsonisation of *M. tb* with immune sera from BCG vaccinated individuals, enhanced intracellular killing through increased phago-lysosome fusion in human macrophages. Antibodies directed against certain antigens (for example, LAM) were able to opsonise bacteria, whereas antibodies of other specificities were not, which

could account for the difference in results between this study (Kumar et al. 2015) and the earlier study by Oh and Straubinger (Oh & Straubinger 1996).

This chapter investigated how different opsonisation conditions affected the production of RNS by MAP infected MDM, in order to understand if this contributed to the reduced intracellular survival observed upon opsonisation with MAP-specific antibody. Surprisingly, it was found that C49 incubated in IS, induced significantly less nitrite secretion than C49 incubated in NS (which was increased compared to C49 incubated in HNS). The concentration of nitrite was generally low (particularly for C49 incubated in HNS or IS), however C49 was previously shown to induce very little nitrite secretion from infected MDM, in chapter 4. The result of this experiment is somewhat incongruous with results from chapter 4, as nitrite secretion was previously shown to correlate with increased microbicidal activity towards MAP, whereas this result suggests it may be induced by the presence of complement, but does not correlate with decreased bacterial survival. It should be noted, that there was much animal-animal variation, with only animal 27 secreting highly elevated levels of nitrite in response to C49 opsonised NS, but this did not correlate with reduced intracellular survival of C49 in MDM from this animal, showing no biologically significant effect of increased nitrite secretion in this context. Kumar et al demonstrated that opsonisation of BCG with antibody increased NO and co-localisation of BCG with iNOS, suggesting that RNS production does play a role in decreased intracellular survival in the presence of antibody (Kumar et al. 2015). However, a major difference between the two studies was that Kumar et al measured intracellular NO by fluorescent microscopy, whereas work presented in this chapter measured secretion of nitrite into the supernatant. This suggests there could still be a role for RNS in reduced intracellular MAP survival and future studies could look at the intracellular co-localisation of MAP with NO, in order to understand this.

Variation between biological replicates was observed throughout this chapter. This is a common problem associated with using primary cells from outbred animals to model infection. It can be accounted for by several different factors, including differences in genotype of the animals. Animal 27 was a Norwegian Red cross, whereas all other animals were Holstein Friesians, which likely accounts for the

differential production of RNS by this animal. Other factors potentially affecting biological variation include environment, age, diet, lactation, and exposure to infection. However, these factors were controlled for as much as possible; all animal used were heifers aged between 6-15 months that were housed in same environment and fed the same diet. It is therefore likely that most of the variation observed can be attributed to genotype.

Collectively, the results of Chapter 5 demonstrate that the response of MDM, and outcome of MAP infection, can be influenced by the route of phagocytosis. Both uptake through C-type lectins, and uptake in the presence of antibody, reduced the intracellular survival of MAP by 24 HPI. This study could have been improved by the inclusion of heat-inactivated sera from MAP-antibody positive cattle, which would have allowed the clear distinction between FcR-mediated phagocytosis and the role of antibody in complement activation; however, this was not included in the experimental design due to a limited supply of sera from MAP-antibody positive cattle. It would be interesting to further elucidate these pathways in the future by knocking down specific receptors with siRNA or blocking the specific receptors with blocking antibodies; this would allow the importance of each specific C-type lectin and FcR to be elucidated. A better understanding of the early interaction of MAP with macrophages, and how MAP engages with specific phagocytic receptors, may assist in the development of new, more effective, vaccines against MAP

.

6 Final Discussion

Johne's disease is a chronic enteritis, caused by MAP infection (referred to as paratuberculosis), and has a detrimental impact on both the beef and dairy industry (McAloon et al. 2016; Richardson & More 2009; Ott et al. 1999). While prevalence in the UK is largely unknown due to the non-notifiable status of the infection, other European countries have estimated paratuberculosis herd-level prevalence to be between 83.3% (Switzerland) and 19% (Austria) (Garcia & Shalloo 2015), causing substantial economic losses.

A meta-analysis by Bastida and Juste determined that vaccination is a useful strategy for preventing production losses from MAP infection and Johne's disease (Bastida & Juste 2011). However, the commercial vaccines currently available lack efficacy, as they cannot prevent infection or faecal shedding of bacteria but merely delay the onset of clinical symptoms (Park & Yoo 2016). In addition, the commercial vaccines available are whole-cell inactivated vaccines that contain an array of antigens which could cause reactivity to ante-mortem diagnostic tests for both paratuberculosis and bovine tuberculosis (Rosseels & Huygen 2008), making their use impractical, particularly in bovine tuberculosis endemic areas. Current paratuberculosis control measures, in the UK, utilise a test-and-cull strategy; however, control is hindered by a lack of sensitive and specific ante-mortem diagnostic tests. Therefore, a novel efficacious vaccine should be developed alongside improved diagnotics with DIVA test capability in order to benefit Johne's disease and partuberculosis control.

The pathogenesis of Johne's disease contributes to the difficulties in controlling the infection (descibed above). MAP is able to evade the host immune response and survive intracellularly within macrophages for a prolonged period. The infected macrophage responds via several mechanisms, including secretion of pro-inflammatory cytokines and chemokines that result in the formation of a granulomatous lesion at the site of infection. Granuloma formation likely contributes to the long subclinical period of paratuberculosis; however, several years later, a change in the immune response (that remains poorly understood) may lead to faecal shedding of MAP, and the eventual development of clinical Johne's disease. The inadequate understanding of immune response over the subclinical period, that leads

either to disease or control of infection, means there is a lack of well-defined correlates of protection or infection. A detailed understanding of the host-pathogen interaction could contribute to identification of correlates of infection, protection, or disease that would significantly benefit disease control strategies.

The over-arching hypothesis of this thesis was that the early macrophage response to MAP likely affects the outcome of the infection, and that the strain of MAP may significantly influence this response. The study aimed to identify early MDM responses that may be important for intracellular bacterial survival or downstream immune responses, analyse and compared the MDM response to the reference strain of MAP (K10) and a recent clinical isolate from a cow with clinical Johne's disease (C49), and assess if the mechanism of uptake impacted the ability of MAP to survive intracellularly. A further understanding of the early MAP-macrophage interaction could highlight pathways that may be of importance in the design of novel efficacious vaccines and diagnostic tests. In addition, an understanding of how the macrophage response differs between the two MAP strains could inform on the reliability of using the reference strain (which is likely to have undergone lab-adaptation) to model the infection, and therefore have a major impact on the design of future studies examining MAP infection.

This study clearly demonstrated several significant differences between the macrophage response to K10, compared to C49. The key difference observed (which informed much of the subsequent work of this thesis) was that K10 had a reduced capacity to survive intracellularly within MDM, compared to C49, suggesting that the virulence of the K10 strain was reduced. Several other notable differences in the macrophage response to each strain were also observed; including significantly increased IL-1β, and IL-10 secretion, as well as increased NOS2 gene expression and nitrite secretion in K10 infected MDM compared to C49 infected cells. This finding suggests that infection experiments utilising K10 may not accurately represent the host-pathogen interaction that leads to paratuberculosis in the field. This should be considered when interpreting the results of studies focusing on K10. The finding that K10 likely has reduced virulence is in agreement with an *in vivo* study by Fernandez at al., which demonstrated that lambs infected with a clinical C-type MAP strain had

higher numbers of intestinal lesions, and higher serum levels of MAP-specific antibody and IFNγ, compared with lambs infected with K10 (Fernández et al. 2014). While the use of K10 remains valid in the study of paratuberculosis, the aim of the study should be considered when selecting which MAP strain to use. For example, the use of K10 may not be optimal in animal challenge studies evaluating pathogenesis or vaccine efficacy. However, as K10 is well characterised, it may be useful for genetic studies examining the role of specific conserved genes in biological processes and host-pathogen interactions. As K10 is the reference strain, its use also allows a direct comparison between multiple studies, whereas results associated with one clinical strain may not be applicable to another strain.

The genome of K10 was first sequenced in 2005 (Li et al. 2005), and remained the only sequenced strain until 2014 (National Center for Biotechnology Information 2017). Thus, K10 has been widely used in the study of host-pathogen interactions, since understanding the genome sequence enabled genetic manipulation (Kugadas et al. 2016; Bannantine et al. 2015; Ghosh et al. 2014). Work described in this thesis identified differences between the genomes of K10 and C49; however, further work is required to understand which genes specific to C49 were responsible for dampening the macrophage response. Targeted gene silencing could be employed to assess the role of the high-effect genetic mutations identified as unique to C49 by the sequencing described in Chapter 4 of this thesis. This would provide an understanding of how specific bacterial genes effect host-pathogen interactions and influence the infection outcome. Clustered regularly interspaced short palindromic repeat (CRISPR) interference has previously been used as a method to efficiently repress expression of target genes in *M. tb*, and is a method that could be utilised for future MAP studies.

The finding that K10 is genetically different, and elicits a different macrophage response, compared to a clinical strain of MAP is in agreement with the wider literature. The phylogeny of different MAP strains has been reported, as well as a strain effect upon lesion structure in lambs (Fernández et al. 2014; Verna et al. 2007; Stevenson 2015; Bryant et al. 2016), suggesting that the genetics of MAP can significantly affect disease progression and infection outcome. It would be

interesting to further elucidate strain-effect on the immune response to MAP *in vitro* as this information could be utilised to identify vaccine candidate antigens that would be cross-protective against multiple field strains. A panel of multiple strains could be included, and co-cultures with other immune cells could be set up to understand how MAP infection affects cell-cell interactions, an aspect of the early immune response that was absent from this study. Intestinal organoids have previously been used to model infections, such as rotavirus (Finkbeiner et al. 2012), and bovine intestinal organoids have recently been established (Hamilton et al. unpublished data). Similar to murine organoids, bovine organoids can be induced to develop M-cells via the Receptor activator of nuclear factor kappa-B ligand (RANKL) and may, therefore, be utilised to demonstrate how different strains of MAP interact with, and invade, the gut epithelium. An accurate understanding of how MAP strains interact with the epithelium is important for future disease control, as epithelial cells contribute to inflammation in response to MAP infection (Everman et al. 2015; Lamont et al. 2012). It is also possible that the manner by which MAP invades the epithelium may affect the phenotype of the bacteria prior to their uptake by macrophages, and thereby affect the macrophage response to infection. Passage of MAP through an epithelial monolayer (MDBK cells) and macrophages *in vitro* has previously been shown to affect the phenotype of MAP upon re-infection of epithelial cells, changing the lipid profile of the bacteria and increasing the inflammatory response of epithelial cells upon reinfection (Everman et al. 2015). The use of organoids containing multiple cell-types would likely increase understanding of how translocation through the epithelium may affect the early immune response and pathogenesis. This would likely be of benefit to the design of improved vaccines, as it may be that targeting translocation across the gut epithelium through a particular mechanism (i.e. via M-cells) could result in a more protective response than other mechanisms of gut invasion.

This study identified several early innate responses that may impact the infection outcome, and warrant further investigation. One such immune response was decreased IL-1β secretion in C49 infected cells compared to K10 infected cells, suggesting that C49 is suppressing IL-1β secretion by infected MDM (likely via a virulence mechanism) and it is therefore likely that IL-1β has protective effects

against MAP. IL-1β is a pleiotropic cytokine, and its role in MAP infection remains poorly understood. Due to the correlation between increased IL-1β secretion of K10 infected cells and decreased intracellular survival of K10, it was hypothesised that IL-1β may directly reduce intracellular MAP survival within macrophages (likely via induction of antimicrobial products). However, IL-1β secretion was dependent on the NLRP3 inflammasome, and knockdown of the NLRP3 inflammasome had no effect on intracellular survival of either K10 or C49 – suggesting that the role of IL-1β in MAP infection is likely unrelated to intracellular survival. A study by Lamont et al. described how MAP infection of bovine epithelial cells (MAC-T cells) resulted in upregulation of IL-1β, and that IL-1β secreted by MAC-T cells had a chemoattractant effect upon macrophages in a co-culture system (Lamont et al. 2012). This finding suggests that IL-1β is important in driving recruitment of immune cells to the site of infection and likely plays a key role in granuloma formation. IL-1β signalling through IL-1R1 has previously been shown to play an important role in granuloma formation in response to *M. tb* infection in mice (Fremond et al. 2007), and IL-1β is associated with multibacillary rather than paucibacillary lesions in ovine paratuberculosis (Alzuherri et al. 1996), further suggesting that this cytokine is important in the development of intestinal lesions. It would be interesting to assess if the strain-specific IL-1β response observed in macrophages is also observed in other cell-types, such as epithelial cells. Again, organoid cultures could be employed to assess the cytokine response of epithelial cells to MAP infection. Establishing co-cultures of bovine intestinal organoids and immune cells, such as macrophages and lymphocytes, would provide understanding of the chemoattractant properties of IL-1β in the context of MAP infection, and expand on the findings of Lamont et al. Gene knockdown of IL-1R1 on cells within this co-culture system would allow assessment of how IL-1β affects chemoattraction and cell-cell interaction.

Subsequent to experiments utilising organoids to assess if IL-1β has a role in lesion development, it may be of benefit to further study the role of IL-1β in MAP infection using a small-animal host that is naturally susceptible to MAP, such as the rabbit. Small-animal infection models can be genetically manipulated with ease, compared to large animals, and IL-1β or IL-1R1 knockout animals would inform on how IL-1β

affects lesion development within the intestine, *in vivo*. If IL-1β secretion is found to have protective effects against MAP, it would likely be of benefit to vaccine design as vaccines and/or adjuvants could target this pathway to confer a protective response. Similarly, the finding that IL-1β produced in response to MAP likely depends upon NLRP3 inflammasome activation, could have important consequences for future MAP vaccines. The current Johne's disease vaccines licenced for cattle (Mycopar and Silirum) both incorporate an oil adjuvant. However, the oil-in-water adjuvant (MF59) has been reported to act independently of NLRP3 activation (Seubert et al. 2011). A clearer understanding of the role of IL-1β in the early response would inform on whether adjuvants targeting NLRP3 could improve protection.

This study demonstrated a clear association between RNS production (but not ROS production) and decreased intracellular survival of MAP. However, the mechanism by which RNS is produced in the context of MAP infection remains to be understood. Expression of the gene encoding iNOS (NOS2) can be induced via several signalling pathways, including cytokine signalling, such as IL-1β, IFNγ and TNFα, as well as through the interaction of certain PAMPs (i.e. LPS) with PRRs. Future studies should investigate the mechanism of RNS production in response to MAP, as it is likely that a vaccine and/or adjuvant targeting this pathway would increase the bactericidal activity of macrophages early in infection, likely altering the infection outcome. For example, if iNOS is primarily induced by signalling of specific cytokines, an effective vaccine would induce early secretion of these cytokines by effector memory T-cells upon subsequent recognition of MAP antigens.

It is likely that a live-attenuated vaccine would be the most effective at inducing protective immunity against MAP, as these vaccines are capable of eliciting both systemic and mucosal immunity due to the diverse range of antigens expressed on their surface (Park & Yoo 2016). Of particular importance for mycobacterial infection, live-attenuated vaccines would be capable of surviving within the host (providing non-sterile immunity), resulting in a strong, protective, long-lasting immune response, due to the prolonged presence of antigen (Waters et al. 2012). In addition, the development of a live-attenuated vaccine is cost-effect compared to

other vaccine types; this is an important aspect of a paratuberculosis vaccine, as control of the disease must be economically beneficial to the farmer. There are currently no commercial live-attenuated vaccines for paratuberculosis and the commercial inactive whole-cell vaccines lack efficacy. However, attempts have been made to develop a live-attenuated MAP vaccine; the Johne's disease integrated program (JDIP), an international research consortium, has identified and evaluated twenty-two live-vaccine candidates using an established standardised testing platform (Bannantine et al. 2014). Knockout mutants, from several different laboratories, were included in the JDIP study; however, none of the mutants out-performed the commercial vaccine Silirum, and did not prevent infection or faecal shedding (Bannantine et al. 2014). A conclusion of the JDIP study was that a detailed understanding the host immune response would benefit the design of a live-attenuated MAP vaccine. This is highlighted by the development of the *M. tb* vaccine strain *ΔfbpAΔsapM*; this mutant lacks Ag85 as well as the acid phosphatase SapM, which is important in restricting phagosome maturation during *M. tb* infection. Macrophages infected with *ΔfbpAΔsapM* were able to undergo phagosome maturation and restrict intracellular growth of the mutant, which subsequently led to increased antigen presentation to T-cells (Saikolappan et al. 2012). A major drawback of developing live-attenuated vaccines against MAP is the issue of cross-reactivity with diagnostics for both paratuberculosis and bovine tuberculosis. However, it has been demonstrated that, while the whole-cell inactive vaccine Silirum can interfere with the single bovine intradermal tuberculin test, the comparative intradermal test had low cross reactivity in cattle (Garrido et al. 2013). It is therefore possible that the comparative intradermal test could also be compatible with a live-attenuated vaccine, although this remains to be tested. MAP antigens known to be absent from vaccine strains could potentially be utilised for paratuberculosis diagnostic tests, alongside vaccination.

The finding that the mechanism of entry impacted the intracellular survival of MAP (via an unknown mechanism) could be of significant importance for the control of paratuberculosis and Johne's disease. Work presented in this thesis demonstrated that incubating MAP in serum containing anti-MAP antibody correlated with decreased intracellular survival of the bacteria within MDM, therefore the presence of anti-

MAP antibody prior to, or during, initial infection is likely to have a protective effect. In agreement with work presented in this thesis, it has been demonstrated that culturing MAP in milk altered the phenotype of the bacteria and that opsonisation with MAP-specific antibodies enhanced bacterial passage through epithelial cells and bactericidal activity of macrophages *in vitro* (Everman & Bermudez 2015; Alonso-Hearn et al. 2010), suggesting that the means by which a calf contracts the bacteria could impact infection outcome and that the presence of antibody during infection is likely protective. A first step to understanding the role of antibody early in MAP infection would be to determine if MAP secreted in milk containing antibody is opsonised at the point of infection. This could be investigated by incubating MAP in antibody-positive milk from a MAP-infected cow, washing, and subsequently incubating the bacteria with an anti-bovine IgG fluorescently labelled antibody, and analysing fluorescence by flow cytometry. The protective role of antibody could then be further investigated *in vitro* by carrying out comparative studies on the macrophage response to opsonised MAP, compared to unopsonised MAP; for example, RNA-Seq could be utilised to investigate differences in macrophage gene expression in the presence of opsonised or unopsonised MAP. To date, there have been no *in vivo* experimental infections examining differences in disease progression between calves given bacteria via different routes (i.e. calves given contaminated faeces, compared to calves given contaminated milk or colostrum). Although, a previous study by Eisenberg et al. demonstrated that there was no correlation between antibody secretion in colostrum of dams, and faecal shedding of MAP by naturally infected daughters. However, the study was discontinued after 2 years, and therefore did not assess how antibody secretion by dams affected the development of clinical disease, or long-term milk production, of daughters (Eisenberg et al. 2015). In addition, the calves in this study were continually exposed to MAP in dust of contaminated barns, meaning it was impossible to determine the time-point and means by which daughters had contracted the bacteria. An *in vivo* infection study is therefore warranted to fully understand if maternal antibody secretion and antibody opsonisation of MAP have a protective effect at the point of infection.

Protective effects of antibody opsonisation were observed in this body of work, and have previously been reported by Everman and Bermudez, although they remain to

be fully understood (Everman & Bermudez 2015). Therefore, it is possible that passive vaccination of neonates may be beneficial for control of paratuberculosis. Pooling of colostrum with high antibody titre has been a practise to improve immunity of calves for several years (Williams et al. 2014). However, pooling of colostrum from MAP milk-ELISA positive dams is impractical due to the risk of bacterial shedding by these animals. MAP is able to withstand both heat-treatment and high pressure processing of milk and colostrum (Verhegghe et al. 2017), therefore it is currently not possible to kill MAP while maintaining immunoglobulin content of milk products. Pooling of colostrum is therefore not recommended on MAP-positive farms (Nielsen et al. 2008; Collins et al. 2010), and is unlikely to be utilised as a method to confer passive immunity to neonates. An alternative method of conferring passive immunity to neonates could be to vaccinate dams at dry-off with a vaccine that would induce a combined immune response. A study by Smith et al. has previously demonstrated that vaccination of dams against *Salmonella enterica* resulted in significantly increased levels of specific antibody against *Salmonella enterica* in neonates (although it as unclear if the presence of these antibodies conferred protection). It is possible that a similar effect could be observed in the calves of dams vaccinated against MAP. A preliminary study could be carried out to assess if current commercial vaccines, such as Silirum, would result in the transfer of passive immunity to calves. Subsequently, long-term challenge studies, assessing faecal shedding, lesion development, and progression to clinical disease, could be carried out to assess the protective effect of passive immunity in MAP infection.

Primary macrophages were used throughout this study, as the response of primary cells is likely to be more representative of natural MAP infection than the response of cell lines, such as BoMac cells (Abendaño, Juste, et al. 2013). In addition, MDM are likely representative of gut macrophages, as host gut macrophages are derived from circulating monocytes and, although resident gut macrophages are typically non-inflammatory, they can be induced to display an inflammatory phenotype in response to infection (similar to MDM) (Bain et al. 2014; Bain et al. 2013). However, the results of this study were compounded by reproducibility issues, due to variation between biological replicates (a recognised issue with work involving primary cells from outbred animals). There is known association between host

genetics and susceptibility to MAP (Gonda et al. 2006; Kirkpatrick & Shook 2011) that may have accounted for the observed variation in the response of macrophages generated from different animals. A recommendation for future studies would be to carry out repeat experiments using MDM generated from the same animal (wherever possible) in order to improve the reliability results for each individual animal, prior to incorporating biological replicates. When substantial variation is observed in a data set, it is advised to increase the sample size to achieve statistical significance; however, an increased sample size was not possible for this project due to time and financial constraints. A priority for future studies of paratuberculosis should be to identify host genetic markers associated with protection (i.e. reduced faecal shedding and lack of clinical disease). It would be of great interest to group animals by their genetic likelihood of developing clinical disease, and carry out comparative studies assessing differences in the host response to MAP between these groups, both *in vitro* and *in vivo*. Previous studies have determined that there is a genetic element to susceptibility to Johne's disease (Küpper et al. 2012; Zare et al. 2014). A better understanding of how the response of resistant animals differs from that of susceptible animals would be invaluable for understanding protection and, therefore, developing more efficacious vaccines and diagnostics. In addition, an improved understanding of the heritability of resistance could allow protection against Johne's disease to be conferred to future generations through breeding programmes.

To summarise, this study clearly demonstrated that bovine MDM respond differently to the reference strain of MAP (K10), compared to a recent isolate from an animal displaying clinical Johne's disease (C49), and demonstrated genetic differences between these two strains that likely account for the altered MDM response. The observed strain-effect on the macrophage response to MAP will be of significance for the design of future studies investigating host-pathogen interactions in the context of MAP infection. In addition, this study identified several MDM responses that are likely important for determining the outcome of infection, including IL-1β, IL-10 and RNS production. The mechanism of phagocytosis affected the ability of MAP to survive intracellularly, which could have a significant impact on the development of the downstream immune response to MAP, and warrants further investigation. These

findings will likely be of benefit for the design of novel efficacious vaccines against paratuberculosis and Johne's disease.

6.1 Conclusion

This body of work has contributed to the field of Johne's disease research, and the key findings reported in this thesis are summarised below:

A. It has been demonstrated that the reference strain of MAP, K10, and the recent clinical isolate, C49, differ in their ability to survive intracellularly within bovine MDM, and that the two strains induce differential MDM immune responses during the first 24 hours of infection. For example, K10 infected MDM demonstrated increased IL-1β, IL-10 and nitrite secretion, compared to C49 infected MDM. This finding suggests that virulence may differ between K10 and recent clinical isolates and will have implications regarding the interpretation of previous literature and the design of future studies examining host-pathogen interactions in the context of MAP infection.

B. The project has contributed to knowledge of the early immune response of MDM to MAP infection (in addition to highlighting how this response differs between the two strains utilised throughout). The early response of macrophages to MAP infection is likely critical in determining downstream immune events and, therefore, infection outcome. Increased understanding of the early immune response is critical for identifying correlates of protection that could be utilised in the screening of novel vaccine strains, and correlates of infection that could be exploited by novel diagnostic tests.
C. The mechanism by which macrophages take up MAP may significantly influence intracellular survival of the bacteria. This finding requires further investigation to fully elucidate the mechanisms by which this occurs, and if the result would have a meaningful effect on the

development of infection and progression to disease *in vivo*. It was demonstrated that incubation of MAP in 10% IS resulted in reduced intracellular survival of MAP; suggesting antibody may have a protective role at early time-points of infection, and that passive immunisation could be investigated as an alternative disease control strategy.

7 References

Abdul-Aziz, M. et al., 2016. Complement factor H interferes with Mycobacterium bovis BCG entry into macrophages and modulates the pro-inflammatory cytokine response. *Immunobiology*, 221(9), pp.944–952.

Abendaño, N., Sevilla, I. a, et al., 2013. Mycobacterium avium subspecies paratuberculosis isolates from sheep and goats show reduced persistence in bovine macrophages than cattle, bison, deer and wild boar strains regardless of genotype. *Veterinary microbiology*, 163(3-4), pp.325–34.

Abendaño, N., Juste, R. a & Alonso-Hearn, M., 2013. Anti-inflammatory and antiapoptotic responses to infection: a common denominator of human and bovine macrophages infected with Mycobacterium avium subsp. paratuberculosis. *BioMed research international*, 2013, p.908348.

Adams, J.L., Collins, M.T. & Czuprynski, C.J., 1996. Polymerase chain reaction analysis of TNF-alpha and IL-6 mRNA levels in whole blood from cattle naturally or experimentally infected with Mycobacterium paratuberculosis. *Canadian journal of veterinary research = Revue canadienne de recherche veterinaire*, 60(4), pp.257–62.

Adams, J.L. & Czuprynski, C.J., 1995. Ex vivo induction of TNF-apha and IL-6 mRNA in bovine whole blood by Mycobacterium paratuberculosis and mycobacterial cell wall components. *Microbial Pathogenesis*, 19(1), pp.19–29.

Aderem, A. & Underhill, D.M., 1999. Mechanisms of Phagocytosis in Macrophages. *Annu. Rev. Immunol*, 17, pp.593–623.

Aderem, A.A. et al., 1985. Ligated complement receptors do not activate the arachidonic acid cascade in resident peritoneal macrophages. *The Journal of experimental medicine*, 161(3), pp.617–22.

Agdestein, A. et al., 2014. Intracellular growth of Mycobacterium avium subspecies and global transcriptional responses in human macrophages after infection. *BMC genomics*, 15(58).

Aktas Cetin, E. et al., 2017. CD163 levels, pro- and anti-inflammatory cytokine

secretion of monocytes in children with pulmonary tuberculosis. *Pediatric Pulmonology*, 52(5), pp.675–683.

Alford, C.E., King, T.E. & Campbell, P.A., 1991. Role of transferrin, transferrin receptors, and iron in macrophage listericidal activity. *Journal of Experimental Medicine*, 174(2).

Alonso-Hearn, M. et al., 2010. A Mycobacterium avium subsp. paratuberculosis LuxR regulates cell envelope and virulence. *Innate immunity*, 16(4), pp.235–47.

Alonso-Hearn, M. et al., 2017. Mycobacterium avium subsp. paratuberculosis (Map) Fatty Acids Profile Is Strain-Dependent and Changes Upon Host Macrophages Infection. *Frontiers in cellular and infection microbiology*, 7, p.89.

Aly, S.S. et al., 2012. Cost-effectiveness of diagnostic strategies to identify Mycobacterium avium subspecies paratuberculosis super-shedder cows in a large dairy herd using antibody enzyme-linked immunosorbent assays, quantitative real-time polymerase chain reaction, and bacte. *Journal of veterinary diagnostic investigation : official publication of the American Association of Veterinary Laboratory Diagnosticians, Inc*, 24(5), pp.821–32.

Alzuherri, H.M., Woodall, C.J. & Clarke, C.J., 1996. Increased intestinal TNF-alpha, IL-1 beta and IL-6 expression in ovine paratuberculosis. *Veterinary immunology and immunopathology*, 49(4), pp.331–45.

Appelberg, R. et al., 1994. Role of interleukin-6 in the induction of protective T cells during mycobacterial infections in mice. *Immunology*, 82(3), pp.361–4.

Arsenault, R.J. et al., 2014. From mouth to macrophage: mechanisms of innate immune subversion by Mycobacterium avium subsp. paratuberculosis. *Veterinary research*, 45(1), p.54.

Arsenault, R.J. et al., 2012. Mycobacterium avium subsp. paratuberculosis inhibits gamma interferon-induced signaling in bovine monocytes: insights into the cellular mechanisms of Johne's disease. *Infection and immunity*, 80(9), pp.3039–48.

Astarie-Dequeker, C. et al., 1999. The mannose receptor mediates uptake of pathogenic and nonpathogenic mycobacteria and bypasses bactericidal responses in human macrophages. *Infection and immunity*, 67(2), pp.469–77.

Atreya, R. et al., 2000. Blockade of interleukin 6 trans signaling suppresses T-cell resistance against apoptosis in chronic intestinal inflammation: evidence in crohn disease and experimental colitis in vivo. *Nature Medicine*, 6(5), pp.583–588.

Attalla, S.A. et al., 2010. Genetic parameters of milk ELISA scores for Johne's disease. *Journal of Dairy Science*, 93(4), pp.1729–1735.

Autschbach, F. et al., 2005. High prevalence of Mycobacterium avium subspecies paratuberculosis IS900 DNA in gut tissues from individuals with Crohn's disease. *Gut*, 54(7), pp.944–949.

Bain, C.C. et al., 2014. Constant replenishment from circulating monocytes maintains the macrophage pool in the intestine of adult mice. *Nature immunology*, 15(10), pp.929–37.

Bain, C.C. et al., 2013. Resident and pro-inflammatory macrophages in the colon represent alternative context-dependent fates of the same Ly6Chi monocyte precursors. *Mucosal Immunology*, 6(3), pp.498–510.

Bajic, G. et al., 2013. Structural insight on the recognition of surface-bound opsonins by the integrin I domain of complement receptor 3. *Proceedings of the National Academy of Sciences of the United States of America*, 110(41), pp.16426–31.

Baldwin, E., 1976. Isoniazid therapy in two cases of Johne's disease: VM/SAC. *Agri Pract*, 71, pp.1359–1362.

Bannantine, J.P. et al., 2014. A rational framework for evaluating the next generation of vaccines against Mycobacterium avium subspecies paratuberculosis. *Frontiers in cellular and infection microbiology*, 4(September), p.126.

Bannantine, J.P. et al., 2015. Mycobacterium avium Subspecies paratuberculosis

Recombinant Proteins Modulate Antimycobacterial Functions of Bovine Macrophages. *PloS one*, 10(6), p.e0128966.

Bannantine, J.P. & Bermudez, L.E., 2013. No holes barred: invasion of the intestinal mucosa by Mycobacterium avium subsp. paratuberculosis. *Infection and immunity*, 81(11), pp.3960–5.

Bartlomiejczyk, M.A. et al., 2014. Interaction of lectin pathway of complement-activating pattern recognition molecules with mycobacteria. *Clinical and experimental immunology*, 178(2), pp.310–9.

Bastida, F. & Juste, R.A., 2011. Paratuberculosis control: a review with a focus on vaccination. *Journal of immune based therapies and vaccines*, 9, p.8.

Bayr, H., 2005. Reactive oxygen species. *Critical Care Medicine*, 33(Suppl), pp.S498–S501.

Beamer, G.L. et al., 2008. Interleukin-10 promotes Mycobacterium tuberculosis disease progression in CBA/J mice. *Journal of immunology (Baltimore, Md. : 1950)*, 181(8), pp.5545–50.

Beard, P.M., Rhind, S.M., et al., 2001. Natural Paratuberculosis Infection in Rabbits in Scotland. *Journal of Comparative Pathology*, 124(4), pp.290–299.

Beard, P.M., Daniels, M.J., et al., 2001. Paratuberculosis Infection of Nonruminant Wildlife in Scotland. *Journal of Clinical Microbiology*, 39(4), pp.1517–1521.

Begg, D.J. et al., 2010. Does a Th1 over Th2 dominancy really exist in the early stages of Mycobacterium avium subspecies paratuberculosis infections? *Immunobiology*, 216, pp.840–846.

Benard, E.L. et al., 2012. Infection of zebrafish embryos with intracellular bacterial pathogens. *Journal of visualized experiments : JoVE*, (61).

Benard, E.L. et al., 2014. Phagocytosis of mycobacteria by zebrafish macrophages is dependent on the scavenger receptor Marco, a key control factor of pro-

inflammatory signalling. *Developmental and comparative immunology*, 47(2), pp.223–33.

Bermudez, L.E. et al., 2010. Peyer's patch-deficient mice demonstrate that Mycobacterium avium subsp. paratuberculosis translocates across the mucosal barrier via both M cells and enterocytes but has inefficient dissemination. *Infection and immunity*, 78(8), pp.3570–7.

Bermudez, L.E., Goodman, J. & Petrofsky, M., 1999. Role of complement receptors in uptake of Mycobacterium avium by macrophages in vivo: evidence from studies using CD18-deficient mice. *Infection and immunity*, 67(9), pp.4912–6.

Berthou, C. et al., 1995. Cord blood T lymphocytes lack constitutive perforin expression in contrast to adult peripheral blood T lymphocytes. *Blood*, 85(6).

Bettelli, E. et al., 2006. Reciprocal developmental pathways for the generation of pathogenic effector TH17 and regulatory T cells. *Nature*, 441(7090), pp.235–238.

Beumer, A. et al., 2010. Detection of Mycobacterium avium subsp. paratuberculosis in Drinking Water and Biofilms by Quantitative PCR. *Applied and Environmental Microbiology*, 76(21), pp.7367–7370.

Bogdan, C., 2001. Nitric oxide and the regulation of gene expression. *Trends in cell biology*, 11(2), pp.66–75.

Borrmann, E. et al., 2011a. Divergent cytokine responses of macrophages to Mycobacterium avium subsp. paratuberculosis strains of Types II and III in a standardized in vitro model. *Veterinary Microbiology*, 152(1-2), pp.101–111.

Borrmann, E. et al., 2011b. Divergent cytokine responses of macrophages to Mycobacterium avium subsp. paratuberculosis strains of Types II and III in a standardized in vitro model. *Veterinary Microbiology*, 152(1-2), pp.101–111.

Botsaris, G. et al., 2016. Detection of viable Mycobacterium avium subspecies paratuberculosis in powdered infant formula by phage-PCR and confirmed by

culture. *International Journal of Food Microbiology*, 216, pp.91–94.

Bowdish, D.M. et al., 2013. Genetic variants of MARCO are associated with susceptibility to pulmonary tuberculosis in a Gambian population. *BMC Medical Genetics*, 14(1), p.47.

Bowdish, D.M.E. et al., 2009. MARCO, TLR2, and CD14 are required for macrophage cytokine responses to mycobacterial trehalose dimycolate and Mycobacterium tuberculosis. *PLoS pathogens*, 5(6), p.e1000474.

Boysen, P. et al., 2006. Bovine CD2 - /NKp46 + cells are fully functional natural killer cells with a high activation status. *BMC Immunology*, 7(1), p.10.

Briken, V., Ahlbrand, S.E. & Shah, S., 2013. Mycobacterium tuberculosis and the host cell inflammasome: a complex relationship. *Frontiers in cellular and infection microbiology*, 3, p.62.

Brooks-Pollock, E. & Keeling, M., 2009. Herd size and bovine tuberculosis persistence in cattle farms in Great Britain. *Preventative Veterinary Medicine*, 92, pp.360–365.

Bryan, L.A. et al., 1988. Immunocytochemical identification of bovine Langerhans cells by use of a monoclonal antibody directed against class II MHC antigens. *Journal of Histochemistry & Cytochemistry*, 36(8), pp.991–995.

Bryan, N.S. & Grisham, M.B., 2007. Methods to detect nitric oxide and its metabolites in biological samples. *Free radical biology & medicine*, 43(5), pp.645–57.

Bryant, J.M. et al., 2016. Phylogenomic exploration of the relationships between strains of Mycobacterium avium subspecies paratuberculosis. *BMC genomics*, 17, p.79.

Buchwalow, I. et al., 2011. Non-specific binding of antibodies in immunohistochemistry: fallacies and facts. *Scientific reports*, 1, p.28.

Bull, T.J. et al., 2007. A Novel Multi-Antigen Virally Vectored Vaccine against Mycobacterium avium Subspecies paratuberculosis N. Ahmed, ed. *PLoS ONE*, 2(11), p.e1229.

Bull, T.J. et al., 2014. Immunity, safety and protection of an Adenovirus 5 prime--Modified Vaccinia virus Ankara boost subunit vaccine against Mycobacterium avium subspecies paratuberculosis infection in calves. *Veterinary research*, 45(1), p.112.

Bustamante, J. et al., 2011. Germline CYBB mutations that selectively affect macrophages in kindreds with X-linked predisposition to tuberculous mycobacterial disease. *Nature Immunology*, 12(3), pp.213–221.

Buvelot, H. et al., 2016. *Staphylococcus aureus* , phagocyte NADPH oxidase and chronic granulomatous disease A. Shen, ed. *FEMS Microbiology Reviews*, 41(2), p.fuw042.

Buza, J.J. et al., 2004. Neutralization of interleukin-10 significantly enhances gamma interferon expression in peripheral blood by stimulation with Johnin purified protein derivative and by infection with Mycobacterium avium subsp. paratuberculosis in experimentally infected cattle with paratuberculosis. *Infection and immunity*, 72(4), pp.2425–8.

Canton, J. et al., 2014. Contrasting phagosome pH regulation and maturation in human M1 and M2 macrophages. *Molecular biology of the cell*, 25(21), pp.3330–41.

Carroll, M. V. et al., 2009. Multiple routes of complement activation by Mycobacterium bovis BCG. *Molecular Immunology*, 46(16), pp.3367–3378.

Cetinkaya, B., Erdogan, H.M. & Morgan, K.L., 1998. Prevalence, incidence and geographical distribution of Johne's disease in cattle in England and the Welsh borders. *The Veterinary record*, 143(10), pp.265–9.

CHeCS, 2016. Cattle Health Certification Standards (CHeCS)Home - Cattle Health Certification Standards (CHeCS). Available at: http://www.checs.co.uk/

[Accessed September 18, 2017].

Chieppa, M. et al., 2003. Cross-Linking of the Mannose Receptor on Monocyte-Derived Dendritic Cells Activates an Anti-Inflammatory Immunosuppressive Program. *The Journal of Immunology*, 171(9).

Chorro, L. et al., 2009. Langerhans cell (LC) proliferation mediates neonatal development, homeostasis, and inflammation-associated expansion of the epidermal LC network. *The Journal of experimental medicine*, 206(13), pp.3089–100.

Cifani, N. et al., 2013. Reactive-Oxygen-Species-Mediated P. aeruginosa Killing Is Functional in Human Cystic Fibrosis Macrophages E. Gulbins, ed. *PLoS ONE*, 8(8), p.e71717.

Clark, D.L. et al., 2008. Detection of Mycobacterium avium subspecies paratuberculosis: comparing fecal culture versus serum enzyme-linked immunosorbent assay and direct fecal polymerase chain reaction. *Journal of dairy science*, 91(7), pp.2620–7.

Clay, H., Volkman, H.E. & Ramakrishnan, L., 2008. Tumor Necrosis Factor Signaling Mediates Resistance to Mycobacteria by Inhibiting Bacterial Growth and Macrophage Death. *Immunity*, 29(2), pp.283–294.

Collins, M.T., Eggleston, V. & Manning, E.J.B., 2010. Successful control of Johne's disease in nine dairy herds: Results of a six-year field trial. *Journal of Dairy Science*, 93(4), pp.1638–1643.

Cooper, A.M., Mayer-Barber, K.D. & Sher, A., 2011. Role of innate cytokines in mycobacterial infection. *Mucosal Immunology*, 4(3), pp.252–260.

Cooper, G., 2000. *The Cell: A Molecular Approach* 2nd ed. M. Sunderland, ed., Sinauer Associates.

Corripio-Miyar, Y. et al., 2015. Phenotypic and functional analysis of monocyte populations in cattle peripheral blood identifies a subset with high endocytic and

allogeneic T-cell stimulatory capacity. *Veterinary research*, 46, p.112.

Cummings, R.D. & McEver, R.P., 2009. *C-type Lectins*, Cold Spring Harbor Laboratory Press.

Danelishvili, L. et al., 2017. The Voltage-Dependent Anion Channels (VDAC) of Mycobacterium avium phagosome are associated with bacterial survival and lipid export in macrophages. *Scientific reports*, 7(1), p.7007.

Davies, L.C. et al., 2013. Tissue-resident macrophages. *Nature Immunology*, 14(10), pp.986–995.

Davis, A.S. et al., 2007. Mechanism of Inducible Nitric Oxide Synthase Exclusion from Mycobacterial Phagosomes. *PLoS Pathogens*, 3(12), p.e186.

Deffert, C. et al., 2014. Bacillus Calmette-Guerin Infection in NADPH Oxidase Deficiency: Defective Mycobacterial Sequestration and Granuloma Formation M. A. Behr, ed. *PLoS Pathogens*, 10(9), p.e1004325.

Dejam, A. et al., 2007. Nitrite Infusion in Humans and Nonhuman Primates. *Circulation*, 116(16).

Delgado, F. et al., 2010. Expression of NRAMP1 and iNOS in Mycobacterium avium subsp. paratuberculosis naturally infected cattle. *Comparative Immunology, Microbiology and Infectious Diseases*, 33(5), pp.389–400.

Dernivoix, K. et al., 2017. Field performance of six Mycobacterium avium subsp. paratuberculosis antigens in a 20 h interferon gamma release assay in Belgium. *Veterinary Immunology and Immunopathology*, 189, pp.17–27.

Desvignes, L., Wolf, A.J. & Ernst, J.D., 2012. Dynamic roles of type I and type II IFNs in early infection with Mycobacterium tuberculosis. *Journal of immunology (Baltimore, Md. : 1950)*, 188(12), pp.6205–15.

Dinarello, C.A., 2009. Immunological and Inflammatory Functions of the Interleukin-1 Family. *Annual Review of Immunology*, 27(1), pp.519–550.

Domingo-Gonzalez, R. et al., 2016. Cytokines and Chemokines in Mycobacterium tuberculosis Infection. *Microbiology spectrum*, 4(5).

Donius, L.R. & Weis, J.H., 2014. Detection of Complement Receptors 1 and 2 on Mouse Splenic B Cells Using Flow Cytometry. In *Methods in molecular biology (Clifton, N.J.)*. pp. 305–310.

Dorman, S.E. & Holland, S.M., 1998. Mutation in the signal-transducing chain of the interferon-gamma receptor and susceptibility to mycobacterial infection. *The Journal of clinical investigation*, 101(11), pp.2364–9.

Doyle, S.E. et al., 2004. Toll-like receptors induce a phagocytic gene program through p38. *The Journal of experimental medicine*, 199(1), pp.81–90.

Dudemaine, P.L. et al., 2014. Increased blood-circulating interferon-γ, interleukin-17, and osteopontin levels in bovine paratuberculosis. *Journal of dairy science*, pp.1–12.

Eisenberg, S.W., Rutten, V.P. & Koets, A.P., 2015. Dam Mycobacterium avium subspecies paratuberculosis (MAP) infection status does not predetermine calves for future shedding when raised in a contaminated environment: a cohort study. *Veterinary Research*, 46(1), p.70.

Elguezabal, N. et al., 2011. Estimation of Mycobacterium avium subsp. paratuberculosis Growth Parameters: Strain Characterization and Comparison of Methods. *Applied and environmental microbiology*, 77(24), pp.8615–8624.

Ellingson, J. et al., 2005. Detection of Viable Mycobacterium avium subsp. paratuberculosis in Retail Pasteurized Whole Milk by Two Culture Methods and PCR. *Journal of Food Protection*, 5, pp.900–1111.

Esquivel-Solís, H. et al., 2013. Nitric oxide not apoptosis mediates differential killing of Mycobacterium bovis in bovine macrophages. *PloS one*, 8(5), p.e63464.

Everman, J.L. et al., 2015. Characterization of the inflammatory phenotype of mycobacterium avium subspecies paratuberculosis using a novel cell culture

passage model. *Microbiology (United Kingdom)*, 161(7), pp.1420–1434.

Everman, J.L. & Bermudez, L.E., 2015. Antibodies against invasive phenotype-specific antigens increase Mycobacterium avium subspecies paratuberculosis translocation across a polarized epithelial cell model and enhance killing by bovine macrophages. *Frontiers in cellular and infection microbiology*, 5(August), p.58.

Fabriek, B.O. et al., 2009. The macrophage scavenger receptor CD163 functions as an innate immune sensor for bacteria. *Blood*, 113(4).

Fadista, J. et al., 2010. Copy number variation in the bovine genome. *BMC genomics*, 11, p.284.

Fawzy, A. et al., 2015. Improvement of sensitivity for Mycobacterium avium subsp. paratuberculosis (MAP) detection in bovine fecal samples by specific duplex F57/IC real-time and conventional IS900 PCRs after solid culture enrichment. *Tropical Animal Health and Production*, 47(4), pp.721–726.

Fecteau, M.-E. & Whitlock, R.H., 2011. Treatment and Chemoprophylaxis for Paratuberculosis. *Veterinary Clinics of North America: Food Animal Practice*, 27(3), pp.547–557.

Feller, M. et al., 2010. Long-Term Antibiotic Treatment for Crohn's Disease: Systematic Review and Meta-Analysis of Placebo-Controlled Trials. *Clinical Infectious Diseases*, 50(4), pp.473–480.

Fernández, M. et al., 2014. Experimental infection of lambs with C and S-type strains of Mycobacterium avium subspecies paratuberculosis: immunological and pathological findings. *Veterinary research*, 45(1), p.5.

Fernández, M. et al., 2017. Macrophage Subsets Within Granulomatous Intestinal Lesions in Bovine Paratuberculosis. *Veterinary Pathology*, 54(1), pp.82–93.

Finkbeiner, S.R. et al., 2012. Stem cell-derived human intestinal organoids as an infection model for rotaviruses. *mBio*, 3(4), pp.e00159–12.

Foddai, A.C.G. & Grant, I.R., 2017. Sensitive and specific detection of viable Mycobacterium avium subsp. paratuberculosis in raw milk by the peptide-mediated magnetic separation-phage assay. *Journal of Applied Microbiology*, 122(5), pp.1357–1367.

Francis, J. et al., 1953. Mycobactin, a growth factor for Mycobacterium johnei. I. Isolation from Mycobacterium phlei. *The Biochemical journal*, 55(4), pp.596–607.

Fratti, R.A. et al., 1997. in phagosomal biogenesis and mycobacterial phagosome maturation arrest. , pp.631–644.

Fremond, C.M. et al., 2007. IL-1 receptor-mediated signal is an essential component of MyD88-dependent innate response to Mycobacterium tuberculosis infection. *Journal of immunology (Baltimore, Md. : 1950)*, 179(2), pp.1178–89.

Fulton, S.A. et al., 2004. Inhibition of major histocompatibility complex II expression and antigen processing in murine alveolar macrophages by Mycobacterium bovis BCG and the 19-kilodalton mycobacterial lipoprotein. *Infection and immunity*, 72(4), pp.2101–10.

Ganusov, V. V. et al., 2015. Evaluating contribution of the cellular and humoral immune responses to the control of shedding of Mycobacterium avium spp. paratuberculosis in cattle. *Veterinary Research*, 46(1), p.62.

Garcia, A.B. & Shalloo, L., 2015. Invited review: The economic impact and control of paratuberculosis in cattle. *Journal of Dairy Science*, 98(8), pp.5019–5039.

García-García, E. & Rosales, C., 2002. Signal transduction during Fc receptor-mediated phagocytosis. *Journal of leukocyte biology*, 72(6), pp.1092–108.

Garrido, J.M. et al., 2013. Paratuberculosis vaccination causes only limited cross-reactivity in the skin test for diagnosis of bovine tuberculosis. *PloS one*, 8(11), p.e80985.

Geijtenbeek, T.B.H. et al., 2003. Mycobacteria target DC-SIGN to suppress dendritic

cell function. *The Journal of experimental medicine*, 197(1), pp.7–17.

GeneTex Inc., 2013. anti-Marco antibody [PLK-1] | GeneTex. Available at: http://www.genetex.com/MARCO-antibody-PLK-1-GTX54470.html [Accessed August 13, 2017].

Geraghty, T. et al., 2014. A review of bovine Johne's disease control activities in 6 endemically infected countries. *Preventive Veterinary Medicine*, 116, pp.1–11.

Ghadiali, A.H. et al., 2004. Mycobacterium avium subsp. paratuberculosis strains isolated from Crohn's disease patients and animal species exhibit similar polymorphic locus patterns. *Journal of clinical microbiology*, 42(11), pp.5345–8.

Ghosh, P. et al., 2012. Genome-wide analysis of the emerging infection with Mycobacterium avium subspecies paratuberculosis in the Arabian camels (Camelus dromedarius). *PloS one*, 7(2), p.e31947.

Ghosh, P., Steinberg, H. & Talaat, A.M., 2014. Virulence and immunity orchestrated by the global gene regulator sigL in mycobacterium avium subsp. paratuberculosis. *Infection and Immunity*, 82(7), pp.3066–3075.

Gomez, L.M. et al., 2006. Analysis of IL1B, TAP1, TAP2 and IKBL polymorphisms on susceptibility to tuberculosis. *Tissue Antigens*, 67(4), pp.290–296.

Gonda, M.G. et al., 2007. Effect of Mycobacterium paratuberculosis infection on production, reproduction, and health traits in US Holsteins. *Preventive Veterinary Medicine*, 80(2-3), pp.103–119.

Gonda, M.G. et al., 2006. Genetic Variation of Mycobacterium avium ssp. paratuberculosis Infection in US Holsteins. *Journal of Dairy Science*, 89, pp.1804–1812.

Gonza, A.M. et al., 2009. Evaluation of four commercial serum ELISAs for detection of Mycobacterium avium subsp . paratuberculosis infection in dairy cows. *The Veterinary Journal*, 180, pp.231–235.

Gopal, R. et al., 2014. Unexpected Role for IL-17 in Protective Immunity against Hypervirulent Mycobacterium tuberculosis HN878 Infection D. M. Lewinsohn, ed. *PLoS Pathogens*, 10(5), p.e1004099.

Goude, R. & Parish, T., 2009. Electroporation of Mycobacteria. In *Methods in molecular biology (Clifton, N.J.)*. pp. 203–215.

Graham, E.M. et al., 2009. Natural killer cell number and phenotype in bovine peripheral blood is influenced by age. *Veterinary Immunology and Immunopathology*, 132(2-4), pp.101–108.

Grant, I.R., Ball, H.J. & Rowe, M.T., 2002. Incidence of Mycobacterium paratuberculosis in bulk raw and commercially pasteurized cows' milk from approved dairy processing establishments in the United Kingdom. *Applied and environmental microbiology*, 68(5), pp.2428–35.

Gringhuis, S.I. et al., 2009. Carbohydrate-specific signaling through the DC-SIGN signalosome tailors immunity to Mycobacterium tuberculosis, HIV-1 and Helicobacter pylori. *Nature Immunology*, 10(10), pp.1081–1088.

Gringhuis, S.I. et al., 2007. C-Type Lectin DC-SIGN Modulates Toll-like Receptor Signaling via Raf-1 Kinase-Dependent Acetylation of Transcription Factor NF-κB. *Immunity*, 26(5), pp.605–616.

Groenendaal, H., Nielen, M. & Hesselin, J.W., 2003. Development of the Dutch Johne's disease control program supported by a simulation model. *Preventive Veterinary Medicine*, 60(1), pp.69–90.

Guilliams, M. et al., 2014. The function of Fcγ receptors in dendritic cells and macrophages. *Nature Reviews Immunology*, 14(2), pp.94–108.

Guo, Y. et al., 2016. EBP50 induces apoptosis in macrophages by upregulating nitric oxide production to eliminate intracellular Mycobacterium tuberculosis. *Scientific Reports*, 6(1), p.18961.

Han, C. et al., 2010. Integrin CD11b negatively regulates TLR-triggered

inflammatory responses by activating Syk and promoting degradation of MyD88 and TRIF via Cbl-b. *Nature Immunology*, 11(8), pp.734–742.

Harding, C. V & Boom, W.H., 2010. Regulation of antigen presentation by Mycobacterium tuberculosis: a role for Toll-like receptors. *Nature reviews. Microbiology*, 8(4), pp.296–307.

Higgins, D.M. et al., 2009. Lack of IL-10 alters inflammatory and immune responses during pulmonary Mycobacterium tuberculosis infection. *Tuberculosis*, 89(2), pp.149–157.

Hope, J.C. et al., 2012. Migratory sub-populations of afferent lymphatic dendritic cells differ in their interactions with Mycobacterium bovis Bacille Calmette Guerin. *Vaccine*, 30(13), pp.2357–2367.

Hope, J.C., Sopp, P. & Howard, C.J., 2002. NK-like CD8(+) cells in immunologically naïve neonatal calves that respond to dendritic cells infected with Mycobacterium bovis BCG. *Journal of leukocyte biology*, 71(2), pp.184–94.

Hostetter, J., Kagan, R. & Steadham, E., 2005. Opsonization effects on Mycobacterium avium subsp. paratuberculosis--macrophage interactions. *Clinical and diagnostic laboratory immunology*, 12(6), pp.793–6.

Hsu, C.-Y., Wu, C.-W. & Talaat, A.M., 2011. Genome-Wide Sequence Variation among Mycobacterium avium Subspecies paratuberculosis Isolates: A Better Understanding of Johne's Disease Transmission Dynamics. *Frontiers in microbiology*, 2, p.236.

Huang, J. & Brumell, J.H., 2009. NADPH oxidases contribute to autophagy regulation. *Autophagy*, 5(6), pp.887–9.

Hughes, M.N., 2008. Chemistry of Nitric Oxide and Related Species. In *Methods in enzymology*. pp. 3–19.

Hughes, V. et al., 2017. Gamma interferon responses to proteome-determined

specific recombinant proteins in cattle experimentally- and naturally-infected with paratuberculosis. *Research in Veterinary Science*, 114, pp.244–253.

Hussain, T. et al., 2016. The role of IL-10 in Mycobacterium avium subsp. paratuberculosis infection. *Cell communication and signaling : CCS*, 14(1), p.29.

Ishigame, H. et al., 2009. Differential roles of interleukin-17A and -17F in host defense against mucoepithelial bacterial infection and allergic responses. *Immunity*, 30(1), pp.108–19.

Ito, H. et al., 2004. A pilot randomized trial of a human anti-interleukin-6 receptor monoclonal antibody in active Crohn's disease. *Gastroenterology*, 126(4), pp.989–96; discussion 947.

Jacobs, A.J. et al., 2016. Antibodies and tuberculosis. *Tuberculosis (Edinburgh, Scotland)*, 101, pp.102–113.

Janagama, H.K. et al., 2006. Cytokine responses of bovine macrophages to diverse clinical Mycobacterium avium subspecies paratuberculosis strains. *BMC microbiology*, 6, p.10.

Jensen, K. et al., 2016. Live and inactivated Salmonella enterica serovar Typhimurium stimulate similar but distinct transcriptome profiles in bovine macrophages and dendritic cells. *Veterinary research*, 47, p.46.

Jensen, K., Anderson, J.A. & Glass, E.J., 2014. Comparison of small interfering RNA (siRNA) delivery into bovine monocyte-derived macrophages by transfection and electroporation. *Veterinary immunology and immunopathology*, 158(3-4), pp.224–32.

Joeris, T. et al., 2017. Diversity and functions of intestinal mononuclear phagocytes. *Mucosal Immunology*, 10(4), pp.845–864.

Jolly, A. et al., 2016. Evidence of a pro-apoptotic effect of specific antibodies in a bovine macrophage model of infection with Mycobacterium avium subsp.

paratuberculosis. *Veterinary Immunology and Immunopathology*, 169, pp.47–53.

Jonkman, J. & Brown, C.M., 2015. Any Way You Slice It-A Comparison of Confocal Microscopy Techniques. *Journal of biomolecular techniques : JBT*, 26(2), pp.54–65.

Juffermans, N. et al., 2000. Interleukin-1 Signaling Is Essential for Host Defense during Murine Pulmonary Tuberculosis. *The Journal of Infectious Diseases*, 182(3), pp.902–908.

Jung, J.-Y. et al., 2013. The intracellular environment of human macrophages that produce nitric oxide promotes growth of mycobacteria. *Infection and immunity*, 81(9), pp.3198–209.

Jungersen, G. et al., 2002. Interpretation of the gamma interferon test for diagnosis of subclinical paratuberculosis in cattle. *Clinical and diagnostic laboratory immunology*, 9(2), pp.453–60.

Jungi, T.W. et al., 1996. Inducible nitric oxide synthase of macrophages. Present knowledge and evidence for species-specific regulation. *Veterinary immunology and immunopathology*, 54(1-4), pp.323–30.

Kabara, E. & Coussens, P.M., 2012. Infection of Primary Bovine Macrophages with Mycobacterium avium Subspecies paratuberculosis Suppresses Host Cell Apoptosis. *Frontiers in microbiology*, 3, p.215.

Kacskovics, I., 2004. Fc receptors in livestock species. *Veterinary Immunology and Immunopathology*, 102(4), pp.351–362.

Kang, P.B. et al., 2005. The human macrophage mannose receptor directs Mycobacterium tuberculosis lipoarabinomannan-mediated phagosome biogenesis. *The Journal of experimental medicine*, 202(7), pp.987–99.

Karlsen, T.A. & Brinchmann, J.E., 2013. Liposome delivery of microRNA-145 to mesenchymal stem cells leads to immunological off-target effects mediated by

RIG-I. *Molecular therapy : the journal of the American Society of Gene Therapy*, 21(6), pp.1169–81.

Karuppusamy, S. et al., 2018. Identification of antigenic proteins from Mycobacterium avium subspecies paratuberculosis cell envelope by comparative proteomic analysis. *Microbiology*, 164(3), pp.322–337.

Kawaji, S. et al., 2007. Detection of Mycobacterium avium subsp. paratuberculosis in ovine faeces by direct quantitative PCR has similar or greater sensitivity compared to radiometric culture. *Veterinary microbiology*, 125(1-2), pp.36–48.

Keller, C. et al., 2006. Genetically determined susceptibility to tuberculosis in mice causally involves accelerated and enhanced recruitment of granulocytes. *Infection and immunity*, 74(7), pp.4295–309.

Kelley, V.A. & Schorey, J.S., 2003. Mycobacterium's arrest of phagosome maturation in macrophages requires Rab5 activity and accessibility to iron. *Molecular biology of the cell*, 14(8), pp.3366–77.

Khader, S.A. et al., 2007. IL-23 and IL-17 in the establishment of protective pulmonary CD4+ T cell responses after vaccination and during Mycobacterium tuberculosis challenge. *Nature Immunology*, 8(4), pp.369–377.

Khalifeh, M.S. & Stabel, J.R., 2004. Effects of gamma interferon, interleukin-10, and transforming growth factor beta on the survival of Mycobacterium avium subsp. paratuberculosis in monocyte-derived macrophages from naturally infected cattle. *Infection and immunity*, 72(4), pp.1974–82.

Khare, S. et al., 2009. Early Phase Morphological Lesions and Transcriptional Responses of Bovine Ileum Infected with *Mycobacterium avium* subsp. *paratuberculosis*. *Veterinary Pathology*, 46(4), pp.717–728.

Khare, S. et al., 2004. Rapid and sensitive detection of Mycobacterium avium subsp. paratuberculosis in bovine milk and feces by a combination of immunomagnetic bead separation-conventional PCR and real-time PCR. *Journal of clinical microbiology*, 42(3), pp.1075–81.

Khare, S. et al., 2012. Systems biology analysis of gene expression during in vivo Mycobacterium avium paratuberculosis enteric colonization reveals role for immune tolerance. *PloS one*, 7(8), p.e42127.

Kirkpatrick, B.W. & Shook, G.E., 2011. Genetic Susceptibility to Paratuberculosis. *Veterinary Clinics of North America: Food Animal Practice*, 27(3), pp.559–571.

Kitani, H. et al., 2011. Isolation and characterization of macrophages from a mixed primary culture of bovine liver cells. *Veterinary Immunology and Immunopathology*, 140(3-4), pp.341–345.

Klein, I. et al., 2007. Kupffer cell heterogeneity: functional properties of bone marrow derived and sessile hepatic macrophages. *Blood*, 110(12), pp.4077–85.

Koets, a et al., 2010. Susceptibility to paratuberculosis infection in cattle is associated with single nucleotide polymorphisms in Toll-like receptor 2 which modulate immune responses against Mycobacterium avium subspecies paratuberculosis. *Preventive veterinary medicine*, 93(4), pp.305–15.

Kralik, P. et al., 2011. Development of a predictive model for detection of Mycobacterium avium subsp. paratuberculosis in faeces by quantitative real time PCR. *Veterinary Microbiology*, 149(1), pp.133–138.

Kralik, P. et al., 2014. Evidence of passive faecal shedding of Mycobacterium avium subsp. paratuberculosis in a Limousin cattle herd. *The Veterinary Journal*, 201(1), pp.91–94.

Kralik, P., Beran, V. & Pavlik, I., 2012. Enumeration of Mycobacterium avium subsp. paratuberculosis by quantitative real-time PCR, culture on solid media and optical densitometry. *BMC research notes*, 5, p.114.

Kruze, J. et al., 2013. Herd-level prevalence of Map infection in dairy herds of southern Chile determined by culture of environmental fecal samples and bulk-tank milk qPCR. *Preventive Veterinary Medicine*, 111(3), pp.319–324.

Krych-Goldberg, M. & Atkinson, J.P., 2001. Structure-function relationships of

complement receptor type 1. *Immunological Reviews*, 180(1), pp.112–122.

Kudahl, A.B. et al., 2007. A stochastic model simulating paratuberculosis in a dairy herd. *Preventive Veterinary Medicine*, 78(2), pp.97–117.

Kudo, K. et al., 2004. Pulmonary collectins enhance phagocytosis of Mycobacterium avium through increased activity of mannose receptor. *Journal of immunology (Baltimore, Md. : 1950)*, 172(12), pp.7592–602.

Kuehnel, M.P. et al., 2001. Characterization of the intracellular survival of Mycobacterium avium ssp. paratuberculosis: Phagosomal pH and fusogenicity in J774 macrophages compared with other mycobacteria. *Cellular Microbiology*, 3(8), pp.551–566.

Kugadas, A. et al., 2016. A Mycobacterium avium subsp. paratuberculosis Predicted Serine Protease Is Associated with Acid Stress and Intraphagosomal Survival. *Frontiers in cellular and infection microbiology*, 6, p.85.

Kumar, P. et al., 2014. Mycobacterium indicus pranii and Mycobacterium bovis BCG lead to differential macrophage activation in Toll-like receptor-dependent manner. *Immunology*, 143(2), pp.258–68.

Kumar, S.K., Singh, P. & Sinha, S., 2015. Naturally produced opsonizing antibodies restrict the survival of Mycobacterium tuberculosis in human macrophages by augmenting phagosome maturation. *Open biology*, 5(12), p.150171.

Küpper, J. et al., 2012. Heritability estimates for Mycobacterium avium subspecies paratuberculosis status of German Holstein cows tested by fecal culture. *Journal of Dairy Science*, 95(5), pp.2734–2739.

van der Laan, L.J.. et al., 1997. Macrophage scavenger receptor MARCO: In vitro and in vivo regulation and involvement in the anti-bacterial host defense. *Immunology Letters*, 57(1-3), pp.203–208.

Lachmann, P.J., 2010. Preparing serum for functional complement assays. *Journal of Immunological Methods*, 352(1-2), pp.195–197.

Lambris, J.D., Ricklin, D. & Geisbrecht, B. V, 2008. Complement evasion by human pathogens. *Nature reviews. Microbiology*, 6(2), pp.132–42.

Lamont, E. a, Xu, W.W. & Sreevatsan, S., 2013. Host-Mycobacterium avium subsp. paratuberculosis interactome reveals a novel iron assimilation mechanism linked to nitric oxide stress during early infection. *BMC genomics*, 14(1), p.694.

Lamont, E.A. et al., 2012. Identification and Characterization of a Spore-Like Morphotype in Chronically Starved Mycobacterium avium Subsp. Paratuberculosis Cultures L. A. Sechi, ed. *PLoS ONE*, 7(1), p.e30648.

Lamont, E.A. et al., 2012. Infection with Mycobacterium avium subsp. paratuberculosis results in rapid interleukin-1β release and macrophage transepithelial migration. *Infection and immunity*, 80(9), pp.3225–35.

Lamont, E.A. et al., 2014. Screening of Mycobacterium avium subsp. paratuberculosis mutants for attenuation in a bovine monocyte-derived macrophage model. *Frontiers in cellular and infection microbiology*, 4, p.87.

Leal, I.S. et al., 1999. Interleukin-6 and interleukin-12 participate in induction of a type 1 protective T-cell response during vaccination with a tuberculosis subunit vaccine. *Infection and immunity*, 67(11), pp.5747–54.

Lee, S.J. et al., 2014. The Mycobacterium avium subsp. Paratuberculosis protein MAP1305 modulates dendritic cell-mediated T cell proliferation through Toll-like receptor-4. *BMB reports*, 47(2), pp.115–20.

Lei, L. & Hostetter, J.M., 2007. Limited phenotypic and functional maturation of bovine monocyte-derived dendritic cells following Mycobacterium avium subspecies paratuberculosis infection in vitro. *Veterinary Immunology and Immunopathology*, 120(3-4), pp.177–186.

Leistikow, R.L. et al., 2010. The Mycobacterium tuberculosis DosR regulon assists in metabolic homeostasis and enables rapid recovery from nonrespiring dormancy. *Journal of bacteriology*, 192(6), pp.1662–70.

Lesniak, A. et al., 2010. Serum heat inactivation affects protein corona composition and nanoparticle uptake. *Biomaterials*, 31(36), pp.9511–9518.

Li, H. et al., 2010. [Clinical analysis of 18 children with disseminated Bacille Calmette-Guérin infection]. *Zhonghua er ke za zhi = Chinese journal of pediatrics*, 48(1), pp.65–8.

Li, L. et al., 2005. The complete genome sequence of Mycobacterium avium subspecies paratuberculosis. *Proceedings of the National Academy of Sciences of the United States of America*, 102(35), pp.12344–9.

Li, X.L. et al., 1998. Induction of interferon synthesis and activation of interferon-stimulated genes by liposomal transfection reagents. *Journal of interferon & cytokine research : the official journal of the International Society for Interferon and Cytokine Research*, 18(11), pp.947–52.

Lima-Junior, D.S. et al., 2013. Inflammasome-derived IL-1β production induces nitric oxide–mediated resistance to Leishmania. *Nature Medicine*, 19(7), pp.909–915.

Lin, P.L. et al., 2006. Early events in Mycobacterium tuberculosis infection in cynomolgus macaques. *Infection and immunity*, 74(7), pp.3790–803.

Linscott, W.D. & Triglia, R.P., 1981. The bovine complement system. *Advances in experimental medicine and biology*, 137, pp.413–30.

Lombard, J.E., 2011. Epidemiology and Economics of Paratuberculosis. *Veterinary Clinics of North America: Food Animal Practice*, 27(3), pp.525–535.

Lukacs, G.L., Rotstein, O.D. & Grinstein, S., 1990. Phagosomal Acidification Is Mediated by a Vacuolar-type H+-ATPase in Murine Macrophages. *The Journal of biological chemistry*, 265(34), pp.21099–21107.

Mabbott, N.A. et al., 2013. Microfold (M) cells: important immunosurveillance posts in the intestinal epithelium. *Mucosal immunology*, 6(4), pp.666–77.

MacHugh, D.E. et al., 2012. Pan-genomic analysis of bovine monocyte-derived macrophage gene expression in response to in vitro infection with Mycobacterium avium subspecies paratuberculosis. *Veterinary research*, 43, p.25.

Mackintosh, C.G. et al., 2016. SOLiD SAGE sequencing shows differential gene expression in jejunal lymph node samples of resistant and susceptible red deer (Cervus elaphus) challenged with Mycobacterium avium subsp. paratuberculosis. *Veterinary Immunology and Immunopathology*, 169, pp.102–110.

MacMicking, J.D. et al., 1997. Identification of nitric oxide synthase as a protective locus against tuberculosis. *Proceedings of the National Academy of Sciences of the United States of America*, 94(10), pp.5243–8.

Magombedze, G., Eda, S. & Stabel, J., 2015. Predicting the Role of IL-10 in the Regulation of the Adaptive Immune Responses in Mycobacterium avium Subsp. paratuberculosis Infections Using Mathematical Models S. E. Hasnain, ed. *PLOS ONE*, 10(11), p.e0141539.

Mangan, P.R. et al., 2006. Transforming growth factor-β induces development of the TH17 lineage. *Nature*, 441(7090), pp.231–234.

Martinez, A.N., Mehra, S. & Kaushal, D., 2013. Role of interleukin 6 in innate immunity to Mycobacterium tuberculosis infection. *The Journal of infectious diseases*, 207(8), pp.1253–61.

Master, S.S. et al., 2008. Mycobacterium tuberculosis Prevents Inflammasome Activation. *Cell Host & Microbe*, 3(4), pp.224–232.

Master, S.S. et al., 2008. Mycobacterium tuberculosis prevents inflammasome activation. *Cell host & microbe*, 3(4), pp.224–32.

Mayer-Barber, K.D. et al., 2010. Caspase-1 independent IL-1beta production is critical for host resistance to mycobacterium tuberculosis and does not require TLR signaling in vivo. *Journal of immunology (Baltimore, Md. : 1950)*, 184(7),

pp.3326–30.

McAloon, C.G. et al., 2016. The effect of paratuberculosis on milk yieldÃ¢â‚¬?A systematic review and meta-analysis. *Journal of Dairy Science*, 99, pp.1449–1460.

McNab, F. et al., 2015. Type I interferons in infectious disease. *Nature Reviews Immunology*, 15(2), pp.87–103.

Merkal, R.S. & Larsen, A.B., 1973. Clofazimine treatment of cows naturally infected with Mycobacterium paratuberculosis. *American journal of veterinary research*, 34(1), pp.27–8.

Merkal, R.S. & Mccullough, W.G., 1982. A New Mycobactin, Mycobactin J, from Mycobacterium paratuberculosis. *Current Microbiology*, 7, pp.333–335.

Mishra, B.B. et al., 2010. Mycobacterium tuberculosis protein ESAT-6 is a potent activator of the NLRP3/ASC inflammasome. *Cellular Microbiology*, 12(8), pp.1046–1063.

Mishra, B.B. et al., 2012. Nitric oxide controls the immunopathology of tuberculosis by inhibiting NLRP3 inflammasome–dependent processing of IL-1β. *Nature Immunology*, 14(1), pp.52–60.

Mitachi, K. et al., 2016. Structure determination of lipopeptides from Mycobacterium avium subspecies paratuberculosis and identification of antigenic lipopeptide probes. *Analytical biochemistry*, 505, pp.29–35.

Möbius, P. et al., 2017. Evaluation of associations between genotypes of Mycobacterium avium subsp. paratuberculsis and presence of intestinal lesions characteristic of paratuberculosis. *Veterinary Microbiology*, 201, pp.188–194.

Momotani, E. et al., 1988. Role of M Cells and Macrophages in the Entrance of Mycobacterium paratuberculosis into Domes of Ileal Peyer's Patches in Calves. *Veterinary Pathology*, 25(2), pp.131–137.

Mondal, D., Sinha, R.P. & Gupta, M.K., 1994. Effect of combination therapy in Mycobacterium paratuberculosis infected rabbits. *Indian journal of experimental biology*, 32(5), pp.318–23.

Monteiro, J.T. et al., 2016. Helicobacter pullorum induces nitric oxide release in murine macrophages that promotes phagocytosis and killing. *Microbiology*, 162(3), pp.503–512.

Mortier, R.A. et al., 2013. Evaluation of age-dependent susceptibility in calves infected with two doses of Mycobacterium avium subspecies paratuberculosis using pathology and tissue culture. *Veterinary Research*, 44(1), p.94.

Mortier, R.A.R., Barkema, H.W. & De Buck, J., 2015. Susceptibility to and diagnosis of Mycobacterium avium subspecies paratuberculosis infection in dairy calves: A review. *Preventive Veterinary Medicine*, 121(3-4), pp.189–198.

Motiwala, A.S. et al., 2004. Molecular epidemiology of Mycobacterium avium subsp. paratuberculosis isolates recovered from wild animal species. *Journal of clinical microbiology*, 42(4), pp.1703–12.

Mucha, R. et al., 2009. Toll-like receptors TLR1, TLR2 and TLR4 gene mutations and natural resistance to Mycobacterium avium subsp. paratuberculosis infection in cattle. *Veterinary immunology and immunopathology*, 128(4), pp.381–8.

Muñoz, M. et al., 2009. Expression of transforming growth factor-beta 1 (TGF-β1) in different types of granulomatous lesions in bovine and ovine paratuberculosis. *Comparative Immunology, Microbiology and Infectious Diseases*, 32(3), pp.239–252.

Murphey, K. & Weaver, C., 2016. *Janeway's Immunobiology* 9th ed., Garland Science.

Murray, R.A. et al., 2007. Mycobacterium leprae inhibits dendritic cell activation and maturation. *Journal of immunology (Baltimore, Md. : 1950)*, 178(1), pp.338–44.

Nakatani, S.M. et al., 2004. Efficient method for mycobacterial DNA extraction in blood cultures aids rapid PCR identification of Mycobacterium tuberculosis and Mycobacterium avium. *European Journal of Clinical Microbiology & Infectious Diseases*, 23(11), pp.851–854.

Nathan, C., 1992. Nitric oxide as a secretory product of mammalian cells. *FACEB*, 6(12), pp.3051–3064.

Nathan, C. & Shiloh, M.U., 2000. Reactive oxygen and nitrogen intermediates in the relationship between mammalian hosts and microbial pathogens. *PNAS*, 97(16), pp.8841–8848.

National Center for Biotechnology Information, 2017. NCBI Genome database. Available at: https://www.ncbi.nlm.nih.gov/genome/browse/?report=2 [Accessed August 23, 2017].

Nielsen, S.S. et al., 2013. Dynamics of Specific Anti-Mycobacterium avium Subsp. paratuberculosis Antibody Response through Age L. A. Sechi, ed. *PLoS ONE*, 8(4), p.e63009.

Nielsen, S.S., Bjerre, H. & Toft, N., 2008. Colostrum and Milk as Risk Factors for Infection with Mycobacterium avium subspecies paratuberculosis in Dairy Cattle. *Journal of Dairy Science*, 91(12), pp.4610–4615.

Nielsen, S.S., Krogh, M.A. & Enevoldsen, C., 2009. Time to the occurrence of a decline in milk production in cows with various paratuberculosis antibody profiles. *Journal of Dairy Science*, 92(1), pp.149–155.

Nielsen, S.S. & Toft, N., 2008. Ante mortem diagnosis of paratuberculosis: A review of accuracies of ELISA, interferon-γ assay and faecal culture techniques. *Veterinary Microbiology*, 129(3-4), pp.217–235.

Nielsen, S.S. & Toft, N., 2014. Bulk tank milk ELISA for detection of antibodies to Mycobacterium avium subsp. paratuberculosis: Correlation between repeated tests and within-herd antibody-prevalence. *Preventive Veterinary Medicine*, 113(1), pp.96–102.

Nimmerjahn, F. & Ravetch, J. V., 2005. Divergent Immunoglobulin G Subclass Activity Through Selective Fc Receptor Binding. *Science*, 310(5753).

Noss, E.H. et al., 2001. Toll-like receptor 2-dependent inhibition of macrophage class II MHC expression and antigen processing by 19-kDa lipoprotein of Mycobacterium tuberculosis. *Journal of immunology (Baltimore, Md. : 1950)*, 167(2), pp.910–8.

Novikov, A. et al., 2011. Mycobacterium tuberculosis Triggers Host Type I IFN Signaling To Regulate IL-1 Production in Human Macrophages. *The Journal of Immunology*, 187(5), pp.2540–2547.

O'Leary, S., O'Sullivan, M.P. & Keane, J., 2011. IL-10 Blocks Phagosome Maturation in *Mycobacterium tuberculosis*– Infected Human Macrophages. *American Journal of Respiratory Cell and Molecular Biology*, 45(1), pp.172–180.

Oh, Y.K. & Straubinger, R.M., 1996. Intracellular fate of Mycobacterium avium: Use of dual-label spectrofluorometry to investigate the influence of bacterial viability opsonization on phagosomal pH phagosome-lysosome interaction. *Infection and Immunity*, 64(1), pp.319–325.

Ohmann, H.B., 1988. In Situ Characterization of Mononuclear Leukocytes in Skin and Digestive Tract of Persistently Bovine Viral Diarrhea Virus-infected Clinically Healthy Calves and Calves with Mucosal Disease. *Vet. Pathol*, pp.25304–309.

Olsen, A. et al., 2016. Targeting Mycobacterium tuberculosis Tumor Necrosis Factor Alpha-Downregulating Genes for the Development of Antituberculous Vaccines. *mBio*, 7(3), pp.e01023–15.

Orpin, P.G., Sibley, R.J. & Komorowski, E., 2012. A voluntary Johne's engagement programme in UK Dairy Herds. In *Proceedings of 3rd ParaTB Forum*. Syndey, pp. 10–19.

Osterstock, J.B. et al., 2007. Contribution of environmental mycobacteria to false-

positive serum ELISA results for paratuberculosis. *Journal of the American Veterinary Medical Association*, 230(6), pp.896–901.

Ott, S.L., Wells, S.J. & Wagner, B.A., 1999. Herd-level economic losses associated with Johne's disease on US dairy operations. *Preventative Veterinary Medicine*, 40(3-4), pp.179–192.

Park, H.-T. & Yoo, H.S., 2016. Development of vaccines to Mycobacterium avium subsp. paratuberculosis infection. *Clinical and experimental vaccine research*, 5(2), pp.108–16.

Park, K.T. et al., 2011. Evaluation of two mutants of Mycobacterium avium subsp. paratuberculosis as candidates for a live attenuated vaccine for Johne's disease. *Vaccine*, 29(29-30), pp.4709–19.

Park, K.T. et al., 2016. Phenotype and Function of CD209+ Bovine Blood Dendritic Cells, Monocyte-Derived-Dendritic Cells and Monocyte-Derived Macrophages. *PloS one*, 11(10), p.e0165247.

Park, K.T., Burnett, S. & Davis, W.C., 2015. Development and characterization of a monoclonal antibody specific for bovine CD209. *Veterinary Immunology and Immunopathology*, 163(3-4), pp.216–220.

Parker, A.E. & Bermudez, L.E., 1997. Expression of the green fluorescent protein (GFP) in Mycobacterium avium as a tool to study the interaction between Mycobacteria and host cells. *Microbial Pathogenesis*, 22, pp.193–198.

Parrish, N., Vadlamudi, A. & Goldberg, N., 2017. Anaerobic adaptation of Mycobacterium avium subspecies paratuberculosis in vitro: similarities to M. tuberculosis and differential susceptibility to antibiotics. *Gut Pathog*, 9.

Pathak, S. et al., 2012. Counting Mycobacteria in Infected Human Cells and Mouse Tissue: A Comparison between qPCR and CFU R. Manganelli, ed. *PLoS ONE*, 7(4), p.e34931.

Payne, J. & Rankin, J., 1961. The pathogenesis of experimental Johne's disease in

calves. *Research in veterinary science*, 2(2), pp.167–174.

Peñuelas-Urquides, K. et al., 2013. Measuring of Mycobacterium tuberculosis growth. A correlation of the optical measurements with colony forming units. *Brazilian journal of microbiology : [publication of the Brazilian Society for Microbiology]*, 44(1), pp.287–9.

Pfaffl, M.W., 2001. A new mathematical model for relative quantification in real-time RT – PCR. , 29(9), pp.16–21.

Pieters, J., 2008. Mycobacterium tuberculosis and the macrophage: maintaining a balance. *Cell host & microbe*, 3(6), pp.399–407.

Plain, K.M. et al., 2014. High-throughput direct fecal PCR assay for detection of Mycobacterium avium subsp. paratuberculosis in sheep and cattle. *Journal of clinical microbiology*, 52(3), pp.745–57.

Plattner, B.L., Doyle, R.T. & Hostetter, J.M., 2009. Gamma-delta T cell subsets are differentially associated with granuloma development and organization in a bovine model of mycobacterial disease. *International journal of experimental pathology*, 90(6), pp.587–97.

Poeck, H. et al., 2010. Recognition of RNA virus by RIG-I results in activation of CARD9 and inflammasome signaling for interleukin 1β production. *Nature Immunology*, 11(1), pp.63–69.

Poirier, V. & Av-Gay, Y., 2012. Mycobacterium tuberculosis modulators of the macrophage's cellular events. *Microbes and Infection*, 14(13), pp.1211–1219.

Pott, J. et al., 2009. Internalization-dependent recognition of *Mycobacterium avium* ssp. *paratuberculosis* by intestinal epithelial cells. *Cellular Microbiology*, 11(12), pp.1802–1815.

Pradhan, A.K. et al., 2011. Molecular epidemiology of Mycobacterium avium subsp. paratuberculosis in a longitudinal study of three dairy herds. *Journal of clinical microbiology*, 49(3), pp.893–901.

Price, S.J. & Hope, J.C., 2009. Enhanced secretion of interferon-gamma by bovine gammadelta T cells induced by coculture with Mycobacterium bovis-infected dendritic cells: evidence for reciprocal activating signals. *Immunology*, 126(2), pp.201–8.

Prinzis, S., Chatterjee, D. & Brennan, P.J., 1993. Structure and antigenicity of lipoarabinomannan from Mycobacterium bovis BCG. *Journal of General Microbiology*, 139(11), pp.2649–2658.

Pritchard, T. et al., 2017. The genetics of antibody response to paratuberculosis in dairy cattle. *Journal of dairy science*, 100(7), pp.5541–5549.

Próchnicki, T. & Latz, E., 2017. Inflammasomes on the Crossroads of Innate Immune Recognition and Metabolic Control. *Cell metabolism*, 26(1), pp.71–93.

Puissegur, M.-P. et al., 2007. Mycobacterial Lipomannan Induces Granuloma Macrophage Fusion via a TLR2-Dependent, ADAM9- and β1 Integrin-Mediated Pathway. *The Journal of Immunology*, 178(5).

Purdie, A. et al., 2012. Expression of genes associated with the antigen presentation and processing pathway are consistently regulated in early Mycobacterium avium subsp. paratuberculosis infection. *Comp. Immunol. Microbiol. Infect. Dis.*, 35, pp.151–162.

Puri, R.V., Reddy, P.V. & Tyagi, A.K., 2013. Secreted acid phosphatase (SapM) of Mycobacterium tuberculosis is indispensable for arresting phagosomal maturation and growth of the pathogen in guinea pig tissues. *PloS one*, 8(7), p.e70514.

Qu, W. et al., 2011. Identification of S-nitrosylation of proteins of Helicobacter pylori in response to nitric oxide stress. *The Journal of Microbiology*, 49(2), pp.251–256.

Radosevich, T.J. et al., 2007. Proteome and differential expression analysis of membrane and cytosolic proteins from Mycobacterium avium subsp. paratuberculosis strains K-10 and 187. *Journal of bacteriology*, 189(3),

pp.1109–17.

Raizman, E.A. et al., 2007. The associations between culling due to clinical Johne's disease or the detection of Mycobacterium avium subsp. paratuberculosis fecal shedding and the diagnosis of clinical or subclinical diseases in two dairy herds in Minnesota, USA. *Preventive Veterinary Medicine*, 80(2-3), pp.166–178.

Rajaram, M.V.S. et al., 2017. M. tuberculosis-Initiated Human Mannose Receptor Signaling Regulates Macrophage Recognition and Vesicle Trafficking by FcRγ-Chain, Grb2, and SHP-1. *Cell reports*, 21(1), pp.126–140.

Redford, P.S. et al., 2010. Enhanced protection to Mycobacterium tuberculosis infection in IL-10-deficient mice is accompanied by early and enhanced Th1 responses in the lung. *European journal of immunology*, 40(8), pp.2200–10.

Reed, J.H. et al., 2013. Complement receptor 3 influences toll-like receptor 7/8-dependent inflammation: implications for autoimmune diseases characterized by antibody reactivity to ribonucleoproteins. *The Journal of biological chemistry*, 288(13), pp.9077–83.

Richardson, E. & More, S., 2009. Direct and indirect effects of Johne's disease on farm and animal productivity in an Irish dairy herd. *Irish veterinary journal*, 62(8), pp.526–32.

Riley, J.K. et al., 1999. Interleukin-10 receptor signaling through the JAK-STAT pathway. Requirement for two distinct receptor-derived signals for anti-inflammatory action. *The Journal of biological chemistry*, 274(23), pp.16513–21.

Roberts, A.L. et al., 2016. The complement receptor 3 (CD11b/CD18) agonist Leukadherin-1 suppresses human innate inflammatory signalling. *Clinical and experimental immunology*, 185(3), pp.361–71.

Rollin, E., Dhuyvetter, K.C. & Overton, M.W., 2015. The cost of clinical mastitis in the first 30 days of lactation: An economic modeling tool. *Preventive Veterinary Medicine*, 122, pp.257–264.

Rosales, C., 2017. Fcγ Receptor Heterogeneity in Leukocyte Functional Responses. *Frontiers in Immunology*, 8, p.280.

Rosales, C. & Uribe-Quero, E., 2017. Phagocytosis: A Fundamental Process in Immunity. *Biomed Res Int*, 2017, p.18.

Rosseels, V. & Huygen, K., 2008. Vaccination against paratuberculosis. *Expert Review of Vaccines*, 7(6), pp.817–32.

Rumsey, J., Valentine, J.F. & Naser, S. a, 2006. Inhibition of phagosome maturation and survival of Mycobacterium avium subspecies paratuberculosis in polymorphonuclear leukocytes from Crohn's disease patients. *Medical science monitor : international medical journal of experimental and clinical research*, 12(4), pp.BR130–R139.

Russell, D.G. et al., 2009. Foamy macrophages and the progression of the human tuberculosis granuloma. *Nature immunology*, 10(9), pp.943–8.

Sadeghi-Shanbestari, M. et al., 2009. Immunologic aspects of patients with disseminated bacille Calmette-Guerin disease in north-west of Iran. *Italian Journal of Pediatrics*, 35(42).

Sahoo, M. et al., 2011. Role of the inflammasome, IL-1β, and IL-18 in bacterial infections. *TheScientificWorldJournal*, 11, pp.2037–50.

Saikolappan, S. et al., 2012. The fbpA/sapM double knock out strain of Mycobacterium tuberculosis is highly attenuated and immunogenic in macrophages. *PloS one*, 7(5), p.e36198.

Salgado, M. et al., 2014. Association between cattle herd Mycobacterium avium subsp. paratuberculosis (MAP) infection and infection of a hare population. *Tropical Animal Health and Production*, 46(7), pp.1313–1316.

Sándor, N. et al., 2013. CR3 is the dominant phagocytotic complement receptor on human dendritic cells. *Immunobiology*, 218, pp.652–663.

Schieber, M. & Chandel, N.S., 2014. ROS function in redox signaling and oxidative stress. *Current biology : CB*, 24(10), pp.R453–62.

Schlesinger, L.S. et al., 1990. Phagocytosis of Mycobacterium tuberculosis is mediated by human monocyte complement receptors and complement component C3. *The Journal of Immunology*, 144(7).

Schorey, J.S., Carroll, M.C. & Brown, E.J., 1997. A Macrophage Invasion Mechanism of Pathogenic Mycobacteria. *Science*, 277(5329).

Secott, T.E., Lin, T.L. & Wu, C.C., 2004. Mycobacterium avium subsp. paratuberculosis Fibronectin Attachment Protein Facilitates M-Cell Targeting and Invasion through a Fibronectin Bridge with Host Integrins. *Infection and Immunity*, 72(7), pp.3724–3732.

Seubert, A. et al., 2011. Adjuvanticity of the oil-in-water emulsion MF59 is independent of Nlrp3 inflammasome but requires the adaptor protein MyD88. *Proceedings of the National Academy of Sciences of the United States of America*, 108(27), pp.11169–74.

Shafran, I., 2000. Isolation of Mycobacterium avium subsp paratuberculosis From Breast Milk of Crohn ' s Disease Patients Antineutrophil Cytoplasmic Antibodies in Turkish Children With Inflammatory Bowel Disease. *The American Journal of Gastroentrology*, 95(4), pp.1999–2000.

Shaughnessy, L.J. et al., 2013. High prevalence of paratuberculosis in rabbits is associated with difficulties in controlling the disease in cattle. *The Veterinary Journal*, 198(1), pp.267–270.

Shin, M.-K. et al., 2015. Whole-blood gene-expression profiles of cows infected with Mycobacterium avium subsp. paratuberculosis reveal changes in immune response and lipid metabolism. *Journal of microbiology and biotechnology*, 25(2), pp.255–67.

Shin, S.J. et al., 2007. Rapid and Reliable Method for Quantification of Mycobacterium paratuberculosis by Use of the BACTEC MGIT 960 System.

Journal of Clinical Microbiology, 45(6), pp.1941–1948.

Shippy, D.C. et al., 2017. Superior Protection from Live-Attenuated Vaccines Directed against Johne's Disease. *Clinical and vaccine immunology : CVI*, 24(1).

Sidoti, F. et al., 2011. Validation and standardization of IS900 and F57 real-time quantitative PCR assays for the specific detection and quantification of *Mycobacterium avium* subsp. *paratuberculosis*. *Canadian Journal of Microbiology*, 57(5), pp.347–354.

Silva, A.R. et al., 2009. Lipid bodies in oxidized LDL-induced foam cells are leukotriene-synthesizing organelles: a MCP-1/CCL2 regulated phenomenon. *Biochimica et Biophysica Acta (BBA) - Molecular and Cell Biology of Lipids*, 1791(11), pp.1066–1075.

Slana, I. et al., 2008. On-farm spread of Mycobacterium avium subsp. paratuberculosis in raw milk studied by IS900 and F57 competitive real time quantitative PCR and culture examination. *International Journal of Food Microbiology*, 128(2), pp.250–257.

Smith, P.D. et al., 2011. Intestinal macrophages and response to microbial encroachment. *Mucosal Immunology*, 4(1), pp.31–42.

Sobotta, K. et al., 2016. Coxiella burnetii Infects Primary Bovine Macrophages and Limits Their Host Cell Response. *Infection and immunity*, 84(6), pp.1722–34.

Sologuren, I. et al., 2011. Partial recessive IFN-γR1 deficiency: genetic, immunological and clinical features of 14 patients from 11 kindreds. *Human molecular genetics*, 20(8), pp.1509–23.

Sommer, S. et al., 2009. Mycobacterium avium subspecies paratuberculosis suppresses expression of IL-12p40 and iNOS genes induced by signalling through CD40 in bovine monocyte-derived macrophages. *Veterinary Immunology and Immunopathology*, 128(1-3), pp.44–52.

Souriau, A. et al., 2017. Identification of new antigen candidates for the early diagnosis of Mycobacterium avium subsp. paratuberculosis infection in goats. *Research in Veterinary Science*, 115, pp.278–287.

Souza, C. et al., 2013. Mannosylated lipoarabinomannans from Mycobacterium avium subsp. paratuberculosis alters the inflammatory response by bovine macrophages and suppresses killing of Mycobacterium avium subsp. avium organisms. *PloS one*, 8(9), p.e75924.

Souza, C.D. et al., 2017. A nano particle vector comprised of poly lactic-co-glycolic acid and monophosphoryl lipid A and recombinant *Mycobacterium avium* subsp *paratuberculosis* peptides stimulate a pro-immune profile in bovine macrophages. *Journal of Applied Microbiology*, 123(1), pp.54–65.

Souza, C.D., 2015. Blocking the mitogen activated protein kinase-p38 pathway is associated with increase expression of nitric oxide synthase and higher production of nitric oxide by bovine macrophages infected with Mycobacterium avium subsp paratuberculosis. *Veterinary Immunology and Immunopathology*, 164(1-2), pp.1–9.

Souza, C.D., Evanson, O.A. & Weiss, D.J., 2006. Mitogen activated protein kinase p38 pathway is an important component of the anti-inflammatory response in Mycobacterium avium subsp. paratuberculosis-infected bovine monocytes. *Microbial Pathogenesis*, 41, pp.59–66.

Souza, C.D., Evanson, O.A. & Weiss, D.J., 2007. Role of the MAPK (ERK) pathway in regulation of cytokine expression by Mycobacterium avium subsp paratuberculosis exposed bovine monocytes. *American Journal of Veterinary Research*, 68(6), pp.625–630.

Stabel, J., 2000. Transitions in immune responses to Mycobacterium paratuberculosis. *Veterinary Microbiology*, 77(3-4), pp.465–473.

Stanley, E.C. et al., 2007. Development of a new, combined rapid method using phage and PCR for detection and identification of viable Mycobacterium

paratuberculosis bacteria within 48 hours. *Applied and environmental microbiology*, 73(6), pp.1851–7.

Stevenson, K., 2015. Genetic diversity of Mycobacterium avium subspecies paratuberculosis and the influence of strain type on infection and pathogenesis: a review. *Veterinary Research*, 46(1), p.64.

Stewart, L.D. et al., 2013. Development of a novel phage-mediated immunoassay for the rapid detection of viable *Mycobacterium avium* subsp. *paratuberculosis*. *Journal of Applied Microbiology*, 115(3), pp.808–817.

Sturgill-Koszycki, S., Schaible ', U.E. & Russell2, D.G., 1996. Mycobacterium-containing phagosomes are accessible to early endosomes and reflect a transitional state in normal phagosome biogenesis. *The EMBO Journal*, 15(24), pp.6960–6968.

Sullivan, B.M. et al., 2005. Increased Susceptibility of Mice Lacking T-bet to Infection with Mycobacterium tuberculosis Correlates with Increased IL-10 and Decreased IFN-γ Production. *The Journal of Immunology*, 175(7).

Sun, K. & Metzger, D.W., 2008. Inhibition of pulmonary antibacterial defense by interferon-γ during recovery from influenza infection. *Nature Medicine*, 14(5), pp.558–564.

Sundaramurthy, V. & Pieters, J., 2007. Interactions of pathogenic mycobacteria with host macrophages. *Microbes and infection / Institut Pasteur*, 9(14-15), pp.1671–9.

Sung, N., Takayama, K. & Collins, M.T., 2004. Possible association of GroES and antigen 85 proteins with heat resistance of Mycobacterium paratuberculosis. *Applied and environmental microbiology*, 70(3), pp.1688–97.

Sweeney, R. et al., 1998. Interferon-gamma and interleukin 4 gene expression in cows infected with Mycobacterium paratuberculosis. *Am J Vet Res.*, 59(7), pp.842–7.

Sweeney, R.W. et al., 2006. Longitudinal Study of ELISA Seroreactivity to *Mycobacterium Avium* subsp. *Paratuberculosis* in Infected Cattle and Culture-Negative Herd Mates. *Journal of Veterinary Diagnostic Investigation*, 18(1), pp.2–6.

Sweeney, R.W., 2011. Pathogenesis of Paratuberculosis. *Veterinary Clinics of North America: Food Animal Practice*, 27(3), pp.537–546.

Sweeney, R.W. et al., 2006. Tissue predilection sites and effect of dose on Mycobacterium avium subs. paratuberculosis organism recovery in a short-term bovine experimental oral infection model. *Research in Veterinary Science*, 80(3), pp.253–259.

Sweet, L. et al., 2010. Mannose Receptor-Dependent Delay in Phagosome Maturation by Mycobacterium avium Glycopeptidolipids. *Infection and Immunity*, 78(1), pp.518–526.

Swift, B.M.C. et al., 2016. Evaluation of the limitations and methods to improve rapid phage-based detection of viable Mycobacterium avium subsp. paratuberculosis in the blood of experimentally infected cattle. *BMC veterinary research*, 12(1), p.115.

Thakur, A. et al., 2013. Cell-mediated and humoral immune responses after immunization of calves with a recombinant multiantigenic Mycobacterium avium subsp. paratuberculosis subunit vaccine at different ages. *Clinical and vaccine immunology : CVI*, 20(4), pp.551–8.

Thomas, G. et al., 2015. Nonclassical patrolling monocyte function in the vasculature. *Arteriosclerosis, thrombosis, and vascular biology*, 35(6), pp.1306–16.

Twort, F.W. & Ingram, G.L.Y., 1912. A Method for Isolating and Cultivating the Mycobacterium enteritidis chronicae pseudotuberculosae bovis, Johne, and some Experiments on the Preparation of a Diagnostic Vaccine for Pseudo-tuberculous Enteritis of Bovines. *Proceedings of the Royal Society of London B:*

Biological Sciences, 84(575).

de Vallière, S. et al., 2005. Enhancement of innate and cell-mediated immunity by antimycobacterial antibodies. *Infection and immunity*, 73(10), pp.6711–20.

Vavra, A.K. et al., 2011. Insights into the effect of nitric oxide and its metabolites nitrite and nitrate at inhibiting neointimal hyperplasia. *Nitric oxide : biology and chemistry*, 25(1), pp.22–30.

Vergne, I. et al., 2005. Mechanism of phagolysosome biogenesis block by viable Mycobacterium tuberculosis. *Proceedings of the National Academy of Sciences of the United States of America*, 102(11), pp.4033–8.

Verhegghe, M. et al., 2017. Reduction of Mycobacterium avium ssp. paratuberculosis in colostrum: Development and validation of 2 methods, one based on curdling and one based on centrifugation. *Journal of Dairy Science*, 100(5), pp.3497–3512.

Verna, A.E. et al., 2007. Variation in the Immuno-pathological Responses of Lambs after Experimental Infection with Different Strains of Mycobacterium avium subsp. paratuberculosis. *Zoonoses and Public Health*, 54(6-7), pp.243–252.

Via, L.E. et al., 1997. Arrest of mycobacterial phagosome maturation is caused by a block in vesicle fusion between stages controlled by rab5 and rab7. *The Journal of biological chemistry*, 272(20), pp.13326–31.

Via, L.E. et al., 2008. Tuberculous granulomas are hypoxic in guinea pigs, rabbits, and nonhuman primates. *Infection and immunity*, 76(6), pp.2333–40.

Volovitz, I. et al., 2016. A non-aggressive, highly efficient, enzymatic method for dissociation of human brain-tumors and brain-tissues to viable single-cells. *BMC Neuroscience*, 17(30).

Vordermeier, H.M. et al., 2009. Viral booster vaccines improve Mycobacterium bovis BCG-induced protection against bovine tuberculosis. *Infection and immunity*, 77(8), pp.3364–73.

Wang, J. et al., 2015. Evaluation of the inflammatory response in macrophages stimulated with exosomes secreted by Mycobacterium avium-infected macrophages. *BioMed research international*, 2015, p.658421.

Waters, W.R. et al., 2012. Bovine tuberculosis vaccine research: historical perspectives and recent advances. *Vaccine*, 30(16), pp.2611–22.

Waters, W.R. et al., 2003. Early induction of humoral and cellular immune responses during experimental Mycobacterium avium subsp. paratuberculosis infection of calves. *Infection and immunity*, 71(9), pp.5130–8.

Weber, B. et al., 2011. CX3CR1 defines functionally distinct intestinal mononuclear phagocyte subsets which maintain their respective functions during homeostatic and inflammatory conditions. *European Journal of Immunology*, 41(3), pp.773–779.

Weiss, D.J. et al., 2005. A critical role of interleukin-10 in the response of bovine macrophages to infection by Mycobacterium avium subsp paratuberculosis. *American journal of veterinary research*, 66(4), pp.721–6.

Weiss, D.J. et al., 2008. Bovine monocyte TLR2 receptors differentially regulate the intracellular fate of Mycobacterium avium subsp. paratuberculosis and Mycobacterium avium subsp. avium. *Journal of leukocyte biology*, 83(1), pp.48–55.

Weiss, D.J. et al., 2002. Differential responses of bovine macrophages to Mycobacterium avium subsp. paratuberculosis and Mycobacterium avium subsp. avium. *Infection and immunity*, 70(10), pp.5556–61.

Weiss, D.J. et al., 2001. Regulation of Expression of Major Histocompatibility Antigens by Bovine Macrophages Infected with Mycobacterium avium subsp. paratuberculosis or Mycobacterium avium subsp. avium. *Infection and Immunity*, 69(2), pp.1002–1008.

Whittington, R.J. et al., 2004. Survival and dormancy of Mycobacterium avium subsp. paratuberculosis in the environment. *Applied and environmental*

microbiology, 70(5), pp.2989–3004.

Whittington, R.J., Marsh, I.B. & Reddacliff, L.A., 2005. Survival of Mycobacterium avium subsp. paratuberculosis in dam water and sediment. *Applied and environmental microbiology*, 71(9), pp.5304–8.

Willcocks, S. et al., 2006. Identification and gene expression of the bovine C-type lectin Dectin-1. *Veterinary immunology and immunopathology*, 113(1-2), pp.234–42.

Williams, D.R. et al., 2014. Effect of Three Colostrum Diets on Passive Transfer of Immunity and Preweaning Health in Calves on a California Dairy following Colostrum Management Training. *Veterinary medicine international*, 2014, p.698741.

Wojciechowski, W. et al., 1999. Attenuation of MHC class II expression in macrophages infected with Mycobacterium bovis bacillus Calmette-Guérin involves class II transactivator and depends on the Nramp1 gene. *Journal of immunology (Baltimore, Md. : 1950)*, 163(5), pp.2688–96.

Wong, D. et al., 2011. Mycobacterium tuberculosis protein tyrosine phosphatase (PtpA) excludes host vacuolar-H+-ATPase to inhibit phagosome acidification. *Proceedings of the National Academy of Sciences of the United States of America*, 108(48), pp.19371–6.

Woo, S.-R. et al., 2006. Bovine monocytes and a macrophage cell line differ in their ability to phagocytose and support the intracellular survival of Mycobacterium avium subsp. paratuberculosis. *Veterinary Immunology and Immunopathology*, 110(1-2), pp.109–120.

Wright, S.D. & Silverstein, S.C., 1983. Receptors for C3b and C3bi promote phagocytosis but not the release of toxic oxygen from human phagocytes. *The Journal of experimental medicine*, 158(6), pp.2016–23.

Wu, C. et al., 2009. A novel cell wall lipopeptide is important for biofilm formation and pathogenicity of Mycobacterium avium subspecies paratuberculosis.

Microbial pathogenesis, 46(4), pp.222–30.

Wu, C. et al., 2007. Invasion and persistence of Mycobacterium avium subsp. paratuberculosis during early stages of Johne's disease in calves. *Infection and immunity*, 75(5), pp.2110–9.

Yamakawa, Y. et al., 2008. Identification and functional characterization of a bovine orthologue to DC-SIGN. *Journal of leukocyte biology*, 83(6), pp.1396–403.

Yan, W., Chen, W. & Huang, L., 2007. Mechanism of adjuvant activity of cationic liposome: Phosphorylation of a MAP kinase, ERK and induction of chemokines. *Molecular Immunology*, 44(15), pp.3672–3681.

Zanetti, S. et al., 2006. "In vitro" activities of antimycobacterial agents against Mycobacterium avium subsp. paratuberculosis linked to Crohn's disease and paratuberculosis. *Annals of clinical microbiology and antimicrobials*, 5, p.27.

Zare, Y. et al., 2014. *Short communication: Heritability estimates for susceptibility to Mycobacterium avium subspecies paratuberculosis infection defined by ELISA and fecal culture test results in Jersey cattle*,

Zhang, H. et al., 2015. Therapeutic Potential of IL-17-Mediated Signaling Pathway in Autoimmune Liver Diseases. *Mediators of inflammation*, 2015, p.436450.

8 Appendices

Appendix A – Media

FBS was purchased from Lonza and batch tested prior to use.

- **Tissue Culture Medium A (TCMa)**
  - *RPMI 1640 with 20% FBS, 4mM L-glutamine and 0.1% 2 β-mercaptoethanol,*
    120U/ml penicillin streptomycin solution

- **Tissue Culture Medium B (TCMb)**
  - *RPMI 1640 with 20% FBS, 4mM L-glutamine and 0.1% 2 β-mercaptoethanol*

- **Tissue culture Medium C (TCMc)**
  - *DMEM without phenol red, supplemented with 20% FBS, 4mM L-glutamine, 0.1% β-mercaptoethanol*

- **Tissue culture media D (TCMd)**
  - *RPMI 1640 without phenol red, supplemented with 20% FBS, 4mM L-glutamine, 0.1% β-mercaptoethanol*

- **7H9/Mycobactin J**
  - *0.26% Middlebrook 7H9 broth, 0.22% glycerol, 0.06% Tween 80, 0.22% Mycobactin J, 10% OADC, in sterile H_2O*

- **7H9/Mycobactin J/30% glycerol**
  - *7H9 + MJ, as described above, with 30% glycerol*

- **7H9/ 30% glycerol**
  - *0.26% Middlebrook 7H9 broth, 0.22% glycerol, 0.06% Tween 80, 10% OADC, 30% glycerol, in sterile H_2O*

- **7H9/2mM $CaCl_2$**
  - *0.26% Middlebrook 7H9 broth, 0.22% glycerol, 0.06% Tween 80, 10% OADC, 2mM $CaCl_2$, in sterile H_2O*

- **7H9/Mycobactin J/Kanamycin**
  - *0.26% Middlebrook 7H9 broth, 0.22% glycerol, 0.06% Tween 80, 0.22% Mycobactin J, 10% OADC, 25µg/ml kanamycin, in sterile H_2O*

- **7H10 agar**
  - *1.9% Middlebrook 7H10 agar powder, 2.5% glycerol, 0.06% aspargine, 10% OADC, 20% heat inactive bovine FCS, in sterile H_2O*

- **7H10 agar/Mycobactin J**
  - *1.9% Middlebrook 7H10 agar powder, 2.5% glycerol, 0.06% aspargine, 0.22% Mycobactin J, 10% OADC, 20% heat inactive bovine FCS, in sterile H_2O*

Appendix B – Buffers and Solutions

- **Phosphate buffered saline**

- **RBC Lysis buffer**
  - *10mM KHCO3, 150mM NH4Cl, 0.1mM EDTA, pH 8.0*

- **PBS/BSA/Azide**
  - 1% BSA, 0.1% NaN_3 in distilled PBS

- **SM buffer**
  - *100mM NaCl, 8mM MgSO4•7H2O, 50mM Tris-Cl*

- **Enzymatic lysis buffer (DNA extraction)**
  - *20 mM Tris-Cl (pH 8.0), 2 mM sodium EDTA, 1.2% Triton® X-100. Immediately before use, lysozyme was added to 20 mg/ml.*

- **TAE buffer**
  - *40 mM Tris (pH 7.6),20 mM acetic acid, 1 mM EDTA*

- **CTAB/NaCl**
  - *4.1% NaCl, 10% CTAB (hexadecyltri-methyl ammoniumbromide) in distilled H_2O*

- **ELISA blocking buffer**
  - *1mg/ml sodium casein in PBS*

Appendix C – Suppliers

- 10mM dNTP mix – Promega (Southampton, UK)
- 10x PCR buffer – Life Technologies (Paisley, UK)
- 13mm diameter glass coverslips – VWR (Leicestershire, UK)
- 25mM $MgCl_2$ - Life Technologies (Paisley, UK)
- 6x loading dye – Thermo Fisher Scientific (Paisley, UK)
- 75cm^3 cell culture flasks – Corning (Flintshire, UK)
- 7H10 agar base – Sigma Aldrich (Dorset, UK)
- 7H9 media base – Sigma Aldrich (Dorset, UK)
- 96 well plates for qPCR – Thermo Fisher Scientific (Paisley, UK)
- AF647 dextran – Life Technologies (Paisley, UK)
- Agarose – Bioline (London, UK)
- Alexa Fluor 350 Carboxylic Acid, bis(triethylammonium) salt – Molecular probes (Paisley, UK)
- β-mercaptoethanol -
- Blood bags with CPDA – Sarstedt (Leicester, UK)
- Brilliant III Ultra-Fast SYBR Green qPCR master mix – Agilent Technologies (Edinburgh, UK)
- CellRoX Deep Red Flow Cytometry Assay kit – Molecular Probes (Paisley, UK)
- D-Mannose – Sigma Aldrich (Dorset, UK)
- DNEasy Blood and Tissue kit – Qiagen (Manchester, UK)
- FACS Flow Sheath fluid – BD Biosciences (Berkshire, UK)
- FBS – Lonza Biologicals (Slough, UK)
- Ferrous Ammonium Sulphate – SLS (Newhouse, UK)
- FITC isomer – Sigma Aldrich (Dorset, UK)
- Gene pulser cuvettes – Bio-Rad (Watford, UK)
- GoScript Reverse Transcription System – Promega (Southampton, UK)
- Griess assay kit – Thermo Fisher Scientific (Paisley, UK)
- Griess Reagent kit – Thermo Fisher Scientific, (Paisley, UK)
- Hyperladder IV – Bioline (London, UK)

- Lymphoprep – Alere Ltd. (Stirling, UK)
- L-glutamine
- Lysozyme – Sigma Aldrich (Dorset, UK)
- Lysozyme – Sigma Aldrich (Dorset, UK)
- Mannan from *Saccharomyces cerevisiae* - Sigma Aldrich (Dorset, UK)
- Mycobactin J – IDVet (Grabels, France)
- NG-Monomethyl-L-arginine, monoacetate salt (L-NMMA) - Thermo Fisher Scientific (Paisley, UK)
- Nuclease free H_2O - Gibco (Paisley, UK)
- OADC – BD Biosciences (Berkshire, UK)
- Opti-MEM I serum free medium - Invitrogen (Paisley, UK)
- Phalloidin 488 – Molecular Probes (Paisley, UK)
- Phrodo dextran – Life Technologies (Paisley, UK)
- pHrodo Red, succinimidyl ester – Molecular Probes (Paisley, UK)
- Polystyrene beads – Polysciences, Inc.(Northampton, UK)
- ProLong Gold Antifade Mountant – Life Technologies (Paisley, UK)
- ReliaPrep RNA Extraction kit – Promega (Southampton, UK)
- RNAiMAX Lipofectamine – Thermo Fisher Scientific (Paisley, UK)
- RPMI 1640, no glutamine, no phenol red – Gibco (Paisley, UK)
- RPMI 1640 media – Sigma Aldrich (Dorset, UK)
- SYBR safe – Invitrogen (Paisley, UK)
- SYTO9 – Life Technologies (Paisley, UK)
- Taq polymerase – Life Technologies (Paisley, UK)
- TritonX-100 – Sigma Aldrich (Dorset, UK)
- TRIzol reagent – Thermo Fisher Scientific (Paisley, UK)
- Trypan blue - Thermo Fisher Scientific (Paisley, UK)
- TrypLE Express – Thermo Fisher Scientific (Paisley, UK)
- Ultra Clear qPCR caps – Thermo Fisher Scientific (Paisley, UK)
- Wizard Genomic DNA purification kit – Promega (Southampton, UK)
- Zombie Aqua – Biolegend (London, UK)

Appendix D - Primers

Bovine primers:

	Application	Forward	Reverse	Product size
MARCO	PCR	GCTGGGCTCTTGGTGATACA	TGCTGCCAGTATCACCCTTG	405
NOS2	PCR	CCCGTCCTTGCATCCTCATT	CCTCCACCTGTTCCTCGTTC	416
LAMP1	PCR	GTGCTCCTCGCCTACCTGAT	GCCCAGACAGACACGCTTTA	772
NOX2	PCR	TCGTCATTACACTGTGCCTGA	ACCAGACCGACTTGAGGATG	416
IL-1β	PCR	AGGTGGTGTCGGTCATCGT	ATTCTTCCCTTCCCTTCTGC	684
IL-6	PCR	CCAGAACGAGTATGAGGGAAA	CAATAAGGACATTCAAGCCACA	523
IL-10	PCR	CTCTGTTGCCTGGTCTTCCT	CACCGCCTTGCTCTTGTT	399
NLRP3	PCR	AAAGGAAGTGGACTGCGAGA	GCCAGGTTGTTGGAGTGTTT	775
GAPDH	PCR	GATGCTGGTGCTGAGTATGTA	ATCCACAACAGACACGTTGGGAG	963 (gDNA)
MARCO	qPCR	ACAACAATGAAACGCAGGCC	TCTTCCTGCCTCTCCCTTGA	140
NOS2	qPCR	GAGGAGATGCTGGAGATGGC	TGAACATAGACCTTGGGCTGG	92
LAMP1	qPCR	CACTCAGACACAAGCCTCACA	ACCCTCCACACTCACCACTC	82
NOX2	qPCR	GTCAAGTGTCCCGTGGTGTC	ACGATGCGGATATGGATGCT	92
IL-1β	qPCR	TCCGACGAGTTTCTGTGTGA	TGTGAGAGGAGGTGGAGAGC	122
IL-6	qPCR	ACCACTCCAGCCACAAACAC	ATGCCCAGGAACTACCACAA	176
IL-10	qPCR	TGGATGACTTTAAGGGTTAC	AGGGCAGAAAGCGATGAC	183
NLRP3	qPCR	GTTGTCCGTTTCCTCTTTGG	AGTGTCTTGGCATTGGCTTT	137
CHAMP1	qPCR	AGCAGTGACCAAGAGCAGGT	TCATAGCACGACAGCAACAA	205
OAS1	qPCR	AGTTCTCCCCCTGCTTCAAC	GCTGCTCCTTACACAGTTGG	114
SPAST	qPCR	CAACACCTGCGTCCCTTT	CGCAGGGCAGATCAGTTT	61

MAP primers:

	Application	Forward	Reverse	Product size
F57	PCR	CGATCCGAATATGTTGTTGC	TGGCGTCAGCTATTGGTGTA	455
F57	qPCR	GACTGGTAGACGCCCATTTC	GCTTAGTTCGCCGCTTGA	90

Appendix E - Antibodies

Primary antibodies							
Antibody	**Manufacturer**	**Cat. No.**	**Clone**	**Conc.**	**Dilution**	**Final conc.**	**Isotype**
Mouse anti-human MARCO	Hycult biotech	HM2208S	PLK-1	0.1mg/ml	N/A		IgG3
Mouse anti-bovine CD209	Monoclonal Antibody Centre	BOV2133	209MD26A	0.5mg/ml	1:50	10µg/ml	IgG2a
Mouse anti-bovine CD163	Monoclonal Antibody Centre	BOV2141	LND68A	0.5mg/ml	1:250	2µg/ml	IgG1
Mouse anti bovine CD32	IAH Compton	N/A	CCG36		1:2000		IgG1
Fcg2R	IAH Compton	N/A	CCG124		1:100		IgM
Mouse anti Bovine MHC Class II DR	AbD Serotec	MCA5656	CC108	0.1mg/ml	1:100	1µg/ml	IgG1
Mouse anti-bovine CD40	IAH Compton	N/A	ILA-158		1:1000		IgG1
Mouse anti-bovine CD11b	Santa Cruz	sc-101829	CC104	0.2mg/ml	1:10		IgG2b
Mouse anti-bovine CD11c	IAH Compton	N/A	IL-A16		1:10		IgG1

Conjugated antibodies							
Antibody	**Manufacturer**	**Cat. No.**	**Clone**	**Conc.**	**Dilution**	**Final Conc.**	**Isotype**
Mouse anti-Human CD16: FITC	AbD Serotec	MCA5665F	KD1	0.1mg/ml	1:10		IgG2a
Mouse anti Human CD14:Alexa Fluor 647	AbD Serotec	MCA1568A647T	TUK4		1:50		IgG2a
Mouse anti Bovine CD172a:RPE-Cy5	AbD Serotec	MCA2041C	CC149		1:100		IgG2b
Mouse anti human CD206:RPE	Beckman Coulter	IM2741	3.29B1.10		1:5		IgG1

Secondary antibodies					
Antibody	**Manufacturer**	**Cat. No.**	**Conc.**	**Dilution**	**Final Conc.**
Goat anti- Mouse IgG (H+L) PE	Southern Biotech	1031-09	0.5mg/ml	1:100	5µg/ml
Goat anti-guinea pig IgG (H+L) CF568	Sigma	SAB4600080	2mg/ml	1:200	10µg/ml
Goat anti-guinea pig IgG (H+L) CF488A	Sigma	SAB4600040	2mg/ml	1:100	20µg/ml
Goat anti-mouse IgG1 FITC	Southern Biotech	1031-02 S.	1mg/ml	1:100	10µg/ml
Goat anti-mouse IgG1 AF647	Life Technologies	A21240	2mg/ml	1:1000	2µg/ml
Goat anti-mouse IgG2a PE	Invitrogen	P-21139	1mg/ml	1:500	2µg/ml
Goat anti-mouse IgG2b FITC	Southern Biotech	1091-02	1mg/ml	1:100	10µg/ml
Goat anti-mouse IgG2b PE	Southern Biotech	1090-09S	0.5mg/ml	1:50	10µg/ml

Isotype Controls		
Antibody	**Manufacturer**	**Cat. No.**
Mouse IgG1 Negative control	Invitrogen	15304401
Mouse IgG2a Negative Control	Invitrogen	15364401
Mouse IgG3 Negative Control	Affymetrix eBioscience	15237377
Mouse IgM Negative Control	Affymetrix eBioscience	15267377

	ELISA antibodies							
	Antibody	**Manufacturer**	**Cat. No.**	**Clone**	**Conc.**	**Dilution**	**Final Conc.**	**Isotype**
Coating antibody	MOUSE ANTI BOVINE INTERLEUKIN-10	AbD Serotec	MCA2110	CC318	0.5mg/ml	1:250	2µg/ml	IgG2b
Detection antibody	MOUSE ANTI BOVINE INTERLEUKIN-10:Biotin	AbD Serotec	MCA2111B	CC320b	0.25 mg	1:125	2µg/ml	IgG1

Appendix F – Assessing co-localisation of MAP with LAMP1 by confocal microscopy

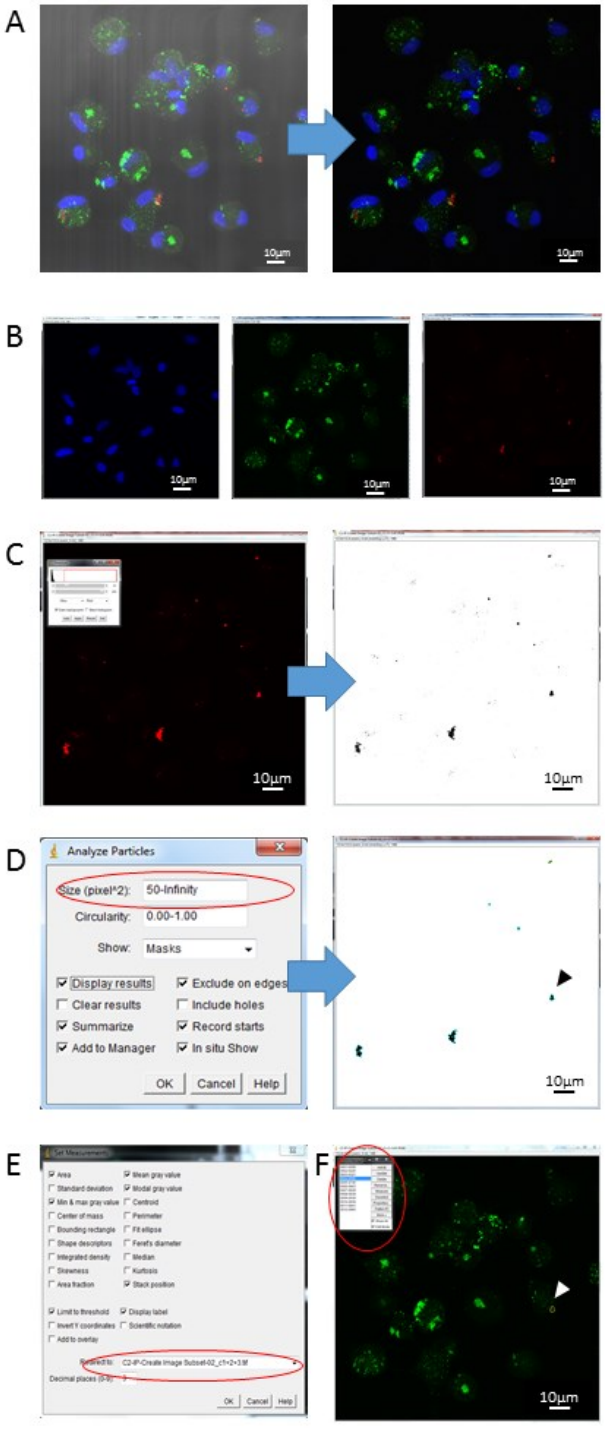

Figure 8-1 Assessing co-localisation of MAP with LAMP1.

The methodology of assessing co-localisation of MAP with LAMP1 by confocal microscopy image analysis is descibed. Images are Maximum Intensity Projections of Z-stacks taken at 1μm intervals vertically through the monolayer (A)Light microscopy channel is removed from image. (B) The fluorescent channels are split using ImageJ software. (C) On the red channel, depicting MAP, a threshold is set, ensuring that all positive staining is covered with minimal background. (D) In the 'Analyse Particles' menu of ImageJ 'Size (pixel^2)' is set to 50-Infinity, so as to only include whole MAP cells in the analysis and further eliminate background. This creates ROIs that can then be applied to another image (E) In the 'Set Measurements' menu of imageJ the 'Redirect to' option (circled in red) is set to the green channel of the same image. This allows the ROIs set up in Figure 8.1 D to be applied to the green channel. Each ROI can then be selected, in turn, to assess if it co-localises with green staining, indicating LAMP1.

Appendix G- Isotype Controls

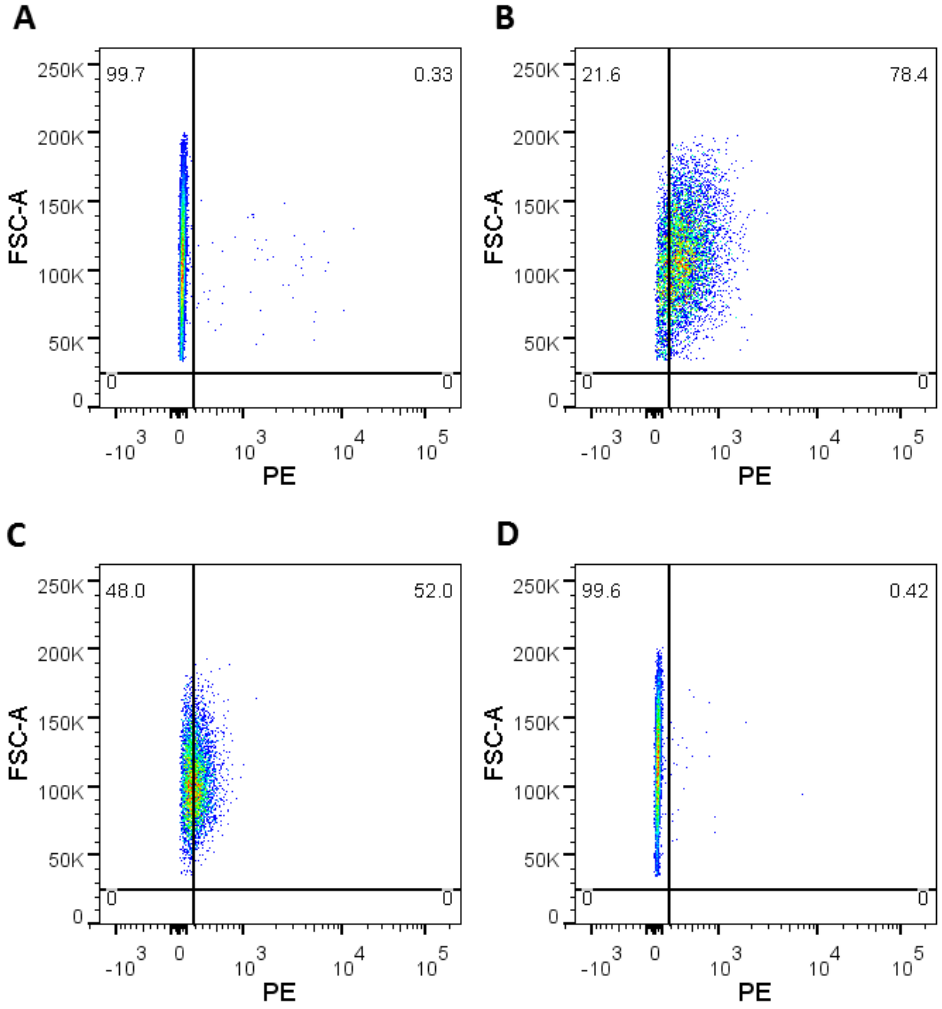

Figure 8-2 Isotype control staining

MDM were gated first by their viability and size and granularity, as depicted in Figure 3-3. Gates were set using unstained controls. (A) Representative IgG1 isotype control (N=5) (B) Representative IgG2a Isotype control (N=3). (C) Representative IgG2b isotype control (N=2). (D) Representative IgG3 Isotype control (N=2). Numbers within gates represent percentage of events